Formation of the Yosemite Creek Granodiorite: a field and geochemical study

by Erik Bliekendaal
Master of Science Thesis Solid Earth
Vrije Universiteit Amsterdam

2012

Preface

My personal interests in geology developed towards the debate of crust-mantle differentiation during my master. The processes involved in crust-mantle differentiation makes the Earth as it is nowadays. The scale of this phenomena exceed all human proportions with a time-scale that spans the complete history of Earth and will continue far into the future. Length and depth scales of the crust-mantle processes are immense with respect to human proportions. I feel it to be a honour to work with and attribute to such a important and interesting subject.

The scientific debate is firm and spreads over a numerous geological disciplines. In my opinion the most interesting of these disciplines are the petrology and geochemistry. Especially the debate with respect to these disciplines is heated and firm due to new geochemical analytical techniques. I hope with this thesis to add another brick of knowledge and data to the great tower of Earth sciences.

My gratitude go to my supervisors, Gareth Davies (Professor at the Vije Universiteit van Amsterdam, department Petrology) and Jonathan Miller (Associate Professor at the San José State University, Department of Geology). Gareth Davies helped to give direction to the research and provided valuable feed-back on the written part of the thesis. Jonathan Miller made the research possible by providing research permits, accommodation and facilitation in California. He gave an extensive field introduction in the granitoïd field relations. I thank both for their intellectual guidance and contribution.

The research was not possible if the Stichting Molengraaff Fonds provided an great financial contribution. My thanks for their contribution.

This research is focussed on a local area within a igneous formation of a plutonic system. Extensive fieldwork and documentation with major and trace element analyse provides a solid base for future work.

The thesis is provided with abundant figures and pictures to illustrate statements with maps, cartoons and field relations. Figures of each single chapter are collected at the end of the chapters to maintain the reading flow and to enhance the overview within the thesis. Figures are categorized by textual appearance and field chronology.

Abstract

A extensive overview of the literature discussion on magma chamber evolution is presented. There are two end-member models, the large magma chamber and the incremental pluton growth. This author considers both models for valid and concludes that only detailed study of a pluton can reveal to what extent which model is most plausible.

From field and geochemical study six units are distinguished in the Yosemite Creek Granodiorite. From most mafic to most felsic the unit are the Diorite to Hornblende-rich Diorite Unit, Fine Grained Quartz Monzodiorite to Granodiorite Unit, Medium Grained Quartz Monzodiorite to Granodiorite Unit, Coarse Grained Granodiorite Unit, Porphyritic Granodiorite Unit and Yosemite Creek Granite Unit.

Two batches are distinguished by their geochemical signature. A mafic batch that is derived from extensive fractional crystallization of a gabbro which is observed as the Diorite to Hornblende-rich Diorite Unit and Fine Grained Quartz Monzodiorite to Granodiorite Unit. The other distinguished increments are a result of assimilation and homogenization in the MASH zone between the “felsic” Yosemite Creek and a parental Yosemite Valley Intrusive Suite Taft Granite. The felsic and mafic increments are thought to be petrogenetically unrelated.

The concluding model considers a MASH zone at the lower crust. In this zone a dacitic melt is formed due to fractional crystallization and assimilation and homogenisation with the host rock. Melt escapes to the upper crust due to the increased buoyancy of the melt. This melt is emplaced as the observed Yosemite Creek units or increments.
A fresh injection of gabbroic melt rapidly intrudes the lower crust. This melt underwent extensive fractional crystallization. Small increments of this melt intrudes in the previous described emplaced increments. From this gabbroic melt a batch is extracted which underwent fractional crystallization of hornblende and inheritance of zircons and plagioclase of a earlier melt before it was emplaced in the upper crust.

Table of content

Figures

1 Introduction

This chapter presents a detailed introduction to the research questions and research set-up. The first sub-chapter consist of a global introduction to the subject, problem statement, research objective and questions, methodology and research approach. The second sub-chapter presents a overview of relevant geology, geological units and geological models.

1.1 Introduction Project

A introduction to the research, research objective and research questions are presented in this chapter. A short lay-out of the methodology and approach is given to gain a impression of the research set-up.

The field work of this research was conducted in collaboration with Jonathan Miller Associate professor at San Jose State University (SJSU) and Martine van der Linde colleague student Vrije Universiteit Amsterdam (VUA). The majority of the lab research was done in collaboration with Martine van der Linde.

1.1.1 Research background

The project was focussed on granitic intrusions which are parts of the Sierra Nevada Batholith in eastern California, and specifically in the North of Yosemite National Park (Figure 1.1a). In this area it is possible to study magma mixing processes and if granitic intrusions are potentially formed of several generations of magma pulses. The main aim is to investigate how the granitic suites are formed.

Granitic plutons are evidence of the fundamental processes that lead to crustal differentiation. Research on plutonic rocks provides a more comprehensive view of the evolution of magma chambers and thereby of Earth's differentiation and evolution.

This research will be complimentary to former studies conducted by previous VUA students and US collaborators. These studies were concentrated on the Yosemite Sentinel Granodiorite and its contact margin with the Yosemite Creek Granodiorite. The granitic entities are located at the margin of the famous Tuolumne Intrusive Suite (TIS). The latter mentioned suite forms a large part of the Yosemite National Park (Figure 1.1b).

A detailed study of the contact boundary between the Yosemite Sentinel Granodiorite and Yosemite Creek Granodiorite was provided by Fulmer and Kruijer (2008). Detailed mapping of the Yosemite Creek Granodiorite is provided by Johnson (unpublished) and, on a more regional scale, by Kistler (1973).

1.1.2 Problem statement

Johnson (unpublished) mapped in detail the lithologies of the Yosemite Creek Granodiorite (YC) and its structural features. The discrimination of rock types is based on the Streckeisen classification of plutonic rocks, structure and grain size. The discriminated units are assumed to originate from the same batch of melt emplaced in several different pulses. However, studies (Huber et al., 1989; Petsche, 2008 and Johnson, unpublished) provide no conclusive petrogenesis with respect to batch relations. It is important to understand these relations for the interpretation of the pluton system and thereby for the discussion on magma chambers.

1.1.3 Research Objective

The objective of this research is to gain more insights of the evolution (e.g. rates of mass addition, mechanisms of magma transfer and storage) of the YC suites and thereby crustal arcs in general. In other words this research would lead to an attempt to discriminated or correlate the YC pulses by their chemical signature. These pulses could form from several magma batches, mixing trends and/or assimilation and hybridization of wall rock and/or older plutons.

Sub-objectives are:

1 Verify units mapped by Johnson (unpublished).
2 Distinguish and map out different pulses if present.
3 Find field relations between the pulses.
4 Characterize the general YC by geochemical signatures.
5 Characterize the geochemical signatures of YC pulses.
6 Determine the role of assimilation, hybridization or mixing trends in the pulses.
7 Relate the YC to other suites/units of the Sierra Nevada Batholith.

1.1.4 Research question

The major research question is: What is the characteristic geochemical signature of Yosemite Creek Granodiorite?

This research question is divided in the follow research questions:

1 Does the YC consist of one magma batch?
2 What is/are the origin(s) of the YC magma batch(es)?
3 Does the YC magma batch assimilate wall-rock on a major scale?
4 To what extent does hybridization occur between the different units?

1.1.5 Hypothesis

The YC consists of several pulses originating from one magma batch. Different magma pulses are partial assimilate and reactivating the older Taft Granite unit. The oldest YC pulses are highly felsic and record the most assimilation. The younger the pulse the more mafic the intrusion become and the lesser assimilation occurs.

1.1.6 Methodology

This research is built up of several phases. The first phase is a literature research, a field research, thin-section analyses, and a XRF major trace-elements analyses. The project was initiated by a detailed analysis of a recent mapping project by an SJSU team and the selection of representative samples. Missing links, "gaps" in the sample coverage and areas of specific importance were identified to be sampled at a later date after completion of an initial geochemistry study of the existing samples. Depending on the progression of the research, isotope analyses and in situ methods can be used to address the research questions in more detail.

After the first phase of research fieldwork was performed. In the field the relationships between granodiorite, enclaves, dikes and other structures are studied. Major-, trace-elements and possible isotope analyse will characterize the origin of identified pulses and their relationship to each other. By analyses of mixing and assimilation an attempt is made to reconstruct the petrogenesis of each YC magma pulse and how these formed individual units.

1.1.7 Approach of research

Detailed lithological contacts and intrusive relations are studied in the field near Ten Lakes and Grant Lake. For location on the map see Figure 3.1. These areas are marked by Johnson (unpublished) as interesting and complex and are assumed to be the location where to find all petrogenetic features of the YC. The general geochemical signature of the YC formation is determined by XRF, major and trace elements, from samples from Johnson (unpublished) and this author in collaboration with M. van der Linde and J. Miller. Major and trace elements will be used to assess hypothesises derived from field studies. A special selection of samples will be used for isotope analyse to detect the relation to other units and the extent of assimilation, hybridization and/or mixing.

1.2 Previous Work: Regional geology

In this subchapter the geology of interest is presented. First a overview is given of the tectonic situation. This is the formation of the Sierra Nevada Batholith at the west-coast of North America. Secondly, a overview is given of the plutonic system with the geological formations. The most relevant units are discussed, such as the Tuolumne Intrusive Suite, Yosemite Valley Intrusive Suite, Yosemite Sentinel Granodiorite and Yosemite Creek Granodiorite.

1.2.1 Sierra Nevada subduction setting

The Sierra Nevada Orogen consists of three major zones, the Western Metamorphic Belt (WMB), the Sierra Nevada Batholith (SNB) and the Eastern Sierra Pendant (ESP) (Figure 1.1a). In total it covers an area of at least 40.000 km^2 near the West coast of North America.

The WMB and ESP manly consist out of Jurassic metavolcanic and metasedimentary rocks (Schweickert et al., 1984). The Sierra Nevada Batholith intruded Precambrian, Paleozoic, and early Mesozoic strata. These can be found as roof pendants, wall-rock and metasedimentary splinters between igneous suites. In general the SNB consist of quartz-bearing granitoid rocks ranging from quartz diorite to leucogranite. Leucogranitic granitoids can contain smaller mafic plutonic masses of diorite, quartz diorite and hornblende gabbro (Chen and Moore, 1982). The SNB is estimated to have a total volume of ~4 x 10^5 km^3 (Titus, 2005).

Within the SNB four major plutons or grouped plutons can be distinguished (Figure 1.1a). These are the Sonora Pluton, Tuolumne Intrusive Suite, John Muir Intrusive Suite and Mount Whitney Intrusive Suite. The Yosemite Batholith consists of two major plutons, the Tuolumne Intrusive Suite and the Yosemite Valley Intrusive Suite. Other important suites are the Yosemite Sentinel Granodiorite, Yosemite Creek Granodiorite, and other small or not identified plutons (Figure 1.1 and Figure 1.2).

Magmatism in SNB Batholith occurd from Jurassic, Triassic and Cretaceous to Late Cretaceous in age (e.g. Coleman and Glazner, 1997; Titus, 2005). The origin of this huge amount of magmatism is due to Mesozoic subduction of the Farralon slab underneath the North American plate (Coleman and Glazner, 1997; Lackey et al., 2008). Magma is generated due to dehydration of the subduction slab, hydration of the mantle wedge and thereby lowering the solidus of the mantle wedge. The latter results in production of magmas (Figure 1.3).

Detailed study by Lackey and co-workers (2005, 2006, 2008) allows distinctions between the relative importance of variation in source, contamination processes and magmatic pulsations by use of O, Sr, Nd and Pb isotopes in the SNB. Doing so, Lackey et al. (2008) proposed a model for the overall evolution of the SNB (Figure 1.3), in majority based on $\delta^{18}O$ isotopes. Discussing the evolution and development of the SNB in its whole is beyond the scope of this thesis. For more information on the evolution of the SNB see Lackey et al. (2008).

1.2.2 Yosemite Batholith

Allaby and Allaby (1993) state that "a batholith is a large igneous intrusion, which may comprise several plutons amalgamated at depth. Most are granitic in composition and their genesis is linked with plate tectonics."

The well developed pluton of the TIS, with clear concentrically zones, is a good case-study to study magma chamber processes and batholiths emplacement (Bateman and Chappell, 1979). Many studies are performed on this pluton, for full references see paragraphs below.

The publication of Huber et al. (1989) combined all available data at that time and made the most complete and probably most cited geological overview of the Yosemite Batholith. In this publication seven plutons or grouped plutons are distinguished (Figure 1.2). The Yosemite Valley Intrusive Suite (Early Cretaceous), Intrusive suite of Merced Peak (mid-Cretaceous), Intrusive suite of Buena Vista Crest (mid-Cretaceous), Intrusive suite of Washburn Lake (mid-Cretaceous), Intrusive suite of Jack Main Canyon (Late Cretaceous), Intrusive suite of Sonora Pass (Late Cretaceous) and the Tuolumne Intrusive Suite (Late Cretaceous).

1.2.2.1 Tuolumne Intrusive Suite

Introduction to the TIS
The TIS was in earlier publications interpreted as a four unit pluton. From old to young these plutons were respectively Kuna Crest Granodiorite, Half Dome Granodiorite, Cathedral Peak Granodiorite and the Johnson Granite Porphyry. In subsequent research the Half Dome Granodiorite was separated into an Equigranular Half Dome Granodiorite and a Porphyritic Half Dome Granodiorite (e.g. Bateman and Chappell, 1979; Huber et al., 1989; Burgess and Miller, 2008; Figure 1.1).

Origin and evolution of the TIS
The general consensus in the literature about the evolution and emplacement of the TIS is that this pluton is built up by several "injection" periods (Figure 1.4). This results in a zoned pluton were age emplacement decreases inward (Bateman and Chappell, 1979). Up to today the exact evolution and emplacement is a topic of debate (e.g. Coleman et al., 2005; Burgess and Miller, 2008; Žák et al., 2009).

A single binary mixing model will not explain all the geochemical variations present in the TIS. More complex models involving fractional crystallization, mixing, assimilation, periodically recharged magmas and magma flows play an important role in evolution and emplacement of the TIS (Burgess and Miller, 2008). Rather than earlier studies were it is stated that the TIS reflects a big magma chamber with normal fractionation trends (e.g. Bateman and Chappell, 1979; Figure 1.4), nowadays the TIS is generally interpreted to be a more complex system made up by continuous pulses of magma derived from a lower crustal MASH zone. Where a TIS-like granitic source mixes with the TIS original source (e.g. Coleman et al., 2004; Gray et al., 2008).

The assembly duration of the TIS is determined to be 8-10 Ma by use of U-Pb geochronology. The emplacement is interpreted to be between 85 and 95 Ma (Coleman et al., 2004; Burgerss and Miller, 2008). Emplacement depth of the TIS is estimated to be ~7- 10 km, based on the use of Al-in hornblende barometry (Žák et al., 2009).

In the literature there is a controversy whether the Yosemite Creek Granodiorite (YC) and Sentinel Granodiorite (YS) should be interpreted as units of the Tuolumne Intrusive Suite (TIS). Calkins (1930), Kistler (1973), Kistler et al. (1986), Kistler en Fleck (1994), Glazner et al. (2004), and Petsche (2008) interpreted the YS and YC as units of the TIS. Other publications and the most recent publications (Bateman and Chappell, 1979; Bateman, 1992; Peck, 2002; Gray et al., 2008; Burgess and Miller, 2008; Paterson et al., 2008; Solgadi and Sawyer, 2008; Fulmer and Kruijer, 2008; Mills et al., 2009; Žák et al., 2009 and Johnson and Glazner, 2010) favor the Huber et al. (1989) interpretation which do not subscribe the YC and YS to the TIS.

The most referred argument to incorporate the YC and YS into the TIS are mineral compositions and general morphological features. Several authors agree that these features resemble those found in the TIS. The most persuasive argument to exclude the granodiorite suites of the TIS is the good concentrically zoning within the TIS. The units in the TIS from in- to outwards become more mafic. The most outward unit, the Kuna Crest, is the most mafic (Figure 1.1 and Figure 1.4). When incorporating the relative felsic YS and YC into the TIS, they will form the most outer unites (Figure 1.1b) and hereby undermining the whole hypothesis of felsic-mafic concentrically zoning in the batholith.

1.2.2.2 Yosemite Valley Intrusive Suite

Introduction to the YVIS
The Yosemite Valley Intrusive Suite (YVIS) is located on the West side of the TIS (Figure 1.1). The Yosemite Creek Granodiorite and the Yosemite Sentinel Granodiorite cross-cut the YVIS in both the northern and southern part of the batholith. Both the YS and YC have an intruding-like relation with the YVIS which can be seen in Figure 1.1 near the eastern margin.

Description of YVIS
YVIS consists of two granitic units, the El Capitan Granite and the Taft Granite. U-Pb age dating yielded between 103 Ma and 100 Ma (Huber et al., 1989; Petsche, 2008). With Taft Granite as a younger unit then the El Capitan (Petsche, 2008). The El Capitan Granite is a coarse-grained, white to light gray biotite granite and biotite granodiorite. It is generally porphyritic with angular potassium feldspar phenocrysts. The Taft Granite is a fine to coarse grained white to gray biotite granite and biotite granodiorite. Occasionally porphyritic with potassium feldspar phenocrysts (Petsche, 2008). Huber et al. (1989), Bateman (1992), Petsche (2008) and Johnson (unpublished) considered the Granite of Rancheria Mountain and Mount Hoffman Granite as units of the El Capitan Granite.

Origin and evolution of the YVIS
Ratajeski et al. (2001) states that in the YVIS numerous mafic bodies are present. Varying from large mafic pods, dykes, swarms of enclaves, enclaves to schlieren. These are considered to be of the same origin, after studying major and trace elements and Nd, Hf, Sr and Pb isotopes. The conclusion of Ratajeski et al. (2001) was that all the felsic and mafic components of the YVIS are derived from the same source. They presume the original source is the trace element-enriched mantle. Partial melting of this enriched mantle results in a primitive arc basalt which by fractionation and/or crustal assimilation results in a non-primitive hydrous mafic magma. These mafic magmas are seen in the field as diorite dykes, diorite complexes and pods. Ratajeski et al. (2001) propose that the previous mentioned non-primitive mafic magma intruded the lower crust to from a hornblende gabbro, which by

partial melting evolves to the low-silica El Capitan Granite (granodiorite). Fractionation of this same batch of melt results in the high silica El Capitan Granite. The Taft Granite is proposed to be a product of fractionation of the high-silica El Capitan Granite (Ratajeski et al., 2001).

1.2.2.3 Yosemite Creek Granodiorite

Introduction to Yosemite Creek Granodiorite
The southern margin of the YC is for its majority a contact with the YS. The middle southern margin of the YC unit is a contact with the YVIS. Margins in the East, West and North are also in contact with the YVIS. Most of the northern margin of the YC has a contact with a undivided granitic body for which the age is estimated as Cretaceous and older then YC and YS (Figure 1.2). The eastern margin of the YC has a complex structure. From regional mapping it appears on the large scale (up to several kilometer) that the YC intrudes the YVIS Taft Granite as bodies and dykes. This observation is just an illustrative description and not an interpretation (Figure 1.1).

Description of Yosemite Creek Granodiorite
The geological relationships of the YC to surrounding rock types are not fully understood. Petsche (2008) made a detailed study of the southern contact zone's of the YC and extrapolated his results to the rest of the YC unit. Extrapolating the southern YC should be valid according to Kistler (1973), Huber et al. (1989) and Bateman (1992). Petsche (2008) described the YC as follows: "The Yosemite Creek Granodiorite is a medium-grained, light-gray to light-tan (where weathered) biotite-hornblende granodiorite; modes locally plot within the quartz diorite and tonalite fields. The color index ranges between 10 and 20 and is normally ~15. Biotite is 2 to 4 mm long, and hornblende is 4 to 8 mm long; they make up ~5 to 10% and ~2 to 8% of the granodiorite, respectively. Elongate aggregates of biotite and hornblende are up to 1 cm long and define a weak to moderately strong magmatic foliation. Boxy (square-shaped in cross-section) plagioclase typically comprises 50 to 60% of the rock, but as little as 30% in some places. It is typically 4 to 6 mm, but may be up to 1 cm long. Plagioclase is weakly aligned parallel to magmatic foliation. Interstitial potassium feldspar is generally less than 5 mm long, and makes up 0 to 10% of the rock. Interstitial quartz is 2 to 12 mm across and constitutes 10 to 20% of the rock."

This description is most consistent for the more southern lithologies of the YC. More north the description becomes less applicable. Hornblende and biotite are more abundant and grain size of these minerals increases. For detail description see chapter 3 Field Results.

Petsche (2008) also reported magmatic structures. He encountered granodiorite dykes, enclaves, enclave swarms, schlieren, aplite and pegmatite dykes. The contact between the YC and YS were described as strongly changing mafic and felsic layers and cumulates with a great variety of grain size distribution.

Origin and evolution of Yosemite Creek Granodiorite
There are no direct age studies performed on the YC but it is interpreted as Late Cretaceous and older then the YS which has been dated at ~93 (error undefined) Ma based on K-Ar (Huber et al., 1989; Petsche, 2008) and ~95± 1 Ma by U-Pb zircon dating (Coleman and Glazner, 1997). Petsche (2008) proposed that the YC is slightly younger than the YS because of the magmatic structures near the contact of the YC and YS. Fulmer and Kruijer (2008)

state on similar arguments that the YS is younger then the YC. The discussion about the age relation depends on the interpretation of the contact between the two suites (Fulmer and Kruijer, 2008). There is no study that clearly describes the origin and evolution of the YC pluton. However, Petsche (2008) concluded that the YC and YS formed in the same magma chamber or in the same magma source region by a deep level of mixing or differentiation.

1.2.2.4 Sentinel Granodiorite by Fulmer and Kruijer

Introduction to the Sentinel Granodiorite
The Yosemite Sentinel Granodiorite is a unit which in most publications has not been assigned to a pluton system (See earlier paragraph about literature discussion on the YC and the YS). This author agrees with the interpretation of a previous study performed by VUA MSc students Fulmer and Kruijer (2008). They performed the first thorough geochemical research on the YS.

The outcrop of the YS unit is made up of two differently orientated lobes (Figure 1.1). The larger (~15 x 20 km^2) relatively homogeneous east-west orientated lobe cross cuts the YVIS. The south-eastern lobe is north-south orientated (~ 15 x 2 km^2), follows the contours of the TIS and appears to be more heterogeneous in shape with the YVIS (Figure 1.1).

Description of Sentinel Granodiorite
The YS is coarse-grained, dark gray, biotite hornblende granodiorite with abundant sphene. (Huber et al., 1989). The emplacement age of the YS is dated by the U-Pb zircon technique by Coleman and Glazner (1997) and resulted in a age of 94.6 ± 1.1 Ma. The YS can contain local distinct granitic and dioritic lithologies.

Origin and evolution of Sentinel Granodiorite
Variations in whole rock Sr-Nd-Hf isotopes could be explained by a minor granite source heterogeneity, intra-pluton magma mixing and hornblende-biotite-plagioclase-titanite fractionation. Zircon Hf isotope data suggests rejuvenation and local mixing in the YS magmatic system with minor crustal contamination (Fulmer and Kruijer, 2008).

The assemblage of the YS is considered to be a crystal mush which has been intruded multiple times by slightly isotopically and chemically heterogeneous magma pulses. Within the pluton there was incomplete mixing but extensive fractional crystallization also occurred. The YS is interpreted to be originated out of a deep younger YVIS unit (Fulmer and Kruijer, 2008).

1.3 Debate on magma chamber concepts

The Sierra Nevada Batholith is a unique study area due to the excellent outcrop of the large granitic area. The numerous studies done on the Sierra Nevada Batholith makes it a hot topic in the scientific geology. Interpretations of different data sets makes a scientist favour a magma chamber model for pluton assembly. There are two end-member models proposed to form a pluton. A large molten magma chamber or incremental growth by stacked sills or laccoliths.

1.3.1 Large magma chamber model

Figure 1.5 shows the processes that would take place in a large magma chamber. Large scale convection will mean that any initial homogeneous magma would mix with new magma injections. Assimilation of country rock would be an ongoing process until solidification at the margin of the pluton (Glazner et al., 2004). These processes would account for the geochemical variations found in plutons. Wall rock material could be found within such a magma chamber, which is called stoping. Large amounts of fractionated crystals accumulate at the magma chamber floor and occasionally near the walls. More large magma chamber structures are discussed in paragraphs below. Diapirism is proposed to bring the large amounts of magma from the asthenosphere to the crust (Hildreth, 1979).

1.3.1.1 Field Evidence

Tuolumne Intrusive Suite as field evidence
The work of Bateman and Chappell (1979) is a good example for they way geologist's interpret plutons and there emplacement. According to these authors the TIS is solely a product of several magma inputs each followed by crystal fractionation. From the rim to the centre of the TIS pluton the units become more felsic. The units are thought to be a direct representation of a large fossil magma chamber. The mafic to felsic trend could be explained by crystal fractionation with the residual magma becoming more felsic. Having several stages of solidification from the outer rim inwards one would expect to have the most felsic unit/melt at the inner part of the pluton (Bateman and Chappell, 1979). Figure 1.4 depicts the envisaged emplacement and evolution of the different stages of TIS in the framework of a large magma chamber system.

Field structures as evidence
Several recent publications support the large magma chamber hypothesises. These are for the majority based on field observations (Paterson et al., 2008 and Paterson, 2009). Paterson (2009) described several magmatic structures observed in the TIS. Structures such as stationary tubes, pipe's, migrating tubes, diapirs, plume heads and troughs. To form these structures one needs a magmatic host which has a high viscosity like a mush. In such a situation minor homogenization by convection and mixing can take place. Structures mentioned before are proposed as evidence for large magma chambers. Paterson et al. (2008) propose a big magma chamber which recycles older chamber parts into younger units.

Field observations against incremental growth
Žák et al. (2009) propose several arguments as to why incremental assemblage of a magma chamber is unlikely. The most important argument they propose is that it is very speculative that different magma inputs of incremental assemblage do not leave any trace in the field, moreover in paragraph 1.3.2.1 Cooling Rims.

Žák et al. (2009) concluded that there is no reason to invoke incremental dyking to explain the TIS pluton construction. Dykes rapidly cool and solidify when emplaced which mean that convective structures, homogenisation, stoping, etc. are very hard to accomplish in an incremental assembly system. Least but not last as evidence in favour for large (over 1000 km^3) magma chambers are caldera eruptions. These are an unequivocal proof that "large" magma chambers must exist (Miller, 2008)

1.3.1.2 Geochemical evidence

Geochemical data in favor for large magma chamber
Burgess and Miller (2008) advocate the large magma chamber theory for the Cathedral Peak Granodiorite, TIS. They use extensive geochemical research (major ,trace elements, isotope and U-Pb geochronology) to argument in favour of the large and dynamic magma system.

Age emplacement of the Cathedral Peak Granodiorite is within a time interval of 2 Ma. This fits the overall agreed life-span of a large hot liquid-like reservoir. Major element trends are compatible with a crystal fractionation system such as supposed in a large magma chamber. Trace element variations are likely to be controlled by magma chamber process rather than incremental interaction in the shallow crust. Variation in REE patterns are most likely controlled by crystal fractionation, which correspond with the large magma chamber model. Sr and Nd isotope data could be interpreted as fractionation in a closed system (Burgess and Miller, 2008). It is suggested that melts interacted with a mush reservoir to sustain the system.

Zircon data on debate
Interpretations of zircon data are the subject of debate due to new measurement techniques and new insights in magmatic systems which reduces analytical errors. Miller et al. (2007) and Burgess and Miller (2008) published zircon ages derived from in situ U-Pb zircon dating. The zircon data define concordant U-Pb ages and have a significantly greater range than the analytical error suggesting the involvement of more than one magma batch. Miller et al. (2007) state that this is due to inheritance of older zircons (antecrysts and xenocrysts). Thereby increasing the measured ages of the zircons and potentially giving a misleading crystallisation age.

1.3.1.3 Heat budget argument

Several authors have argued that rejuvenation and fresh injection of magma can sustain a large mush magma chamber for considerately long periods. For instance Huber et al. (2009) pointed that big ignimbrite magma chambers survive despite the rapid cooling of large chambers in the upper crust. They state that amalgamation, rejuvenation and pulsed magma batches could assemblage, maintain and sustain big magma chambers because of the latent heat buffering due to fractional crystallisation.

Thermal modelling by Bartley et al. (2006) suggest that a large volume of incremental magma can result in a volume where the solidus is above the 650 °C. Taking this into account and the statements mentioned above by Huber et al. (2009) it is plausible that large magma chamber-like environments do exist.

1.3.2 Incremental pluton growth model

The incremental pluton growth model is a hypothesis to explain plutons which contain strong geochemical variations on a small scale (hand sample). It is stated that these plutons are constructed out of several inputs of magma (Figure 1.6). The source of the inputs is the lower crust where strong heterogeneity can occur. It is assumed that magma inputs interact at source level as well as at emplacement level. These interactions can vary from assimilation, hybridization and mixing.

Coleman et al. (2004) states that large ignimbrite magma chambers can occur but are uncommon. Incrementally assembled plutons seem more valid for the majority of plutons. Stacking of sills, incremental growth, to form plutons and batholiths is also proposed by Menand (2007). This latter mentioned publication is consistent with the ideas of incremental growth and strengthened the position of the incremental growth on behalf of challenging space and stacking of the sills.

1.3.2.1 Field evidence

Field observations
Glazner et al. (2004) summarizes several compelling arguments advocating incremental pluton growth. These field evidences, based on xenoliths that only can be attained by dyking, corresponds with the idea of incremental pluton growth. Other examples are dyke amalgamation, wall-rock inside the pluton, xenoliths of metamorphic wall-rock (size: 250 x 20 m^2) surrounded by dykes and formations with swarms of mafic enclaves near magmatic contacts with a more homogeneous interior.

Moreover, Glazner and Bartley (2006) argue that stoping is not a volumetrically significant process in the emplacement of most plutons. They state, just as in Bartley et al. (2006), that most interpretations of stoping are xenoliths that are enclosed by dyke swarms with little to no assimilation of the xenolith. Xenoliths engulfed by magma are suspected to be rare. Bartley et al. (2006) proposes a syntaxial and antitaxial sill stacking to explains the xenoliths in the solidified magmas.

Cooling rims
There is an ongoing discussion about incremental growth concerning rim structures (e.g. Bateman, 1992; Coleman et al., 2005; Bartley et al., 2006). Initially it is assumed that increments would generate cooling-rims near the margin of the increment. This would mean that in a pluton which consist out of amalgamated increments it should show physical remnants of the rims by composition and/or mineral grain size. However such field relations are not observed. The absence of cooling rims or compositional variation rims to the plutons are suggested to be arguments in favour for large magma chambers, Žák et al. (2009) and paragraph 1.3.1.1 Field observations against incremental growth.

Bartley et al. (2006) strongly disagree. It is proposed that rims probably do not form at all even against colder wall rock. Similar composition in increments would not form any rims either. Slight variations might be found if input compositions do vary (Bartley et al., 2006). Even so, if rims would form when increments are emplaced, recrystallization by emplacement of a new increment would anneal all previous rim-like cooling structures (Bartley et al., 2006). According to Bartley et al. (2006) it can be stated that the absence of cooling rims or compositional variation rims is not a argument to dismiss the incremental growth model.

1.3.2.2 Geochemical evidence

Zircons as evidence for incremental pluton growth

Miller (2008) published a summary on the debate of crustal differentiation concerning magma chamber assemblage (e.g. Jellinek and De Paolo, 2003; Coleman et al, 2004; Glazner et al., 2004; Bachmann and Bergantz, 2004, 2006; Matzel et al., 2005; Miller et al., 2007; Lipman, 2007; Glazner et al., 2008). High precision U-Pb zircon studies resulted in new insights of the assemblage of magma chambers. The time span of crystallization of individual mapped units exceeded the time span of solidification. Crystallization refer to the initiation to form solid state phases in the melts. Solidification refer to a system which contain no significant amounts of melt anymore. All the melts of the batch or pluton are changed to their solid state phases. Thus, minerals (zircons) have a longer crystallization time span then what is calculated for the time span of solidification for the whole pluton.

Moreover, Glazner et al. (2004) concluded based on zircon crystallization ages that the TIS and other plutons must have grown by incremental emplacement. The age range of zircons with respect to the pluton volume must have exceeded the estimated cooling time of the pluton. This would mean that the total pluton was not in a liquid-like state at a specific time. In other words, such as Glazner et al. (2004) calculated, a TIS-like volume of a pluton would become magmatic immobile within 500,000 years. The zircon ages for the Half Dome Granodiorite (a inner TIS unit) are spread over 3 m.y. of solidification. Hereby, Coleman et al. (2004) concluded that such a magmatic system can only be attained by several different intrusions.

Zircon isotopes

Extensive isotope work on O and Hf done by Kemp et al. (2007) advocates incremental pluton growth. This isotope study is done on zircons which gives insights in the processes played in the magma chamber. Kemp et al. (2007) propose that the data measured can only be interpreted as a complex mixing and assimilation process which started in a MASH zone and continued in the crust by smaller pulses of magma intrusions (Figure 1.6). Which can not be obtained by large magma chambers.

1.3.2.3 Seismic argument

Seismic interpretations are the subject of debate with respect to the pluton formation models. Seismic surveys failed to spot large molten magma chambers. It is proposed that only small "chambers" exist which can not be detected by seismic survey because of a too small seismic resolution (Coleman et al., 2004). However a combination of electrical and seismic methods reveal a melt of at least 20% beneath the central Andes. It is suggested that large magma bodies can exist except that there constructed with a large solid crystalline framework and not as a gigantic tank (Glazner et al., 2004). This interpretation corresponds with the model proposed by Kemp et al. (2007).

1.3.3 Summary

Considering all the evidence large liquid-like magma chambers did exist and probably still exist but have not yet been discovered by conventional seismic techniques. It is likely that both magma "reservoir" concepts do exist. It is also not rejectable that both concepts play a integrated role in pluton formation. All discussed arguments for the pluton systems are plausible and seem valid.

This author would like to make a remark on publications discussing observed structures in plutons that are presented as evidence for large magma chambers. They state that these kind of structures are not possible to occur in sills or laccoliths. As remark, in the literature there are no publications that these structures can occur in large magma chambers.
Taking in account the heat buffering of stacking sills or laccoliths it is not unthinkable that these structures occur outside large magma chambers. In a system with contrasting thermal boundaries, which could take place in stacking magma sills, one could imagine flow structures from lower hot material rising through a more solidified colder upper sill. This makes it plausible that the large magma chamber structures observed by Paterson et al. (2008) and Paterson (2009) can be the result of internal processes involved in the incremental assemblage of the pluton.

In summary the paradigm of the magma chamber is still open for debate and for now it seems both end member concepts are plausible. This author considers that both concepts are valid and concludes that only high precision geochemical studies can reveal to what extent the two concepts play a part in the evolution of a specific pluton.

Figure 1.1
Modified after Fulmer and Kruijer (2008) and Žák et al. (2009).

(a) Location map of the Sierra Nevada batholith (SNB) along with the general relationships with the Eastern Sierra Pendant (ESP), Tuolumne Intrusive Suite (TIS) and the Western Metamorphic Belt (WMB). After Žák (2009). Four late Cretaceous intrusive suites (Sonoma, Tuolumne, John Muir, and Mount Whitney) are also designated. The dashed square is the area of this research. **(b)** Simplified geologic map of Yosemite National Park modified after Huber et al. (1989), showing the Yosemite Valley Intrusive Suite (YVIS), Yosemite Creek Granodiorite (YC), Yosemite Sentinel Granodiorite (YS), and the concentrically zoned Tuolumne Intrusive Suite (TIS, including Kuna Crest Granodiorite, Equigranular Half Dome Granodiorite, Porphyritic Half Dome Granodiorite, Cathedral Peak Granodiorite, and Johnson Granite Porphyry). The outline of the Yosemite National Park is shown in light gray. Superimposed on the geologic map are recent U-Pb zircon ages (Coleman and Glazner, 1997; Coleman et al., 2004; Burgess and Miller, 2008). **(c)** The approximate pluton emplacement ages of the units shown in the geologic map.

Abbreviations in the figure relate to the simplified abbreviations in this thesis or used by Huber et al. (1989). Not all abbreviations used by Huber et al. (1989) are copied. Simplified abbreviations for YS and YC are used because emplacement timing of plutons discussed in this research are all Cretaceous. Huber et al. (1989) used a extra timing abbreviation (e.g. Ks = Cretaceous Sentinel Granodiorite; Figure 1.2). In this thesis the names of the units are used to make the abbreviations. YS = Yosemite Sentinel Granodiorite; YC = Yosemite Creek Granodiorite; YVIS = Yosemite Valley Intrusive Suite; other abbreviations see Figure 1.1 and Figure 1.2.

Figure 1.2
Geological map of Yosemite National Park and vicinity, California by Huber et al. (1989). First page is the northern half of the map, second page is the southern half of the map. The third page is a explanation of the map. In the explanation the major suites are indicated.

Figure 1.3
Model for the origin of the distinct δO^{18} belts of the central Sierra Nevada depicts the general view of the SNB subduction systems with dehydration of the slab, hydration and melt generation in the mantle wedge, the mixing, assimilation, storage and homogenization location (MASH) and crustal interaction with the magma. Adopted from Lackey et al. (2008).

(a) Early Cretaceous setting before voluminous magmatism, showing distinct basement and lithospheric mantle domains, overlying sediments, and older plutons. The Foothills and eastern Sierra crustal breaks are shown as trans-crustal; '?' symbols indicate uncertainty of the geometry and depth of the PA/NA break. The transition from oceanic to North American lithospheric mantle is also uncertain, although an east-dipping contact is inferred. **(b)** By 110 Ma, increased magmatism mobilized accreted supracrustal rocks into the western SNB high-δO^{18} belt, inboard of the low-δO^{18} belt. A relatively shallow western MASH zone resulted in widespread crustal melting. **(c)** At 90 Ma, transpression and increased rates of subduction facilitated emplacement of voluminous eastern SNB magmas from lithospheric mantle sources. Intra-arc shortening by lithospheric under-thrusting temporarily stifled magmatism, possibly inserting Proterozoic lower crust into the sub-arc mantle. 'Eclogitic root' refers to eclogitic residues expelled from the MASH zone.

Figure 1.4
Four stages of TIS emplacement. **(a)** First stage: Emplacement of the Kuna Crest; **(b)** Second stage: emplacement of the Halve Dome Granodiorite; **(c)** Third stage Porpheritic Halve Dome Granodrioite; **(d)** Fourth stage: Emplacement of the Cathedral Peak Granodiorite and the Tom Johnson Granodiorite. In white are the areal extent of the envisioned liquid magma (Bateman and Chappell, 1979). For abbreviations see Figure 1.1.

Figure 1.5
Big magma chamber model to illustrate possible processes which could play a role in formation of a batholith (Glazner et al., 2004; Fulmer and Kruijer, 2008).

Figure 1.6
A deep crustal hot zone is the location where batches of differentiated melts are extracted to the shallow crust. At the shallow crust small magmatic reservoirs form where the different melt batches can interact with each other. This latter location is also known as the mush zone. The magma-crust interactions forming strong geochemical variations on small scale (hand specimen) outcrops. Illustrated are the deep crustal melt and the shallow crust melt interaction (Kemp et al., 2007).

Figure 1.1

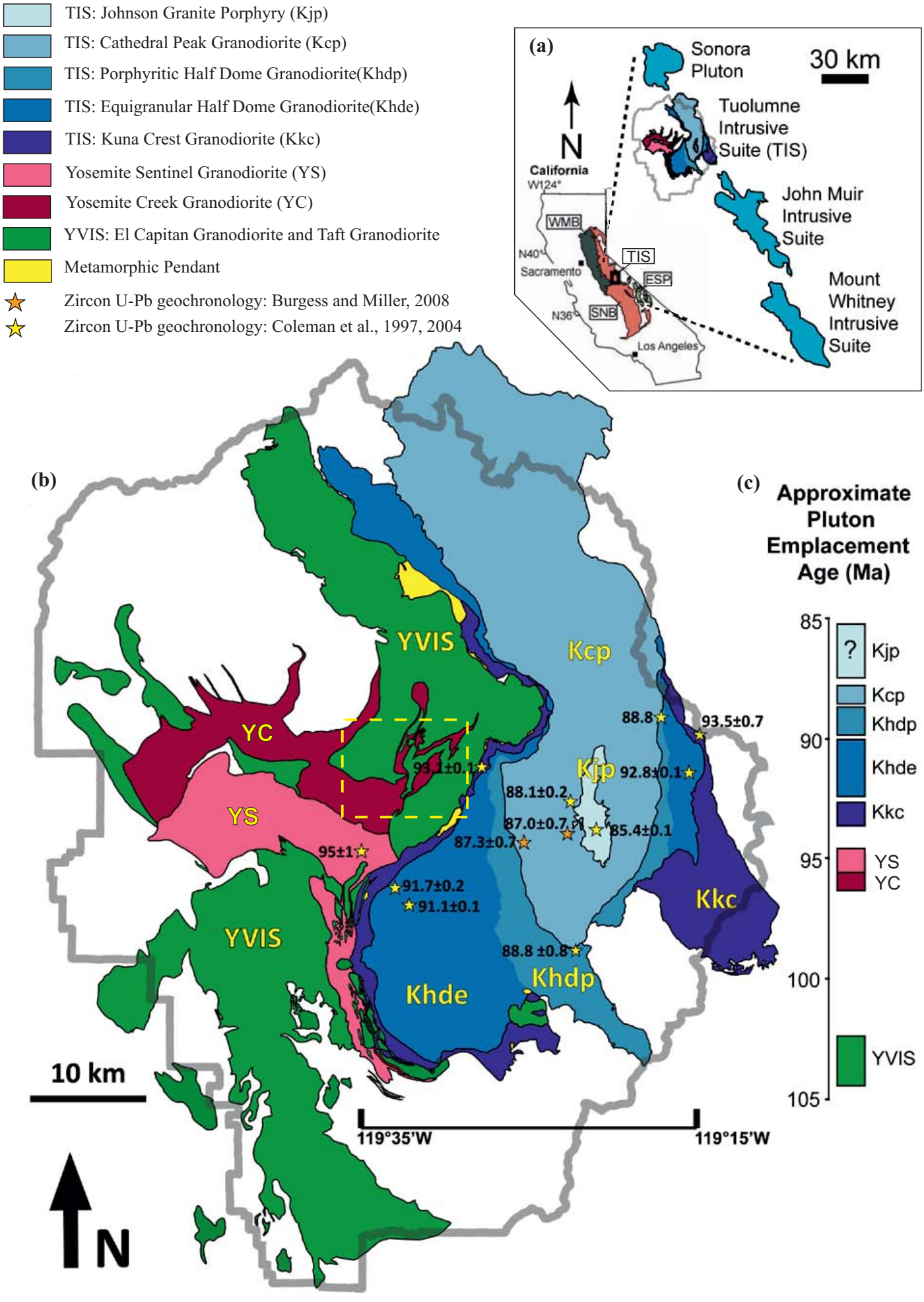
TIS: Johnson Granite Porphyry (Kjp)
TIS: Cathedral Peak Granodiorite (Kcp)
TIS: Porphyritic Half Dome Granodiorite(Khdp)
TIS: Equigranular Half Dome Granodiorite(Khde)
TIS: Kuna Crest Granodiorite (Kkc)
Yosemite Sentinel Granodiorite (YS)
Yosemite Creek Granodiorite (YC)
YVIS: El Capitan Granodiorite and Taft Granodiorite
Metamorphic Pendant
Zircon U-Pb geochronology: Burgess and Miller, 2008
Zircon U-Pb geochronology: Coleman et al., 1997, 2004
(a)
Sonora Pluton
30 km
Tuolumne Intrusive Suite (TIS)
John Muir Intrusive Suite
Mount Whitney Intrusive Suite
N
California
W124°
WMB
N40°
Sacramento
TIS
ESP
SNB
N36°
Los Angeles
(b)
YVIS
Kcp
YC
YS
Kjp
Kkc
Khde
Khdp
88.8
93.5±0.7
93.1±0.1
92.8±0.1
88.1±0.2
87.0±0.7
85.4±0.1
87.3±0.7
95±1
91.7±0.2
91.1±0.1
88.8 ±0.8
10 km
119°35'W
119°15'W
N
(c)
Approximate Pluton Emplacement Age (Ma)
85
90
95
100
105
?
Kjp
Kcp
Khdp
Khde
Kkc
YS
YC
YVIS

Figure 1.2

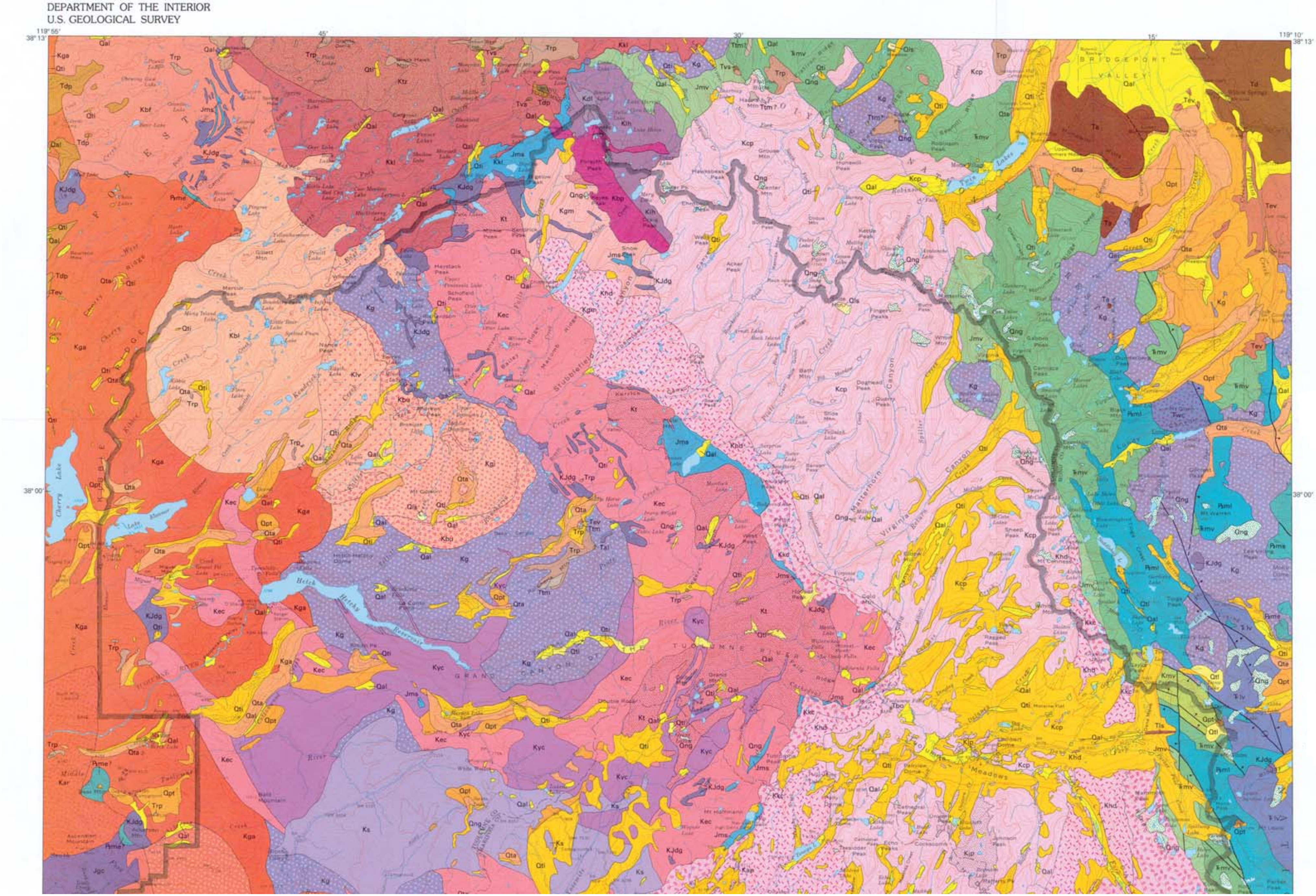

DEPARTMENT OF THE INTERIOR
U.S. GEOLOGICAL SURVEY
BRIDGEPORT VALLEY
TUOLUMNE RIVER
GRAND CANYON OF THE

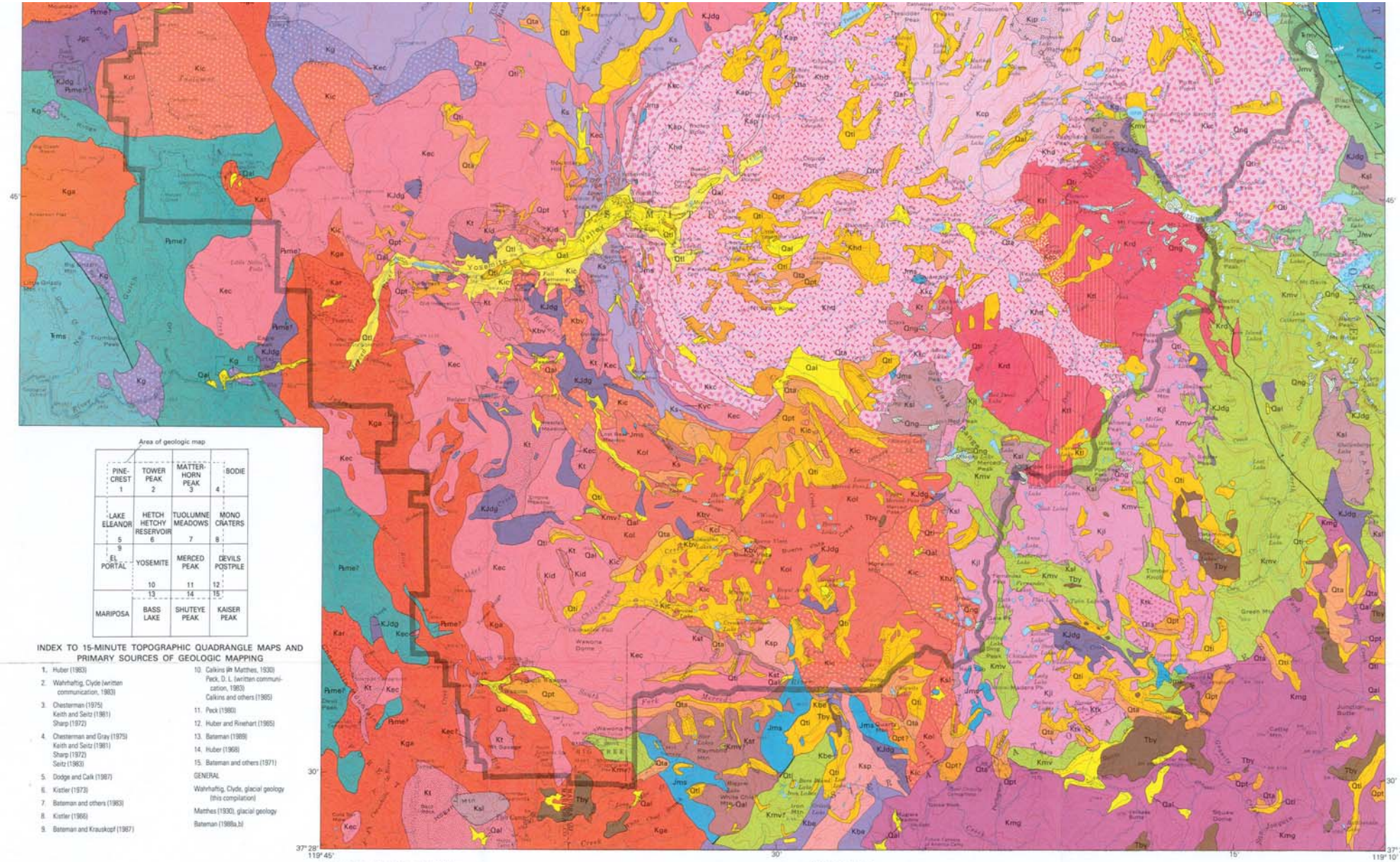

Area of geologic map

PINE-CREST 1	TOWER PEAK 2	MATTER-HORN PEAK 3	BODIE 4
LAKE ELEANOR 5	HETCH HETCHY RESERVOIR 6	TUOLUMNE MEADOWS 7	MONO CRATERS 8
EL PORTAL 9	YOSEMITE 10	MERCED PEAK 11	DEVILS POSTPILE 12
MARIPOSA 13	BASS LAKE 14	SHUTEYE PEAK 15	KAISER PEAK

INDEX TO 15-MINUTE TOPOGRAPHIC QUADRANGLE MAPS AND PRIMARY SOURCES OF GEOLOGIC MAPPING

1. Huber (1983)
2. Wahrhaftig, Clyde (written communication, 1983)
3. Chesterman (1975)
   Keith and Seitz (1981)
   Sharp (1972)
4. Chesterman and Gray (1975)
   Keith and Seitz (1981)
   Sharp (1972)
   Seitz (1983)
5. Dodge and Calk (1987)
6. Kistler (1973)
7. Bateman and others (1983)
8. Kistler (1966)
9. Bateman and Krauskopf (1987)
10. Calkins (in Matthes, 1930)
    Peck, D. L. (written communication, 1983)
    Calkins and others (1985)
11. Peck (1980)
12. Huber and Rinehart (1965)
13. Bateman (1989)
14. Huber (1968)
15. Bateman and others (1971)

GENERAL

Wahrhaftig, Clyde, glacial geology (this compilation)

Matthes (1930), glacial geology

Bateman (1989a,b)

37° 28'
119° 45'
30'
15'
37° 28'
119° 10'
45'
30'

Base from U.S. Geological Survey. Compiled from 1:62,500-scale 15-minute quadrangle maps, surveyed 1947–68
Universal Transverse Mercator projection

16°
TRUE NORTH
MAGNETIC NORTH
APPROXIMATE MEAN DECLINATION, 1987

SCALE 1:125 000
2 0 2 4 6 8 10 MILES
2 0 2 4 6 8 10 KILOMETERS

CONTOUR INTERVAL 200 FEET
DOTTED LINES REPRESENT 100-FOOT CONTOURS
NATIONAL GEODETIC VERTICAL DATUM OF 1929

CALIF
AREA OF MAP

INTERIOR—GEOLOGICAL SURVEY, RESTON, VA.—1989—G89293

Geology compiled by N. K. Huber, P. C. Bateman, and Clyde Wahrhaftig, 1981–85, from sources indicated

GEOLOGIC MAP OF YOSEMITE NATIONAL PARK AND VICINITY, CALIFORNIA

Compiled by
N. King Huber, Paul C. Bateman, and Clyde Wahrhaftig

1989

Explanation Figure 1.2

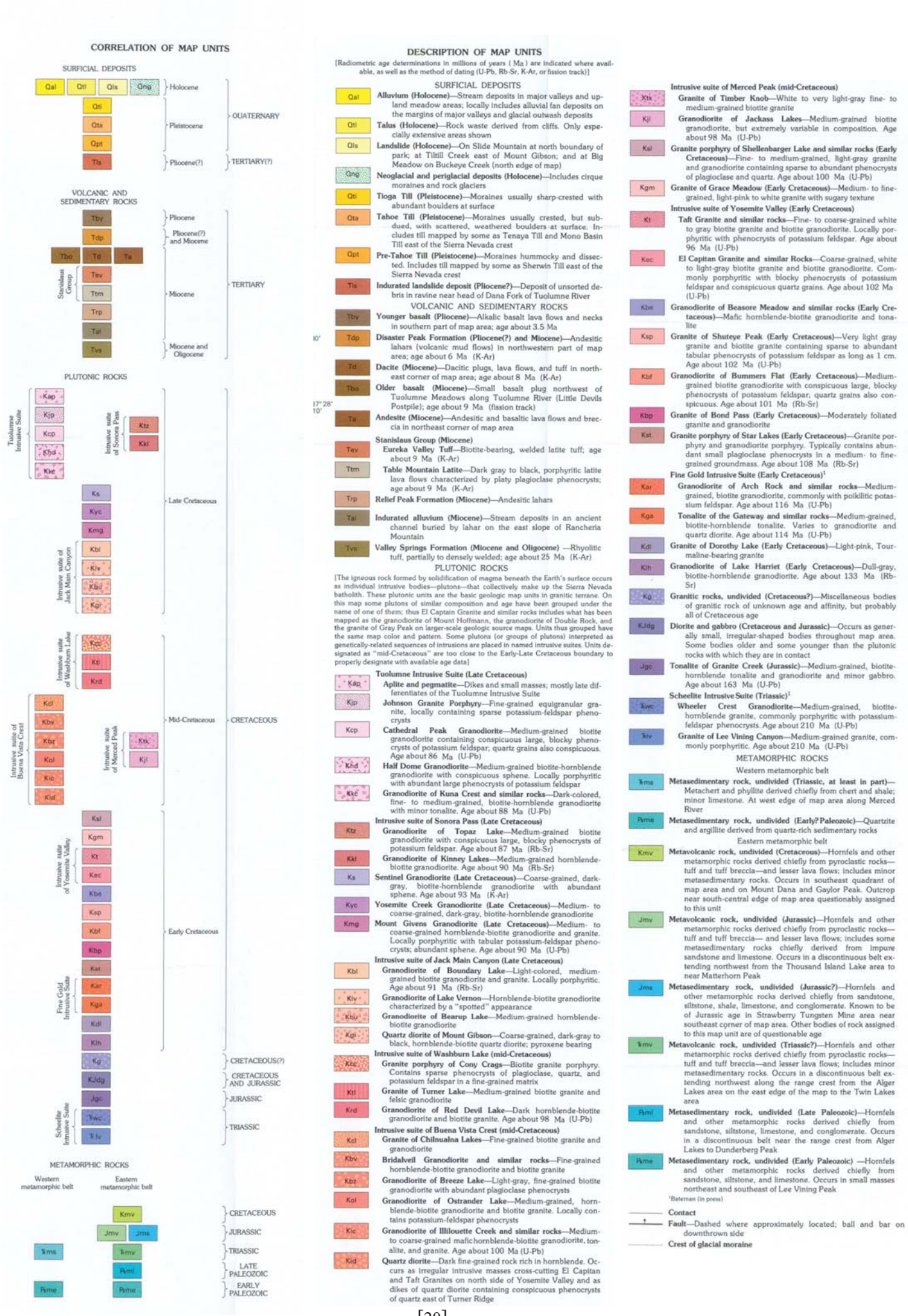

DESCRIPTION OF MAP UNITS

[Radiometric age determinations in millions of years (Ma) are indicated where available, as well as the method of dating (U-Pb, Rb-Sr, K-Ar, or fission track)]

SURFICIAL DEPOSITS

Qal **Alluvium (Holocene)**—Stream deposits in major valleys and upland meadow areas; locally includes alluvial fan deposits on the margins of major valleys and glacial outwash deposits

Qtl **Talus (Holocene)**—Rock waste derived from cliffs. Only especially extensive areas shown

Qls **Landslide (Holocene)**—On Slide Mountain at north boundary of park; at Tiltill Creek east of Mount Gibson; and at Big Meadow on Buckeye Creek (north edge of map)

Qng **Neoglacial and periglacial deposits (Holocene)**—Includes cirque moraines and rock glaciers

Qti **Tioga Till (Pleistocene)**—Moraines usually sharp-crested with abundant boulders at surface

Qta **Tahoe Till (Pleistocene)**—Moraines usually crested, but subdued, with scattered, weathered boulders at surface. Includes till mapped by some as Tenaya Till and Mono Basin Till east of the Sierra Nevada crest

Qpt **Pre-Tahoe Till (Pleistocene)**—Moraines hummocky and dissected. Includes till mapped by some as Sherwin Till east of the Sierra Nevada crest

Tls **Indurated landslide deposit (Pliocene?)**—Deposit of unsorted debris in ravine near head of Dana Fork of Tuolumne River

VOLCANIC AND SEDIMENTARY ROCKS

Tby **Younger basalt (Pliocene)**—Alkalic basalt lava flows and necks in southern part of map area; age about 3.5 Ma

Tdp **Disaster Peak Formation (Pliocene(?) and Miocene)**—Andesitic lahars (volcanic mud flows) in northwestern part of map area; age about 6 Ma (K-Ar)

Td **Dacite (Miocene)**—Dacitic plugs, lava flows, and tuff in northeast corner of map area; age about 8 Ma (K-Ar)

Tbo **Older basalt (Miocene)**—Small basalt plug northwest of Tuolumne Meadows along Tuolumne River (Little Devils Postpile); age about 9 Ma (fission track)

Ta **Andesite (Miocene)**—Andesitic and basaltic lava flows and breccia in northeast corner of map area

Stanislaus Group (Miocene)

Tev **Eureka Valley Tuff**—Biotite-bearing, welded latite tuff; age about 9 Ma (K-Ar)

Ttm **Table Mountain Latite**—Dark gray to black, porphyritic latite lava flows characterized by platy plagioclase phenocrysts; age about 9 Ma (K-Ar)

Trp **Relief Peak Formation (Miocene)**—Andesitic lahars

Tal **Indurated alluvium (Miocene)**—Stream deposits in an ancient channel buried by lahar on the east slope of Rancheria Mountain

Tva **Valley Springs Formation (Miocene and Oligocene)** —Rhyolitic tuff, partially to densely welded; age about 25 Ma (K-Ar)

PLUTONIC ROCKS

[The igneous rock formed by solidification of magma beneath the Earth's surface occurs as individual intrusive bodies—plutons—that collectively make up the Sierra Nevada batholith. These plutonic units are the basic geologic map units in granitic terrane. On this map some plutons of similar composition and age have been grouped under the name of one of them; thus El Captain Granite and similar rocks includes what has been mapped as the granodiorite of Mount Hoffmann, the granodiorite of Double Rock, and the granite of Gray Peak on larger-scale geologic source maps. Units thus grouped have the same map color and pattern. Some plutons (or groups of plutons) interpreted as genetically-related sequences of intrusions are placed in named intrusive suites. Units designated as "mid-Cretaceous" are too close to the Early-Late Cretaceous boundary to properly designate with available age data]

Tuolumne Intrusive Suite (Late Cretaceous)

Kap **Aplite and pegmatite**—Dikes and small masses; mostly late differentiates of the Tuolumne Intrusive Suite

Kjp **Johnson Granite Porphyry**—Fine-grained equigranular granite, locally containing sparse potassium-feldspar phenocrysts

Kcp **Cathedral Peak Granodiorite**—Medium-grained biotite granodiorite containing conspicuous large, blocky phenocrysts of potassium feldspar; quartz grains also conspicuous. Age about 86 Ma (U-Pb)

Khd **Half Dome Granodiorite**—Medium-grained biotite-hornblende granodiorite with conspicuous sphene. Locally porphyritic with abundant large phenocrysts of potassium feldspar

Kke **Granodiorite of Kuna Crest and similar rocks**—Dark-colored, fine- to medium-grained, biotite-hornblende granodiorite with minor tonalite. Age about 88 Ma (U-Pb)

Intrusive suite of Sonora Pass (Late Cretaceous)

Ktz **Granodiorite of Topaz Lake**—Medium-grained biotite granodiorite with conspicuous large, blocky phenocrysts of potassium feldspar. Age about 87 Ma (Rb-Sr)

Kkl **Granodiorite of Kinney Lakes**—Medium-grained hornblende-biotite granodiorite. Age about 90 Ma (Rb-Sr)

Ks **Sentinel Granodiorite (Late Cretaceous)**—Coarse-grained, dark-gray, biotite-hornblende granodiorite with abundant sphene. Age about 93 Ma (K-Ar)

Kyc **Yosemite Creek Granodiorite (Late Cretaceous)**—Medium- to coarse-grained, dark-gray, biotite-hornblende granodiorite

Kmg **Mount Givens Granodiorite (Late Cretaceous)**—Medium- to coarse-grained hornblende-biotite granodiorite and granite. Locally porphyritic with tabular potassium-feldspar phenocrysts; abundant sphene. Age about 90 Ma (U-Pb)

Intrusive suite of Jack Main Canyon (Late Cretaceous)

Kbl **Granodiorite of Boundary Lake**—Light-colored, medium-grained biotite granodiorite and granite. Locally porphyritic. Age about 91 Ma (Rb-Sr)

Klv **Granodiorite of Lake Vernon**—Hornblende-biotite granodiorite characterized by a "spotted" appearance

Kbu **Granodiorite of Bearup Lake**—Medium-grained hornblende-biotite granodiorite

Kgl **Quartz diorite of Mount Gibson**—Coarse-grained, dark-gray to black, hornblende-biotite quartz diorite; pyroxene bearing

Intrusive suite of Washburn Lake (mid-Cretaceous)

Kcc **Granite porphyry of Cony Crags**—Biotite granite porphyry. Contains sparse phenocrysts of plagioclase, quartz, and potassium feldspar in a fine-grained matrix

Kt **Granite of Turner Lake**—Medium-grained biotite granite and felsic granodiorite

Krd **Granodiorite of Red Devil Lake**—Dark hornblende-biotite granodiorite and biotite granite. Age about 98 Ma (U-Pb)

Intrusive suite of Buena Vista Crest (mid-Cretaceous)

Kcl **Granite of Chilnualna Lakes**—Fine-grained biotite granite and granodiorite

Kbv **Bridalveil Granodiorite and similar rocks**—Fine-grained hornblende-biotite granodiorite and biotite granite

Kbz **Granodiorite of Breeze Lake**—Light-gray, fine-grained biotite granodiorite with abundant plagioclase phenocrysts

Kol **Granodiorite of Ostrander Lake**—Medium-grained, hornblende-biotite granodiorite and biotite granite. Locally contains potassium-feldspar phenocrysts

Kic **Granodiorite of Illilouette Creek and similar rocks**—Medium- to coarse-grained mafic hornblende-biotite granodiorite, tonalite, and granite. Age about 100 Ma (U-Pb)

Kid **Quartz diorite**—Dark fine-grained rock rich in hornblende. Occurs as irregular intrusive masses cross-cutting El Capitan and Taft Granites on north side of Yosemite Valley and as dikes of quartz diorite containing conspicuous phenocrysts of quartz east of Turner Ridge

Intrusive suite of Merced Peak (mid-Cretaceous)

Ktk **Granite of Timber Knob**—White to very light-gray fine- to medium-grained biotite granite

Kjl **Granodiorite of Jackass Lakes**—Medium-grained biotite granodiorite, but extremely variable in composition. Age about 98 Ma (U-Pb)

Ksl **Granite porphyry of Shellenbarger Lake and similar rocks (Early Cretaceous)**—Fine- to medium-grained, light-gray granite and granodiorite containing sparse to abundant phenocrysts of plagioclase and quartz. Age about 100 Ma (U-Pb)

Kgm **Granite of Grace Meadow (Early Cretaceous)**—Medium- to fine-grained, light-pink to white granite with sugary texture

Intrusive suite of Yosemite Valley (Early Cretaceous)

Kt **Taft Granite and similar rocks**—Fine- to coarse-grained white to gray biotite granite and biotite granodiorite. Locally porphyritic with phenocrysts of potassium feldspar. Age about 96 Ma (U-Pb)

Kec **El Capitan Granite and similar Rocks**—Coarse-grained, white to light-gray biotite granite and biotite granodiorite. Commonly porphyritic with blocky phenocrysts of potassium feldspar and conspicuous quartz grains. Age about 102 Ma (U-Pb)

Kbe **Granodiorite of Beasore Meadow and similar rocks (Early Cretaceous)**—Mafic hornblende-biotite granodiorite and tonalite

Ksp **Granite of Shuteye Peak (Early Cretaceous)**—Very light gray granite and biotite granite containing sparse to abundant tabular phenocrysts of potassium feldspar as long as 1 cm. Age about 102 Ma (U-Pb)

Kbf **Granodiorite of Bummers Flat (Early Cretaceous)**—Medium-grained biotite granodiorite with conspicuous large, blocky phenocrysts of potassium feldspar; quartz grains also conspicuous. Age about 101 Ma (Rb-Sr)

Kbp **Granite of Bond Pass (Early Cretaceous)**—Moderately foliated granite and granodiorite

Kst **Granite porphyry of Star Lakes (Early Cretaceous)**—Granite porphyry and granodiorite porphyry. Typically contains abundant small plagioclase phenocrysts in a medium- to fine-grained groundmass. Age about 108 Ma (Rb-Sr)

Fine Gold Intrusive Suite (Early Cretaceous)[1]

Kar **Granodiorite of Arch Rock and similar rocks**—Medium-grained, biotite granodiorite, commonly with poikilitic potassium feldspar. Age about 116 Ma (U-Pb)

Kga **Tonalite of the Gateway and similar rocks**—Medium-grained, biotite-hornblende tonalite. Varies to granodiorite and quartz diorite. Age about 114 Ma (U-Pb)

Kdl **Granite of Dorothy Lake (Early Cretaceous)**—Light-pink, Tourmaline-bearing granite

Klh **Granodiorite of Lake Harriet (Early Cretaceous)**—Dull-gray, biotite-hornblende granodiorite. Age about 133 Ma (Rb-Sr)

Kg **Granitic rocks, undivided (Cretaceous?)**—Miscellaneous bodies of granitic rock of unknown age and affinity, but probably all of Cretaceous age

KJdg **Diorite and gabbro (Cretaceous and Jurassic)**—Occurs as generally small, irregular-shaped bodies throughout map area. Some bodies older and some younger than the plutonic rocks with which they are in contact

Jgc **Tonalite of Granite Creek (Jurassic)**—Medium-grained, biotite-hornblende tonalite and granodiorite and minor gabbro. Age about 163 Ma (U-Pb)

Scheelite Intrusive Suite (Triassic)[1]

Kwc **Wheeler Crest Granodiorite**—Medium-grained, biotite-hornblende granite, commonly porphyritic with potassium-feldspar phenocrysts. Age about 210 Ma (U-Pb)

Trv **Granite of Lee Vining Canyon**—Medium-grained granite, commonly porphyritic. Age about 210 Ma (U-Pb)

METAMORPHIC ROCKS

Western metamorphic belt

Trms **Metasedimentary rock, undivided (Triassic, at least in part)**—Metachert and phyllite derived chiefly from chert and shale; minor limestone. At west edge of map area along Merced River

Pzme **Metasedimentary rock, undivided (Early? Paleozoic)**—Quartzite and argillite derived from quartz-rich sedimentary rocks

Eastern metamorphic belt

Kmv **Metavolcanic rock, undivided (Cretaceous)**—Hornfels and other metamorphic rocks derived chiefly from pyroclastic rocks—tuff and tuff breccia—and lesser lava flows; includes minor metasedimentary rocks. Occurs in southeast quadrant of map area and on Mount Dana and Gaylor Peak. Outcrop near south-central edge of map area questionably assigned to this unit

Jmv **Metavolcanic rock, undivided (Jurassic)**—Hornfels and other metamorphic rocks derived chiefly from pyroclastic rocks—tuff and tuff breccia— and lesser lava flows; includes some metasedimentary rocks chiefly derived from impure sandstone and limestone. Occurs in a discontinuous belt extending northwest from the Thousand Island Lake area to near Matterhorn Peak

Jms **Metasedimentary rock, undivided (Jurassic?)**—Hornfels and other metamorphic rocks derived chiefly from sandstone, siltstone, shale, limestone, and conglomerate. Known to be of Jurassic age in Strawberry Tungsten Mine area near southeast corner of map area. Other bodies of rock assigned to this map unit are of questionable age

Trmv **Metavolcanic rock, undivided (Triassic?)**—Hornfels and other metamorphic rocks derived chiefly from pyroclastic rocks—tuff and tuff breccia—and lesser lava flows; includes minor metasedimentary rocks. Occurs in a discontinuous belt extending northwest along the range crest from the Alger Lakes area on the east edge of the map to the Twin Lakes area

Pzmi **Metasedimentary rock, undivided (Late Paleozoic)**—Hornfels and other metamorphic rocks derived chiefly from sandstone, siltstone, limestone, and conglomerate. Occurs in a discontinuous belt near the range crest from Alger Lakes to Dunderberg Peak

Pzme **Metasedimentary rock, undivided (Early Paleozoic)** —Hornfels and other metamorphic rocks derived chiefly from sandstone, siltstone, and limestone. Occurs in small masses northeast and southeast of Lee Vining Peak

[1]Bateman (in press)

Contact

Fault—Dashed where approximately located; ball and bar on downthrown side

Crest of glacial moraine

Figure 1.3

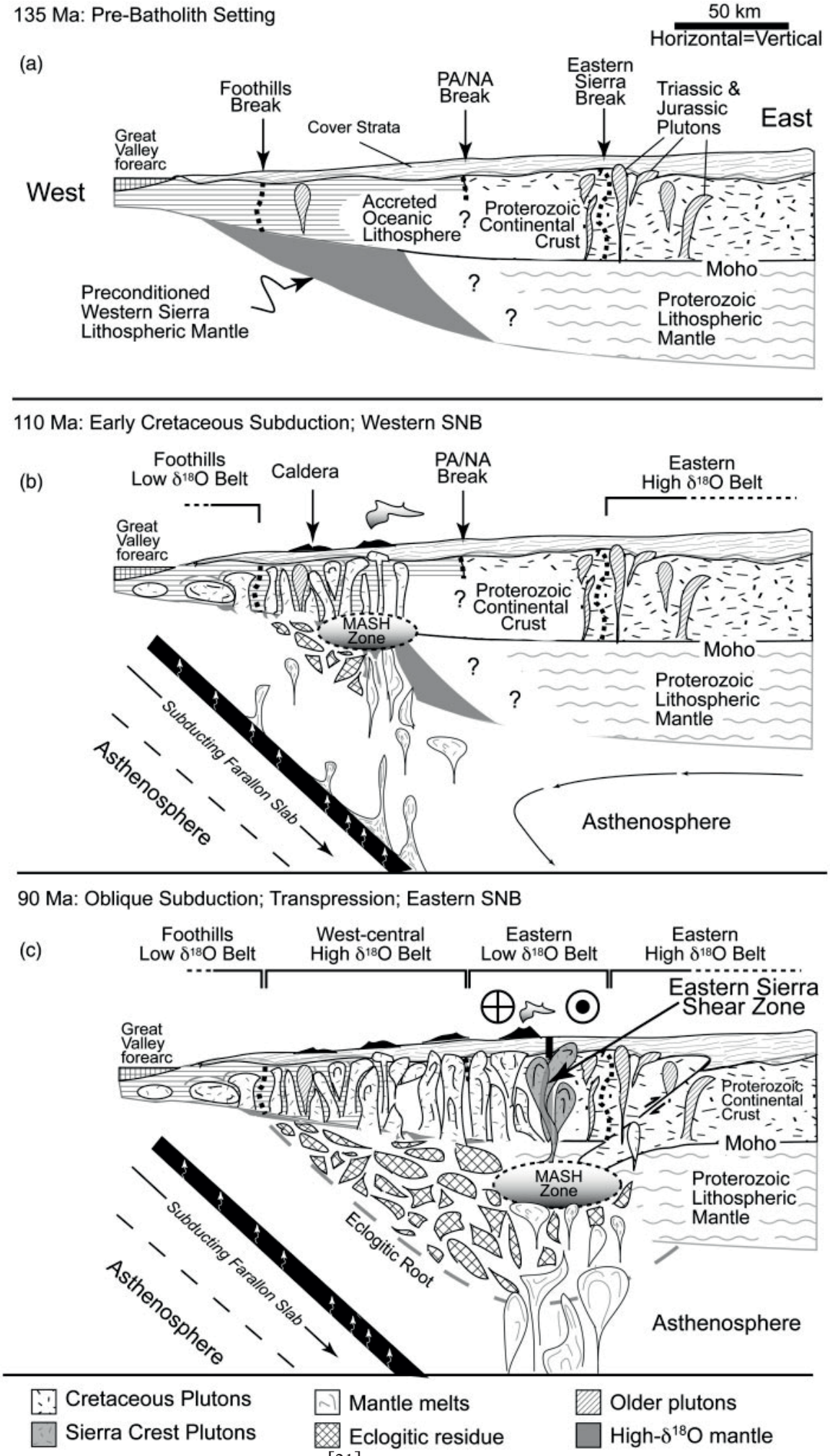
135 Ma: Pre-Batholith Setting
50 km
Horizontal=Vertical
(a)
Foothills Break
PA/NA Break
Eastern Sierra Break
Triassic & Jurassic Plutons
East
Cover Strata
Great Valley forearc
West
Accreted Oceanic Lithosphere
?
Proterozoic Continental Crust
Moho
Preconditioned Western Sierra Lithospheric Mantle
?
?
Proterozoic Lithospheric Mantle
110 Ma: Early Cretaceous Subduction; Western SNB
(b)
Foothills Low δ18O Belt
Caldera
PA/NA Break
Eastern High δ18O Belt
Great Valley forearc
?
Proterozoic Continental Crust
MASH Zone
Moho
?
?
Proterozoic Lithospheric Mantle
Subducting Farallon Slab
Asthenosphere
Asthenosphere
90 Ma: Oblique Subduction; Transpression; Eastern SNB
(c)
Foothills Low δ18O Belt
West-central High δ18O Belt
Eastern Low δ18O Belt
Eastern High δ18O Belt
Eastern Sierra Shear Zone
Great Valley forearc
Proterozoic Continental Crust
Moho
MASH Zone
Proterozoic Lithospheric Mantle
Eclogitic Root
Subducting Farallon Slab
Asthenosphere
Asthenosphere
Cretaceous Plutons
Sierra Crest Plutons
Mantle melts
Eclogitic residue
Older plutons
High-δ18O mantle

Figure 1.4

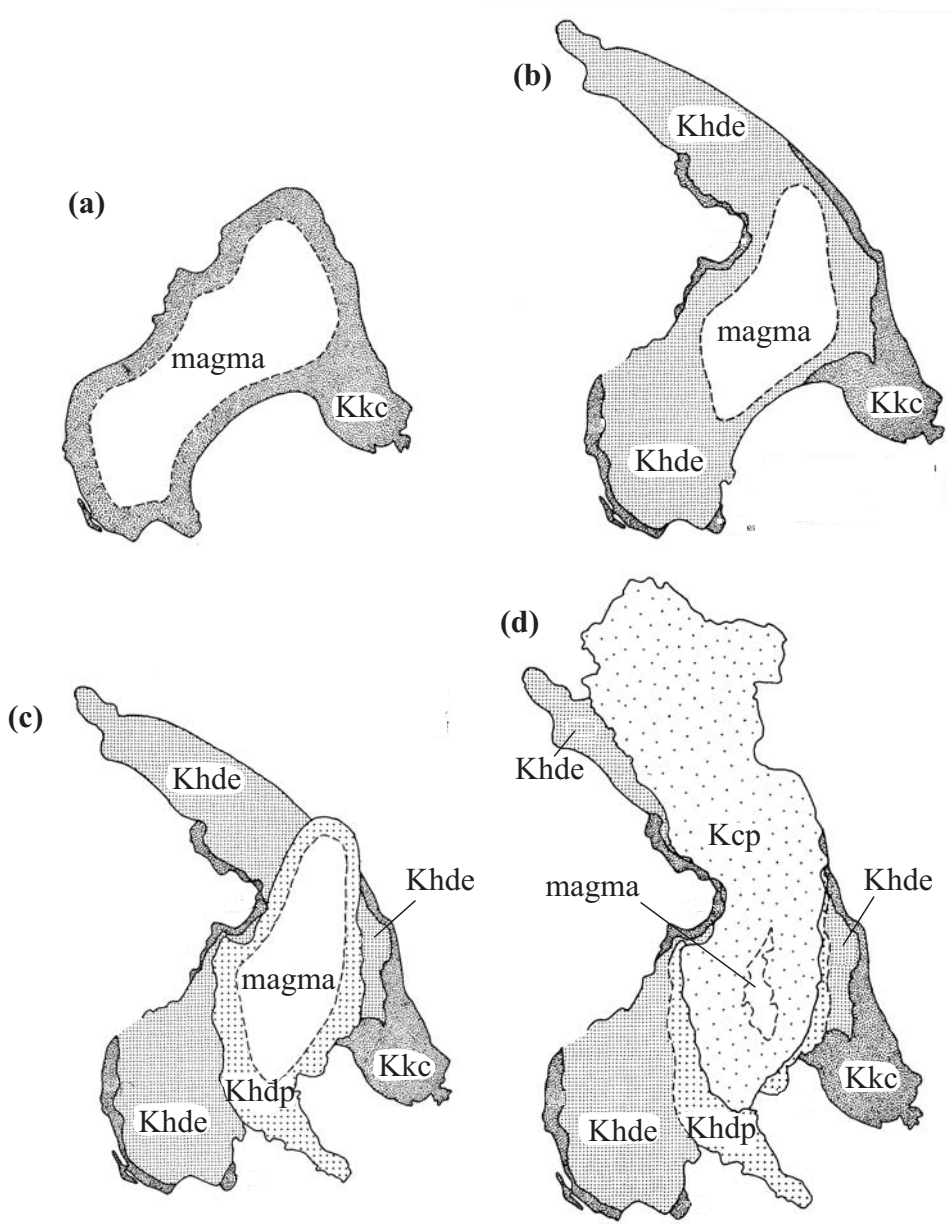

Figure 1.5

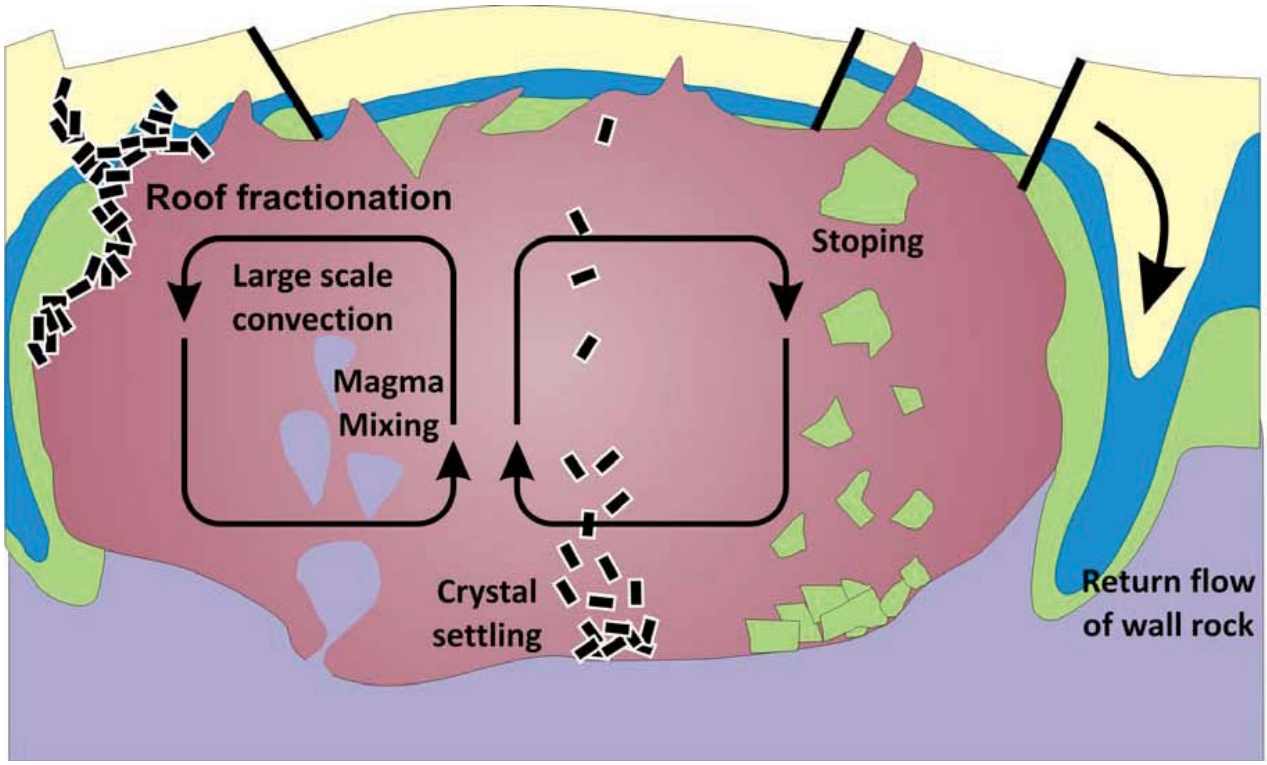

Figure 1.6

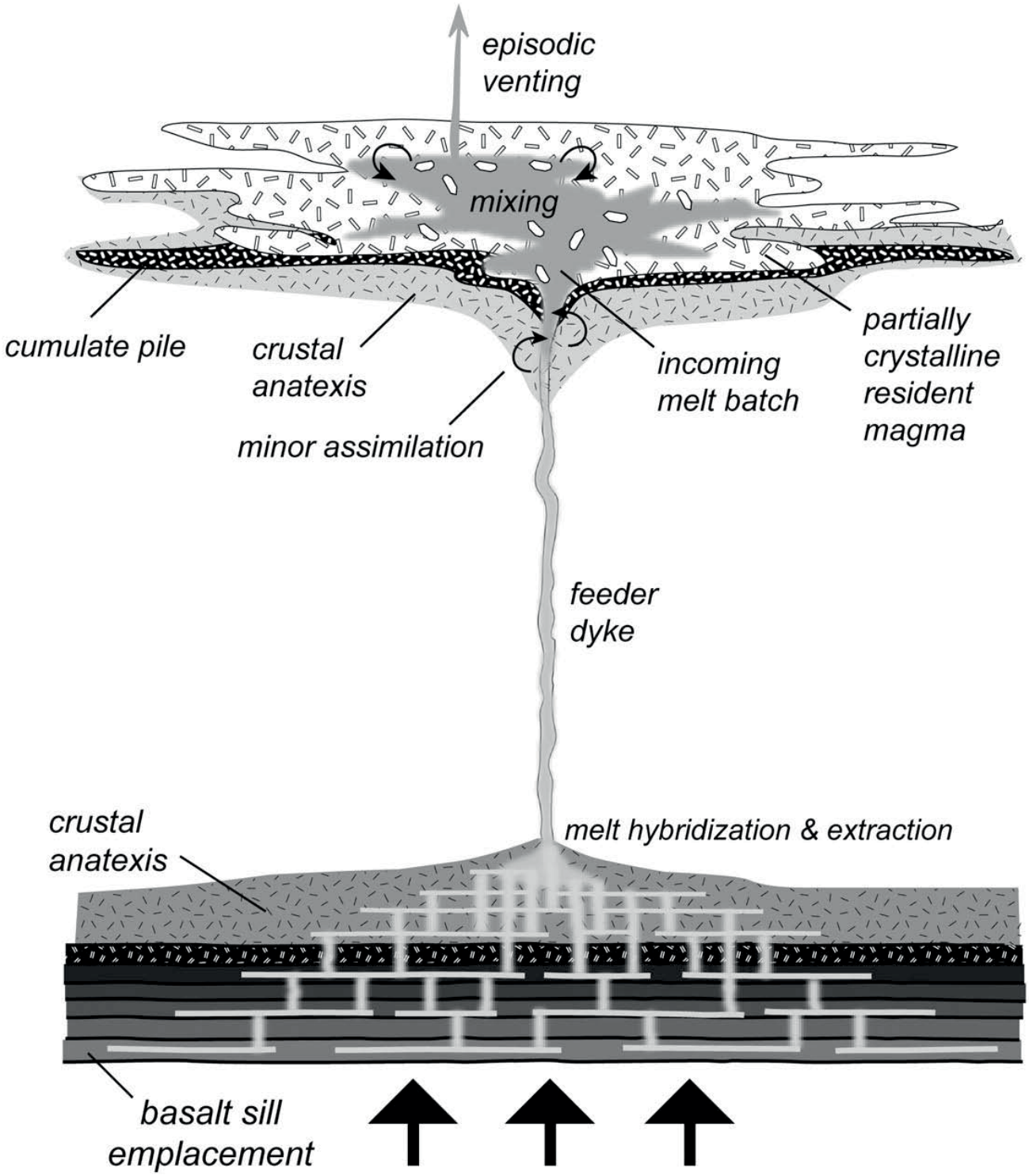
episodic
venting
mixing
cumulate pile
crustal
anatexis
minor assimilation
incoming
melt batch
partially
crystalline
resident
magma
feeder
dyke
crustal
anatexis
melt hybridization & extraction
basalt sill
emplacement

2 Methods

In this chapter the sampling technique, sample preparation and sample analyses are discussed. 24 samples were provided by a previous research (Johnson, unpublished), 60 samples were collected by Martine van der Linde and this author. All samples were processed at the VUA in a collaboration between Martine van de Linde and this author. An initial crush was done by Martine van der Linde at the SJSU by use of a jaw crusher. This concerned the samples collected for this research and was performed to reduce shipment costs.

2.1 Field sampling

Samples taking in the field which were representative of the lithology that was questioned at that time. Weathered rims were removed to gain a fresh sample. Samples sizes could vary depending on the availability to collect pieces of the rock. A optimal size would have a diameter of 15 centimetre and has a weight varying between 200-500 gram.

2.2 Sample preparation

All samples taken by this research group and Johnson (unpublished) were used for analyses. Thin-sections were fabricated of each sample. All samples were reduced in grain size and homogenised. Beads and pellets for XRF analyse were made out of the homogenised rock-powders.

2.2.1 Thin-section

Thin-sections are used for petrographical study and are fabricated in the laboratory of the VUA. For the petrographical study there should be noted that unpolished thin-sections of 120 to 130 micron were used instead of the normal 30 micron. These abnormal thickness is necessarily for potential future research using in situ microbeam techniques. A drawback of this thickness is that mineral characteristics can deviate with respect to the normal used classification techniques. For instance hornblende in these thin-sections also can appear as opaque minerals.

2.2.2 Sample reduction: Crushing and Milling

Steps in sample size reduction are: the jaw crusher, milling and planetary milling. The jaw crusher consist out of two metal plates. One of these plates moves back and forth hereby decreasing the distance between the two. Samples put in the jaw crusher were crushed which reduces the sample size to dice or have a dice size. The jaw crusher is thoroughly rinsed with ethanol between every sample-crush to reduce any contamination.

Step two is the first milling process. This is a jar of 30 cm in diameter. The inside is laid in with agate. A agate ring is placed in the jar and a agate cylinder is placed inside the ring. The sample pieces are placed between the jar, the ring and the cylinder. When centrifuging samples sizes are reduced to a fine (0.1 to 1.0 mm) powder. The mill is cleaned with quartz sand and de-mineralized water to rinse the agate parts of the mill. Afterwards the jar and its parts are rinsed with de-mineralized water and dried with ethanol.

The second milling process, the planetary mill, reduces the sample size even more and provides a excellent homogeneity of the sample. The jars for the planetary mill are 10 cm in diameter, are made out of agate and contain five agate balls with a diameter of two centimetre. Grain sizes are reduced to <0,1 micrometre and homogenized. The agate jars with balls are rinsed with quartz sand and de-mineralized water by running the planetary mill again. Afterwards the jars and balls are rinsed with de-mineralized water and dried with ethanol.

2.2.3 Beads and Pellets preparation

Pressed pellets were fabricated to measure the trace elements. In this research all the trace elements sets were used and measured. This includes the majorsrh 1-4 (Fe_2O_3, MnO, Ti_2O, CaO, K_2O, P_2O_5 , SiO_2, Al_2O_3, MgO, Na_2O, BaO) Spel (Nb, Y, Zr, Sr, U, Rb, Th, Pb) Metals (Ga, Zn, W, Ta, Cu, Hf, Er, Ni, Yb, Dy), Reehex 27 (La, Ce, Pr, Nd, Sm) and VCCBS (V, Cr, Co, Ba, Sc, Er, Hf). Beads are fabricated to measure major elements with a higher accuracy then those obtained with the pressed pellet. Measurements can be viewed in the appendix of this thesis.
Roughly 12 gram of each powdered sample was heated over night in a oven at 110˚C before beads or pellets were fabricated. This heat treatment is necessarily to lose all the remaining moisture in the sample.

Pellets are a combination of an organic binder and sample powder which are compressed together. 4.500 gram of dried sample powder is weighted. The organic binder (EMU 120 ED) is added, this is precisely 10% of the carefully weighted sample powder. This mixture is placed in a agate jar with three agate balls. The jar is placed in a shaker to homogenize the total mass. The homogenized powder is then placed in a aluminium cup and pressed with an X-press pelletizer. 20 tons of pressure are performed over 60 seconds to comprise a pellet. Afterwards the pressure is released over a period of 30 to 120 seconds. In most cases a pellet with a nice smooth surface is formed. High silica samples with a smooth surface were hard to fabricate. These pellets often crumbled when pressure was released.

Beads are fused glass comprised out of 1.000 gram of baked sample powder and 4.000 gram of Spectroflux 110. Spectroflux 110 is a mixture of lithiumtetraborate and lithiummetaborate. Baked sample powder is sample powder that is baked in a oven at 1000˚C for 30 min. This is necessarily to lose all organic material and to determine water and other volatiles by loss on ignition. The combination of 1.000 gram baked sample powder and 4.000 gram Spectroflux 110 is homogenized in a shaker. This mixture is placed in a platinum crucible and heated at roughly 1200˚C in the PerlX3. The PerlX3 pours the melt on a casting plate. When cooled a glass bead is formed.

2.2.4 X-Ray Fluorescence spectrometry

X-Ray Fluorescence spectrometry measurements where performed at the Vrije Universiteit Amsterdam (VUA) by use of the Pananalytical MagiXPro X-Ray Fluorescence (XRF) Spectrometer made by Phillips. The important parts of the XRF machine consist out of the X-ray tube, the sample location, collimator, an analyzer crystal and a detector (Figure 2.1).

A XRF machine radiates X-rays to a bead or pellet. The radiation is produced by the interaction of a Tungsten filament and Rhodium anode. In the XRF-tube the X-ray radiation is formed due to an electron beam originated out of a Tungsten (cathode) filament under a vacuum condition.

The high voltage on the Rhodium anode is 60kV and the high current is 60mA for trace elements. For the major elements 40kV-90mA is used. The electron beam and Rhodium interacts and produces the X-ray. X-ray – electron (sample) interaction produces fluorescence of all elements that interact with the X-ray beam. A collimator and a diffraction device (crystal) are used to select a specific wavelength. Each wavelength is specific for an element. A proportional counter or scintillation detector is used to measure the specific wavelength. Matrix corrections and standard calibrations are preformed on the measured wavelengths. Finally weight percentage oxides and parts per million of trace elements are obtained for the measured sample. For a more detailed explanation see Schlotz and Uhlig (2006).

Calibrations are done by use of measured standards. Pellet and bead standards are AGV-1, BHVO-2, BCR-2 and GSP-1. The measured values for the standards are presented in the appendix. The measured values of the standards fall within the excepted standard deviation range as presented in Fulmer and Kruijer, 2008. The standard deviation is for its maximum 2.5. In other words this would mean that samples are measured with a maximum error of 5%. Standard deviation calculations for the XRF at the VUA are from Fulmer and Kruijer (2008).

Figure 2.1

The Pananalytical MagiXPro X-Ray Fluorescence (XRF). Indicated are the most essential parts of the XRF. Rh = Rhodium anode. Modified after Schlotz and Uhlig (2006).

Figure 2.1

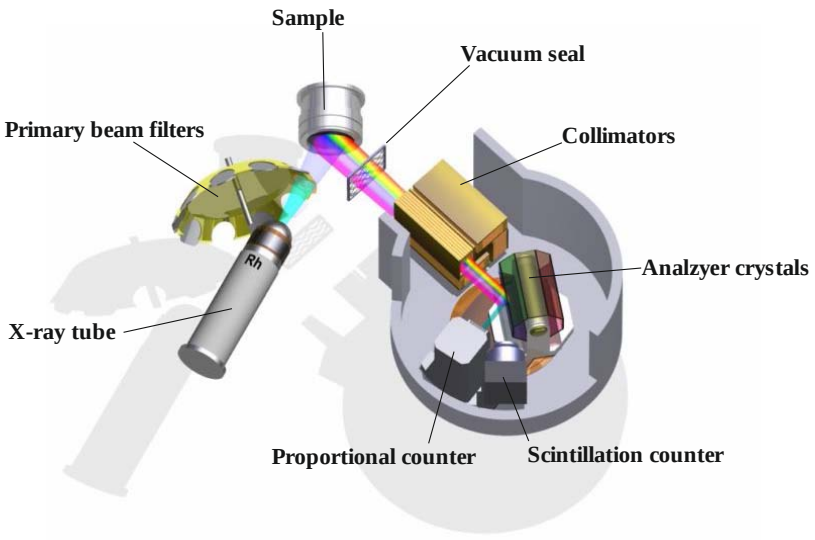

3 Field Observations

In this chapter field observations are presented. A short introduction to the field area is given. The fieldwork area is divided into three separate localities. Each locality contains a description of the characteristic lithological units, enclaves/xenoliths and dykes. Descriptions are made out of observations done by this author. At the end of this chapter a overview and integration of the three localities is presented.

3.1 Field area

This section starts with presenting a general introduction to the field area and its vicinity. The introduction consist out of the descriptions of the location, the accessibility, the used maps and the studied locations.

3.1.1 Location

Fieldwork was performed in the Yosemite National Park. This is a famous national park in California. Over three million tourist visit this park each year in the short period it is opened. The park is famous due to its wild life, gorgeous meadows, clear creeks, high waterfall and lovely forests. Last but not least its granitic mountains. The beauty of the hills and mountains astonishes everyone. Rock climbers, hikers, cyclists, motorcyclists, fishermen and campers are delighted to be in Yosemite National Park.

The field work was performed near the Ten Lakes Trail. This is a hiking trail starting from Highway 120 and going North to Grand Mountain and thereby crossing Half Moon Meadow, Grant Lakes, Ten Lakes and finally going up to the Tuolumne Peak (Figure 3.1). After the Tuolumne Peak the trail returns to Highway 120. The field work was concentrated on the first part of the trail near Grant Lakes and Ten Lakes (Figure 3.2b).

3.1.2 Accessibility

There is one big road crossing the Yosemite National Park. Highway 120 is a direct road which travels from East California to West Nevada. The areas near Highway 120 have numerous hiking trails. Most of these trail link up. One could walk for days in a circle. The more southern and northern areas of the park are almost inaccessible.

The area of interest to this research is accessible by hiking the Ten Lakes trail. The Grant Lakes and Ten Lakes can be reached after roughly six hours walk, depending on the conditions. Most field points where off the trail. Off trail hiking is not allowed without a specific research permit. Most areas were open of vegetation with single high trees.

3.1.3 Field and Geological Maps

Geological maps were available, published by Kistler et al. (1973) and Huber et al. (1989). The map which is most relevant for this study was the detailed map of Johnson (unpublished). Johnson (unpublished) studied the lithology and structural features, between Mount Hoffman, Tuolumne Peak, Grand Mountain, Double Rock and Highway 120 (Figure 3.1).

Johnson (unpublished) distinguished several units. The two major formations distinguished were the Yosemite Creek Granodiorite (YC) and the Yosemite Valley Intrusive Suite (YVIS). The map of Johnson (unpublished) can be divided into two major zones. The north-east side is dominantly Taft Granite and the south-west side El Capitan, a YVIS unit. The Yosemite Creek Granodiorite is located near the north-west side of the El Capitan zone and somewhat randomly located in the Taft Granite zone (Figure 3.2).

The units mapped as YC were: Coarse-grained granodiorite; medium-grained granodiorite to tonalite; mafic quartz diorite to diorite; porphyritic granodiorite, tonalite, “Myriad” zone intruding Taft Granite and “Myriad” zone intruding Taft and El Capitan Granites. The Myriad zones are highly intrusive areas where large parts are intruded by younger batches. Johnson (unpublished) invoked the “Myriad” terminology. The large extent of intrusion makes it a zone which is clearly different then other units in the area and is chaotic due to extensive dyking and remobilization of older and younger units.

In the YVIS Johnson (unpublished) distinguished the Taft Granite and the El Capitan Granite. The El Capitan Granite was divided in the units: Diorite, Mt. Hoffman Granodiorite, Double Rock Granodiorite, Equigranular granite and medium-grained granite.

3.1.4 Sample location

The field area is divided in several smaller field localities (Figure 3.2c, d, e and f). These areas are characteristic on local scale. The locations studied are the areas near Grant Lakes, Ten Lakes and the more southern area near Highway 120 (Figure 3.2b). From now on this latter mentioned area is revered to as the Porphyritic Granodiorite area. For sample locations see Figure 3.2a and appendix list with GPS points.

Figure 3.2a includes sample points. Sample names/locations are renamed on this map to reduce clotting. Other figures of Figure 3.2 contain no sample references to reduce clotting. In this thesis written references are the original sample name/location. For explanation of the map sample points and original sample points see Figure 3.2 Legend.

3.2 Grant Lakes

The area studied near Grant Lakes are differently interpreted by Kistler (1973) and Johnson (unpublished). For interpretation of Kistler (1973) see also Huber et al. (1989) and Figure 1.2. Kistler (1973) interpreted the igneous rocks near Grant Lakes as Taft Granite. Johnson (unpublished) interpreted the igneous rocks directly around and between the lakes as Mt. Hoffman Granodiorite. The latter mentioned unit contacts with the Taft Granite and, as Johnson (unpublished) mapped it, YC "medium-grained granodiorite to tonalite" unit.

The study area of Grant Lakes is roughly 1 km^2, well exposed with 50% outcrop and accessible by a tough hike. Descriptions are taken during a hike, starting at the middle of the southern margin of the eastern lake of Grant Lakes and going South. The observations are made over an area of 500 meters (Figure 3.2a, d). Samples near Grant Lakes are: BL-4A to BL-4H, BL-5A to BL-5E, BL-6A, 37A SJSU, 37D SJSU and 37G SJSU. Total samples taken in this area: 17.

3.2.1 Lithologies in Grant Lakes region

Near Grant Lakes several subdivisions in lithologies can be made. The first and the most abundant group is a quartz monzodiorite to granodiorite. Rock mineralogy varies between: feldspars: 45% to 60%; quartz: 10% to 35%; biotite: 5% to 15%; hornblende: 0% to 30%; sphene: <1%. Grain size varies between minerals: feldspars: 2 to 5 mm; quartz: 2 to 4 mm; biotite: 1 to 2 mm; hornblende: 2 to 10 mm; sphene: <1 mm. Quartz monzodiorite can contain foliations of mafic minerals. Samples taken (Figure 3.2a): BL-4C and BL-4H (Figure 3.6 BL-4C, BL-4H).

Thin-section (TS) study on BL-4C and BL-4H are roughly consistent with the field description. Detailed description of the mineralogy of BL-4C: Quartz makes up 10% of the TS and occurs mostly in the matrix; is colourless in plane polarized light (ppl); grain size ranging from 0.5 to 1 mm; shape is interstitial and anhedral; relief is high versus balsam. Plagioclase makes up 40% of the TS; is white in ppl; grain size varies between 1 to 2 mm; shape is equidimensional and euhedral; relief is positive versus biotite; contains well developed lamella twins especially in the core of the minerals, contains simple twinning and zoning. Alkali feldspar makes up 15% of the total TS; is white in ppl; grain size is 1 mm; the shape is equidimensional and euhedral; relief is positive versus balsam; contains simple twinning and zoning. Pyroxene makes up 5% of the total TS; cleavage is poorly developed; is light brownish in ppl; grain size is 0.1; is prismatic in shape and euhedral to subhedral developed; strong positive versus biotite. Apatite makes up 5% of the TS; is colourless in ppl; grain size varies between 0.2 to 0.5; has well developed cleavages formed and the mineral is anhedral to subhedral developed; relief is negative versus plagioclase. Hornblende makes up 5% of the TS; cleavage is strong developed; colour is dark green to yellow greenish in ppl; grain sizes vary between 0.1 to 1.0 mm; is prismatic shaped with well developed cleavages and the mineral is anhedral developed; relief is positive versus quartz. Opaque minerals make up 10% of the TS; grain size vary between 0.5 and 1.0 mm; equidimensional to cubic shaped and subhedral developed; relief is positive versus biotite.

Detailed description of the TS of sample BL-4H: quartz (20%), up to 4 mm, anhedral; plagioclase (30%) up to 4 mm, zoned; alkali feldspar (25%), 2 to 4 mm; biotite (10%), 0.1 to 2; opaque (10%), 0.1 to 2; hornblende (5%), 0.1 to 2. One apatite mineral is observed (chlorapatite?), 0.2 mm, greenish in ppl and hexagonal in shape.

The second lithology is porphyritic granodiorite to tonalite. Mineral abundance ranges between: feldspars: 40% to 60%; quartz: 30%; biotite: 5% to 10%; hornblende: 0% to 25%. Grain size varies between minerals: feldspars: 1 to 15 mm; quartz: 1-15 mm; biotite: <1 to 2 mm; hornblende: not present to 10 mm. Samples taken (Figure 3.2a): BL-6A (Figure 3.6 BL-6A).
Detailed TS description of sample BL-6A: quartz (10%), 1 to 2 mm; feldspar (30%) 1.0 to 1.5 mm; plagioclase (20%) 1 to 4 mm; biotite (5%), 0.1 to 2.0 mm; opaque (5%), 0.1 to 2.0 mm hornblende (2%), 0.1 mm. Quartz inclusions (< 0.1 mm) in feldspar and plagioclase minerals. Remarkable is the absence (or low amount of) twinning and zoning in the feldspars. The sample is slightly weathered.

3.2.2 Xenoliths and enclaves in Grant Lakes region

In the Grant Lakes area there are abundant granitic xenoliths and enclaves varying from angular to stretched. These granitic xenoliths and enclaves occur in the lithological groups mentioned in paragraph 3.2.1 as well as in a fine grained granodiorite sheet (Figure 3.3 a, b, c, g, h, i, j). The porphyritic granodiorite to tonalite can also hold xenoliths of the quartz monzodiorite to granodiorite (Figure 3.3 g).

The latter mentioned lithology is addressed below in paragraph 3.2.3. Mineral abundance of the granitic xenoliths and enclaves ranges between: feldspars: 55% to 60%; quartz: 35% to 40%; biotite: 5%. Grain size varies between minerals: feldspars: 3 to 10 mm; quartz: 2 to 8 mm; biotite: 1 to 2 mm. Samples taken: BL-4A, BL-4B, BL-5A and BL-5B (Figure 3.6). Detailed TS study reveals that sample BL-4A contain chloritized biotites and strongly altered alkali feldspars.

Sizes of granitic xenoliths vary greatly, ranging from a decimetre up to two meters in length. Most xenoliths are angular but occasionally margins are rounded or spherical elongated (e.g. Figure 3.3 a, g, h, i, j). Stretched granitic strings can be a few centimetres to a few decimetres in length. Angular xenoliths and stretched enclaves do not occur together on local scale (Figure 3.3 a, c). Occasionally near xenoliths reaction rims and clusters of more mafic minerals can be found (Figure 3.3 a, b, c, f).

Near an area of a fine grained granodiorite sheet, see paragraph 3.2.3 and Figure 3.3 d, fine grained mafic enclaves occur in the quartz monzodiorite to granodiorite. These enclaves have mineral abundance of: feldspars: 20%; quartz: 10%; biotite: 20%; hornblende: 50%; Grain size are < 1mm except for hornblendes which is 2 to 5 mm. Sizes of the enclaves vary from 2 to 10 cm in diameter and the shape randomly from spherical, elongated to blocky. The edges are rounded. The density of enclaves is roughly 50 per square meter (Figure 3.3 g).

3.2.3 Dykes and sheets in Grant Lakes region

A large fine grained granodiorite sheet intrudes the quartz monzodiorite to granodiorite unit (Figure 3.3 d). The strike of the sheet is NE 025° with a dip 15° SE. The sheet is at least 80 meters in length and is 15 meters in width. The contact of the sheet with the quartz monzodiorite to granodiorite unit is intrusive. A small network of minor veins and dykes, originated in the sheet, cut into the surrounding lithology (Figure 3.3 e). The mineral abundance of this sheet is: feldspars: 30%; quartz: 40%; biotite: 20%; sphene: 10. Grain size varies between minerals: feldspars: 1 mm; quartz: 1 mm; biotite: <1 mm; sphene: 1 to 2 mm. Sample taken BL-4G (Figure 3.6).
Detailed TS description of sample BL-4G: The matrix is fine grained (0.3 to 0.5 mm); quartz (30%); alkali feldspar (30%); plagioclase (12%); opaque (20%); biotite (8%). Low amount of chlorite (<1 mm) and a few myrmekite alterations. All plagioclase minerals are strongly altered. Phenocrysts of plagioclase and alkali feldspars grain size vary between 5 to 10 mm.

At sample location 4 the dominant lithology is classified as the quartz monzodiorite to granodiorite unit. This outcrop has abundant xenoliths and enclaves, see paragraph 3.2.2. Striking are the dykes. One granite dyke intrudes through the quartz monzodiorite to granodiorite unit into a large granitic xenoliths (Figure 3.3 g). The dyke is at least five meters in length and 5 to 15 cm in width. The mineral composition is as follows: feldspar: 35%; quartz: 50%; biotite: 5%. Grain sizes vary from 2 to 3 mm. Sample taken: BL-4F (Figure 3.6).

Pegmatite dykes intrudes all previous mentioned units, dykes, xenoliths and enclaves. The exception is that no pegmatic dyke is observed in the fine grained granodiorite sheet. The pegmatite dykes can vary from a thickness of a centimetre to decimetre thick. The rock mineralogy of the dykes: feldspar: 77%; quartz: 20%; biotite: 2,5%; sphene <1%. Grain sizes are: feldspar: 4 to 20 mm; quartz: 4 to 15 mm; biotite: 1 mm; sphene: <1 mm. Sample taken: BL-4D (Figure 3.6). TS study reveal that plagioclase minerals are strongly altered.

3.2.4 Schlieren in Grant Lakes region

Schlieren are mesocratic strings enriched in mafic minerals usually hornblende and biotite. These strings can be stacked and together creating a layered zone of a more mafic and felsic compositions. The thickness of these stacked layers can rang up to several decimetres. The length of the strings can vary from several centimetres up to several meters. In the Grant Lakes area schlieren are solely a feature that occur near contact margins with granitic xenoliths (Figure 3.3 g). In this particular situation the schlieren formed in the quartz monzodiorite to granodiorite unit.

Another feature discovered near Grant Lake is a cluster of biotite minerals that is roughly 15 centimetres in diameter. This cluster is located near the contact margin of a granitic xenoliths. Interpretations of this biotite cluster is speculative but fits the description of a cross section of a single schlier (Figure 3.3 f).

3.3 Ten Lakes

The map of Kistler (1973) and Johnson (unpublished) are in their major features in consensus with each other. Johnson (unpublished) invoked the unit "myriad zone intruding Taft" in the YC formation which Kistler (1973) interpreted as Taft Granite.

The study area of Ten Lakes is roughly 2,5 km^2 (Figure 3.2 e), moderately exposed with 25% outcrop and easy accessible by hikes when reached the Ten Lakes "plateau". Most observations are made near sample location 8. Interesting contact relations are extensively studied North of the hiking trail. The Myriad zone was observed during a though hike up-hill. Samples taken near Ten Lakes are: BL-1A to BL-1C, BL-2A to BL-2D, BL-3A to BL-3F, BL-8A to BL-8G, BL-10A, BL-11A and BL-12A to BL-12B (Figure 3.2). Total samples taken in this area: 22.

3.3.1 Lithologies in Ten Lakes region

As shown in Figure 3.2 the majority of Ten Lakes is mapped as granite. The rock mineralogy of the granites vary from: feldspars: 45% to 55%; quartz: 35% to 45%; biotite: <1% to 4%; hornblende: up to 7.5%; sphene: up to <1%; garnet: up to 1%. Grain size varies between minerals: feldspars: 3 to 10 mm; quartz: 2 to 5 mm; biotite: <1 to 2 mm; hornblende: <1 to 6 mm; sphene: <1 mm. Samples BL-1C, BL-3F and BL-8F (Figure 3.6).
Detailed TS study on previous mentioned samples are consistent with field observations and contain similar rock mineralogy. Rock mineralogy: quartz (45%), 5mm; plagioclase (45% to 55%), 1 to 3 mm; biotite (3%), 0.5 to 1 mm, subhedral formed, minor chloritizatoin near the mineral rims; opaque (2% to 7 %), 2 to 3mm, anhedral; Sphene (no to <3%), < 1mm. Sample BL-3F is strongly weathered and contain a lot of pertitic dissolution.

The granites are generally very felsic. The most mafic component of Ten Lakes can be described as diorite to hornblende-rich diorite that occasionally is feldspar porphyritic. Rock mineralogy can be described as follows: feldspars: 20% to 40%; quartz: up to 15%, local occasionally up to 35%; biotite: <1% to 10%; hornblende: 40% to 70%. Grain size diameters varies little between the minerals: feldspars: <1 to 5 mm; quartz: <1 to 2 mm; biotite: <1 to 1 mm; hornblende: <1 to 10 mm. Samples taken (Figure 3.2): BL-1A, BL-3A, BL-8A and BL-8D (Figure 3.6).
Detailed TS study on the granitic samples reveal the follow rock mineralogy: quartz (0% to 5%), 0.5 to 1.0 mm; plagioclase (7% to 25%), 0.5 to 1.0 mm, minor degree of pertitic dissolution; alkali feldspar (15% to 20%), 0.5 to 2; biotite (15% to 30%), 0.2 to 2.0 mm, anhedral formed; opaque (10% to 25%), 0.5 to 1.0 mm, subhedral; hornblende (10% to 25%), 0.1 to 4.0 mm, subhedral to anhedral; Sphene (<1%), < 1mm, can occur as inclusions in plagioclase.

Between the felsic granite and the mafic hornblende-rich diorites a more felsic diorite can be distinguished in the field (e.g. Figure 3.4 b, e, f, g,). The change of the felsic to mafic units can be as less as 1 to 2 meters, but in general the distance will be 10 to 20 meters. This less felsic granodiorite will be revered to as a fine to medium grained quartz monzodiorite to granodiorite. The rock mineralogy can be described as follows: feldspars: 30% to 60%; quartz: 5% to 30%; biotite: 5% to 30%; hornblende: up to 30%. Grain size ranges from: feldspars: <1 to 10 mm; quartz: <1 to 3 mm; biotite: <1 to 6 mm; hornblende: <1 to 10 mm. Samples taken (Figure 3.2): BL-2C, BL-3B, BL-8B, BL-8G and BL-12B (Figure 3.6). The

diorite to hornblende-rich diorite and the fine to medium grained quartz monzodiorite to granodiorite are mapped by Johnson (unpublished) as mafic quartz diorite to diorite.
Rock mineralogy of the samples: quartz (20% to 40%), 1 to 5 mm; plagioclase (10% to 20%), 1 to 5 mm, occasionally zoned, slightly altered core, simple twinning; alkali feldspar (15% to 40%), 2 to 5, occasionally zoned; pyroxene (up to 5%), 0.5 to 1.0 mm; biotite (10% to 15%), 0.5 to 1.0 mm, occasionally chloritized near the mineral rims; opaque (up to 5 %), 0.2 to 3.0 mm; hornblende (5% to 10%), 0.5 to 1.0 mm. Deviating samples: BL-3B contains 5% apatite and BL-12B contain strong altered plagioclase minerals and myrmekite alteration.

3.3.2 Xenoliths and enclaves in Ten Lakes region

Xenoliths and enclaves can be grouped into two major groups. The first group comprises granitic xenoliths and enclaves in the quartz monzodiorite to granodiorite unit. The second group is made up of diorite to hornblende-rich diorite enclaves in the quartz monzodiorite to granodiorite unit. However, some enclaves do not follow this description.

First group of xenoliths vary greatly in size and shape. Small angular centimetre to mineral scale clusters of granitic material can be distinguished in the quartz monzodiorite to granodiorite unit, especially near contact margins with the granite unit (Figure 3.4 h, j1, j2). Occasionally up to metre scale stretched enclave-like structure of granite are found, these have similar characteristics as enclaves (Figure 3.4 i). Composition and grain sizes are similar as described in the granite unit. Granitic xenoliths are also observed in finer grained granitic dykes, which intruded the granitic unit (Figure 3.4 y1, y2).

The second group, the diorite to hornblende-rich diorite enclaves are several centimetre to decimetre in diameter. The shapes are spherical and occasionally stretched (Figure 3.4 b, e, f, g, o). In local areas the enclaves have crenulated margins (Figure 3.4 e, m, n). Mineralogical and grain size variations are similar to those described for the quartz monzodiorite to granodiorite units.

The origin and significance of quartz monzodiorite to granodiorite enclave-like structures in (leuco)granitic rocks are unclear (Figure 3.4 k). These structures can be either enclaves or xenoliths. If they are xenoltihs they are fully surrounded by intruding (leuco)granitic dykes. If they are enclaves the granitic host rock most have been remobilize to such a extent that it can incorporate enclaves.

The “Myriad zone intruding Taft Granite” is a interesting area. Here are almost all rock types and field relations previously described observed together in outcrop scale (Figure 3.4 f, p, t, u, v, w, x). Quartz monzodiorite to granodiorite enclave or xenoliths can be observed in the diorite to hornblende-rich diorite unit and vice versa. Quartz monzodiorite to granodiorite enclaves or xenoliths can be observed in the granite unit (Figure 3.4 w).

3.3.3 Dykes in Ten Lakes region

There are several granitic dykes in the area of Ten Lakes. Length, width and composition vary greatly. Most granitic dykes are thick and cut through the diorite to hornblende-rich diorite unit. The thickness varies between 90 to 120 centimetre. The length of the dykes ranges from ten to several tens of meters (Figure 3.4 r). Occasionally small (2 to 3 meters in length and 2 to 5 cm thick) shallow angle dykes of several centimetre thick intruding other monzodiorite dykes or the quartz monzodiorite to granodiorite unit (Figure 3.4 d, s1, s2). Also mafic diorite enclaves can be intruded by granitic dykes (Figure 3.4 t, x). The "myriad zone intruding Taft granite" is full of smaller granitic dykes which intruding the diorite to hornblende-rich diorite unit (Figure 3.4 f, p). In one outcrop an aplite dyke is observed which intrudes a thick granite dyke (Figure 3.4 y1). Mineral abundances in the granitic dykes vary greatly: feldspars: 50% to 70%; quartz: 20% to 45%; biotite: 5% to 10%; garnet: up to 5%. Grain size ranges from: feldspars: 1 to 5 mm; quartz: 1 to 5 mm; biotite: 1 to 3 mm; garnet: 1 to 3 mm. Samples taken: BL-2A, BL-9C and BL-10A (Figure 3.6).

Leucogranitic dykes intrude all units and dykes (Figure 3.4 f, p, y1). No inter-relations with respect to pegmatite or aplite dykes are observed. Rock mineralogy: feldspars: 20% to 60%; quartz: 30% to 65%; biotite: 5%; hornblende: up to 10%; garnet: up to 5%. Grain size ranges from: feldspars: 1 to 2 mm; quartz: 1 to 4 mm; biotite: <1 to 3 mm; garnet: 1 to 3 mm. Sample taken BL-12A (Figure 3.6).

At least four (sample location 2, 3, 9 and 10) diorite dykes are present that intrude the granitic unit or with the porphyritic diorite (Figure 3.4 a, q, r). Dimensions of the dykes vary greatly. Thicknesses are typically several decimetres and the length of the dykes vary from 20 meters to several hundred of meters. All dykes are intruded almost vertically. Mineral abundances of the diorite dykes: feldspars: 40%; quartz: 10%; biotite: 0% to 5%; hornblende: 50%. Grain size ranges from: feldspars: <1 to 3 mm; quartz: <1 to 3 mm; biotite: <1 to 2 mm; hornblende: <1 to 10 mm. Sample taken BL-3C (Figure 3.6).

3.3.4 Schlieren in Ten Lakes region

Schlieren are rare near Ten Lakes and only one time observed at the north-western margin of the quartz monzodiorite to granodiorite unit (Figure 3.4 z1, z2). The schlieren follow the contact margin with the granite unit. The schlieren consist of three parallel mafic alignments, several meters in length and roughly 20 centimetres thick.

3.4 Porphyritic Granodiorite

The porphyritic granodiorite formation refers to the most southern few kilometres of the Ten Lakes Trail. Johnson (unpublished) mapped a part of this area. He distinguished the porphyritic granodiorite and the coarse-grained granodiorite (Figure 3.2). Kistler (1973) mapped this area as Yosemite Creek Granodiorite with Yosemite Sentinel Granodiorite at the southern margin (Figure 1.2). Fulmer and Kruijer (2008) distinguished a transitional YS to YC unit (Figure 3.2, unit abbreviation Kysc).

The study area of Grant Lakes is roughly 4 km^2, with low outcrop exposure (up to 10%) in the lower valley and near the meadows (Figure 3.1). These areas are good accessible by trail hiking. Outcrop exposure gets better with higher altitude and can be as high as 90% of the area. The rather shallow surface and low vegetation makes the area good accessible by hiking. Samples taken from the Porphyritic Granodiorite Unit are (Figure 3.2): BL-7A, BL-13A to BL13F, BL14A to BL14E, BL-15A, BL-15B, BL-16A, BL17A, BL-17B, BL-18A to BL-18C. Total samples taken in this area: 20.

3.4.1 Lithologies in Porphyritic Granodiorite region

There are two lithologies distinguishable. A porphyritic granodiorite and a coarse-grained granodiorite. The major distinction between the two can be made by the grain size of the feldspars. The big feldspars are characteristic for the porphyritic granodiorite. The contact between the two units is a gradational zone of 30 meters. Grain sizes slightly changes from one unit into the other.

Mineral abundances of the porphyritic granodiorite can be described as follows: feldspars: 35% to 50%; quartz: 20% to 35%; biotite: 5% to 15%, hornblende: 5% to 30%; sphene: up to <5%. Grain size varies between: feldspars: 1 to 10 mm; quartz: 1 to 3 mm; biotite: 2 to 8 mm; hornblende: 1 to 5 mm; sphene: <1 to 3mm. Samples taken: BL-13A, BL-14A, BL-16A and BL-18D (Figure 3.6).
TS study reveal a rock mineralogy of: quartz (20 to 40%), 2 to 10 mm, anhedral; plagioclase (15 to 20%), 2 to 20 mm, euhedral to subhedral, occasionally zoned, slightly altered core, closely spaced lamella, simple twinning; alkali feldspar (15 to 40%), 2 to 10, euhedral, occasionally zoned; pyroxene (5%), 0.5 to 1.0 mm, prismatic, diamond shaped, euhedral formed; biotite (10%), 0.5 to 1.0 mm, anhedral to subhedral formed, occasionally chloritized near the mineral rims; opaque (5 %), 0.2 to 5.0 mm, anhedral; hornblende (5 to 10%), 0.5 to 1.0 mm, anhedral.

The rock mineralogy of the coarse-grained granodiorite: feldspars: 40% to 50%; quartz: 30%; biotite: 10% to 20%; hornblende: 10% to 20%; sphene: <1% to 1%. Grain size varies between: feldspars: 1 to 8 mm; quartz: 2 to 7 mm; biotite: 1 to 5 mm; hornblende: <1 to 10 mm; sphene: <1 to 2 mm. Samples taken: BL-17A, BL-18A and BL-18B (Figure 3.6).
TS study is roughly consistent with field observations. Rock mineralogy: quartz (20% to 33%), 2 to 5 mm, anhedral; plagioclase (30%), 2 to 5 mm,euhedral to subhedral, lamella twins, strong altered mineral cores, zoned, simple twinning, quartz inclusions; alkali feldspar (15% to 30%), 2 to 5 mm, euhedral, simple twinning, zoned; pyroxene (2% to 5%), 0.5 mm, prismatic, diamond shaped, euhedral formed, opaque inclusions; biotite (5% to 10%), 0.1 to 2 mm, anhedral to subhedral formed, occasionally chloritized at the margins of the mineral; hornblende (or chlorite) (5%), dark green to yellow, 1 mm, platy, anhedral to subhedral; opaque (5%), 0.2 to 1.0 mm, equidimensional and cubic, subhedral to anhedral; sphene

(<1%), 0.1 mm, cubic, subhedral to anhedral. The abnormal thickness of the thin-section changes the crossed plane polarized view and hereby the birefringes. This makes it very hard to distinguish hornblende from chlorite.

3.4.2 Xenoliths and enclaves in Porphyritic Granodiorite region

In the Porphyritic Granodiorite area there is only one type of xenolith distinguishable. These xenoliths are situated in the fine grained hornblende-rich monzodiorite sheet. Xenoliths are spherical with a diameter varying between 10 and 20 centimetres. The mineral abundance and grain sizes are identical to the porphyritic granodiorite. See also paragraph 0 on mafic sheet andFigure 3.5 (f), (g) and (h).

Other xenoliths can be described as mafic, hornblende-rich granodiorite, enclaves. These enclaves can be observed as individual enclaves, grouped enclaves and as enclave swarms (Figure 3.5 a, b, c, d, e, q, s, x, y, z1, z2, z3). Diameter of the enclaves vary from several centimetres to several decimetres (Figure 3.5 a, b, c, d, e). Enclave density is 10% to 20% of whole rock. The compositions of enclaves do vary. End-member compositions can occur near each other. Rock mineralogy ranges from: feldspars: 20% to 40%; quartz: 10% to 40%; biotite: up to 5%, hornblende: 25% to 50%; sphene: <1%. Grain size varies between: feldspars: <1 to 5 mm; quartz: <1 to 4 mm; biotite: 1 to 3 mm; hornblende: <1 to 3 mm; sphene: <1 mm. Hornblende minerals can occur in clusters

A striking observation of the enclaves of the Porphyritic Granodiorite Unit is their heterogeneous nature, most notable in the largest enclaves. These zones are more felsic, usually exist near enclave margins and contain large feldspars, up to 5 mm. Occasionally these zones occur as bands between the mafic enclaves (Figure 3.5 q, s).

In several outcrops (sample location 13, 14, 17 and 18) phenocryst could be distinguished in enclaves. In the fine grained (1 mm) hornblende-rich matrix the following phenocrysts were observed: feldspar (50%) 5-10 mm, quartz (20%) 4-5 mm and hornblende (30%) 4-5 mm. A good illustration of the phenocrysts are given in the thin-sections of sample BL-14B, BL-14D and BL-14E (Figure 3.6). Locally, feldspar phenocryst have a corona of hornblende minerals. Samples taken: BL-13B, BL-14D, BL-14E, BL-17B and BL-18C.
TS study reveal that the enclave samples have roughly the same rock mineralogy: in general fine grained (0.5 to 2 mm); quartz (10% to 20%); alkali feldspar (10% to 25%); hornblende (20% to 40%); opaque (5% to 20%); biotite (20% to 30%); pyroxene (up to 10%). Sample BL-17B have plagioclase phenocrysts up to 1.5 cm with strong altered zones.

3.4.3 Dykes in Porphyritic Granodiorite region

There are several types of dykes distinguishable. Large (~5 x 20 m) mafic sheet (dyke), coarse-grained granodiorite dykes intruding into porphyritic granodiorite, porphyritic granodiorite dyke intruding in coarse-grained granodiorite, leucogranite dykes and pegmatite dykes. Samples taken: BL-13C to BL-13F.

The mafic sheet is a fine grained hornblende-rich monzodiorite. Rock mineralogy: feldspars: 38%; quartz: 10%; biotite: <5%, hornblende: 45%; sphene: <1%. Grain size varies between: feldspars: 1 to 2 mm; quartz: 1 to 4 mm; biotite: 1 mm; hornblende: 1 to 2 mm; sphene: <1 to 1 mm. Near the margin of the sheet, enclave-like strings occur. The porphyritic granodiorite intrudes into the margins of the mafic sheet to form enclave-like structures (Figure 3.5 a).

The fine grained hornblende-rich monzodiorite sheet is intruded by a diorite dyke. This dyke intrudes in the hornblende-rich monzodiorite and the porphyritic granodiorite intrusions which are situated within the hornblende-rich monzodiorite sheet (Figure 3.5 i). This diorite dyke is originated out of the Porphyritic Granodiorite Unit (Figure 3.5 j).

Pegmatite dykes near this particular outcrop (sample location 13) are roughly a decimetre thick. The strike of these dykes seems to follow structures in the mafic sheet and its "elongated marginal enclaves" (Figure 3.5 b). Their mineralogy is roughly: K-feldspar: 40%; plagioclase: 25%; quartz: 30%; biotite: <5%. Grain sizes ranges from several millimetres to over a centimetre. Except for biotite minerals, they only occur as 2 to 3 mm grains. In the north-eastern area pegmatite dykes are present as long stretched intrusions.

Minor variations are seen in the intrusions of coarse-grained granodiorite dykes into the Porphyritic Granodiorite Unit. The composition of the intrusion fully fit the description of the coarse-grained granodiorite unit (Figure 3.5 r). Near sample location 16 a porphyritic granodiorite dyke intrudes in the coarse-grained granodiorite. The length of the dyke is roughly 4 meters, the thickness varies between 20 and 50 cm (Figure 3.5 p).

One notable dyke occurs that is parallel to but 30 m South of the contact between the coarse-grained granodiorite and the porphyritic granodiorite (Figure 3.5 k, l, m, n, o). Orientation in plane: NE 031°/54°. This dyke is at least 300 to 400 meters long. At its thickest this dyke is over a meter thick. To the most eastern edge of the dyke it thins out to a decimetre thick. The most striking feature of this dyke is that the majority is leucogranitic. But the dominant lithology in the centre of the dyke is hornblende-rich quartz monzodiorite. The mafic centre dies out to the East remaining is solely the leucogranite dyke. Occasionally a small enclave-like hornblende-rich quartz monzodiorite structure can be found in the centre of the dyke (Figure 3.5 m).
The leucogranite dyke intrudes the Porphyritic Granodiorite Unit with a sharp contact. The contact between the leucogranite and the hornblende-rich quartz monzodiorite in the centre of the dyke appears to be co-magmatic due to crenulated margins (Figure 3.5 n, o). Felsic strings of minerals and elongated enclaves can be linked to the margins of the leucogranitic outer-dyke.

The hornblende-rich quartz monzodiorite has an estimated mineralogy of (Figure 3.6 sample 15): quartz: 50% (?); feldspar: <5% (?); biotite: 1%; hornblende: 44%. Grain size is very fine grained: <1 mm. Biotite minerals can be up to 1 mm and quartz minerals can be up to 2 mm. Feldspars and quartz minerals are too fine grained to be distinguished.

The leucogranite rock mineralogy is: K-feldspar: 30%; plagioclase: 40%; quartz: 25%; biotite: 5%. Grain size varies between: K-feldspars: 5 to 15 mm; plagioclase: 1 to 2 mm; quartz: 1 to 3 mm; biotite: 1 to 5 mm.

3.4.4 Schlieren in Porphyritic Granodiorite region

Near areas with high compositional contrasts between mafic and felsic lithologies schlieren can occur. The schlieren are characterised by hornblende-rich strings and/or feldspar-rich strings. Most the hornblende-rich strings are a few centimetres thick (Figure 3.5 t, u, v, w).

In the eastern part of the Porphyritic Granodiorite Unit near the contact with the coarse-grained granodiorite, many schlieren and schlier-complexes can be distinguished. Complex schlier structures are often accompanied with swarms of small enclaves (Figure 3.5 v, y, z2). Occasionally schlieren can be found that have dyke-like characteristics (Figure 3.5 t, u). They stretch for several tens of meters, are several decimetres thick and have a mafic boundary with the "host" rock. Occasionally circular schlieren can be found (Figure 3.5 w).

3.5 Summary field results

Lithologies previous described can be generalized to the follow units. From South to North these units are: porphyritic granodiorite, coarse-grained granodiorite, granite, fine to medium grained quartz monzodiorite to granodiorite, diorite to hornblende-rich diorite (occasionally feldspar porphyritic) and (fine grained) quartz monzodiorite to granodiorite. Geochemical data should support or reject petrogenetic relationships between the different graitoids.

Granitic xenoliths occur in several varieties. Except in the southern Porphyritic Granodiorite Unit these xenoliths are present in all other rock types. Occasionally xenoliths of host rocks can be found in intruded sheets or dykes, for example, xenoliths of quartz monzodiorite to granodiorite in medium grained quartz monzodiorite to granodiorite; medium grained quartz monzodiorite to granodiorite in fine grained granodiorite sheet and quartz monzodiorite to granodiorite xenoliths in the granite unit. The myriad zone seems to be an exception. All lithologies contain xenoliths of other lithologies.

The most common xenoliths are mafic enclaves. Enclave characteristics are hornblende rich, fine grained (minerals of 1 mm in diameter), usually spherical in shape, ranging in diameter from decimetre to several decimetres and occasionally porphyritic in quartz and feldspar minerals. The majority of the enclaves would be classified as a diorite to hornblende-rich diorite. In the coarse-grained granodiorite and porphyritic granodiorite enclaves can be found near the margins of diorite to hornblende-rich (grano)diorite dykes or sheets. Dyke-like swarms and pods of enclaves also occur in these area, in contrast with the more northern units. In the quartz monzodiorite to granodiorite enclave occur more randomly.

In the total study area fine grained mafic sheets, ranging from granodiorite to hornblende-rich monzodiorite, intrude medium to coarse-grained granodioritic units. These sheets are mostly large in size, stretching for several tens of meters. Occasionally such a sheet can contain host rock material. Contact relations with the host rock varies.

Granitic and leucogranitic dykes intrudes all other units and structures present except for pegmatite and aplite dykes. (Leuco)Granitic dykes are not observed in the coarse-grained granodiorite unit. These dykes stretches for several tens of meters and their thickness might vary greatly (1 to 50 m). Contacts are always sharp with the host rock.

Pegmatite dykes are common and stretches for several meters, are roughly a decimetre thick, contain large K-feldspars and plagioclase and intrudes all other units. In the Porphyritic Granodiorite Unit several pegmatite dykes occur near a hornblende-rich monzodiorite sheet. The pegmatite dykes seems to follow the intrusion and enclave structures of the sheet. Rarely aplite dykes are observed. When observed they intrude all other units and structures with sharp contacts.

Schlieren occur in quartz monzodiorite to granodiorite units and the Porphyritic Granodiorite Unit. It is common to encounter schlieren near large xenoliths, especially granitic xenoliths. Occasionally schlieren occur near mafic intrusions. In the porphyritic granodiorite schlieren occur in complex structures ranging from broad bands, dyke-like strings, circular shapes and irregular stacked schlieren.

Figure 3.1

Topographical map of Ten Lakes and vicinity. Modified after Quadrangles 7.5 minute series (Topographic): Yosemite Falls, Ten Lakes, Falls Ridge and Tenaya Lake. Original scale 1:24 000. Contour interval 40 feet. Magnetic North 15°/267mils. Red line = primary highway; dashed red/white line = secondary highway; black line = light-duty road; small black line = unimproved road; dashed black line = hiking trail; blue lines = creek. National Geodetic Vertical datum of 1929. Produced by the United States geological Survey. Compiled from imagery taken 1984 and 1985. Photo inspected using imagery dated 1992; no major culture or drainage changes observed. Boundaries verified and names revised 1994. North American Datum of (NAD 27). Projection and 10000-foot ticks: California Coordinate System, zone 3 (Lambert Conformal Conic). Blue 1000-meter Universal Transverse Mercator ticks, zone 11. North American Datum of 1983 (NAD 83) is shown by dashed corner ticks. The value of the shift between NAD 27 and NAD 83 for 7.5-minute intersection are obtained from National Geodetic Survey NADCON software.

Figure 3.2

Geological Map of Ten Lakes and vicinity, modified after Fulmer and Kruijer (2008) and Johnson (unpublished). For explanation see Legend. For scale see scale bar in figures. Sample names/locations are renamed on map (a) to reduce clotting. Other figures of Figure 3.2 contain no sample references names to reduce clotting. For explanation of the map, sample points and original sample points see Figure 3.2 Legend. Samples taken by Johnson are labelled as SJSU and are taken in summer 2008 and 2009. Samples taken by Bliekendaal and Van der Linde are labelled as BL in summer 2010.

(a) Geological Map of Ten Lakes and vicinity. Portrayed are the geological units and sample locations. **(b)** Geological map overlain on the topographical map of Figure 3.1. In this figure geological units with respect to the field morphology and field characteristics are showed. Notable intrusions are indicated in white, not to scale. For geological explanation see (a) and Legend. For topographical map information see Figure 3.1 text. **(c)** This figure shows locations of enlarged localities of (d), (e) and (f). **(d)** Enlarged locality of Grant Lakes. **(e)** Enlarged locality near Ten Lakes. **(f)** Enlarged locality of Porphyritic Granodiorite. **(Legend)** explanation of Geological Map of Ten Lakes and vicinity.

Figure 3.1

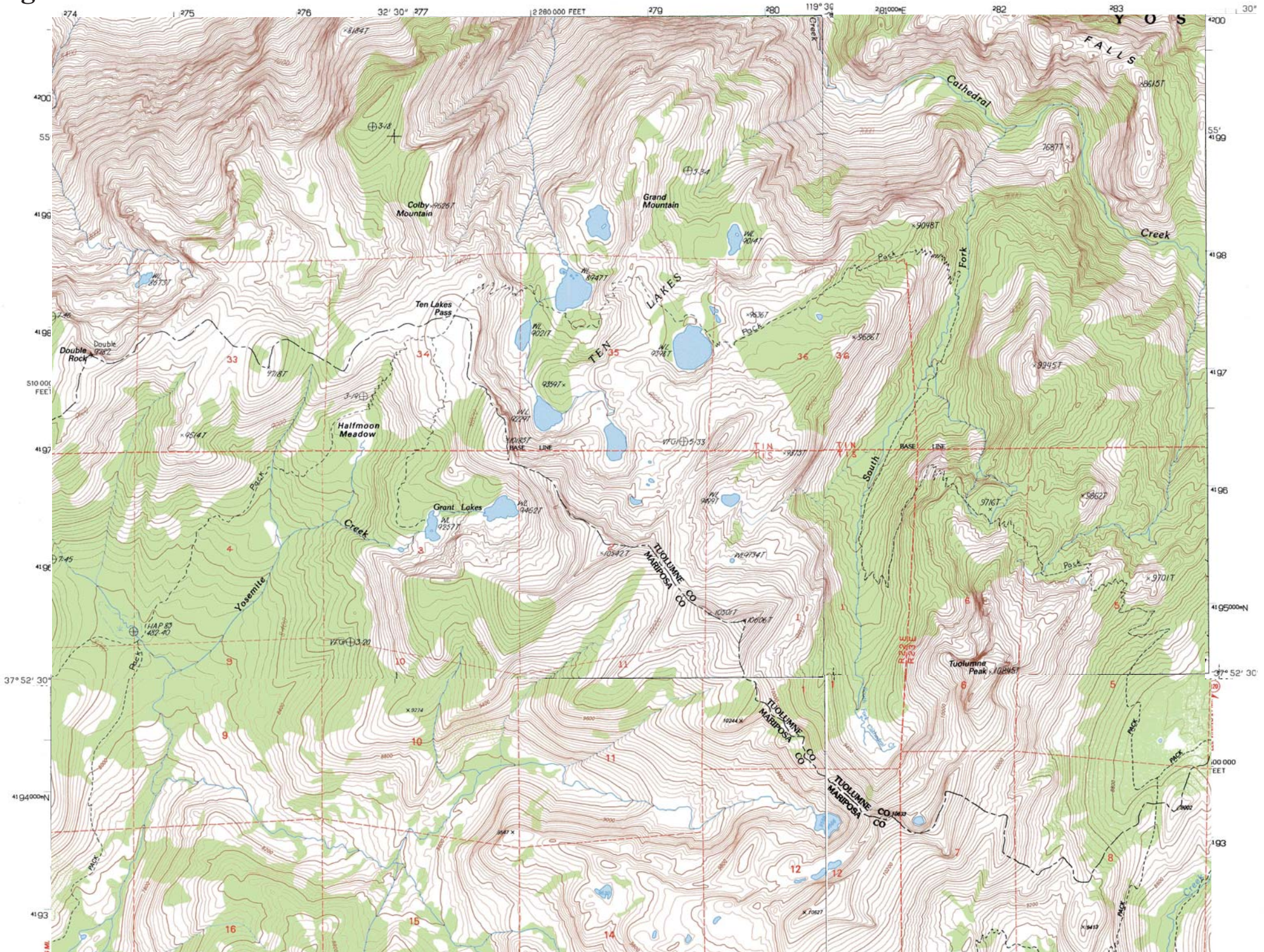
Colby Mountain
Grand Mountain
Ten Lakes Pass
TEN LAKES
Halfmoon Meadow
Grant Lakes
Double Rock
Cathedral
Creek
Fork
South
Yosemite
Creek
TUOLUMNE MARIPOSA CO
Tuolumne Peak
BASE LINE
TIN IS

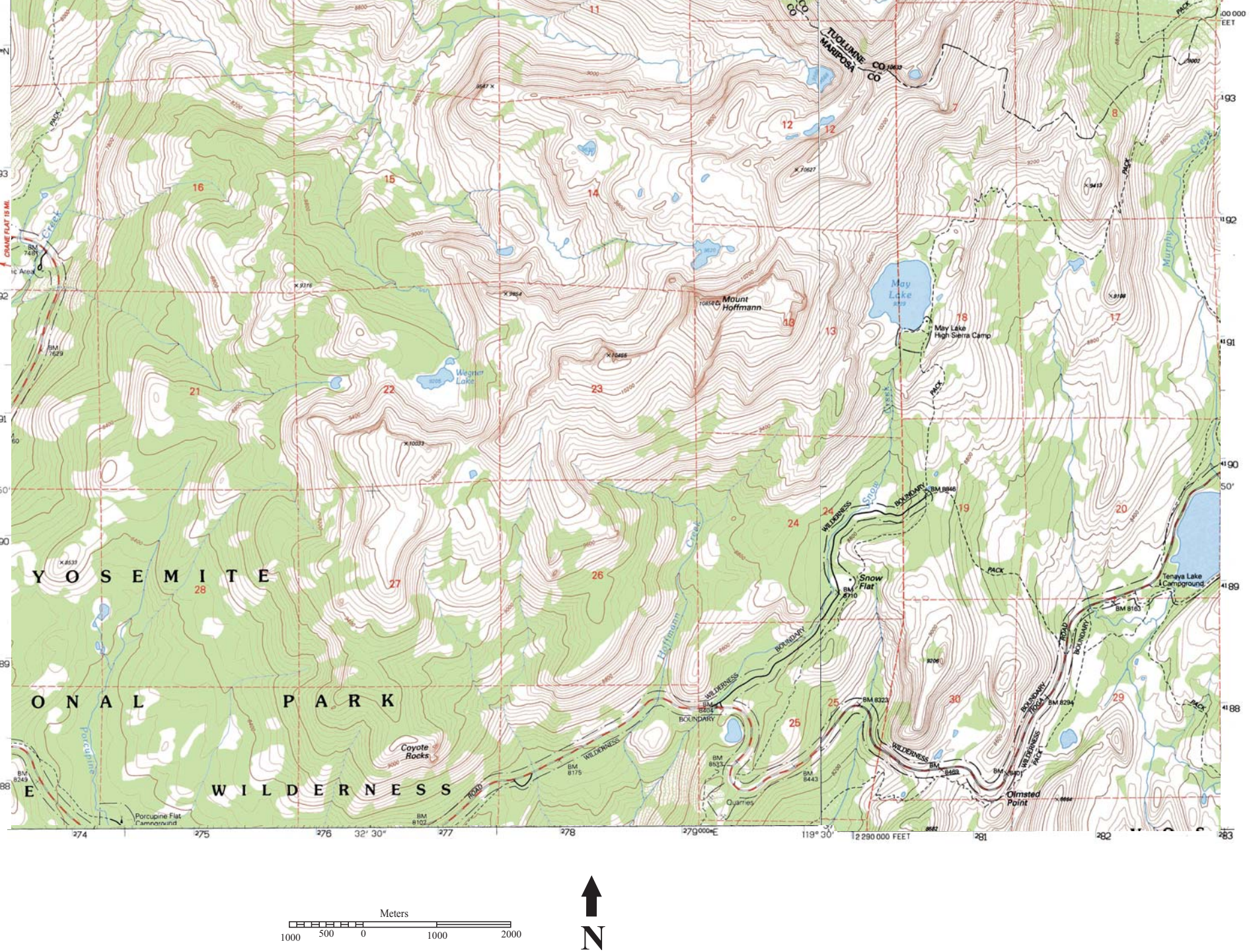
Mount Hoffmann
May Lake
May Lake High Sierra Camp
Wegner Lake
Snow Flat
Tenaya Lake Campground
Olmsted Point
Coyote Rocks
Porcupine Flat Campground
Quarries
Hoffmann Creek
Murphy Creek
Porcupine Creek
CRANE FLAT 15 MI.
TUOLUMNE
MARIPOSA
CO
WILDERNESS
BOUNDARY
ROAD
PACK
Y O S E M I T E
O N A L P A R K
E W I L D E R N E S S
Meters
1000 500 0 1000 2000
N

Figure 3.2(a)

Geological Map of Ten Lakes and vicinity

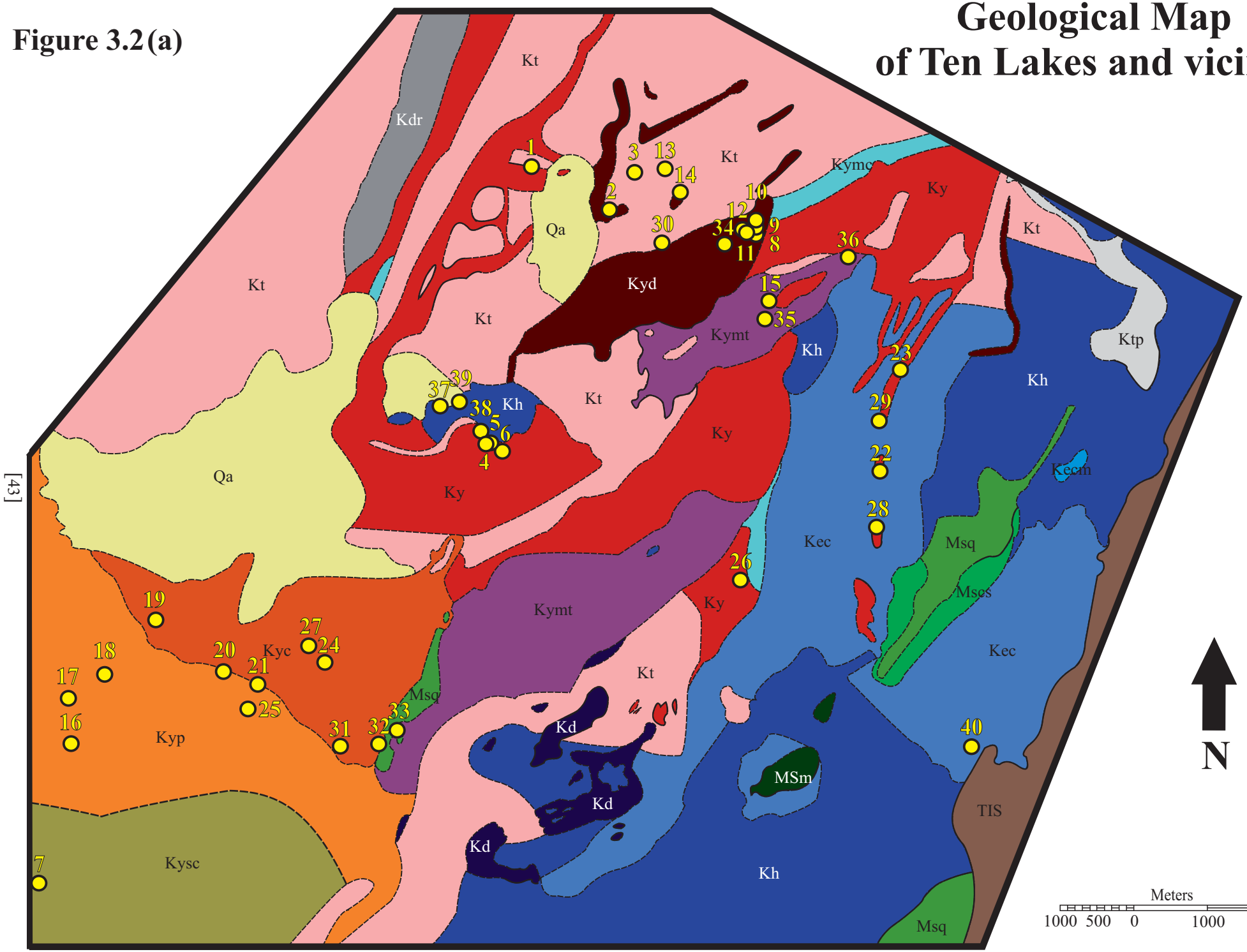

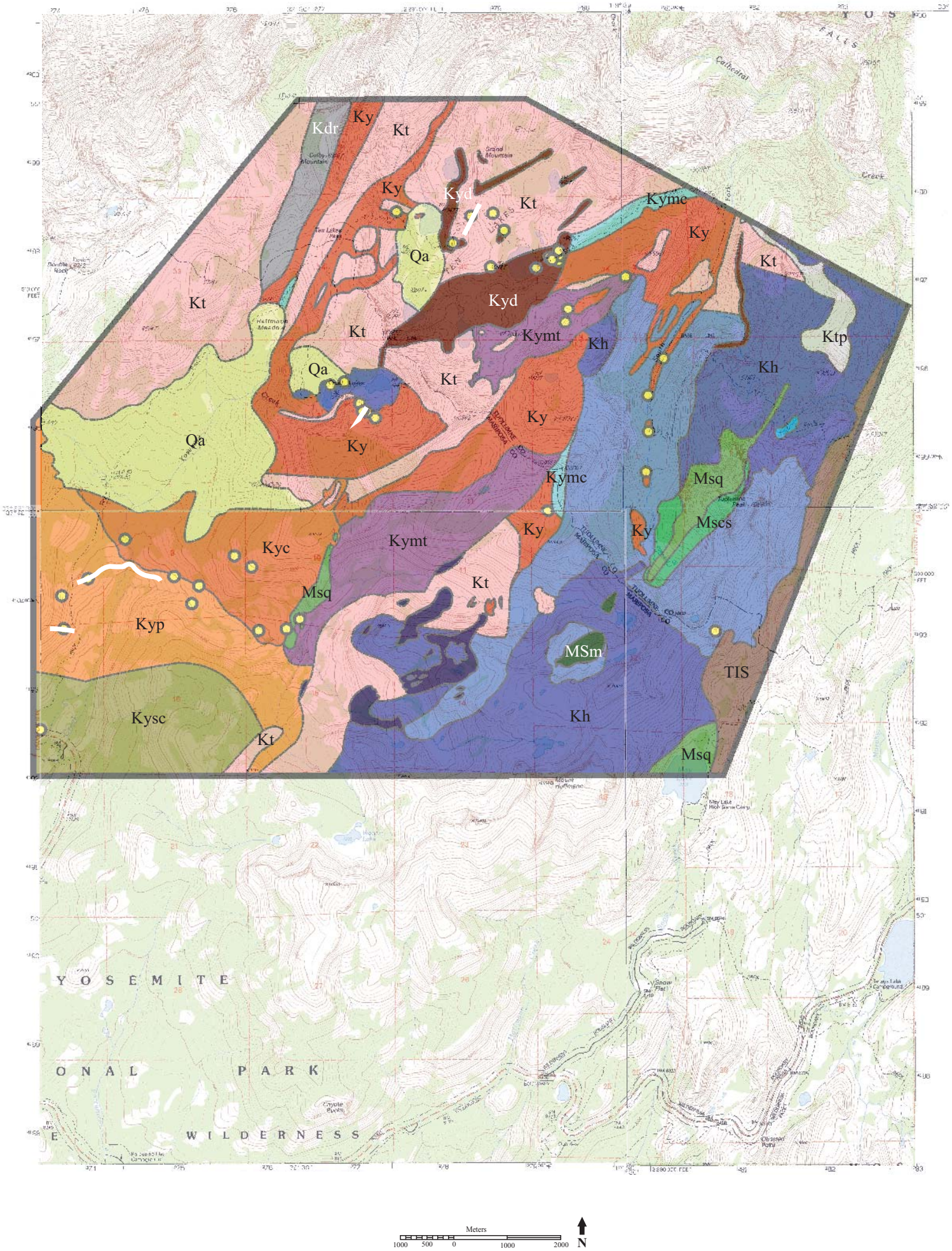
Kdr
Ky
Kt
Kyd
Qa
Kymc
Kymt
Kh
Ktp
Msq
Mscs
Kyc
Kyp
Kysc
MSm
TIS
Meters
1000 500 0 1000 2000
N
YOSEMITE
WILDERNESS

(b)

(c)

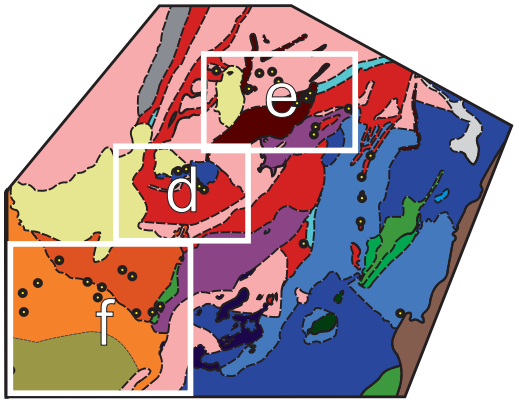
e
d
f

(d)

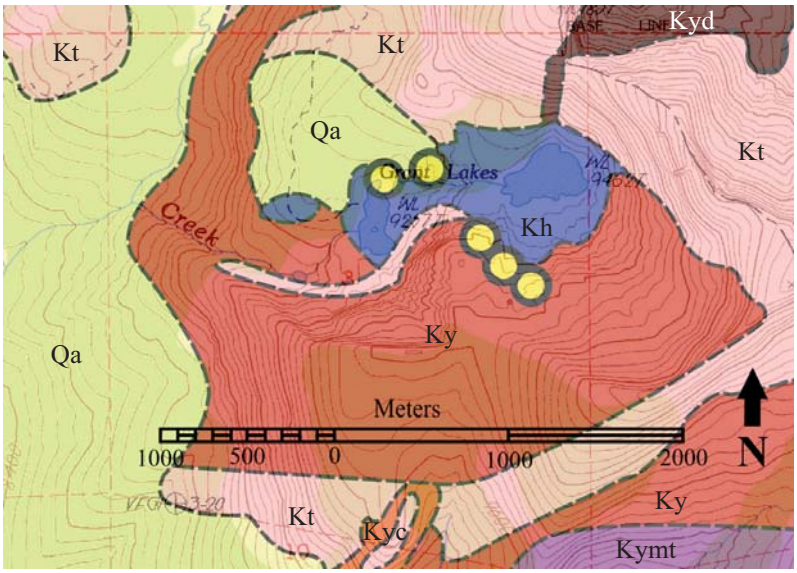
Kyd
Kt
Kt
Qa
Kt
Creek
Kh
Ky
Qa
Meters
1000
500
0
1000
2000
N
Ky
Kt
Kyc
Kymt

(e)

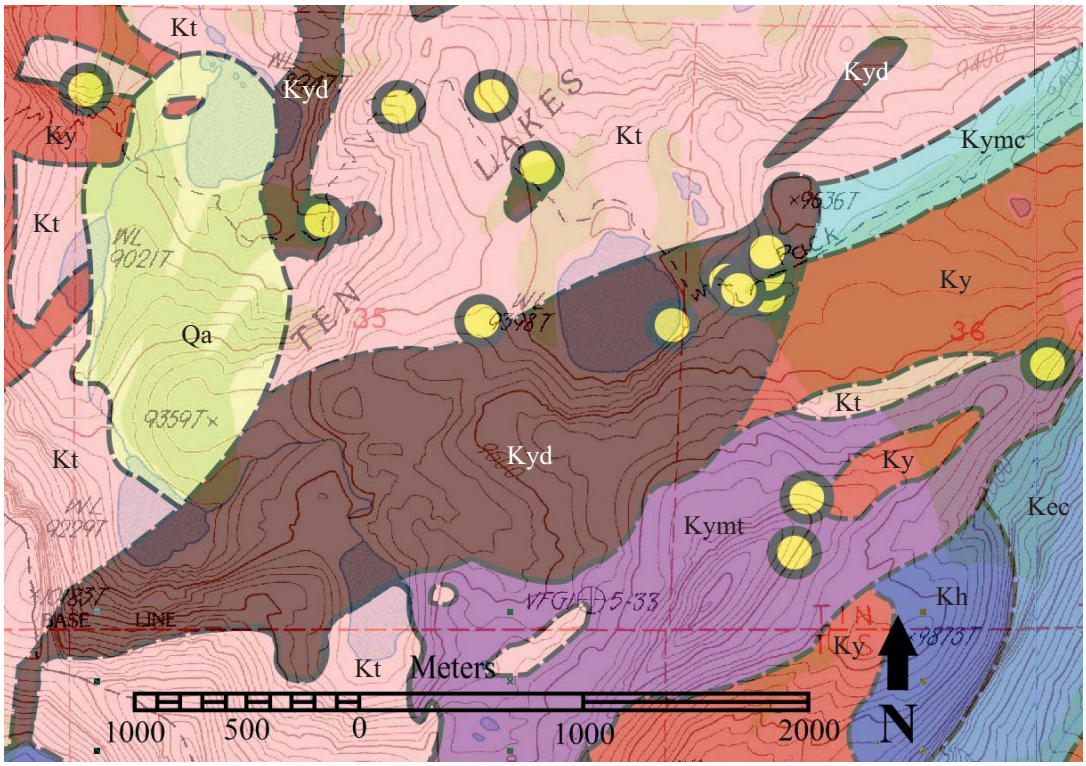
Kt
Kyd
Ky
LAKES
Kt
Kyd
Kymc
Kt
Ky
Qa
Kt
Kyd
Ky
Kt
Ky
Kec
Kymt
Kh
Ky
Kt
Meters
1000
500
0
1000
2000
N

(f)

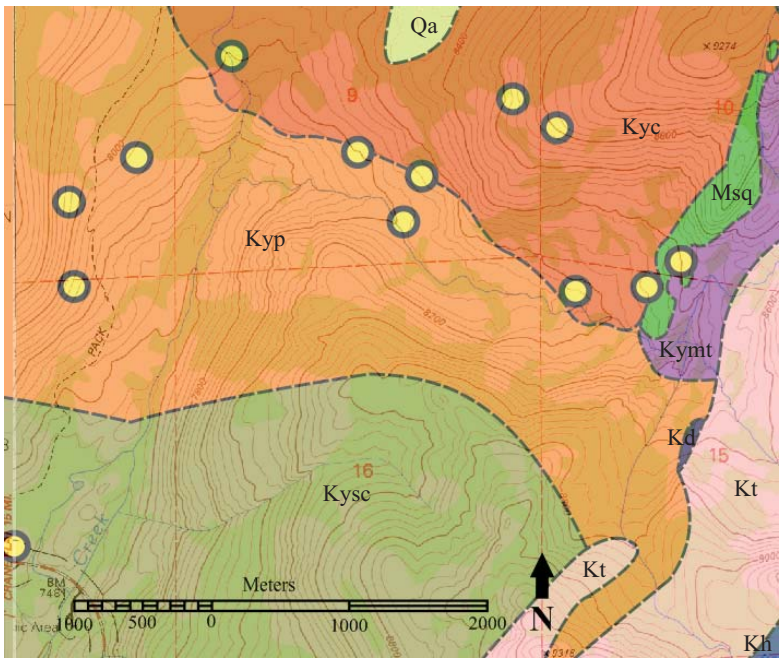
Qa
Kyc
Msq
Kyp
Kymt
Kd
Kysc
Kt
Meters
1000
500
0
1000
2000
N
Kt
Kh

Legend:
Geological Map of Ten Lakes and vicinity

Qa — Quaternary Alluvium

TIS — Tuolumne batholith

Unit contact

Approximate unit contact

Yosemite Sentinel Granodiorite

Kysc — Transitional Yosemite Sentinel Granodiorite - Yosemite Creek Granodiorite

14 — Sample location with reference number to sample name

Yosemite Creek Granodiorite

YC

Kyd — diorite to hornblende-rich diorite

Ky — fine to medium grained quartz monzodiorite to granodiorite

Kyc — Coarse-grained granodiorite

Kyp — Porphyritic granodiorite

Kymt — Myriad zone intruding Taft Granite

Kymc — Myriad zone intruding Taft and El Capitan Granites

Ktp — Granodiorite North of Tuolumne Peak

Yosemite Valley Intrusive Suite

YVIS

Kt — Taft Granite

El Capitan Granite (105 - 102 Ma)

Kd — Diorite

Kh — Mt. Hoffman Granodiorite

Kdr — Double Rock Granodiorite

Kec — Equigranular Granite

Kecm — Medium-graained Granite

Metasedimantary unites

Msq — Quartzite

Mscs — Calc-Silicate

MSm — Marble

Map number corresponding to sample name

1	BL-1	21	BL-18
2	BL-2	22	05E SJSU
3	BL-3	23	05G SJSU
4	BL-4	24	11C SJSU
5	BL-5	25	11F SJSU
6	BL-6	26	19J SJSU
7	BL-7	27	20B SJSU
8	BL-8A/D	28	23B SJSU
9	BL-8B	29	24A SJSU
10	BL-8C	30	25B SJSU
11	BL-8E/F	31	31C SJSU
12	BL-9	32	31I-2 SJSU
13	BL-10	33	31H SJSU
14	BL-11	34	33F SJSU
15	BL-12	35	34C SJSU
16	BL-13	36	35I SJSU
17	BL-14	37	37A SJSU
18	BL-15	38	37D SJSU
19	BL-16	39	37G SJSU
20	BL-17	40	40B SJSU

Figure 3.3

Field pictures to illustrate field relations near Grant Lakes. Hammer and/or two Euro coin for scaling.

(a) Location: near sample 4. Granitic angular xenoliths (Taft Granite) in a foliated quartz monzodiorite. Xenoliths fall apart in to lose minerals, see lowest square and (c). Upper square indicate location of schlieren, figure (b). Lowest square indicates figure (c). **(b)** Schlieren near the margin of a granitic xenoliths (xenoliths left of figure). **(c)** String of minerals originated out of the granitic xenoliths. Upper arrow indicates location of xenoliths. Lower arrow indicates lower part of the mineral string. **(d)** Location: vicinity of sample 5. Fine grained granodiorite sheet of 15 meters in width and at least 80 meters in length intruding into the fine grained quartz monzodiorite to granodiorite unit. Yellow dashed lines indicate the boundaries of the sheet. **(e)** Location near sample 6. Contact relation of sheet (d) with surrounding lithology. Veins and dykes originate out of the sheet, indicated by red arrows. Yellow dashed line indicates the boundary of the sheet, sheet is the lower part of the figure. **(f)** Location near sample 6. Mafic minerals are clusters of biotite. Right side of dashed yellow line is a granitic xenoliths (Taft Granite). Mafic zone can be interpreted as a cross-section of a schlier. **(g)** Location: near sample 5. Quartz monzodiorite to granodiorite with granitic xenoliths (most left and most right arrow) and hornblende-rich diorite enclaves (middle two arrows). A horizontal and a vertical (indicated by the hammer) granite dyke which intrudes the large granitic xenoliths. **(h)** Location: near sample 5. Stretched granitic enclaves in fine grained quartz monzodiorite to granodiorite unit, red arrow. **(i)** Location: near sample 6. Granitic xenoliths (Taft Granite) in fine grained quartz monzodiorite to granodiorite unit. **(j)** Location: near sample 5. Stretched granitic enclaves in fine grained quartz monzodiorite to granodiorite unit

Figure 3.3

(a)

(b)

(c)

(d)

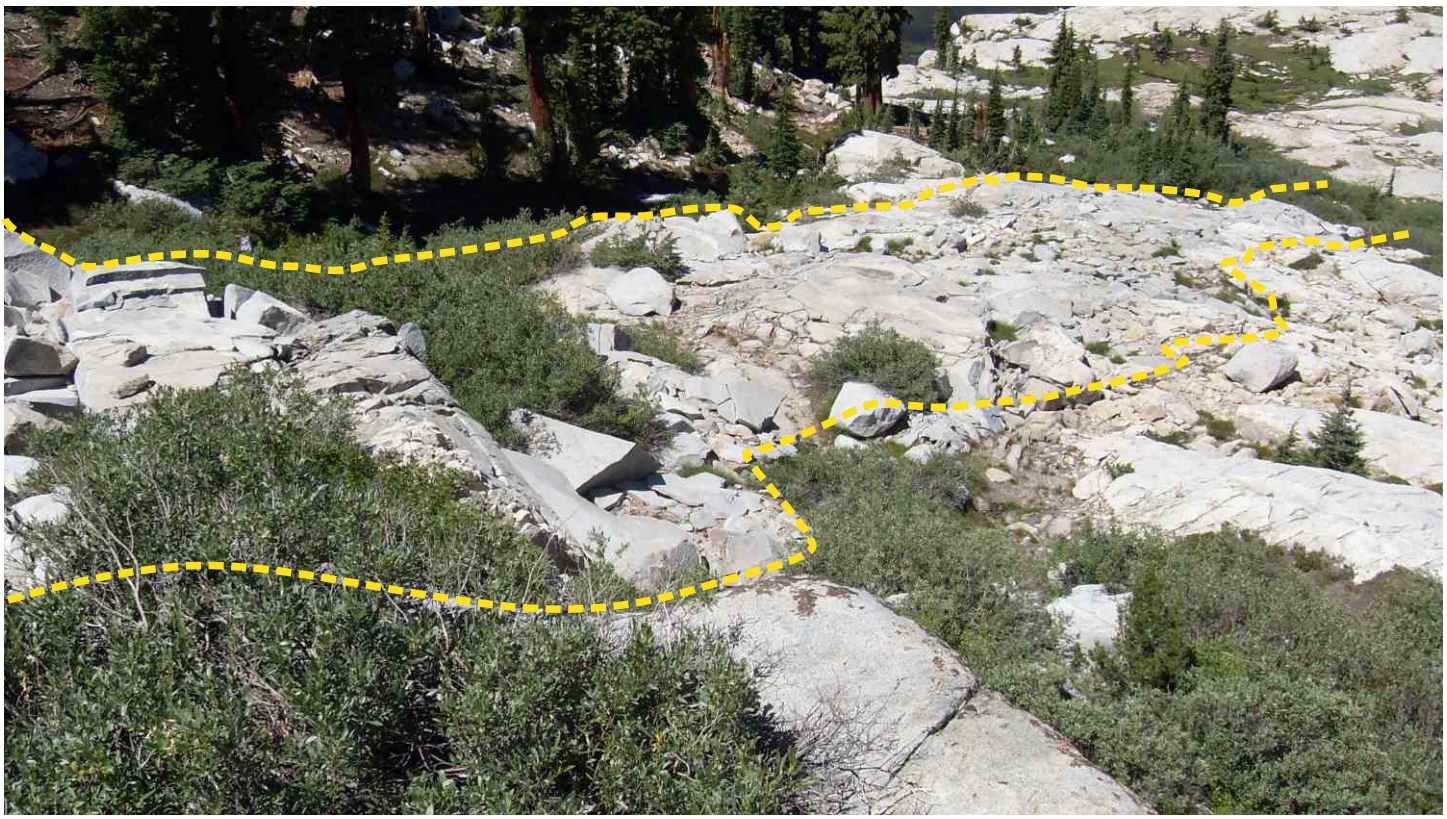

(e)

(f)

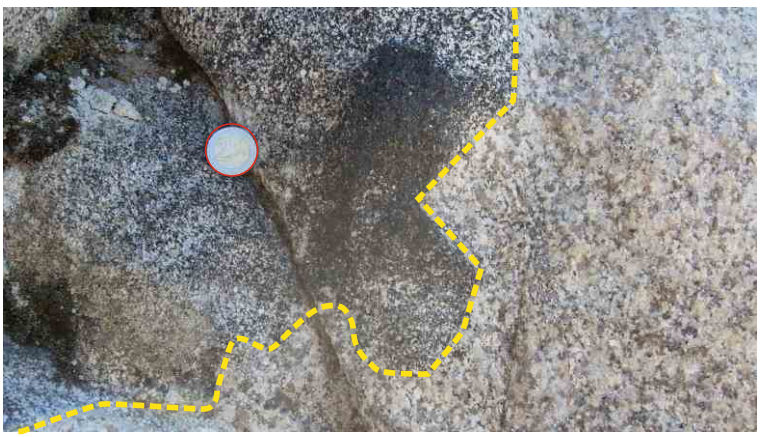

(g)

(h)

(i)

(j)

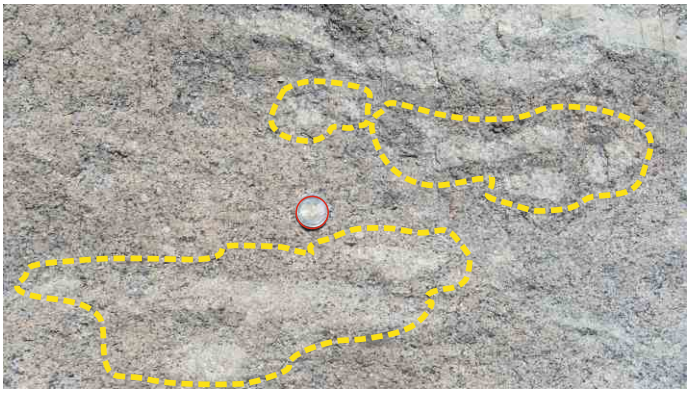

Figure 3.4

Field pictures to illustrate field relations near Ten Lakes. Hammer and/or two Euro coin for scaling.

(a) Location: sample 3. Total outcrop is viewed by figures (a), (b), (c) and (d). View (a) is to the North. Envisioned is a granodiorite dyke (yellow dashed lines) intruding into the Taft Granite. Contact is sharp. Diorite originate out of a granodiorite body viewed at the lower part of figure (a) (near the back-pack) and in figure (b). **(b)** Same outcrop as (a), view to the South. Location of the hammer indicates the granodiorite lithology. Upper red arrow indicates mafic enclaves (diorite to hornblende-rich diorite). Lower arrow indicates felsic zone with large (up to 2 cm) needle hornblendes. **(c)** Same outcrop as (a), view is a close-up of the granodiorite dyke. Location of (c) in (a) is the location where the people are standing. View is to the East. **(d)** Same outcrop as (a). Location is at the right edge of (b). A granitic dyke is illustrated in the yellow dashed lines. Dominant lithology is diorite to hornblende-rich diorite. **(e)** Location: sample 6. Viewed is a contact relation between the medium grained quartz monzodiorite to granodiorite unit and diorite to hornblende-rich diorite unit. In this particular outcrop the lithologies are granodiorite and porphyritic diorite. Contact relations: granodiorite intrudes into the diorite, dyke most right arrow; Granodiorite enclave in diorite, upper arrow; lower two arrows indicting diorite enclaves in the granodiorite. **(f)** Location: Myriad zone, roughly 200 to 300 meters West of sample location 12. Viewed are xenoliths of the diorite to hornblende-rich diorite unit in the medium grained quartz monzodiorite to granodiorite unit. Indicated by yellow dashed lines and red arrows are late stage leucogranitic intrusions. **(g)** Location: near sample 8. Lithology porphyritic diorite (diorite to hornblende-rich diorite unit) is intruded by porphyritic granodiorite (medium grained quartz monzodiorite to granodiorite), indicated by yellow dashed lines. Upper three arrows indicating porphyritic granodiorite enclaves in the porphyritic granodiorite. The lower arrows indicates a porphyritic diorite enclave in the porphyritic granodiorite. **(h)** Location: most North of sample location BL-8. Indicated is the contact relation between the Taft Granite and the quartz monzodiorite to granodiorite unit. Granitic strings originated out of the Taft Granite move into the granodioritic lithology. String composition is felsic. When increasing distance from the contact margin the felsic strings can be as thick as a single mineral. **(i)** Location: Sample BL-10. Lithologies viewed: left side of the figure is granitic (Taft Granite) and the right side of the figure is granodioritic (medium grained quartz monzodiorite to granodiorite unit). Envisioned are stretched enclave-like features (indicated by arrows) of granitic material in the granodiorite. **(j1)** Location: Sample BL-11. Lithologies viewed: left side of the figure is granitic (Taft Granite) and the right side of the figure is granodioritic (medium grained quartz monzodiorite to granodiorite unit). Shown is a early stage of xenolith formation. The granodiorite intrudes into the granite whereby the granite falls apart in a xenoliths and xenolithic minerals. Arrow indicated location of (j2). **(j2)** Location: Sample BL-11. Xenolith formation of Taft Granite in medium grained quartz monzodiorite to granodiorite unit. From left to right (see arrows) a mixing zone of granitic minerals and granodioritic minerals. Density of granitic minerals decreases to the right. **(k)** Location: sample location near BL-8. Quartz monzodiorite to granodiorite enclaves or xenoliths surrounded by (leuco)granitic lithology. **(l)** Location: near contact boundary between Kymt and Kyd, between sample BL-8 and BL-12. Medium grained quartz monzodiorite to granodiorite unit intruded the diorite to hornblende-rich diorite unit. Dyke between yellow dashed lines. Arrow indicates quartz monzodiorite to granodiorite enclaves. **(m)** Location: sample BL-8. Diorite to hornblende-rich diorite enclaves in medium grained quartz monzodiorite to granodiorite unit with crenulated contact. **(n)** Location: sample BL-8. Diorite to hornblende-rich diorite unit and the medium grained quartz monzodiorite to granodiorite unit with crenulated contact. **(o)** Location: sample BL-1. Cross-section of a diorite to hornblende-rich diorite dyke and consist mostly out of enclaves. Directly surrounding lithology is granodioritic. Dyke is located in a Taft Granite are. **(p)** Location: near sample BL-12, Myriad zone. Leucogranitic dykes intruding into a granodiorite. **(q)** Location: sample BL-10. diorite dyke intruding Taft Granite. Length of dyke is over 200 meters. **(r)** Location: sample BL-8. Diorite to hornblende-rich diorite unit which is intruded by a thick granitic dyke (red arrow) and diorite dyke (yellow dashed lines). **(s1)** Location: Sample BL-8. Horizontal granitic dyke (yellow dashed lines) in the diorite to hornblende-rich diorite unit. **(s2)** Location: Sample BL-8. Granitic dykes (e.g. red arrow) in the diorite to hornblende-rich diorite unit. **(t)** Location: Kymt, 200 to 300 meters West of sample BL-12. Diorite to hornblende-rich enclaves (red arrow) in medium grained quartz monzodiorite to granodiorite. Leucogranitic dyke intruding both (yellow dashed lines). **(u)** Location: near (p). Magmatic relation unclear. Leucogranitic zones and quartz monzodiorite to granodiorite zone (dyke?). Arrow indicates small leucogranitic dyke. **(v)** Location: near (t). Quartz monzodiorite to granodiorite enclave/xenoliths/dyke? (blue dashed lines) in diorite to hornblende-rich diorite unit. Both units are intruded by leucogranitic dyes. **(w)** Location: near (t). Angular quartz monzodiorite to granodiorite enclaves in granitic lithology (Taft Granite?). **(x)** Location: near (t). Diorite to hornblende-rich diorite enclaves (yellow dashed lines) in leucogranitic lithology. One enclave is cross-cut by a leucogranitic dyke (red dashed lines). Granitic xenoliths surrounded by mafic minerals (blue dashed lines).

(y1) Location: Sample BL-10. Granitic dyke of 1.5 m thick and 40 meters in length (yellow dashed lines). Direction of dyke: strike 030°NE and dipping near vertical. Pegmatite dyke near horizontal (blue dashed lines). Dyke contains granitic (Taft Granite) xenoliths, see (y2). **(y2)** Location: sample location BL-10. Taft Granite xenoliths in granitic dyke (y1) which intruded the Taft Granite unit with sharp contacts. **(z1)** Location: (h). Contact between the medium grained quartz monzodiorite to granodiorite unit and the Taft Granite (lower felsic part of figure). Indicated by the red arrow are schlieren in the medium grained quartz monzodiorite to granodiorite unit. **(z2)** Location: One meter to the right of (z1). Schlieren at the left side of the figure or also seen in (z1). Red arrow indicates a medium grained quartz monzodiorite to granodiorite dyke in the Taft Granite.

Figure 3.4

(a)

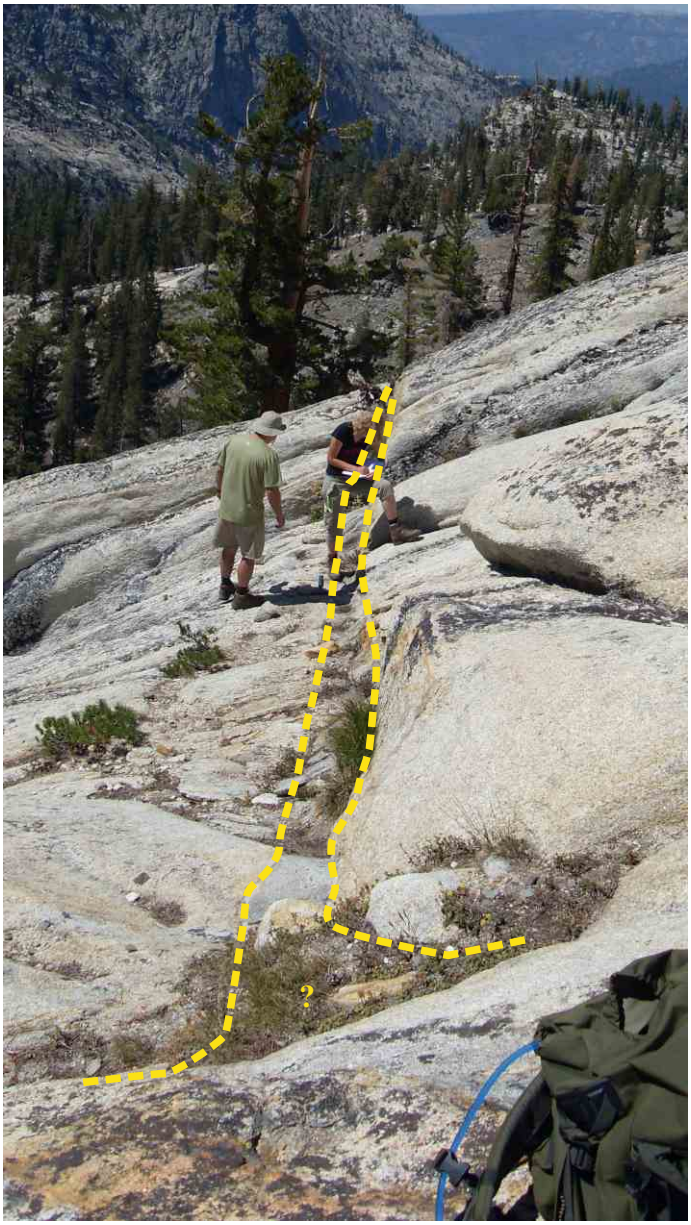

(b)

(c)

(d)

(e)

(f)

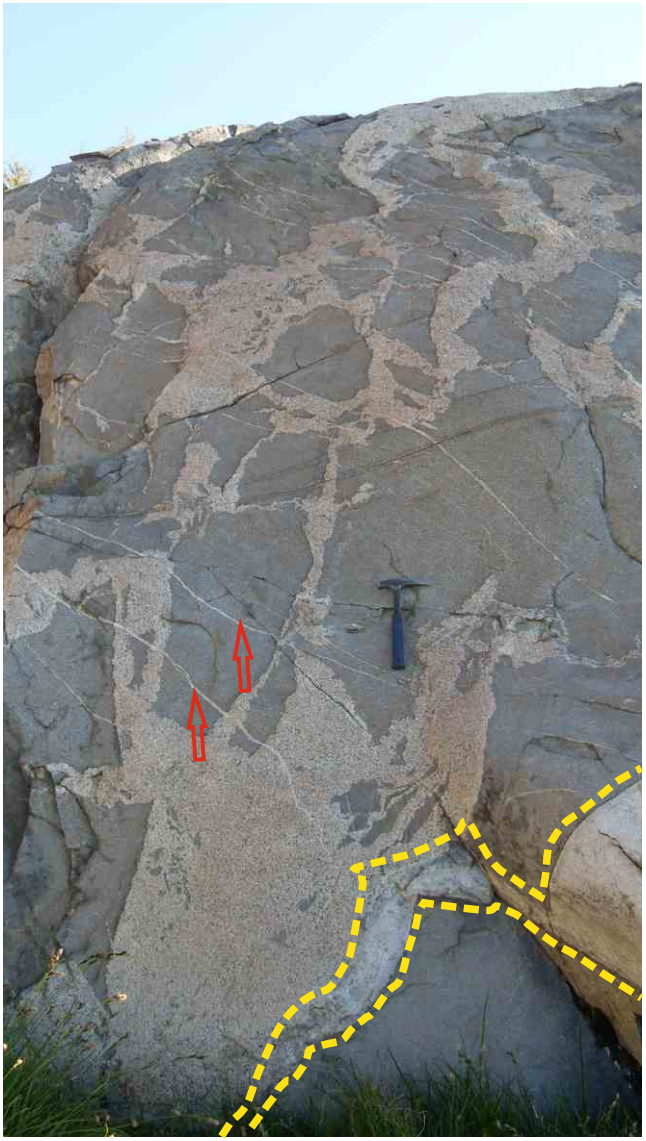

(g)

(h)

(i)

(j1)

(j2)

(k)

(l)

(m)

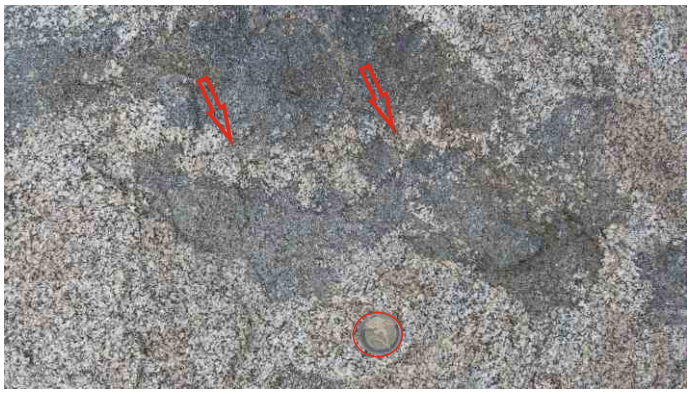

(n)

(o)

(p)

(q)

(r)

(s1)

(s2)

(t)

(u)

(v)

(w)

(x)

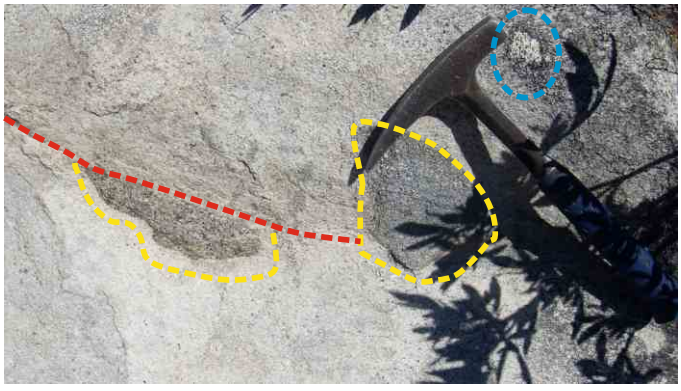

(y1)

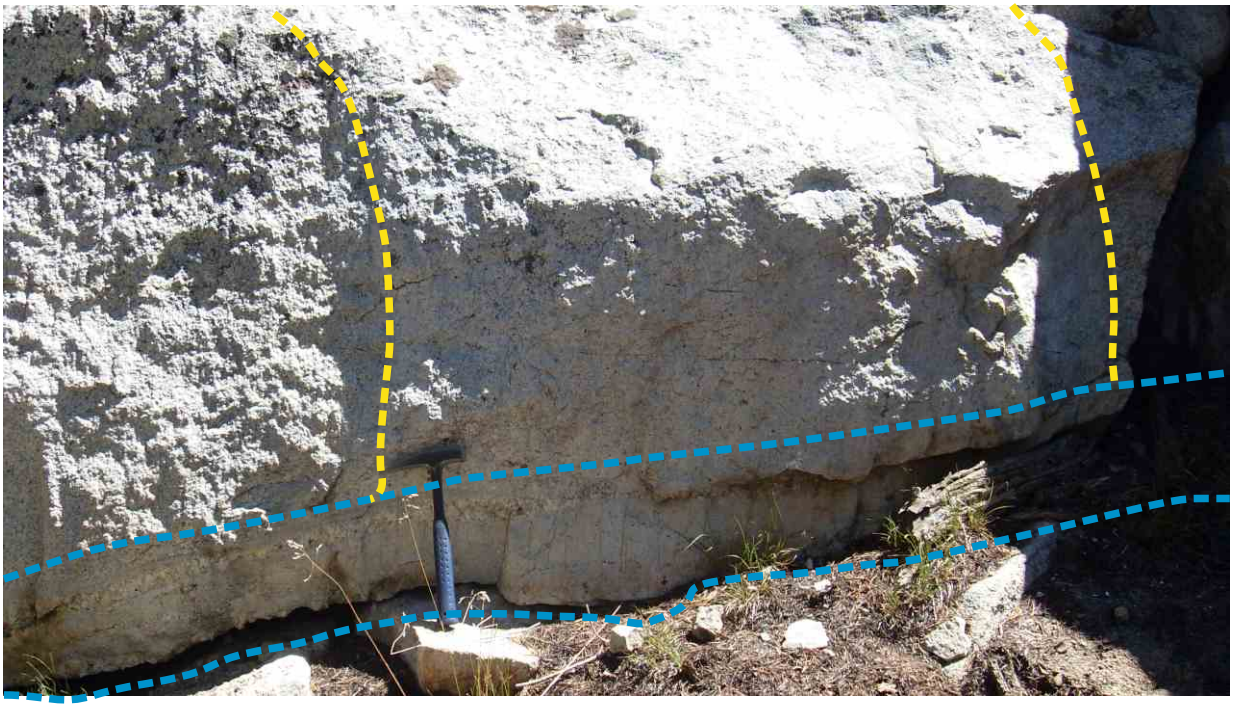

(y2)

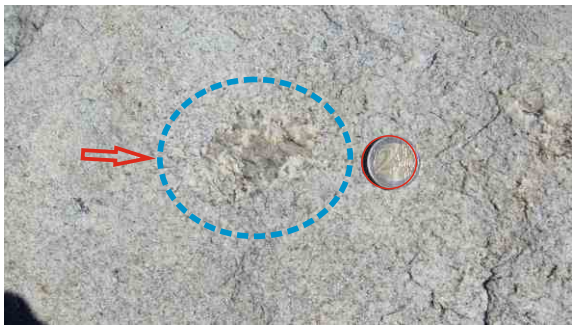

(z1)

(z2)

Figure 3.5

Field pictures to illustrate field relations in the Porphyritic Granodiorite Unit. Hammer and/or two Euro coin for scaling.

(a) Location: Sample location BL-13. Viewed is the margin of a diorite to hornblende-rich monzodiorite sheet in Porphyritic Granodiorite. Lower red arrow indicated granodioritic material that intrudes into the hornblende-rich monzodiorite sheet. The upper red arrow indicates a hornblende-rich monzodiorite enclave. Between the two yellow dashed lines is a zone envisioned where enclaves "fall off" the mafic sheet into the Porphyritic Granodiorite. **(b)** Location: near (a). Cross-section view at the margin of the sheet. Red arrow indicates a enclave. The yellow dashed lines indicate a pegmatite dyke which follows the margin of the mafic sheet and enclaves. **(c)** Location: sample location BL-14. Between the yellow dashed lines a enclave swarm is indicated in the Porphyritic Granodiorite Unit. These enclaves are interpreted as one hornblende-rich diorite dyke that fell-out into enclaves. Most enclaves incorporated quartz and feldspar phenocrysts, see thin-sections Figure 3.6 sample BL-14 and (e). **(d)** Location: sample location BL-13. Small slightly stretched hornblende-rich diorite enclave in porphyritic granodiorite. **(e)** Location: sample location BL-14. Hornblende-rich diorite enclave with feldspar and quartz phenocrysts in porphyritic granodiorite. **(f)** Location: sample location BL-13. Hornblende-rich diorite sheet with granodioritic enclaves, indicated by the red arrow. **(g)** Location: sample location BL-13. Fine grained hornblende-rich monzodiorite sheet with a felsic zone, indicated by yellow dashed line. This felsic zone is interpreted as a xenolith. **(h)** Location: sample location BL-13.The fine grained hornblende-rich monzodiorite sheet with a granodioritic xenoliths (or intrusion). **(i)** Location: sample location BL-13; view to the North. The fine grained hornblende-rich monzodiorite sheet is intruded by a diorite dyke. This dyke intrudes in the hornblende-rich monzodiorite and the porphyritic granodiorite intrusions which are situated within the hornblende-rich monzodiorite sheet. This diorite dyke is originated out of the Porphyritic Granodiorite Unit, (j). **(j)** Location: (i), view to the South. Diorite dyke in porphyritic granodiorite. Yellow dashed lines indicate the dyke. This dyke probably originate from the question mark area and intrudes through the porphyritic granodiorite into the hornblende-rich monzodiorite sheet (i). **(k)** Location: sample location BL-15. Leucogranitic dyke that stretches for several hundreds of meters in the Porphyritic Granodiorite Unit. The margins of this dyke are leucogranitic. The inner part of the dyke is a hornblende-rich quartz monzodiorite. The leucogranitic contact with the host rock is sharp. The contact between the leucogranite and quartz monzodiorite is co-magmatic, (l), (n), (o). **(l)** Location: (k), 200-300 meters more to the East. Same leucogranitic dyke with the inner-dyke of quartz monzodiorite. Red arrow indicates felsic strings or enclaves originated from the leucogranitic margins. **(m)** Location: (l), 200 meters more to the East. Same dyke as (k) and (l) only thinner and the inner quartz monzodiorite almost disappears and fades-out. Upper red arrow indicates the fading quartz monzodiorite. The Lower red arrow indicates enclaves that are cross-cut by the leucogranitic dyke. **(n)** Location: (k). Same dyke as (k). Leucogranitic contact with the quartz monzodiorite. Crenulated contact (red arrow) and felsic strings originated out of the leucogranitic margin. **(o)** Location: (k). Same dyke as (k). Viewed are the felsic minerals near the contact between the leucogranitic margin and the quartz monzodiorite (left red arrow). Right red arrow indicates a mafic enclave near a felsic enclave within the inner quartz monzodiorite. **(p)** Location: sample location BL-16. A porphyritic granodiorite dyke in the coarse-grained granodiorite unit. Dyke indicated by dashed yellow lines. **(q)** Location: roughly 100 meters South of sample location BL-17. A "mafic" enclave swarm with varies compositions in the Porphyritic Granodiorite Unit. Upper arrow indicates a felsic enclave, roughly similar as the host rock. Middle arrow indicates a porphyritic felsic enclave which is granodioritic in composition. Most lower arrow indicates a hornblende-rich diorite enclave. **(r)** Location: near sample location BL-18. A coarse-grained granodiorite dyke or body in the Porphyritic Granodiorite Unit. **(s)** Location: near sample location BL-17. Large mafic enclave swarm in the Porphyritic Granodiorite Unit which is dominantly composed out of hornblende-rich quartz monzodiorite. Arrow indicates a felsic porphyritic transitional zone between the enclave and host rock. **(t)** Location: near sample location BL-17. A schlier with a mafic right side and a felsic left side. Near the hammer a pegmatite intrudes the schlier. **(u)** Location: near sample location BL-17. A dyke-like structure which is slightly more mafic than the porphyritic granodiorite host rock. Near the edges of this dyke-like structure mafic minerals are accumulated (upper red arrow). Lower red arrow indicates a pegmatite dyke. **(v)** Location: near sample location BL-17. A concentrically stacked schlieren complex. Arrows indicating different schlieren. **(w)** Location: near sample location BL-17. Schlieren in the Porphyritic Granodiorite Unit. Upper arrow indicates more felsic circular strings. The lower arrow indicates circular schlieren, together they form a dyke-like feature. **(x)** Location: sample location BL-18. Coarse-grained granodiorite with a swarm of small enclaves. Between the yellow dashed lines a dyke-like system is envisioned (sink-hole?). Which is partly filled by the enclave swarms and schlieren, left arrow. Right arrow indicates figure (x) and (z1). **(y)** Location: (x). Enclave swarm with a boudin-structure (arrows). **(z1)** Location: (x). A schlieren complex which is cross-cut by the dyke-like sink-hole structure of (x).

(z3) Location: (x). Arrow indicates location (z1). Yellow dashed line indicates the dyke-like structure of (x). Viewed are the cumulates of enclaves "buried" by schlieren. **(z2)** Location: sample BL-18. Swarm of enclaves (accumulate of enclaves) which are overlaid by schlieren.

Figure 3.6

Thin-sections are labeled with their sample name. The sample names are constructed out of the first letter of the family name of this author and co-worker Martine van der Linde. B = Bliekendaal; L = Linde; number refers to sample location and the last letter refers to the order of sample picking. E.g. BL-1B refers to a sample taken by this research group at site 1, second sample. Thin-sections of the sample taken by Johnson (unpublished) are archived at the SJSU and not directly available for study. Figures are on true scale.

Figure 3.5

(a)

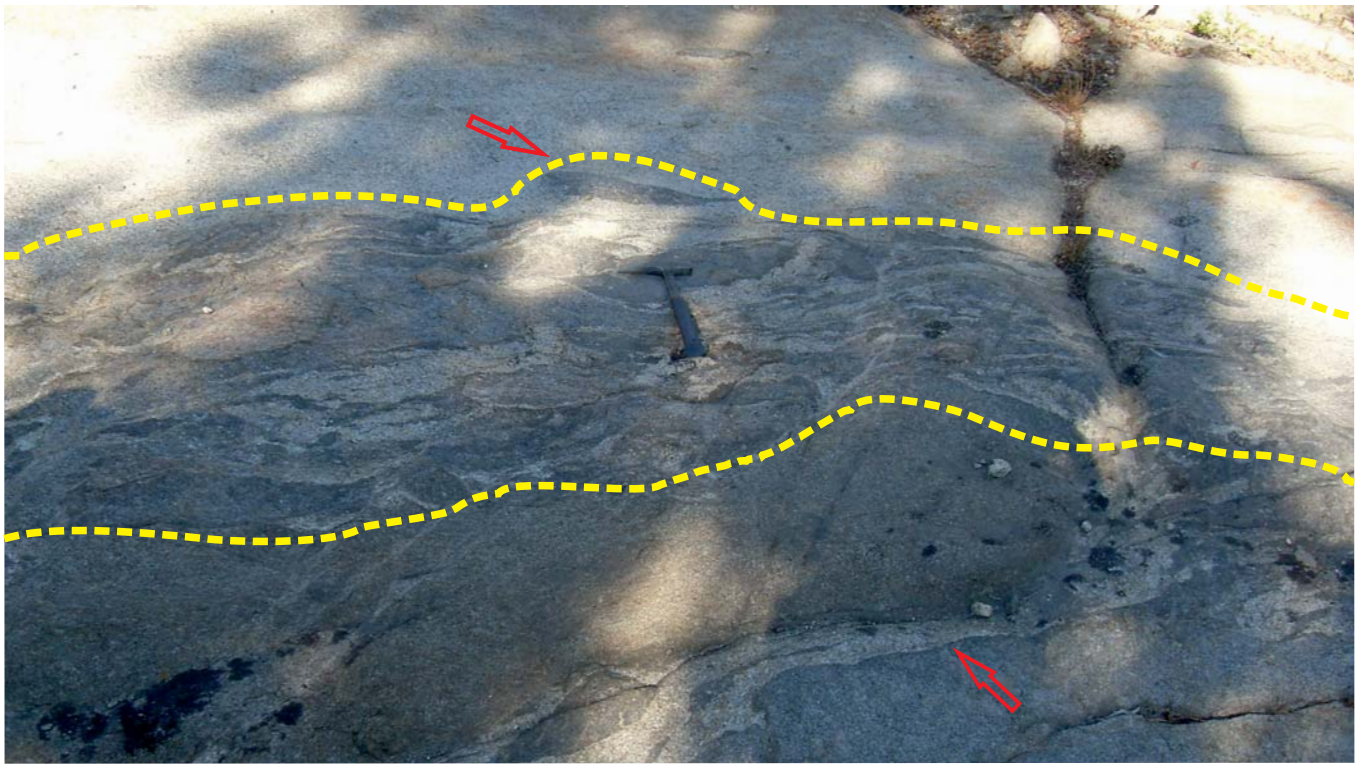

(b)

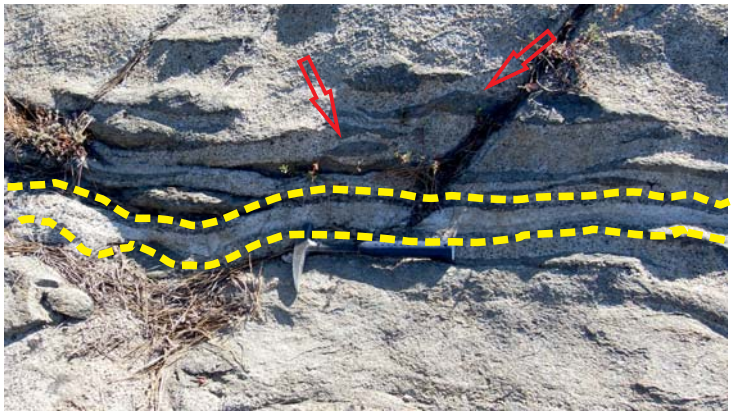

(c)

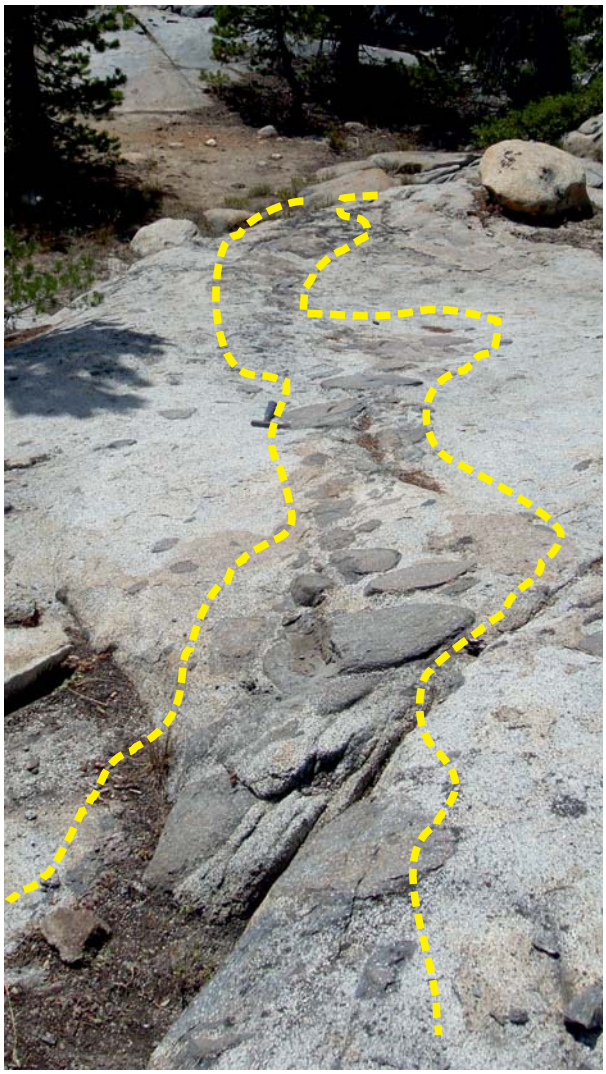

(d)

(e)

(f)

(g)

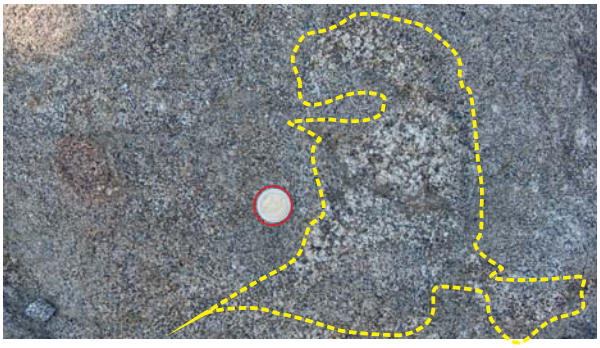

(h)

(i)

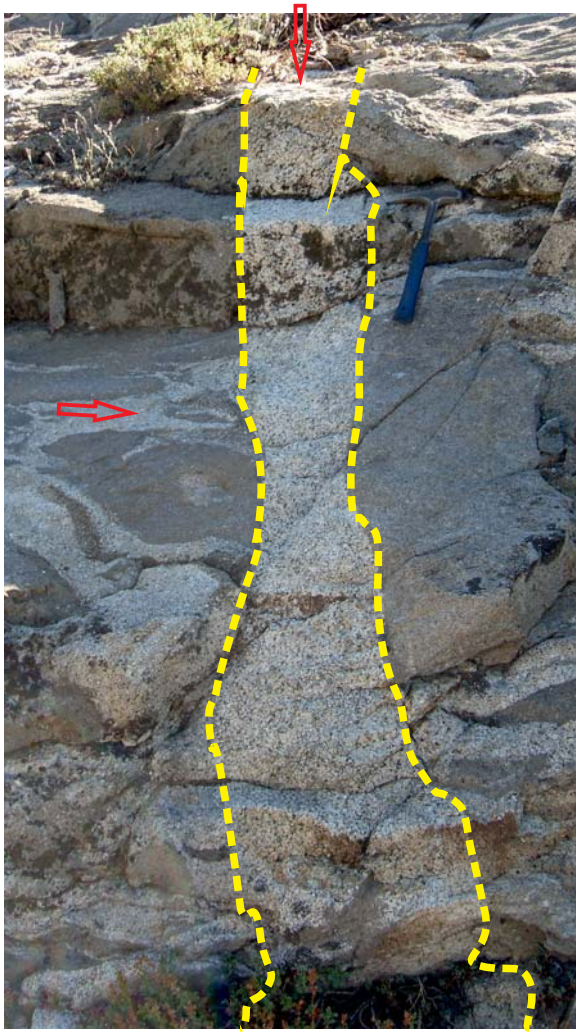

(j)

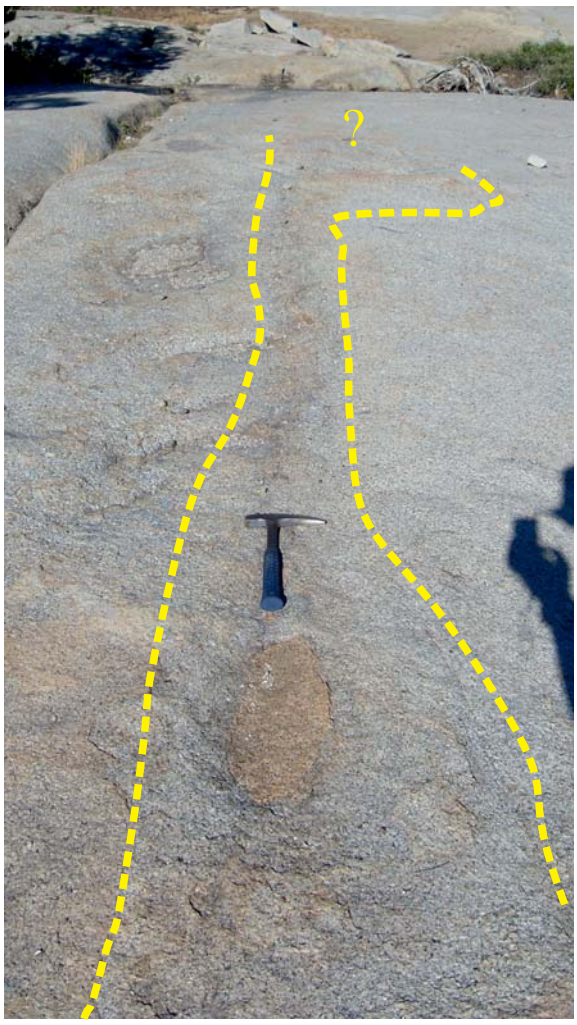

(k)

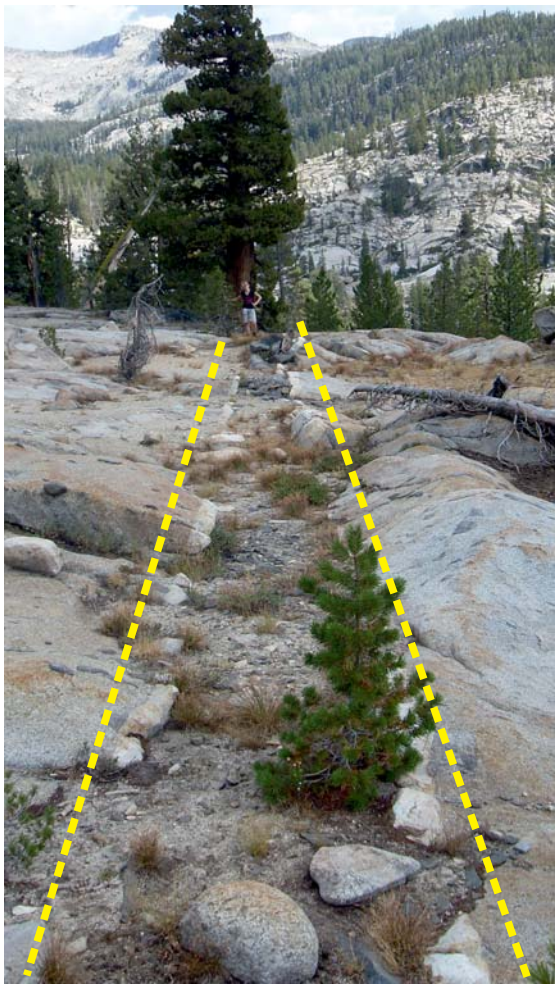

(l)

(m)

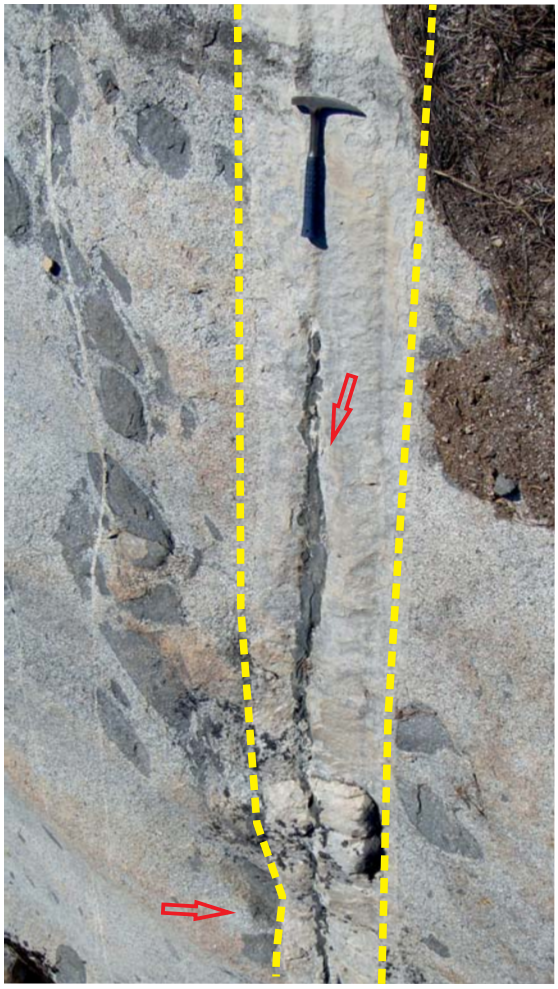

(n)

(o)

(p)

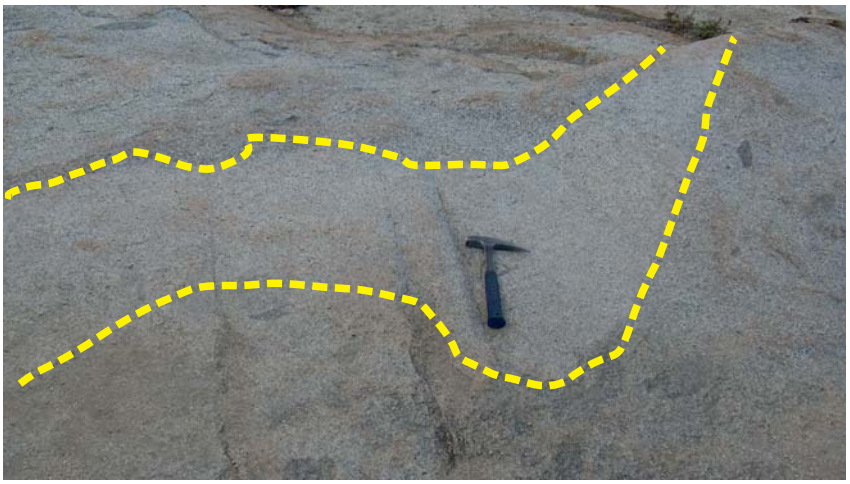

(q)

(r)

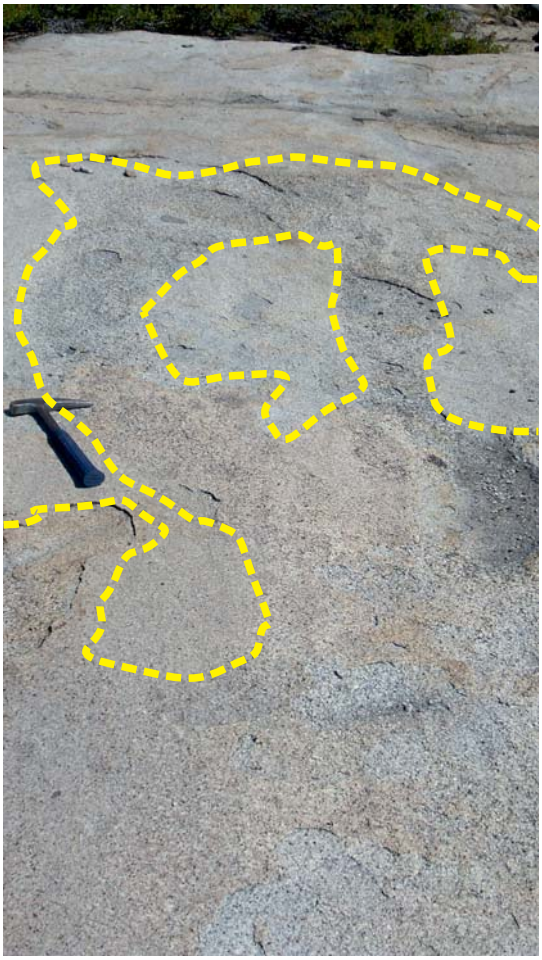

(s)

(t)

(u)

(v)

(w)

(x)

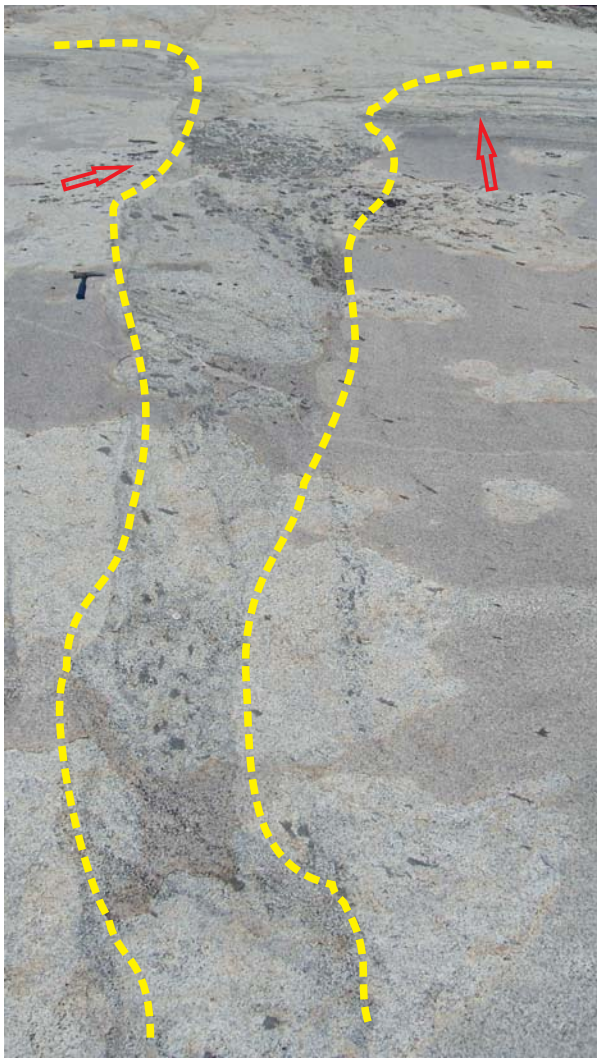

(y)

(z1)

(z2)

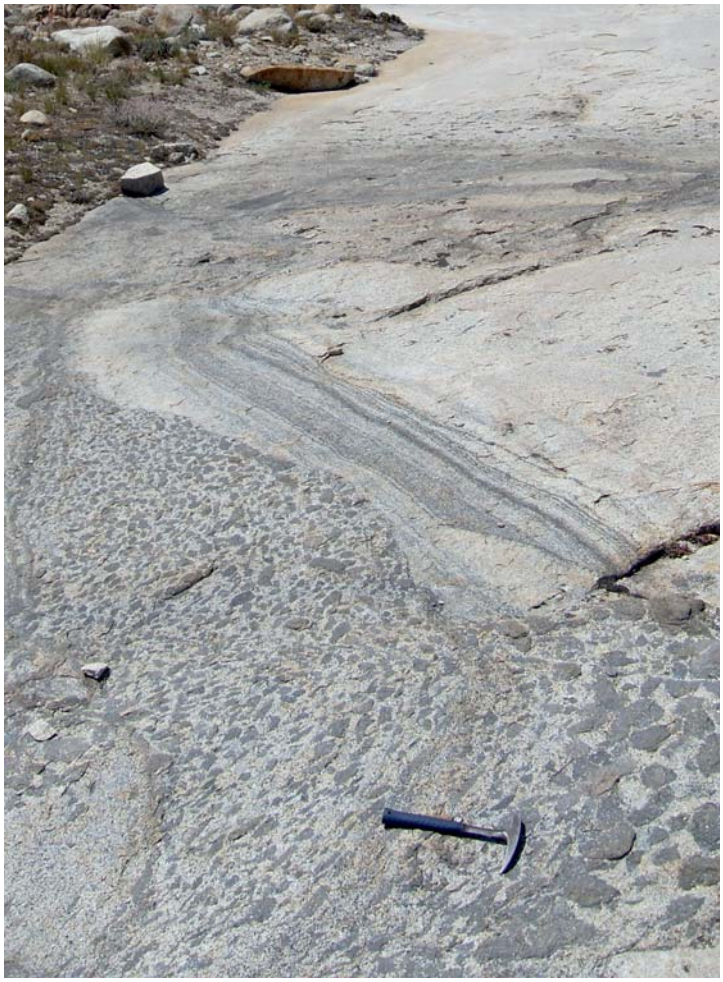

(z3)

Figure 3.6

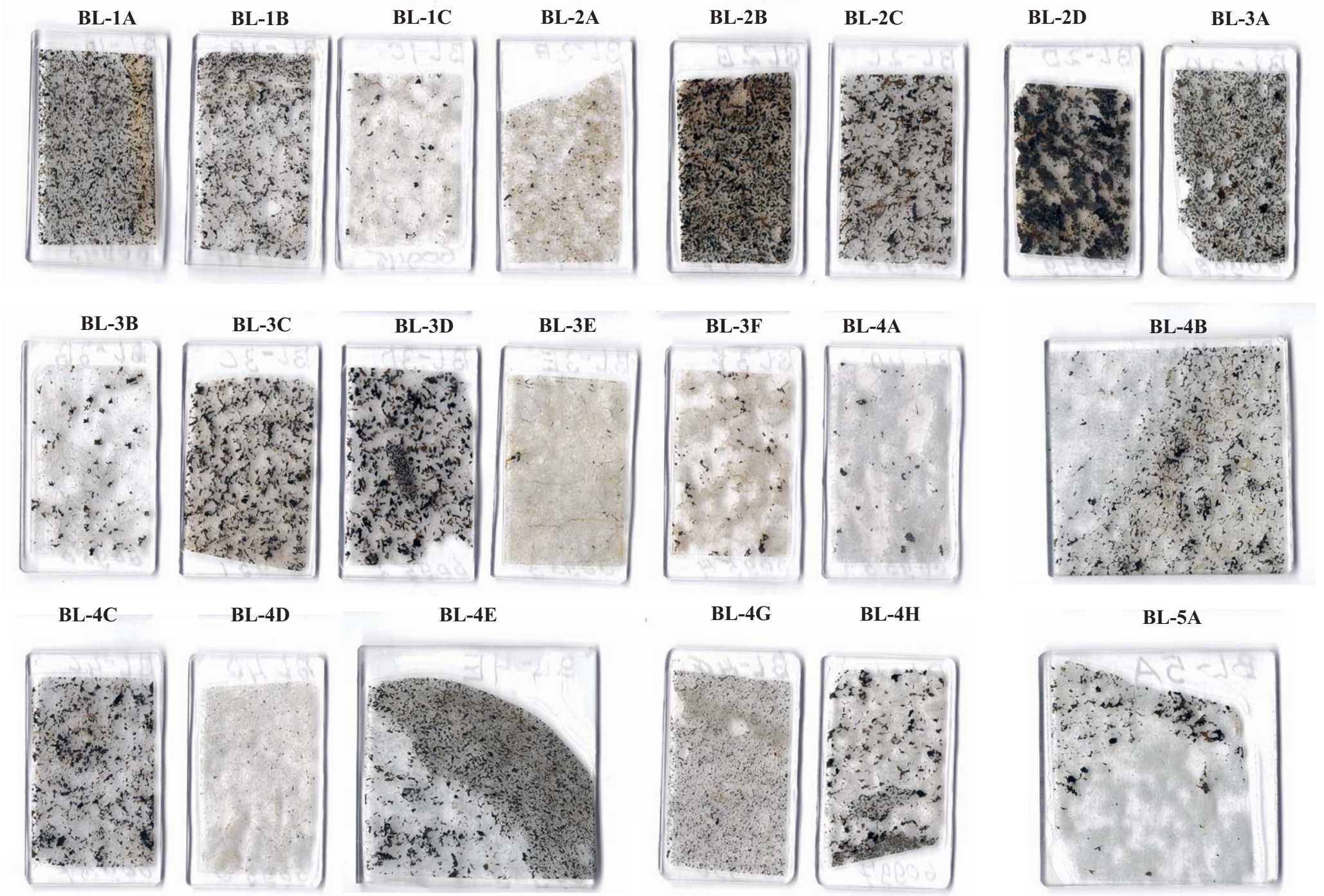
BL-1A
BL-1B
BL-1C
BL-2A
BL-2B
BL-2C
BL-2D
BL-3A
BL-3B
BL-3C
BL-3D
BL-3E
BL-3F
BL-4A
BL-4B
BL-4C
BL-4D
BL-4E
BL-4G
BL-4H
BL-5A


BL-5B


BL-5D


BL-5E


BL-6A


BL-7A


BL-8A


BL-8B


BL-8C


BL-8D


BL-8E


BL-8F


BL-8G


BL-9A


BL-9C


BL-10A


BL-11A


BL-12A


BL-12B


BL-13A


BL-13B

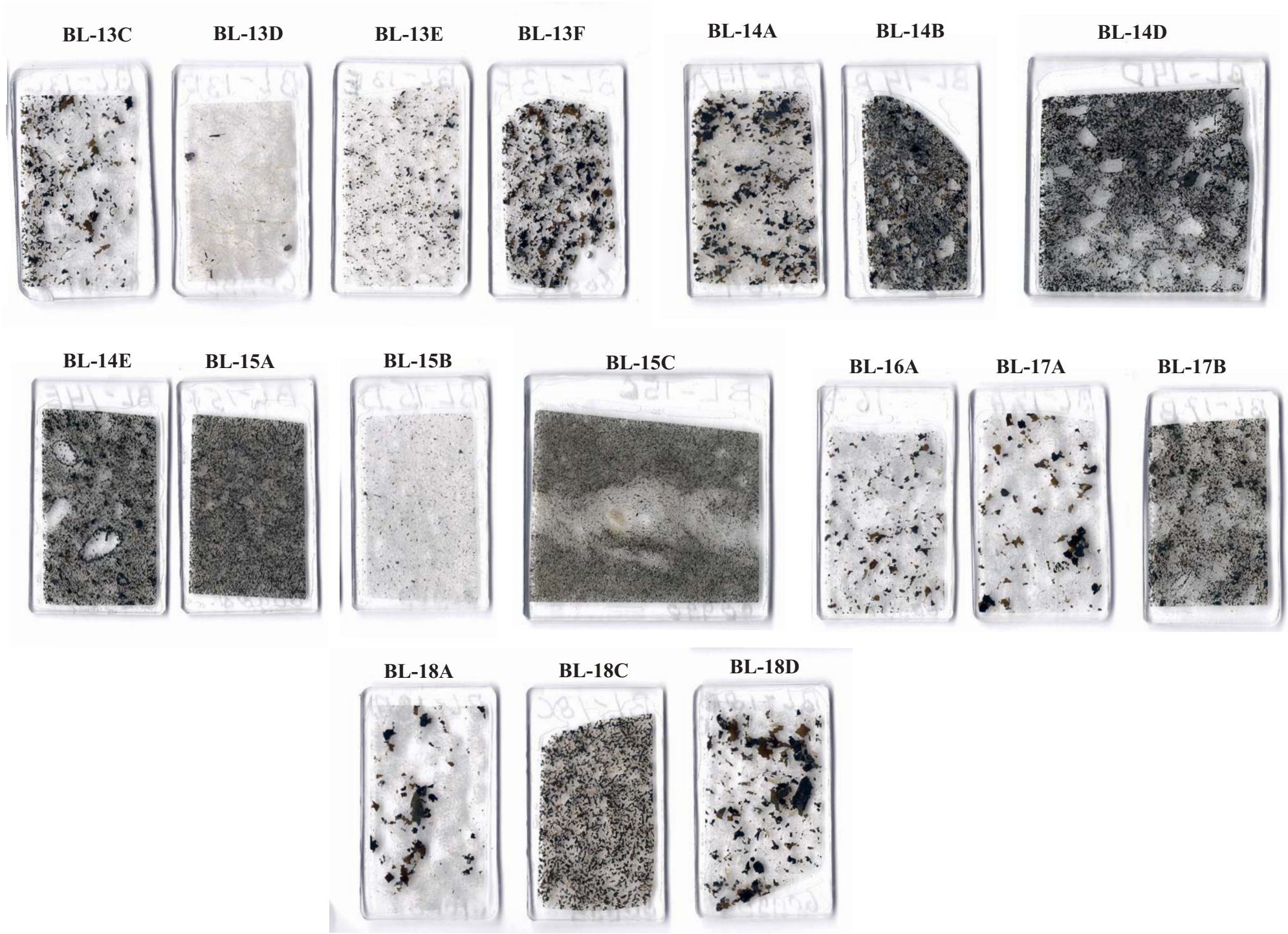
BL-13C
BL-13D
BL-13E
BL-13F
BL-14A
BL-14B
BL-14D
BL-14E
BL-15A
BL-15B
BL-15C
BL-16A
BL-17A
BL-17B
BL-18A
BL-18C
BL-18D

[69]

4 Results: Major and Trace elements

Whole rock geochemistry is based on XRF-analyses of beads and pellets as discussed in Chapter 2 Methods. The data provided by XRF-analyses data are presented in this chapter. Interpretations and conclusions derived from these data are discussed in Chapter 5 Discussion.

This chapter is divided into two sub-chapter, the first sub-chapter is on major elements and the second sub-chapter is on trace elements. The major-oxides are viewed in a Total Alkali Silicate (TAS) diagram, Alkali-Iron-Magnesium (AFM) diagram, Harker variation diagram (major-oxides versus silica) and Fenner type diagram (major-oxides versus magnesium-oxide). The trace elements are viewed in trace elements versus silica graphs, trace elements versus trace elements and trace element normalised diagrams.

Note that referring to “field units” the subdivision made in Chapter 3 Field Observations is used. Referring to “field classification” a more arbitrary classification taken from the field is meant.

4.1 Major-oxides

The major-oxide data are presented in two ways. The first is based on the lithological sub-divisions introduced in the previous chapter and the second way is based on CIPW normative mineral calculations (Johannsen, 1931), Figure 4.1. The first way presents the geochemical signature of the YC without the magmatic structures like xenoliths, enclaves, dykes and sheets. These features are left out intentionally to illustrate the geochemical signature of the YC “proper”. The second way of presenting the data is introduced to combine the samples of Johnson (unpublished) with samples taken by this author. Samples collected by Johnson (unpublished) are not classified in the field and are not described with local contact relations. Hereby an uniform subdivision of field classification can’t be used. Another advantage of using the CIPW normative mineral calculation is to eliminate the arbitrary classification made in the field.

The units distinguished by use of the CIPW normative mineral calculation are: Yosemite Creek (YC) Granite (GT), YC GT dyke, YC Granodiorite (GD), YC Quartz Monzodiorite (QM), YC QM dyke, YC QM enclave, YC Monzodiorite (MD), YC MD enclave, YC MD sheet, YC MD dyke, YC Gabbro (GA), Yosemite Valley Intrusive Suite (YVIS) GT, YVIS QM and YVIS MD.

4.1.1 Major-oxides of field units

The whole rock geochemistry determined on the YC granitoids records a general binary system that is best seen in Figure 4.2 and Figure 4.4. The binary system ranges from mafic to felsic, respectively (hbl-rich) diorite to granite. With increasing silica the units are respectively: Diorite to Hornblende-rich Diorite Unit, Fine Grained Quartz Monzodiorite to Granodiorite Unit, Porphyritic Granodiorite Unit, Medium Grained Quartz Monzodiorite to Granodiorite Unit, Coarse Grained Granodiorite Unit and Granite Unit. The composition of the entire YC suite do not define coherent variations that can be described as a single liquid line of descent. For example, the Medium Grained Quartz Monzodiorite to Granodiorite Unit, the Porphyritic Granodiorite Unit and Coarse Grained Granodiorite Unit have similar SiO_2 contents (60% to 72%) but a significant range in total alkali contents (5.5 to 7.2) (Figure 4.2a). Al_2O_3, FeO*, P_2O_5, TiO_2, CaO and MgO record negative correlations with increasing SiO_2. K_2O and Na_2O have a positive correlation with increasing SiO_2 (Figure 4.4a).

The Fine Grained Quartz Monzodiorite to Granodiorite Unit slightly deviate from the trend line in all the major-oxide graphs. The Granite Unit is relative low in Na_2O with respect to "normal" evolved igneous rocks. Remarkable is the high silica (77%) in one fine grained quartz monzodiorite to granodiorite sample. This sample plots as a tonalite in the CIPW normative calculations.

4.1.2 Major-oxides of combined sample group

In this sub-chapter the combined sample groups are present in several graphs. Sample differentiation is based on the CIPW normative mineral calculation.

The total alkali silica (TAS) diagram (Figure 4.2) shows the classifications of the samples with respect to plutonic classification after Middlemost (1994), Rollinson (1993) and Kotková (2007). By increasing the silica concentration total alkali concentration is also increased. The normal maturity trend would be from gabbro to granite. Most samples fit this trend, however the majority of the quartz monzodiorite and mafic enclaves are alkali enriched.

The granitic and granodiorite samples plotted in major-oxides versus silica graphs form a single liquid line of descent with little scatter. The quartz monzodiorite samples are more scattered and two clusters of samples are distinguishable. This is especially visible in the Al_2O_3, MgO, P_2O_5, BaO and Na_2O versus (vs.) SiO_2 graphs (Figure 4.4b). Monzodiorite and gabbroic samples fit the single liquid line of descent, except in the graph of P_2O_5 vs. SiO_2 are the samples scattered. Enclaves, dykes and sheets do not stand out of the trend, except for granitic dykes which contain abundant K_2O.

Taking all samples analysed into account a similar liquid line of descent as described in paragraph 4.1.1 can be observed for the Fenner type diagrams. The major-oxides vs. MgO record a inverse relationships compared to silica variations (Figure 4.4c). The scatter in these graphs of the quartz monzodiorite samples are less with respect to the monzodiorite in major-oxides vs. SiO_2. Notable is that the quartz monzodiorite and the granodiorite samples overlap in the Fenner type diagrams. The monzodiorite and gabbro samples are more scattered, however they still fit the trend of the single liquid line of descent. Notable is that the mafic enclaves plot near the "edges" of the single liquid line of descent. The enclaves are slightly depleted in FeO*, TiO_2 and CaO and enriched in K_2O, Na_2O and P_2O_5 (Figure 4.4c). Other outliners of the single liquid line of descent in the Fenner type diagrams plot in the same range as the outliners of the Harker variation graphs (Figure 4.4).

Samples plotted in the AFM diagram (Figure 4.3) follow the liquid line of descent in the calc-alkaline domain. One gabbro plots above the calc-alkaline - tholeiitic boundary. Gabbroic and monzodioritic samples are relative high in iron and magnesium, plotting in the less maturated domain of the AFM diagram. Mafic enclaves plot between these less maturated samples and the quartz monzodiorite and granodiorite samples. Striking is the overlap between the quartz monzodiorite and granodiorite samples. Several granodiorite samples and granite samples are alkali-rich. In this diagram three quartz monzodiorite samples, six granodiorite samples overlap with a cluster of granite samples. Granitic dyke samples plot the most to the alkali corner of all the samples.

4.2 Trace elements

Due to different compatibility characteristics of trace elements mineral fractionation trends can be deduced. A clear way to illustrate these trends is by plotting trace element versus silica (Figure 4.5), trace elements versus trace elements (Figure 4.6) and trace element normalised diagrams (Figure 4.7).

4.2.1 Trace elements versus silica

In the next paragraph trace element versus silica graphs are presented. The results and the interpretation of these results are discussed in Chapter 5 Discussion.

All sample groups, except for the gabbroic samples and monzodiorite sheets, are scattered in the Rb vs. SiO_2 graph. Rb concentration ranges between ~50 to ~200 part per million (ppm) (Figure 4.5). Ba concentrations of granitic samples range between 0 to ~1500 ppm and granitic enclave up to ~2500 ppm. Ba concentrations for the quartz monzodiorite and granodiorite sample groups range between ~500 to ~1500 ppm (Figure 4.5). The monzodiorite and gabbroic samples are less scattered for Ba and vary near the 500 ppm, except for one monzodiorite sample. Nb concentrations varying between the ~2 to ~20 ppm with a few monzodiorite outliners up to ~37 ppm (Figure 4.5). Most concentrations of La range between ~5 and ~30 ppm. Remarkable is that granodiorite La concentrations are concentrated between the ~30 and ~50 ppm with a few outliners ranging from ~50 up to ~120 ppm (Figure 4.5). Ni concentrations are mostly concentrated between ~5 and ~10 ppm. The monzodiorite, gabbros and two granitic samples are more scattered and can rang up to ~45 ppm (Figure 4.5). Concentrations for Sr are less scattered then previous presented trace elements, except for a few outliners. Sr concentration for granitic samples range between 0 and ~500 ppm; granodiorite samples range between ~400 and ~500 ppm and the quartz monzodiorite, monzodiorite and gabbro samples range between ~500 and ~800 ppm (Figure 4.5). Zr concentrations vary greatly, granitic samples range between the ~10 and ~150 ppm. Two clusters of granitic dykes can be distinguished in Zr concentrations, first cluster near ~200 ppm and a second cluster between 0 and ~80 ppm. Granodiorite Zr concentrations range between ~80 and ~250 ppm. Three clusters of quartz monzodiorite can be distinguished in the Zr concentrations. First group between ~50 and ~150 ppm; second group between ~200 and ~350 and the third between ~450 and ~550 ppm. The monzodiorite and gabbro Zr concentrations are concentrated between ~30 and ~150 ppm. Concentrations for Y are concentrated between the ~2 and ~30 ppm. Monzodiorite and gabbro Y concentrations ranges between ~12 and ~58 ppm.

4.2.2 Trace elements versus trace elements

Trace elements vs. trace elements graphs (Figure 4.6) are presented because they contribute e.g. for classify tectonic setting and to quantify fractional crystallization, moreover in Chapter 5 Discussion. Trace element versus trace element graphs show more scatter with respect to trace elements vs. silica graphs. However the trace element concentrations are the same as presented in the previous paragraph.

La concentrations for the granodiorite samples ranging from ~30 to ~50 ppm (Figure 4.6). For a few outliners and the granodiorite samples La concentrations range between ~5 to ~30 ppm. Felsic samples are slightly more depleted in Sm (range between ~0 and ~3 ppm) than the more mafic samples (range between ~2 and ~8 ppm). For Rb concentrations, the more felsic samples are enriched (range between the ~100 and ~210 ppm) and mafic components are depleted (range between ~20 and ~150 ppm). Similar observation as for Rb can be made for Th concentrations. Felsic samples are high for Th (generally up to ~30 ppm) and low for mafic components (< 10 ppm). The Yb vs. La, Rb vs. La, Nb vs. Ba and Rb vs. Ba graphs show too much scatter to distillate any significant remarks for this presentation (Figure 4.6). Further descriptions concerning these graphs can be read in Chapter 5 Discussion.

4.2.3 Trace element normalised diagrams

Trace element normalised diagrams are used to show the behaviour of incompatible (trace) elements. This author chose to use trace element normalised diagrams instead of REE and LILE graphs to limit the missing elements in the graphs. Whole rock XRF data is used to produce these diagrams, data sets are discussed in Chapter 2 sub-chapter Beads and Pellets preparation. Trace element normalised diagrams are grouped to the CIPW normative mineral calculation groups (YV GT, YV GT dyke, YV GT enclave, YV TO, YV GD, YV GD dyke, YV QM, YV QM dyke, YV QM enclave, YV MD, YV MD dyke, YV MD sheet, YV MD enclave, YV GA, YVIS GT, YVIS QM and YVIS MD), see sub-chapter 4.1.

4.2.3.1 Normalization sample

Measured values are normalized to the granodiorite of sample BL-4H which is assigned to the unit of the (Medium Grained) Quartz Monzodiorite to Granodiorite Unit. This sample is chosen because it satisfies to the follow demands: sampled by own means, representative sample of the outcrop, interpreted as host rock and YC “proper”, fits on the single liquid line of descent and is a roughly average for the sample group. All the samples are normalized to sample BL-4H and are shown in Figure 4.7b. Statements on enrichment and depletion are relative to sample BL-4H (black line in the diagrams, from now on referred to as “normalization line”).

In Figure 4.7a is the trace element normalised diagram of sample BL-4H is shown, which is normalized to chondrite to illustrate the trace element signature. This sample show high enrichment in less incompatible elements and less enrichment in the more incompatible elements. P is very low (~0.5) and is notable because it sticks out of the general trace element trend. In subsequent section all values are compared to BL-4H and data reported as relative enrichment or depletion to the values in BL-4H.

4.2.3.2 Yosemite Creek Granite's

The YV GT show one dominant signature. The elements range between La and Yb are slightly depleted. In general Th, U and K are enriched (Figure 4.7b). The YV GT dyke show two dominant signatures. First dominant signature shows scatter for the less incompatible elements (Rb to K). For the more incompatible elements (Nb to Yb) sample BL-3E, BL-4D, BL-8C show depletion and a similar signature as observed for the YV GT group. The second group in the YC GT dyke (sample BL-2A and BL-13E) show scatter of the element concentrations near one times BL-4H (Figure 4.7b). Rb to K in sample BL-4A are enriched and show no scatter (Figure 4.7b). The YV GT enclave (sample BL-4A) show great scatter for the more incompatible elements (Nb to Yb) however all elements are depleted relative to BL-4H.

4.2.3.3 Yosemite Creek Granodiorite and Tonalite

The trace element normalised diagram of the YV GD show little scatter (0.5 to 2.0) and generally all elements plot near the normalization line with the exception of sample BL-11C, BL-17A and BL-31I-2 SJSU. Notable is the low concentration of Nb in sample BL-11C and BL-17A (Figure 4.7b). There are two samples in the YV GD dyke group sample BL-3D and sample BL-4G. Sample BL-3D shows scatter (0.3 to 3.2) near the normalization line, comparable to the dominant signature of the YV GD group. Sample BL-4G show little (~up to 0.5) depletion for the more incompatible elements (La to Yb) and scatter (between 0.6 to 3.2) for the Rb to K. Similar dominant signature is observed in the YV GT group (Figure 4.7b). Little scatter can be observed for the YV TO (sample BL-3B). Notable is that almost all the elements are depleted except for U (~1.0) and Sr (~1.2) (Figure 4.7b).

4.2.3.4 Yosemite Creek Quartz Monzodiorite

For the YV QM three dominant signatures can be observed. First group, sample 24A SJSU and 24A-2 SJSU show enrichment (~1.0 to 3.0) for almost all the elements. The second group, the most dominant one (85% of the samples), is a signature which shows scatter (0.3 and 2.0) near the normalization line, notable is the low Th (0.1) in sample BL-8E. The third group, sample BL-4C shows little (1.0 to 1.3) enrichment for almost all the elements and show remarkable resemblance with signatures of YV GD (Figure 4.7b). Sample BL-13C, the YV QM dyke group, show scatter near the normalization line and show resemblance with the YV QM group, however Ti and Y are more depleted. YV QM enclave group, sample BL-17D, show a depletion for the less incompatible elements (Rb to K). The other elements (Nb to Yb) show scatter (0.5 to 2.2) near the normalization line (Figure 4.7b).

4.2.3.5 Yosemite Creek Monzodiorite and Gabbro

The YV MD show a depletion for the less incompatible elements (Rb to Ce) and a scattered trend for the other more incompatible elements. Notable are the enrichment of P and Ti. The YV MD group shows resemblance with the signature of sample BL-17B (YV QM enclave) (Figure 4.7b). Almost all elements range from Rb to Ce show a depletion in the YV MD sheet group, notable are the very depleted Th (~0.14), U (~0.04) and Zr (0.2 to 0.5) values. The more incompatible elements (Sr to Yb) show in general a high enrichment (up to 4), except for Hf (~0.6) and Zr (0.2 to 0.5) which are depleted (Figure 4.7b). The samples of YV MD enclave show a lot of scatter (between ~0.02 and ~9.0) for the less incompatible elements (Rb to K). A dominant signature of scatter near the normalization line is distinguishable for the more incompatible elements (Nb to Yb). Sample BL-4E does not correspond with the dominant signature of the YV MD enclave group, notable is the low Sr concentration of BL-4E (Figure 4.7b). The YV GA samples are in general depleted for the less incompatible elements (Rb to K), notable is the low value of U (~0.04) for all the YC GA samples. For the other elements, except for Zr, an enrichment or less depletion with increasing incompatibility is observed (Figure 4.7b).

4.2.3.6 The Yosemite Valley Intrusive Suite

The samples of the YVIS GT show a lot of scatter (range between <0.01 to 5.3). There is no dominant trend distinguishable. The elements Th, U and K are enriched up to a factor of 8. The more incompatible elements (Nb to Yb) show a depletion, up to 0.01. Notable is the depletion (near 0.0001) of Ba and Sr in the samples BL-10A and BL-11A (Figure 4.7b). The YVIS QM have compositions comparable to BL-4H. Sample 37G SJSU is slightly (up to 1.4) enriched in all the elements except for Ba which is depleted (0.7). Sample 40B SJSU is in general slightly depleted (down to ~0.8) except for Rb, Y and Sr which are enriched (up to ~2.2). These samples show resemblances with the YV GD group. Sample 25B SJSU, YVIS MD group, is very scatter (0.1 to 4.0) and show depletion in the less incompatible elements (Rb to K) and a scatter in the more incompatible elements (Sr to Yb). Notable is the high (~4.0) Ti concentration and the depletion of Zr (~0.5).

4.3 Summary major and trace elements

An uniform classification is introduced to combine all the samples and reduce any arbitrary field classification. For further discussions this step in data processing should always been kept in mind. The projection of the data is viewed in Harker variation diagrams, Fenner type diagrams, single trace elements and trace element normalised diagrams normalized to a representative granodiorite sample.

There is a clear single liquid line of descent in increasing mineral maturity with correlated major elements, such as one would expect for an evolved igneous study area. However, single samples as well as clustered samples can deviate from the liquid line of descent, especially for the Quartz Monzodiorite unit and the Fine Grained Quartz Monzodiorite to Granodiorite.

Most trace elements show scattered graphs which make direct interpretations difficult, however some trends can be distinguished as well as clustered sample groups. Interpretations and fractional crystallization quantifications based on these figures are presented in Chapter 5 Discussion.

Trace element normalised diagrams show one or several dominant signatures in the trace elements. YC “proper” units provide signatures with minor scatter. Enclaves and dyke show more scatter in general. Most granitic and granodioritic samples are enriched in less incompatible elements (Rb to U) and depleted in the more incompatible elements (Nb to Yb). Quartz monzodiorite samples show irregular scatter with compositions comparable with BL-4H for all the trace elements. The mafic samples, monzodiorites and gabbros, show depletion for the less incompatible elements (Rb to U) and enrichment for the more incompatible elements (Nb to Yb), except for Zr which is in general slightly depleted.

Figure 4.1
(a) Classification by use of QAPF diagram based on CIPW normative mineral calculation. Samples are grouped by field classification. **(b)** QAPF diagram based on CIPW normative mineral calculation to reclassify and combine all samples in an uniform classification for further analyses.

Figure 4.2
(a) Total alkali silicate diagram of field units. **(b)** Total alkali silicate diagram of all samples. Plotted in plutonic classification diagram, modified after Middlemost (1994), Rollinson (1993) and Kotková (2007).

Figure 4.3
Alkali-Iron-Magnesium diagram (AFM) to illustrate alkaline and tholeiitic division.

Figure 4.4
(a) Harker variation diagrams of the field units. **(b)** Harker variation diagrams, major-oxides versus silica, of combined samples. Illustrating depletion or enrichment of a major element with respect to increasing mineral maturity (quarts controlled), which is concentrated on felsic samples. **(c)** Fenner type diagrams, major-oxides versus magnesium-oxide, of combined samples. Illustrating depletion or enrichment of a major element with respect to increasing mineral maturity (olivine controlled), which is concentrated on mafic samples.

Figure 4.5
Trace elements versus silica. Illustrating depletion or enrichment of a trace element with respect to mineral maturity.

Figure 4.6
Trace elements versus trace elements. Indicating mobility of a trace element with respect to other trace elements which is related to their compatibility nature. This is indicative for specific mineral crystal fractionation.

Figure 4.7
Trace element normalised diagrams, which show trace elements of a sample with respect to a “average” YC granodiorite. Trace element normalised diagrams are indicative for the rock source and rock evolution. Also it makes comparison available between all the samples. **(a)** Trace element normalised diagram of sample BL-4H, the “average” YC granodiorite, normalized to chondrite to illustrate the trace element signature. **(b)** Trace element normalised diagrams of the YV samples normalized to “average” YC granodiorite. See text for explanation. **(c)** Trace element normalised diagrams of the YVIS samples normalized to “average” YC granodiorite.

Figure 4.1a

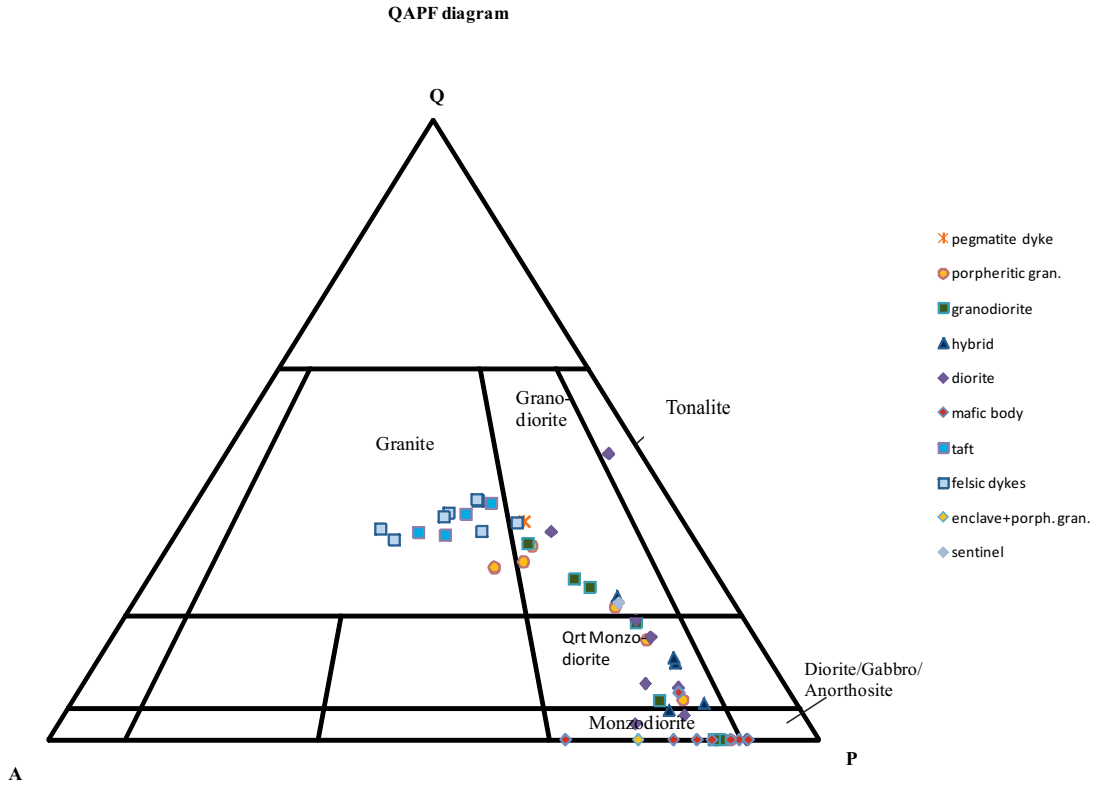

Figure 4.1b

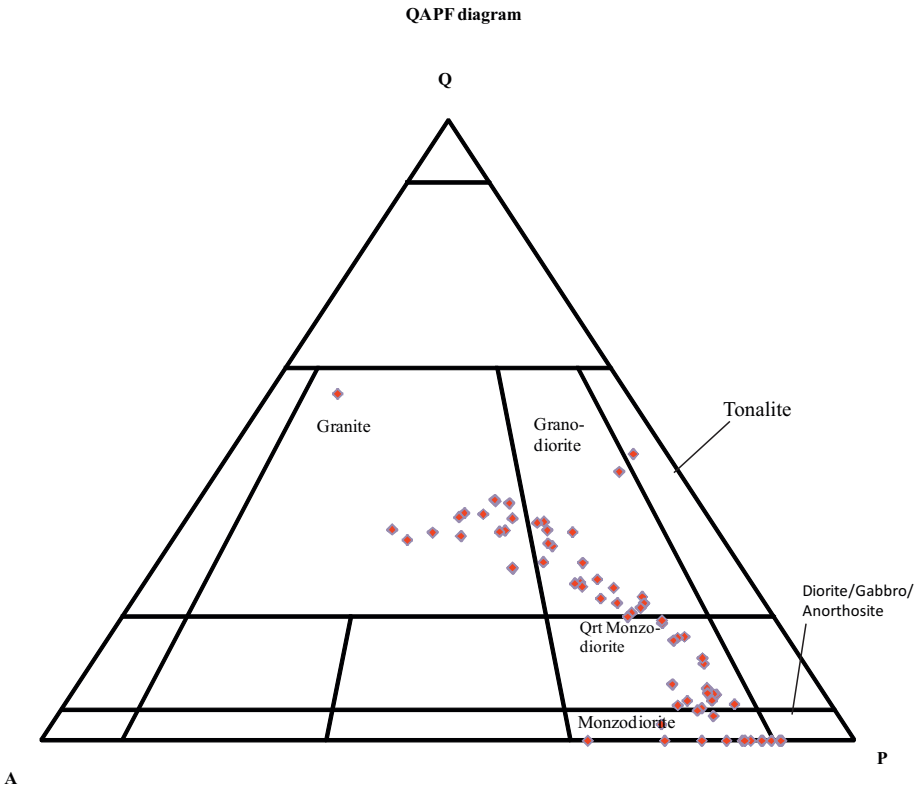

Figure 4.2a

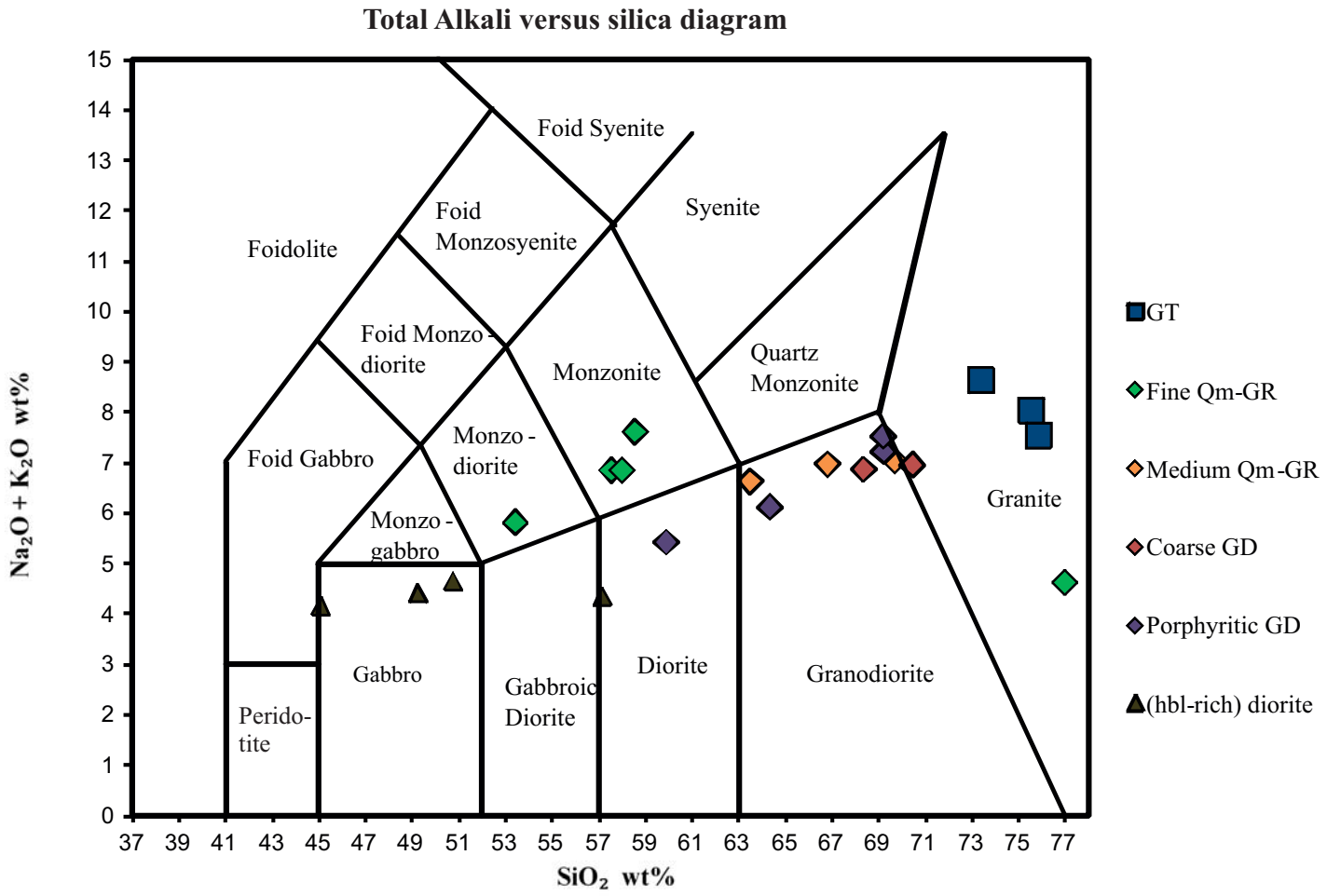

Figure 4.2b

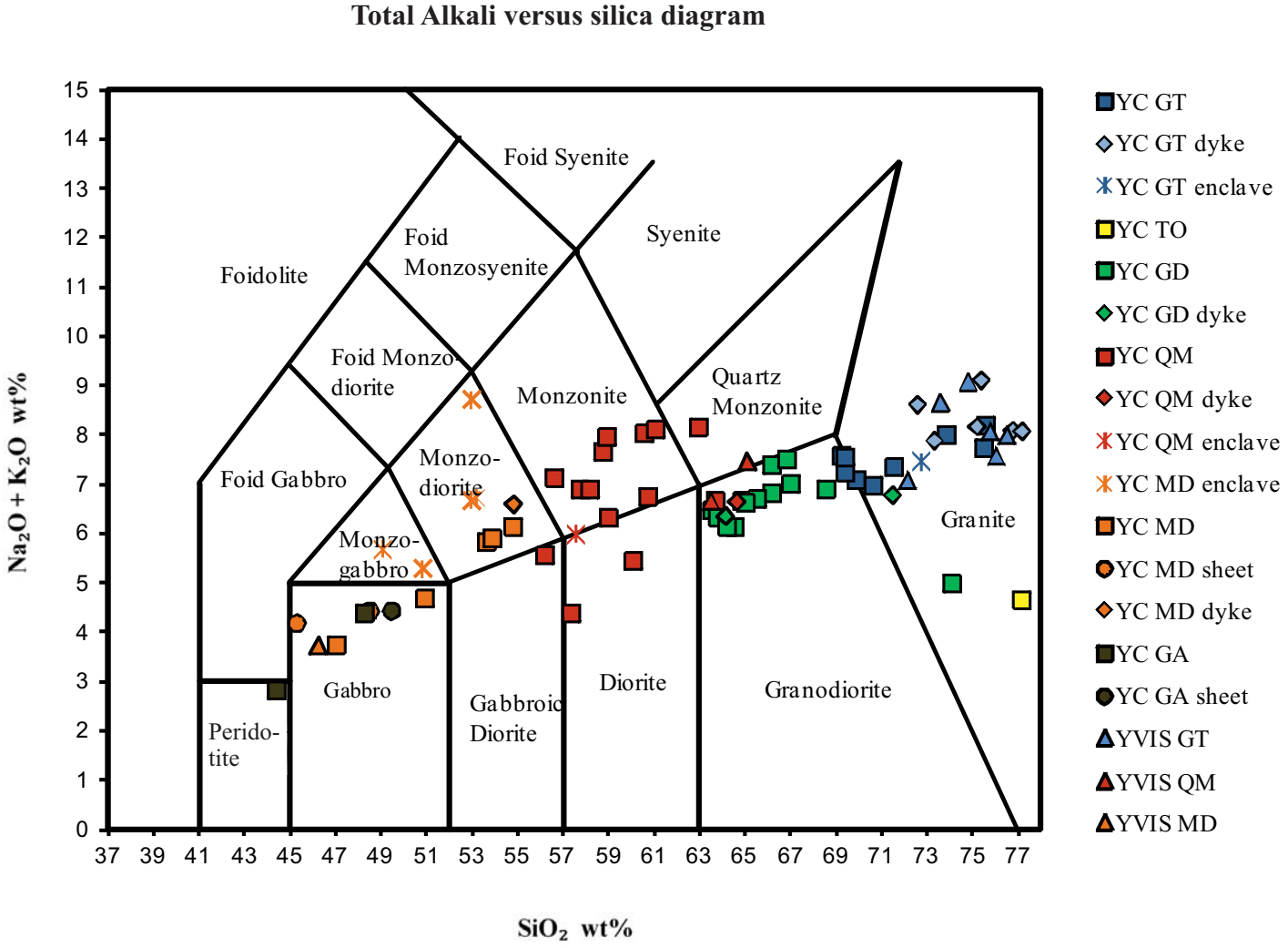

Figure 4.3

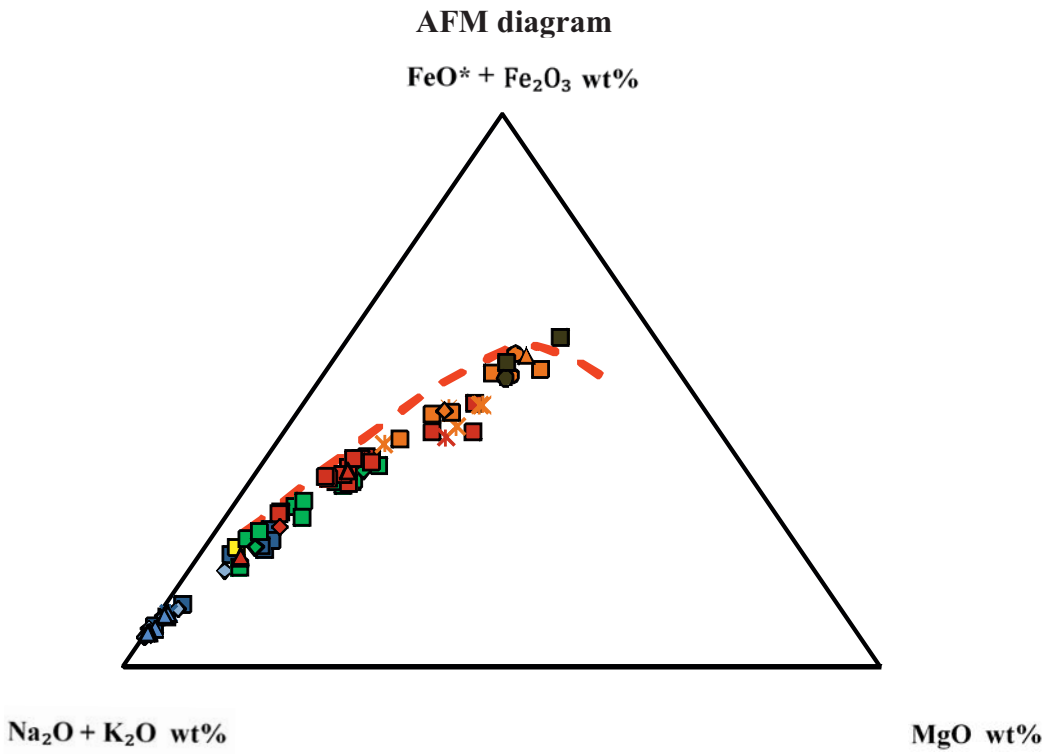

Figure 4.4a

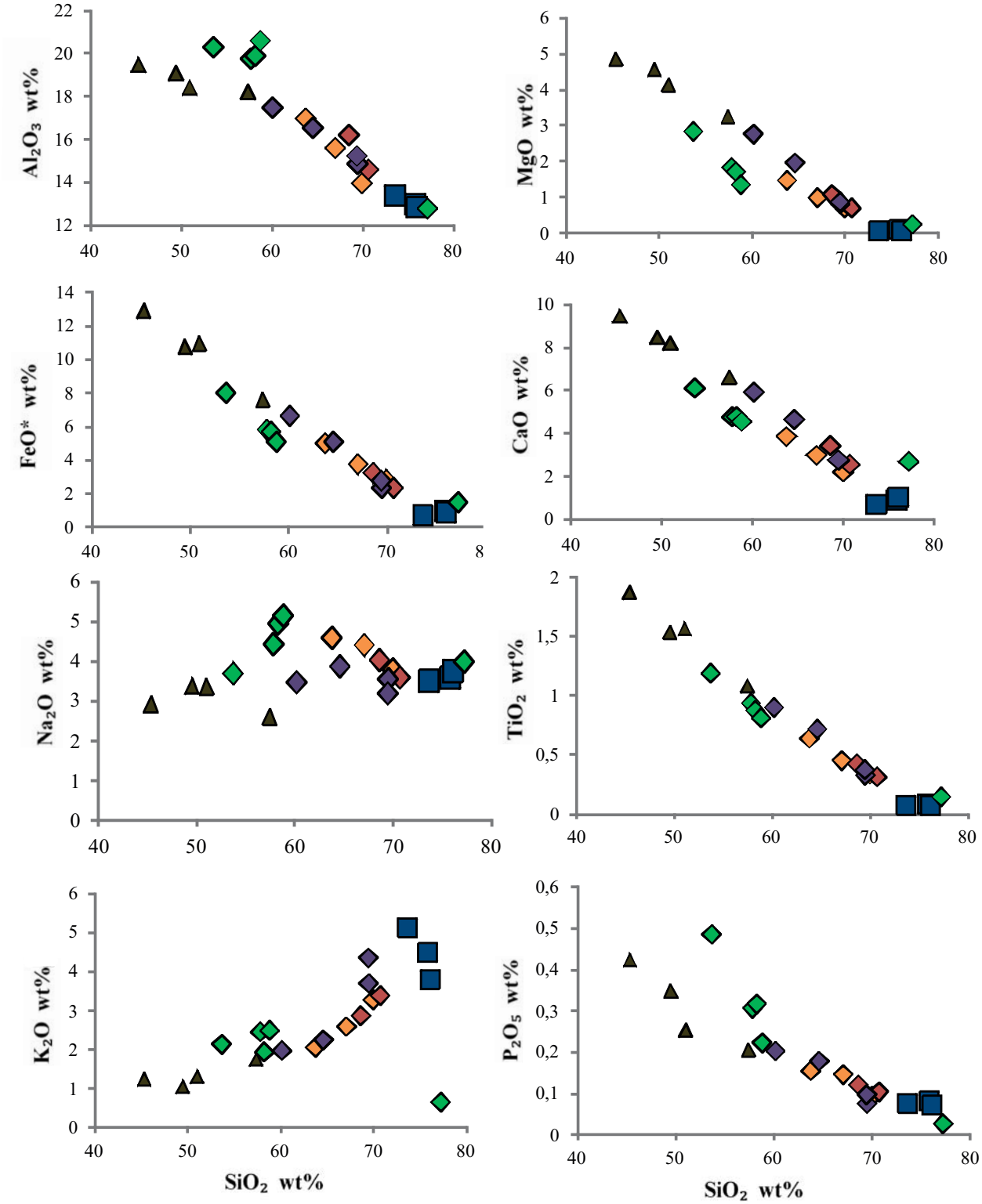
Al2O3 wt%
MgO wt%
FeO* wt%
CaO wt%
Na2O wt%
TiO2 wt%
K2O wt%
P2O5 wt%
SiO2 wt%
SiO2 wt%
GT
Fine Qm-GR
Medium Qm-GR
Coarse GD
Porphyritic GD
(hbl-rich) diorite

Figure 4.4b

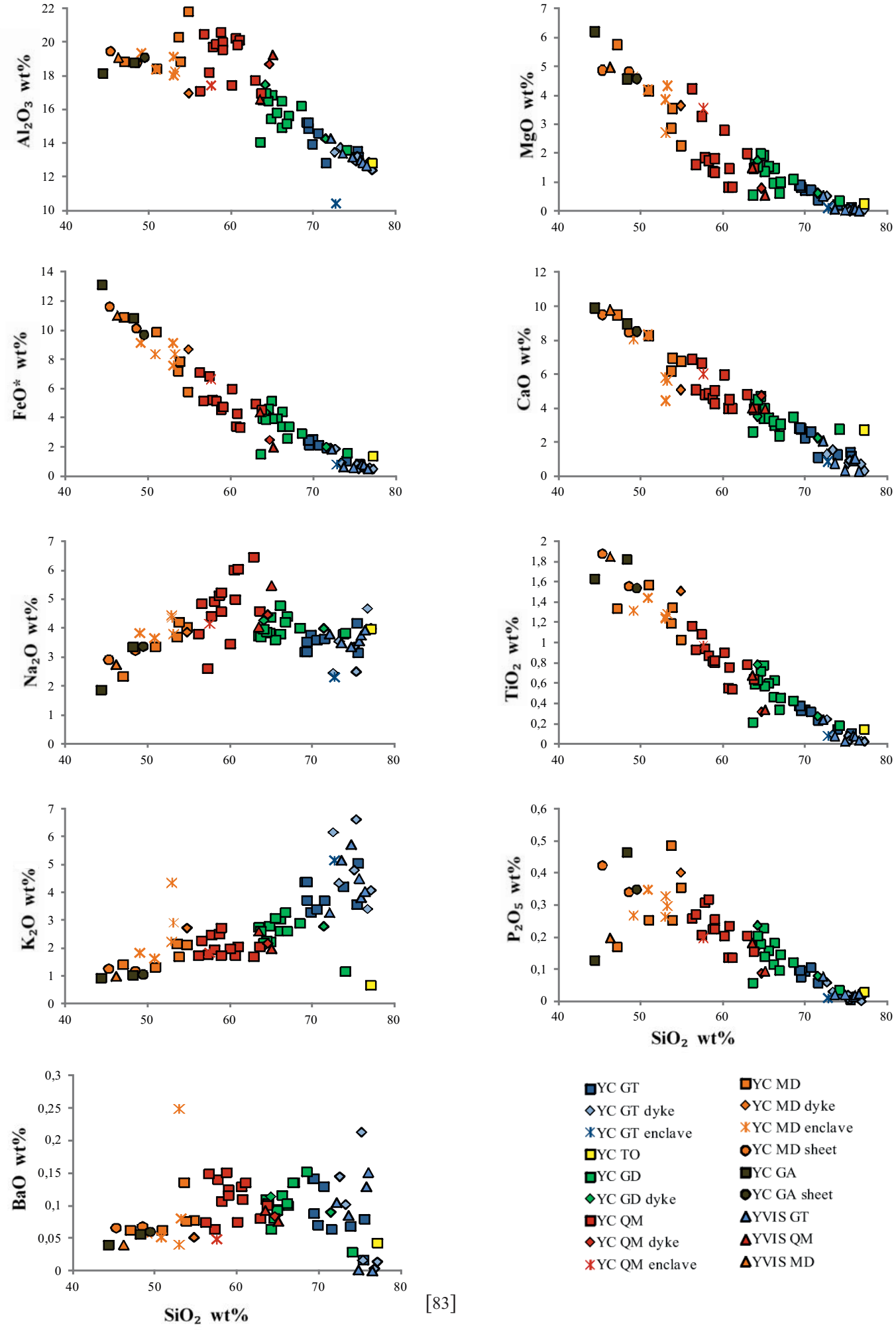
Al2O3 wt%
MgO wt%
FeO* wt%
CaO wt%
Na2O wt%
TiO2 wt%
K2O wt%
P2O5 wt%
BaO wt%
SiO2 wt%
SiO2 wt%
YC GT
YC GT dyke
YC GT enclave
YC TO
YC GD
YC GD dyke
YC QM
YC QM dyke
YC QM enclave
YC MD
YC MD dyke
YC MD enclave
YC MD sheet
YC GA
YC GA sheet
YVIS GT
YVIS QM
YVIS MD

Figure 4.4c

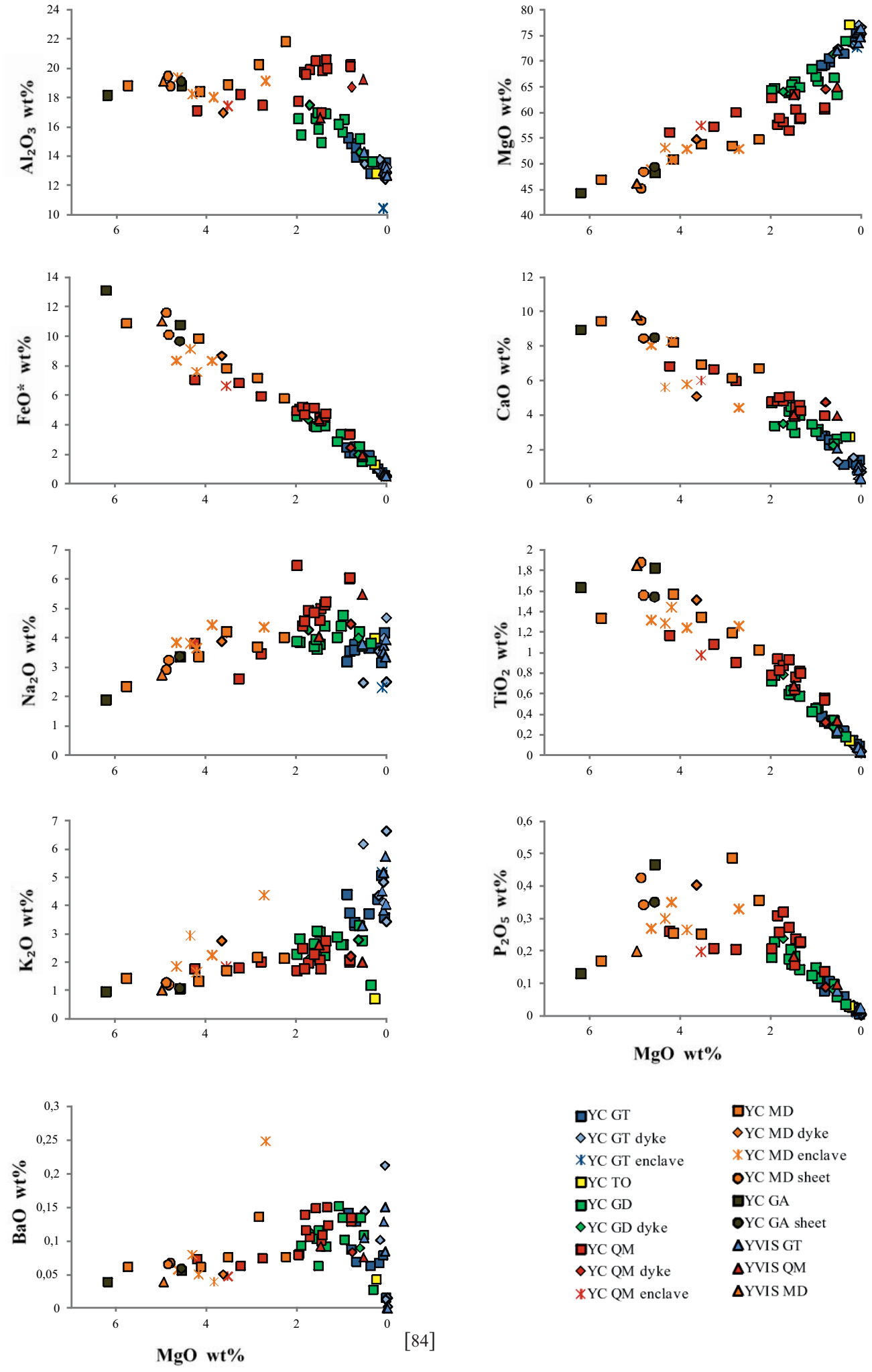
Al2O3 wt%
MgO wt%
FeO* wt%
CaO wt%
Na2O wt%
TiO2 wt%
K2O wt%
P2O5 wt%
BaO wt%
MgO wt%
MgO wt%
YC GT
YC GT dyke
YC GT enclave
YC TO
YC GD
YC GD dyke
YC QM
YC QM dyke
YC QM enclave
YC MD
YC MD dyke
YC MD enclave
YC MD sheet
YC GA
YC GA sheet
YVIS GT
YVIS QM
YVIS MD

Figure 4.5

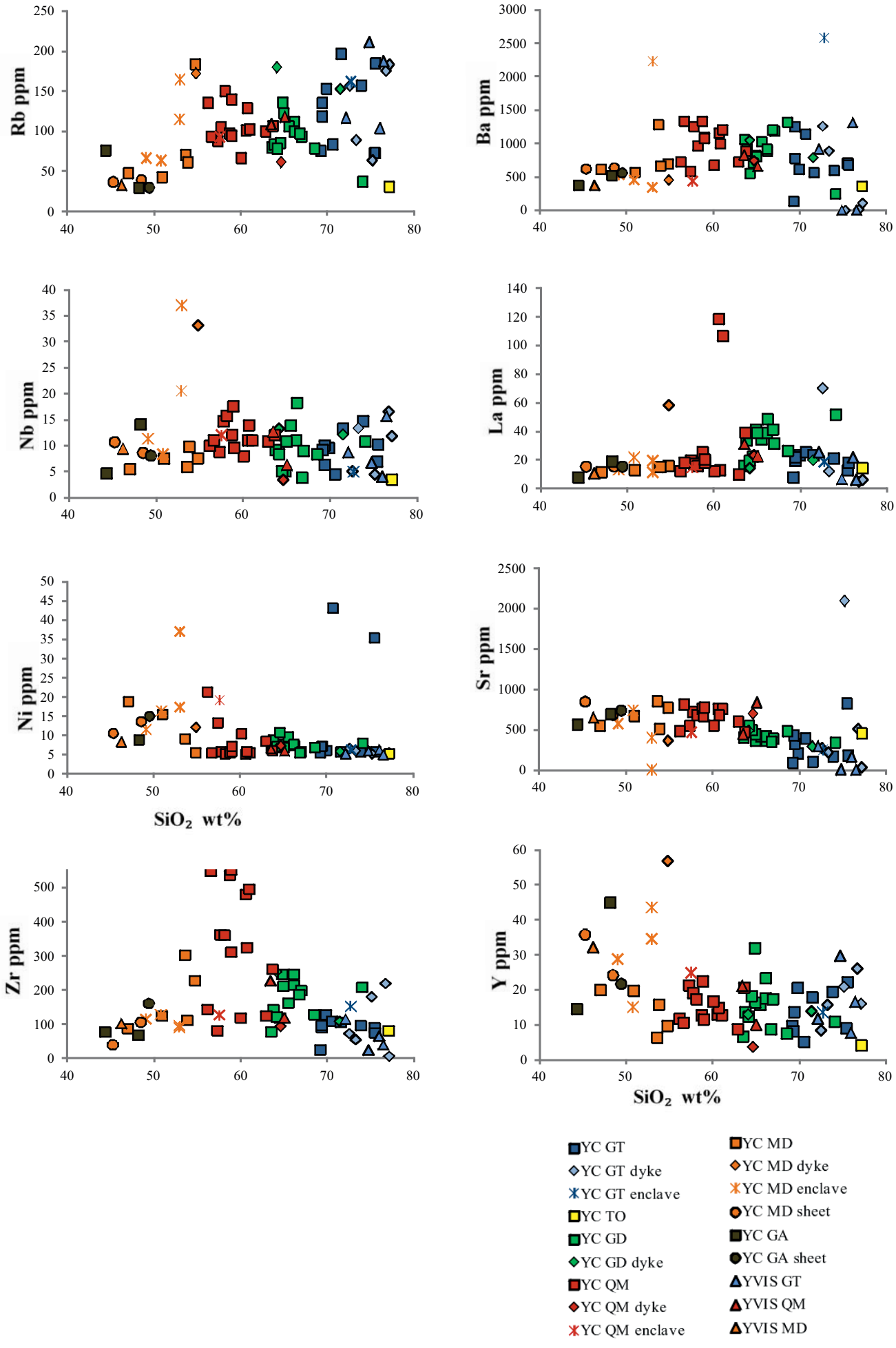
Rb ppm
Ba ppm
Nb ppm
La ppm
Ni ppm
Sr ppm
Zr ppm
Y ppm
SiO2 wt%
SiO2 wt%
YC GT
YC GT dyke
YC GT enclave
YC TO
YC GD
YC GD dyke
YC QM
YC QM dyke
YC QM enclave
YC MD
YC MD dyke
YC MD enclave
YC MD sheet
YC GA
YC GA sheet
YVIS GT
YVIS QM
YVIS MD

Figure 4.6

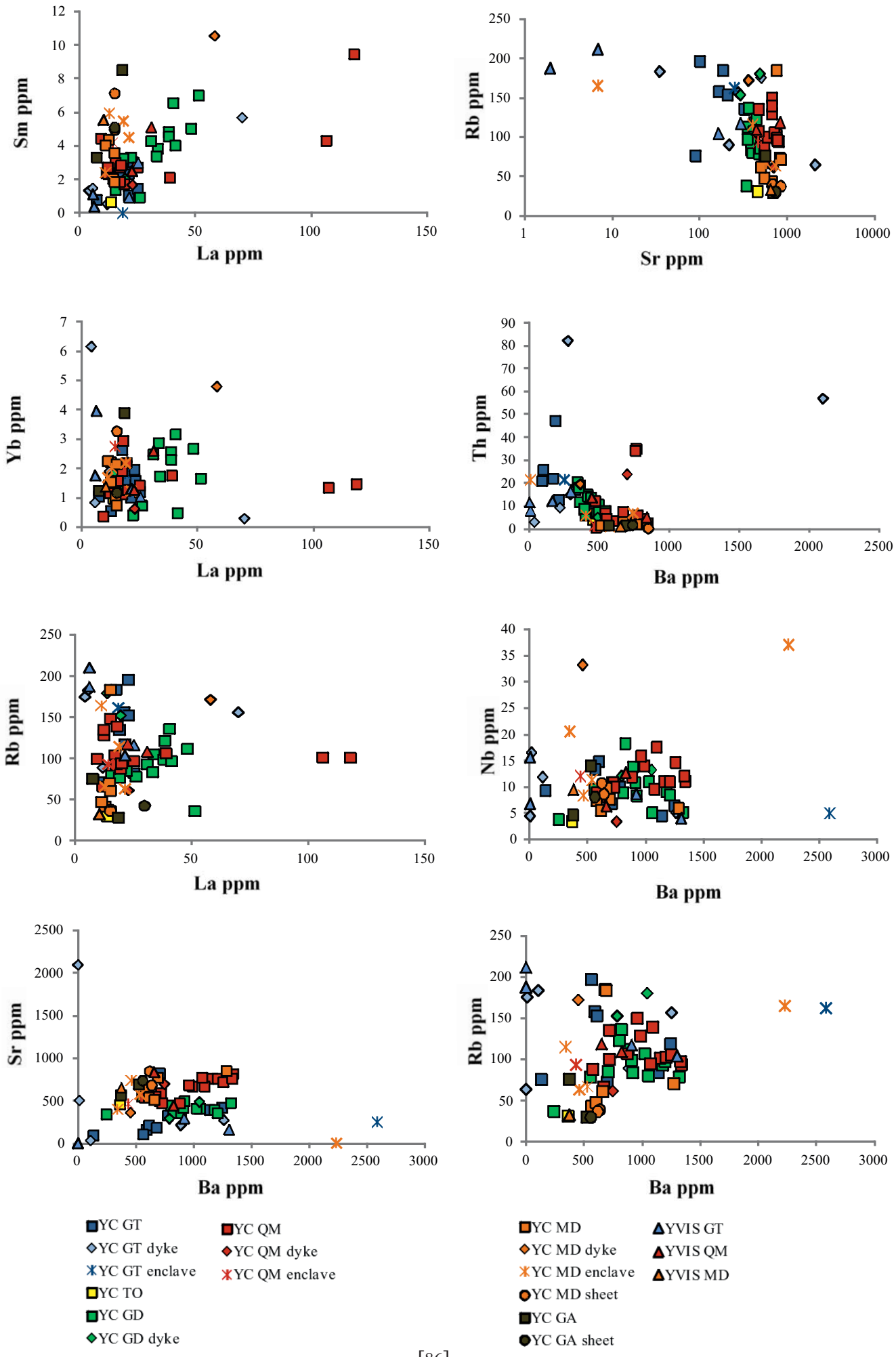
Sm ppm
La ppm
Rb ppm
Sr ppm
Yb ppm
La ppm
Th ppm
Ba ppm
Rb ppm
La ppm
Nb ppm
Ba ppm
Sr ppm
Ba ppm
Rb ppm
Ba ppm
YC GT
YC GT dyke
YC GT enclave
YC TO
YC GD
YC GD dyke
YC QM
YC QM dyke
YC QM enclave
YC MD
YC MD dyke
YC MD enclave
YC MD sheet
YC GA
YC GA sheet
YVIS GT
YVIS QM
YVIS MD

Figure 4.7a

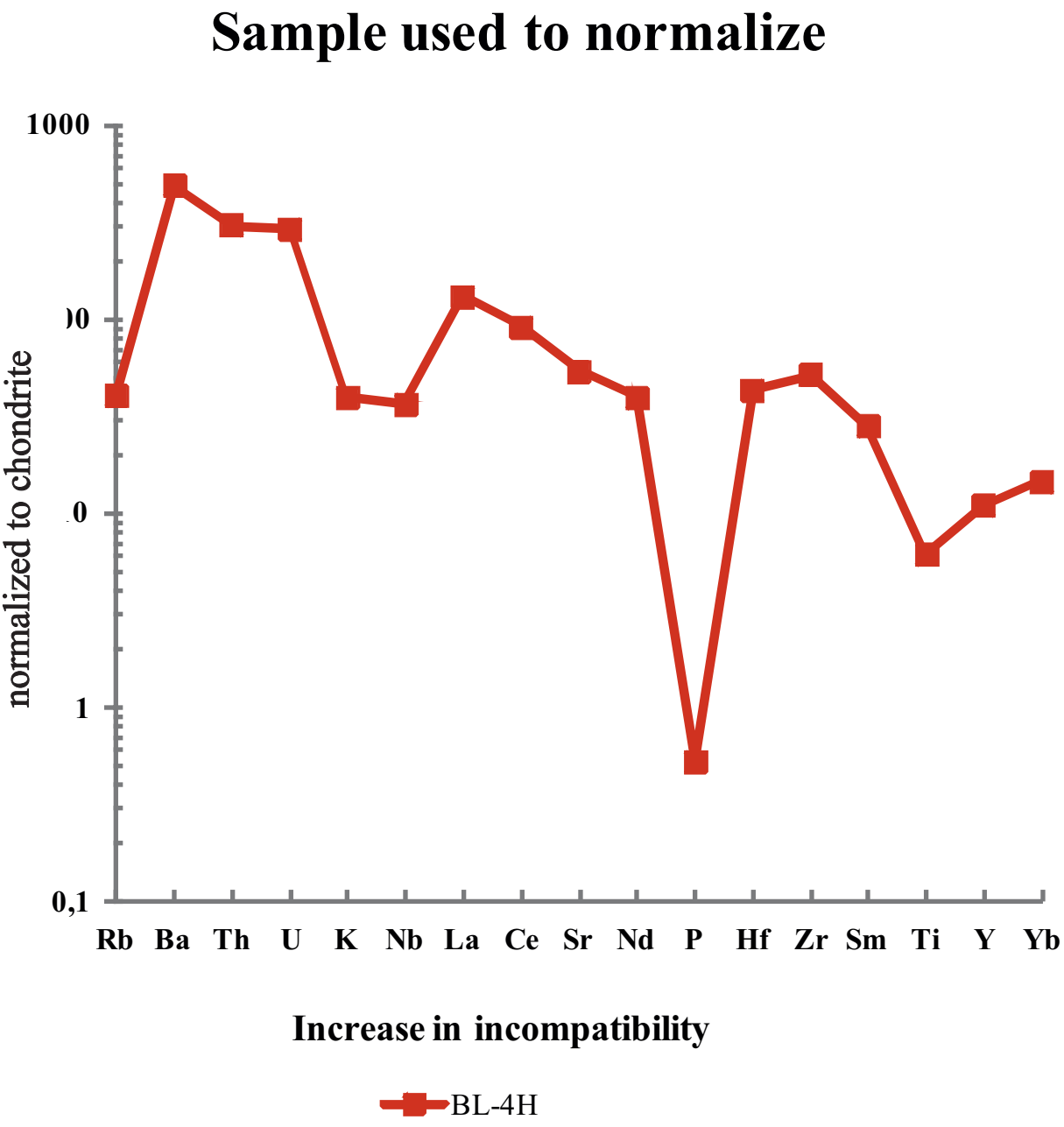
Sample used to normalize
1000
)0
.0
1
0,1
normalized to chondrite
Rb Ba Th U K Nb La Ce Sr Nd P Hf Zr Sm Ti Y Yb
Increase in incompatibility
BL-4H

Figure 4.7b

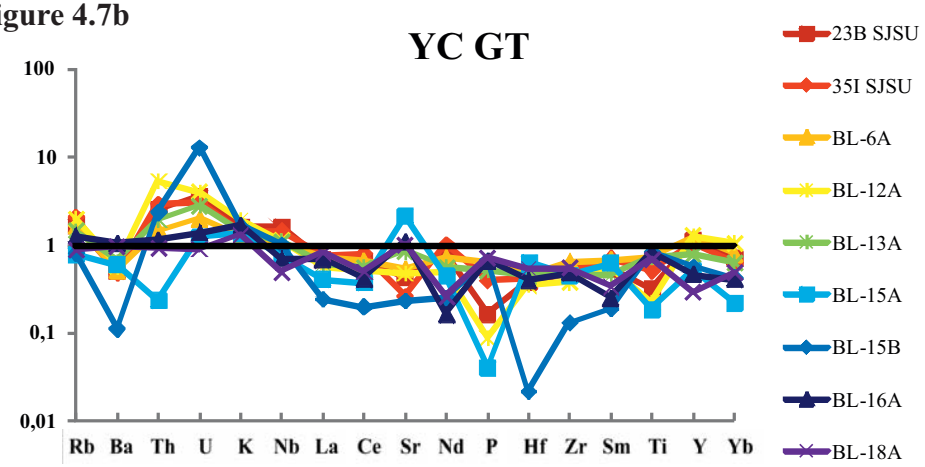
YC GT
100
10
1
0,1
0,01
Rb Ba Th U K Nb La Ce Sr Nd P Hf Zr Sm Ti Y Yb
23B SJSU
35I SJSU
BL-6A
BL-12A
BL-13A
BL-15A
BL-15B
BL-16A
BL-18A

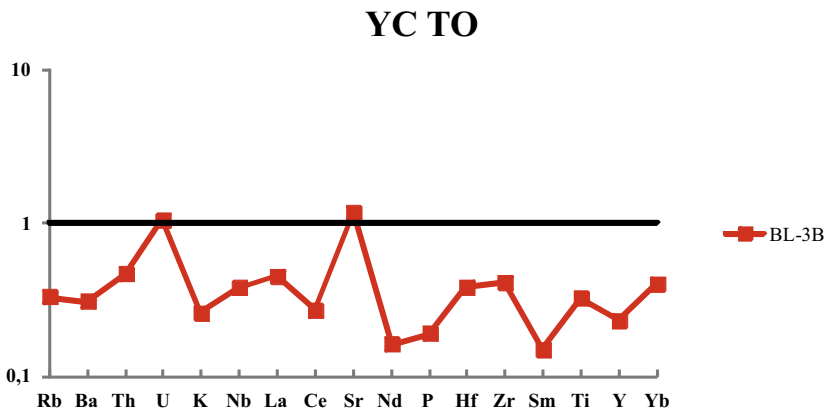
YC TO
10
1
0,1
Rb Ba Th U K Nb La Ce Sr Nd P Hf Zr Sm Ti Y Yb
BL-3B

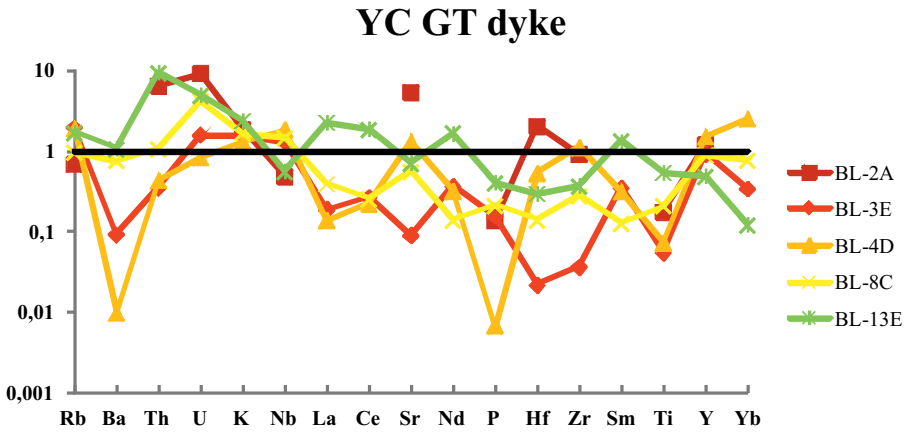
YC GT dyke
10
1
0,1
0,01
0,001
Rb Ba Th U K Nb La Ce Sr Nd P Hf Zr Sm Ti Y Yb
BL-2A
BL-3E
BL-4D
BL-8C
BL-13E

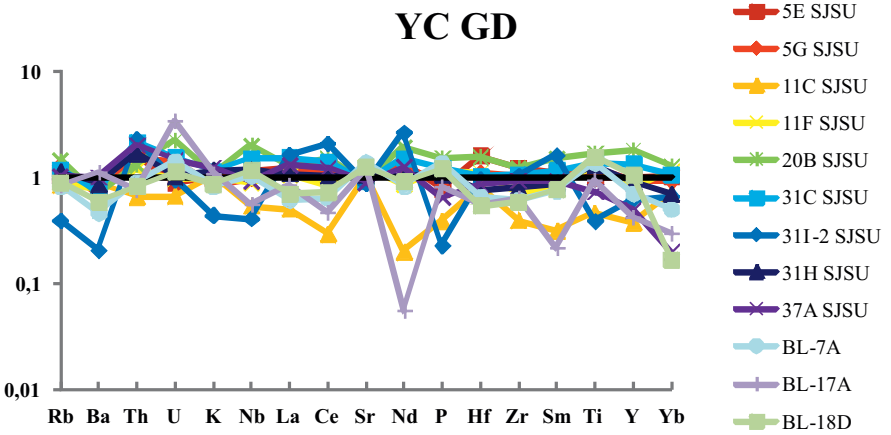
YC GD
10
1
0,1
0,01
Rb Ba Th U K Nb La Ce Sr Nd P Hf Zr Sm Ti Y Yb
5E SJSU
5G SJSU
11C SJSU
11F SJSU
20B SJSU
31C SJSU
31I-2 SJSU
31H SJSU
37A SJSU
BL-7A
BL-17A
BL-18D

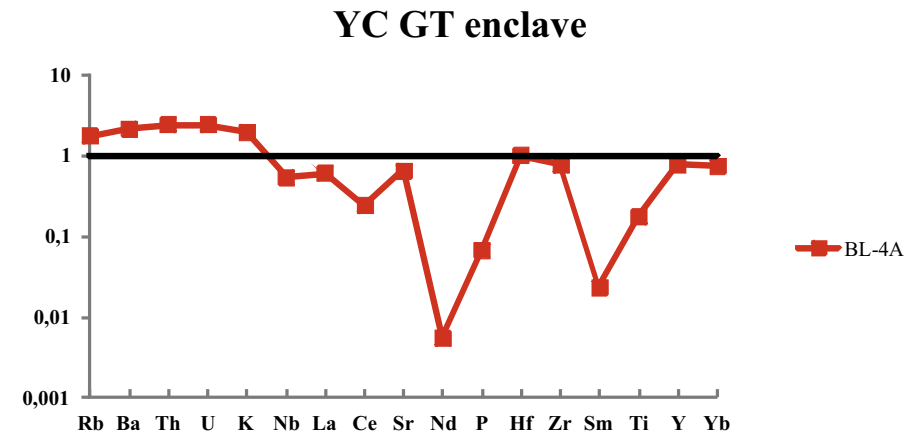
YC GT enclave
10
1
0,1
0,01
0,001
Rb Ba Th U K Nb La Ce Sr Nd P Hf Zr Sm Ti Y Yb
BL-4A

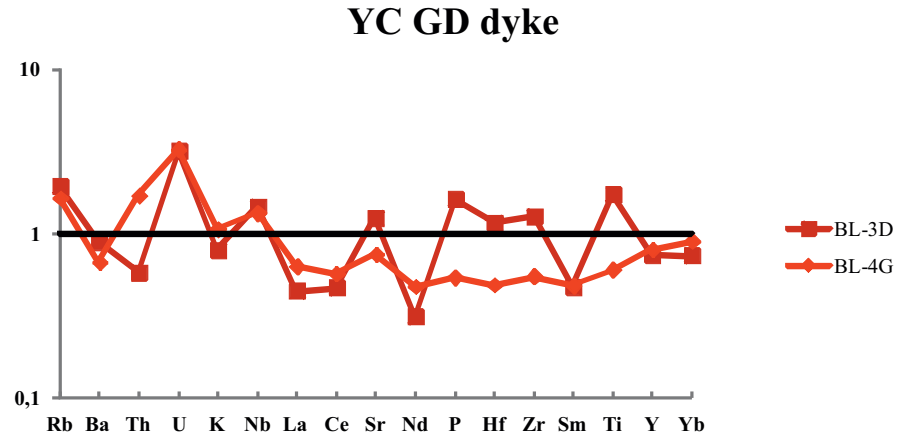
YC GD dyke
10
1
0,1
Rb Ba Th U K Nb La Ce Sr Nd P Hf Zr Sm Ti Y Yb
BL-3D
BL-4G

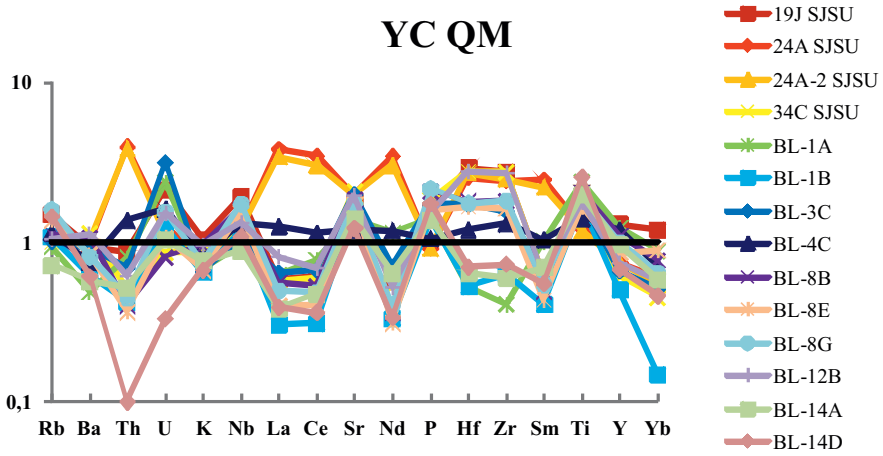
YC QM
10
1
0,1
Rb Ba Th U K Nb La Ce Sr Nd P Hf Zr Sm Ti Y Yb
19J SJSU
24A SJSU
24A-2 SJSU
34C SJSU
BL-1A
BL-1B
BL-3C
BL-4C
BL-8B
BL-8E
BL-8G
BL-12B
BL-14A
BL-14D

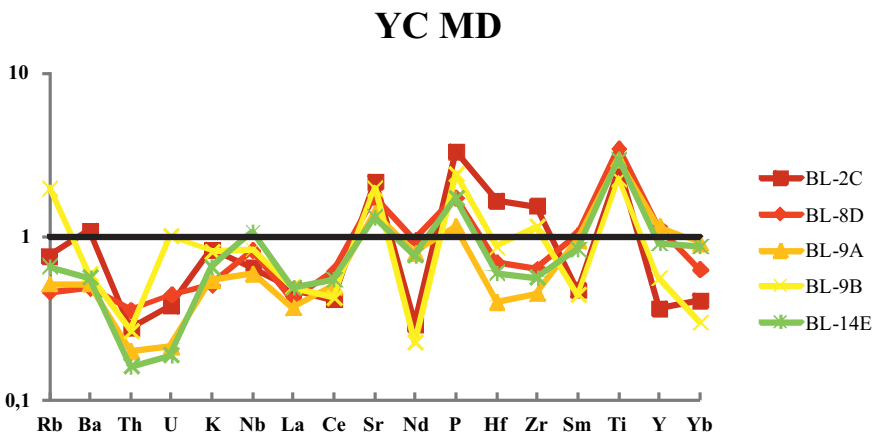
YC MD
10
1
0,1
Rb Ba Th U K Nb La Ce Sr Nd P Hf Zr Sm Ti Y Yb
BL-2C
BL-8D
BL-9A
BL-9B
BL-14E

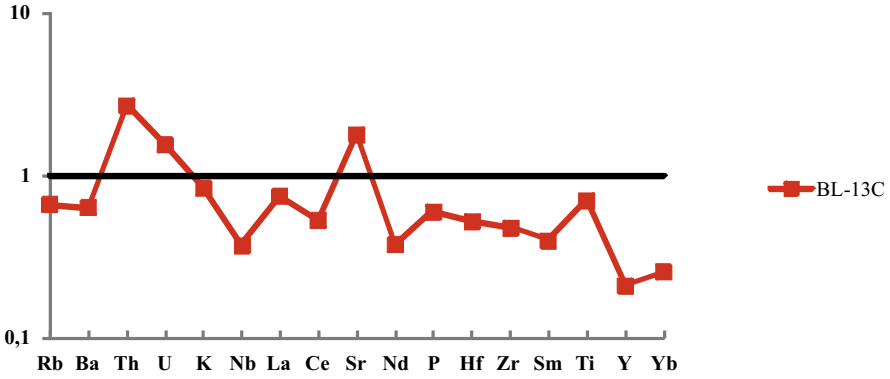
YC QM dyke
10
1
0,1
Rb Ba Th U K Nb La Ce Sr Nd P Hf Zr Sm Ti Y Yb
BL-13C

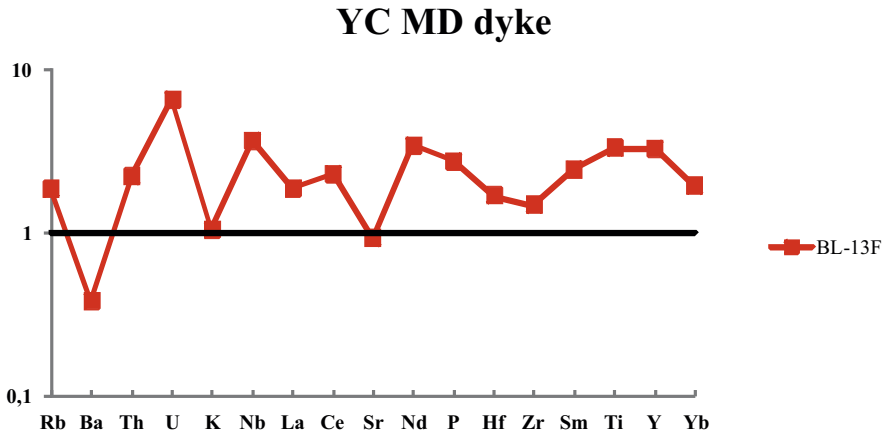
YC MD dyke
10
1
0,1
Rb Ba Th U K Nb La Ce Sr Nd P Hf Zr Sm Ti Y Yb
BL-13F

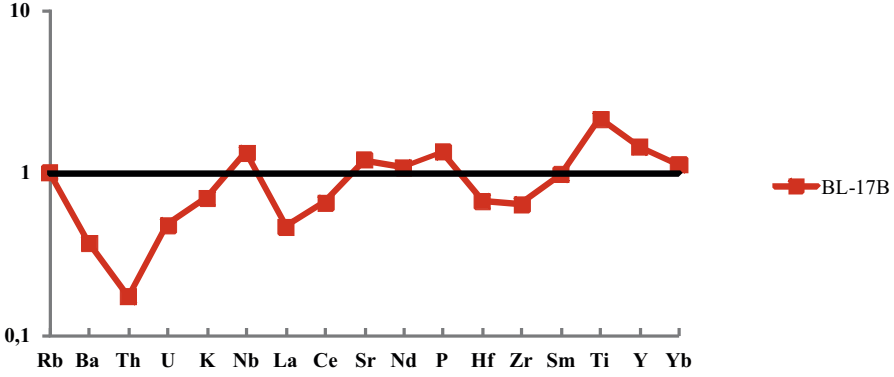
YC QM enclave
10
1
0,1
Rb Ba Th U K Nb La Ce Sr Nd P Hf Zr Sm Ti Y Yb
BL-17B

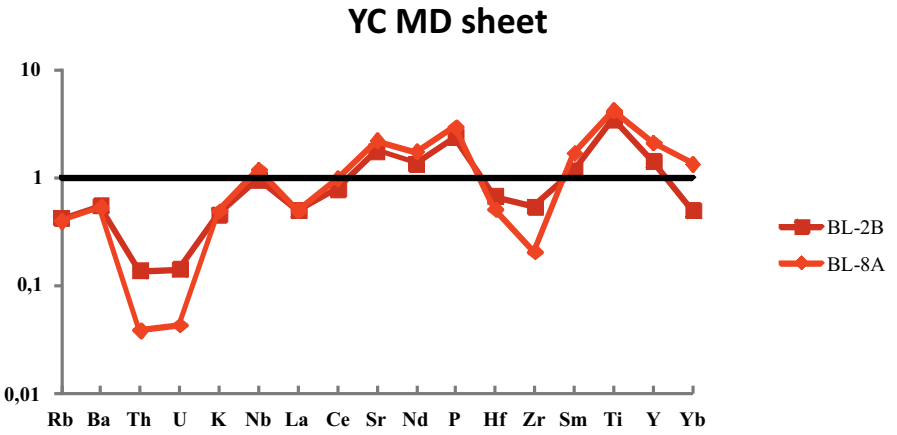
YC MD sheet
10
1
0,1
0,01
Rb Ba Th U K Nb La Ce Sr Nd P Hf Zr Sm Ti Y Yb
BL-2B
BL-8A

Figure 4.7c

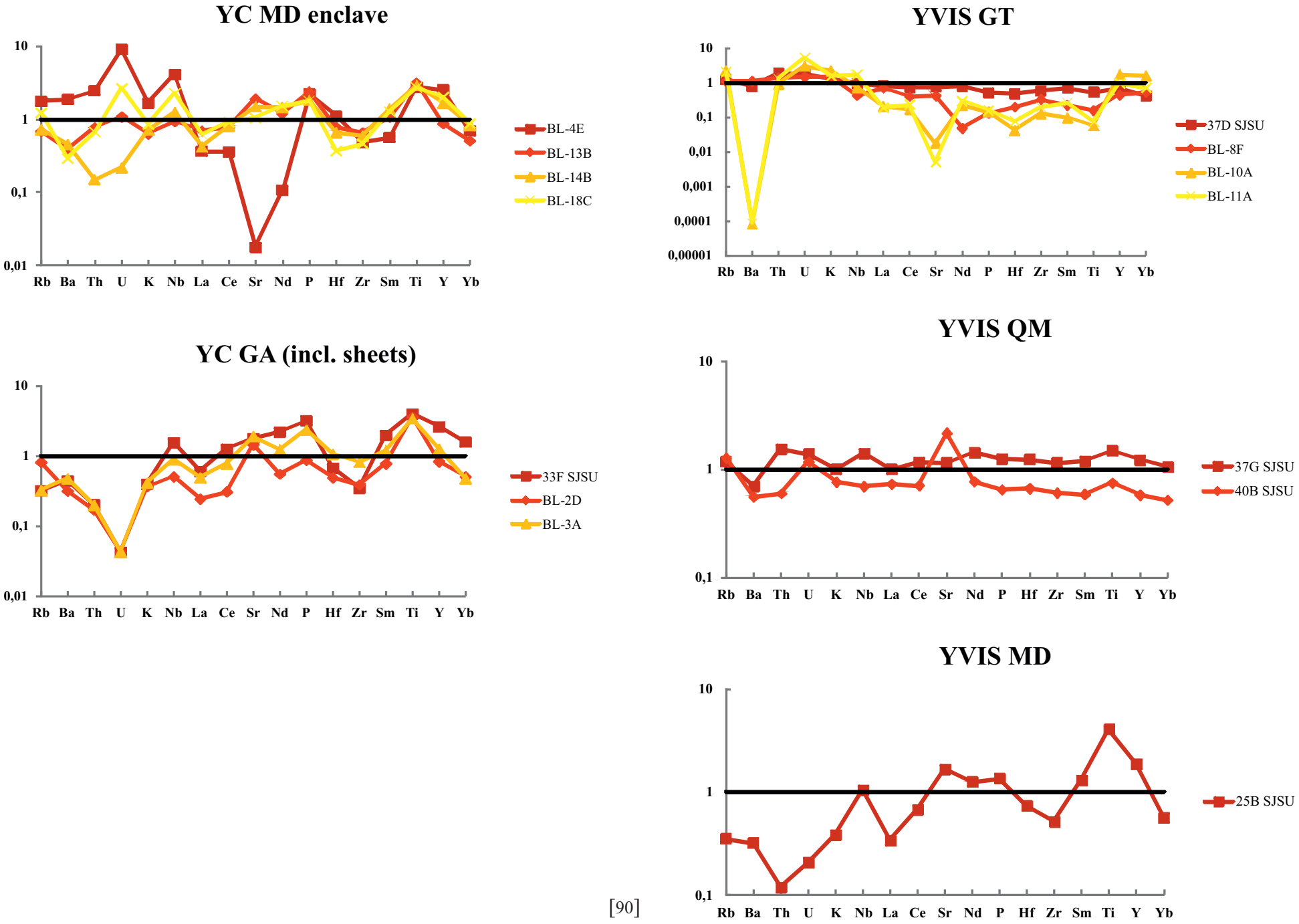
YC MD enclave
10
1
0,1
0,01
Rb Ba Th U K Nb La Ce Sr Nd P Hf Zr Sm Ti Y Yb
BL-4E
BL-13B
BL-14B
BL-18C
YVIS GT
10
1
0,1
0,01
0,001
0,0001
0,00001
Rb Ba Th U K Nb La Ce Sr Nd P Hf Zr Sm Ti Y Yb
37D SJSU
BL-8F
BL-10A
BL-11A
YC GA (incl. sheets)
10
1
0,1
0,01
Rb Ba Th U K Nb La Ce Sr Nd P Hf Zr Sm Ti Y Yb
33F SJSU
BL-2D
BL-3A
YVIS QM
10
1
0,1
Rb Ba Th U K Nb La Ce Sr Nd P Hf Zr Sm Ti Y Yb
37G SJSU
40B SJSU
YVIS MD
10
1
0,1
Rb Ba Th U K Nb La Ce Sr Nd P Hf Zr Sm Ti Y Yb
25B SJSU

5 Discussion

The discussion is divided in to two topics, the field results and the geochemical results. From the field results three hypothesis are proposed. The geochemical data are used to verify or reject these hypothesises. Chapter 6 Conclusion and recommendation will state the most plausible hypothesis, answer the research questions and verify with the research objectives.

5.1 Field results

In this section the field results are discussed and interpreted. Lithological units are divided into formations and possible relations are proposed. Inferred intrusive relations are based on observations related to dykes, schlieren, enclaves and xenoliths.

Before stating arguments based on magmatic relations the definition of a "melt" should be presented. This author agrees with the interpretations and definitions proposed by Vigneresse et al. (1996) on solid-liquid transitions (Figure 5.1). In summary Vigneresse et al. (1996) state that a melt can be mobile over large distances (crustal scale) if there is 20-25% liquid present; ~55% of solid phases in a melt forms a randomly packed framework in which particles can sustain stress and between ~72% and 75% of solid phases the system becomes locked. Hereby this author defines a solid rock when a "melt" contains roughly 75% or more of solid phases.

5.1.1 Lithologies

Different lithologies in Chapter 3 Field Observations are mentioned and already interpreted by assigning the outcrop lithologies to one of the units. The Yosemite Creek Granodiorite Formation (after Huber et al., 1989) consists of porphyritic granodiorite, coarse-grained granodiorite, fine to medium grained quartz monzodiorite to granodiorite, diorite to hornblende-rich diorite (occasionally feldspar porphyritic) and fine grained quartz monzodiorite to granodiorite (this research). For the discussion of the field results the fine to medium grained quartz monzodiorite to granodiorite and the (fine) grained quartz monzodiorite to granodiorite can be grouped together as quartz monzodiorite to granodiorite. Near Ten Lakes this unit shows grain size variety which can be smaller than 1 mm in diameter.
Granite lithologies can be attributed to the Taft Granite Formation (after Huber et al., 1989). Leucogranite lithologies are not necessarily directly linked to the Taft Granite, see 5.1.2 for further discussion. Petrogenetic relations between the YC units are discussed in 5.1.5 and 5.2.3.

The contact between the Transitional Yosemite Sentinel Granodiorite – Yosemite Creek Granodiorite and the Yosemite Porphyritic Granodiorite has not been observed. The transition is gradational and very hard to distinguish (this research). Several interpretations are made in the literature in relation to this locality (Fulmer and Kruijer, 2008; Petsche, 2008). Based on observations this author agrees with the interpretations made by Fulmer and Kruijer (2008) and adopted the estimated contact boundary as proposed by Fulmer and Kruijer (2008) (Figure 3.2).

5.1.1.1 Taft Granite margins

There are no direct contacts observed between the Diorite to Hornblende-rich Diorite Unit and the Taft Granite. No contact relations between Taft Granite and the Porphyritic Granodiorite unit and Taft Granite and the Coarse Grained Granodiorite unit are observed due to inaccessible terrain (Figure 3.2b).

Taft Granite vs. Granodiorite

Contact relations between the Taft Granite and the units of the YC are diverse. In Figure 3.4a a contact between Taft Granite and YC is shown (contact is near the horizontal dashed line). The contact is sharp, with the lithology at the contact being of the YC is granodiorite. The granodiorite thickness is up two to three meters and then gradationally turns in to diorite to hornblende-rich diorite. Near sample point 6 similar contacts are observed, however the granodiorite thickness is several tens of meters thick. Figure 3.4h, i, j1, j2, z1, z2 show the contact relation between the Taft Granite and the YC. The YC units in these figures are medium grained quartz monzodiorite to granodiorite, except for Figure 3.4h which is (fine grained) quartz monzodiorite to granodiorite.

Taft Granite vs. Quartz Monzodiorite to Granodiorite

Figure 3.4h shows a Taft Granite which is incorporated into the YC (fine grained) quartz monzodiorite to granodiorite unit. The lower part of the figure, near the hammer-head, is "solid" Taft Granite. Near the handlebar of the hammer you see strings originating out of the Taft Granite. The composition compositions of the stringers are similar as that of the granite, thickness of the strings vary from a decimetre thick to mineral size thickness. At the sample point of Figure 3.4h the YC is incorporated in the Taft Granite. In Figure 3.4i Taft Granite xenoliths are incorporated into the YC host rock. Figure 3.4j1, j2 show Taft Granite which is in the process of being assimilated by the YC (quartz monzodiorite to granodiorite). In Figure 3.4j1 the YC intrudes into the Taft. Figure 3.4j2 show Taft Granite which is mixing with YC, amount of Taft Granite minerals decreasing to the right. This last mentioned figure is interpreted as assimilation of Taft Granite into YC. Figure 3.4z1, z2 shows a contact with schlieren in the YC as well as an intrusion of YC into the Taft Granite.

Interpretation

In summary, the contact between the Taft Granite and the YC can be sharp, however in most (75%) observations the contact is irregular. The irregularity is caused by intrusions of YC into Taft Granite and assimilation of the Taft Granite into the YC. To create the assimilate structures discussed in previous paragraphs, the contact margins of the Taft Granite must have been partially molten for at least 25%. The YC is likely to have been a mobile melt with a maximum of 50% of solid phases to bring in enough heat for partial melting and assimilation of the contact margin of the Taft Granite.

From literature it is made possible to quantify temperature relations. A granodiorite at shallow crustal depth (not shallower then 4 km (~ 0.1 GPa) of depth, see Chapter 1) with abundant H_2O begins to melt between 600° - 700°C (Winter, 2001). Feldspars of the Taft Granite assimilated into the YC are intact this suggest that the maximum temperature can not be higher than 900° C (Winter, 2001). The magmatic source (subduction zone) is water-rich and there are abundant water bearing mineral phases such as hornblende minerals. Based on these observations and interpretations this author made the assumption that the system is water saturated which is necessarily for the temperature statements mentioned above.

5.1.1.2 Coarse Grained Granodiorite Unit and the Porphyritic Granodiorite Unit

Contact margin

The contact relationship between the Coarse Grained Granodiorite Unit and the Porphyritic Granodiorite Unit is gradational. The transitional zone is roughly 30 meters wide and follows the whole length of the contact. The transition is a change in grain size, which decreases to the North. The units are interpreted to be strongly related to each other because of the observed transitional zone, the compositional resemblances and grain size resemblances, moreover in Chapter 3 Field Observations and 5.2.

Interpretation

There are two ways to interpret the relation between the Coarse Grained Granodiorite Unit and the Porphyritic Granodiorite Unit. The first interpretation is a source or facies difference. The other interpretation would be a product of mixing.

The Coarse Grained Granodiorite Unit and the Porphyritic Granodiorite Unit can be interpreted as two different facies of one single magma batch. Facies difference could be due to a different magma source injection or change in the composition of the magma injection. The other hypothesis to explain the facies difference would be that the Porphyritic Granodiorite Unit inherited the feldspars that are characteristic for the porphyritic structure. In this hypothesis the "pre-" or "proper" Porphyritic Granodiorite Unit should be similar to the Coarse Grained Granodiorite Unit. The feldspars could be inherited from a host rock such as the Taft Granite.

5.1.1.3 Diorite to Hornblende-rich Diorite Unit

Contact margin

Near contacts with the Taft Granite a transitional zone of quartz monzodiorite to granodiorite can be observed. Thickness of the quartz monzodiorite to granodiorite range from one meter up to several tens of meters. Notable is the increase in diorite to hornblende-rich diorite enclaves towards the Diorite to Hornblende-rich Unit, see 5.1.2. All the contacts of the Diorite to Hornblende-rich Diorite Unit are with the Quartz Monzodiorite to Granodiorite Unit (Figure 3.4b, e, g, n). The contact between the units ranges from sharp to crenulated. Near the contact enclaves and dykes are observed. Notable is that both units show intrusive relations with the other unit, moreover in 5.1.2 and 5.1.3..

Interpretation

The discussion in previous section indicates that both lithologies were partially molten (or less than 55% solidified) when emplaced. More quantification on percentages of liquid phases and solid phases are performed in 5.1.2.

The observation that only diorite to hornblende-rich diorite lithologies have contact margins with granodioritic lithologies can suggest two things. Either the dioritic lithologies and granodioritic lithologies are emplacement related. Meaning that they are emplaced near the same localities perhaps due to reusing of intrusive contacts from the older granodioritic units. Or the granodioritic lithologies are a product of assimilation and homogenization between the Diorite to Hornblende-rich Diorite Unit and the Taft Granite Unit.

5.1.2 Xenoliths and enclaves

To understand the relations of the enclaves and there surrounding it is necessarily to understand the liquid-solid transition. This author adopts the classification proposed by Vigneresse et al. (1996) (Figure 5.1). Vigneresse et al. (1996) distinguishes two processes, partial melting and crystallization. This author refers to process of partial melting when stating percentages of liquid phases. When stating percentages in solid phases the process of crystallization is meant.

Some enclaves show a degree of homogenization with their host rock. The homogenization process depends on the size of a enclave and on the water content. From Baker (1991) there can be stated that almost all enclaves from 5 cm in diameter and a temperature above 800°C are homogenized within 10^3 yr. For larger enclaves, from 50 cm in diameter, with a temperature above 800°C are homogenised within 10^5 yr.

5.1.2.1 Granite xenoliths and enclaves

In Quartz Monzodiorite to Granodiorite Units
Granitic angular xenoliths observed in quartz monzodiorite to granodiorite lithologies are interpreted as solid (<20% liquid phases; Vigneresse et al., 1996) Taft Granite blocks which are fully surrounded by quartz monzodiorite to granodiorite melt (Figure 3.3 a, g, h, i, j). Partial melting of the Taft Granite results in xenoliths that contain mineral strings (Figure 3.3c, j2). These melts contain less than 20% solid phases and hereby it can assimilate Taft Granite feldspars. This interpretation is based on the rotating Taft Granite feldspar minerals. Granitic enclaves of Figure 3.3h, j and Figure 3.4i are interpreted as Taft Granite xenoliths that are assimilated by the Quartz Monzodiorite to Granodiorite Unit. They form spherical shapes because they are to a higher degree partially molten than the angular xenoliths, for at least 20-25% of liquid phases (Vigneresse et al., 1996). These features of Taft Granite incorporated into the YC can be interpreted as small scale wall and roof stooping.

5.1.2.2 Quartz monzodiorite to granodiorite xenoliths and enclaves

In Diorite to Hornblende-rich Diorite Units
One type of quartz monzodiorite to granodiorite enclaves is observed in the Diorite to Hornblende-rich Diorite Unit (Figure 3.4e, g, l). Viewing Figure 3.4e, g it directly shows that the Quartz Monzodiorite to Granodiorite Unit forms enclaves in the Diorite to Hornblende-rich Diorite Unit and vice versa. Figure 3.4l shows strong amorphous enclaves. Taking observations of diorite to hornblende-rich diorite enclaves with crenulating margins in the Quartz Monzodiorite to Granodiorite Unit into account (Figure 3.4m, n), an interesting interpretation can be made. Both the units where, at least near the margins, magmatic mobile. This author, based on Vigneresse (1996), concludes that these melts contained less than 50% of solid phases by partial melting and/or crystallization.

In Taft Granite and other granitic lithologies
Quartz monzodiorite to granodiorite enclaves or xenoliths are observed in granitic lithologies (Figure 3.4k, w). The question is if the xenoliths/enclaves are surrounded by granitic intrusions and hereby in situ or if they are assimilated into the granitic body. Another model would be that the quartz monzodiorite to granodiorite xenoltihs/enclaves were injected into the granitic bodies.
However, this statement can be probably rejected because the xenoltih/enclaves are angular which suggest that they were near solid (over 55% of solid phases) when emplaced. Interpretations are speculative because the granitic bodies do not resemble dyke-like structures. Dyke-like structures would favour the hypothesis that quartz monzodiorite to granodiorite intruded the granitic bodies. Based on other field observations of (leuco)granitic dykes this author favours the model that (leuco)granitic bodies intruded into or near the Quartz Monzodiorite to Granodiorite Unit whereby parts of quartz monzodiorite to granodiorite are assimilated into the granitic bodies resulting in the xenoliths.

5.1.2.3 Diorite to hornblende-rich diorite xenoliths and enclaves

In Coarse Grained Granodiorite Unit and Porphyritic Granodiorite Unit
The diorite to hornblende-rich diorite enclaves in the Porphyritic Granodiorite Unit and Coarse Grained Granodiorite Unit are different with respect to the enclaves in the Quartz Monzodiorite. The difference is that these enclaves vary strongly in shape, composition and structure amongst neighbouring enclaves (Figure 3.5d, e, q, s). The shapes can be spherical or more elongated, the composition vary the most with respect to the amount of hornblende and feldspar minerals and the structure ranges from fine grained to porphyritic. Thin-sections BL-13B and BL-14D show most contrasting composition and structure, other resembling enclaves are BL-14B, BL-17B and BL-18C.

Figure 3.5a shows an enclaves swarm that is located at the margin of a large mafic body (also discussed in Chapter 3 Field Observations). This enclave feature is interpreted as a transitional zone between the mafic body and the Porphyritic Granodiorite Unit. The porphyritic granodiorite contained over 20% of liquid phases due to partial melting and the diorite body consisted out of less than 50% solid phases (Vigneresse et al., 1996; Figure 5.1). The enclave swarm shown in Figure 3.5c is interpreted as a mafic dyke that intruded the Porphyritic Granodiorite Unit which had 55% or less solid phases. The mafic dyke consisted out of less than 20% solid phases, minerals could still rotate in the enclave. The change in composition and structures in the enclaves are interpreted as partial mixing of the enclaves with the porphyritic granodiorite surrounding lithology. Especially Figure 3.5m, q shows the mixing. The feldspar minerals in porphyritic enclaves are interpreted as assimilated feldspars of the Porphyritic Granodiorite Unit into the mafic enclaves. Thin-section of BL-14E show a hornblende-corona around a feldspar and quartz mineral clusters. The first quenching mineral when cooling the diorite to hornblende-rich diorite enclave are mafic minerals such as hornblende. When assimilating a cool mineral cluster into the hot enclave hornblende will settles at the clusters margins.

The enclaves of Figure 3.5x, y, z2 form a large (200 square meter) complex with mafic accumulates and schlieren (Figure 3.5z1, z3) in the Porphyritic Granodiorite Unit. Figure 3.5x is interpreted as a channel or sink hole which is partly filled by mafic accumulates. These mafic accumulates are transported over 1 meter (from the right arrow to the left arrow in figure). Figure 3.5y show the mafic accumulates of different layers of diorite to hornblende-rich diorite enclaves, sizes of enclaves vary per layer. Striking are the boudin-sheared layers, indicated by the arrows. Accommodating these shear components suggest a melt of 55 to 75% solid phases for these layers. This area of enclaves and schlieren is interpreted as a margin of a magma chamber/reservoir which is at least several tens of meters in dimension.

Coarse Grained Granodiorite Unit
Interpretations stated for the mafic enclaves in the Porphyritic Granodiorite Unit and the mixing is similar for the Coarse Grained Granodiorite Unit and there enclaves. There should be stated that in the Coarse Grained Granodiorite Unit similar mafic accumulates (enclave swarm) are observed as shown in Figure 3.5m, q. However, one mafic pod is more hornblende-rich with respect to the mentioned figures.

5.1.2.4 Porphyritic granodiorite xenoliths and enclaves

Figure 3.5f, g, h show enclaves and xenoliths of porphyritic granodiorite in a diorite to hornblende-rich diorite sheet. Amongst these features different degree of homogenization occurs. The sheet intruded into the Porphyritic Granodiorite unit, incorporate porphyritic granodiorite xenoliths. Partial melting of the xenoliths is higher than 20% of liquid phases and probably over 800°C. Several xenoliths were more homogenized because either they were hotter or the time of homogenization was longer with respect to enclaves.

Enclaves are a result of melt interaction of the sheet with the host rock. To form the enclaves in both the units (Figure 3.5a, f) less than 50% of solid phases formed by partial melting and the temperature/time ratio was relative low (T <800°C and/or short cooling time, 10^3 yr) to minimize homogenization. The xenoliths and enclaves are interpreted as mixing relationships between the sheet and the Porphyritic Granodiorite Unit host rock.

5.1.3 Dykes and sheets

Dykes are a good indication to construct a chronological emplacement model. The intrusions are discussed in the next paragraphs sorted by the lithology of the intrusion and intrusive host rock. The sub-chapters are (grano)diorite dykes, granitic intrusions, porphyritic granodiorite and the coarse grained granodiorite intrusions and the Myriad zone.

5.1.3.1 (Grano)diorite dykes

Intruding Taft Granite
(Grano)diorite dykes can intrude into the Taft Granite (Figure 3.4a, c, q). Notable is that the granodiorite dyke of Figure 3.4a originates out of the Quartz Monzodiorite to Granodiorite Unit at the Taft Granite margin. The contacts of the dyke are sharp meaning that the Taft Granite was in solid state (over 70% of solid phases when intruded).

Intruding Quartz Monzodiorite to Granodiorite unit
(Grano)diorite dykes are common throughout the study area. The largest sheet observed is a fine grained granodiorite sheet (Figure 3.3d) which intruded into the Quartz Monzodiorite to Granodiorite Unit. The contact relation is shown in Figure 3.3e which is a branch of the large intrusion. This branch intruded into the margins of the Quartz Monzodiorite to Granodiorite Unit. The large sheet might be correlated to the diorite to hornblende-rich diorite zone between Grant Lakes and Ten Lakes. Figure 3.2b shows that this sheet could be linked to the southern "tail" of the diorite to hornblende-rich diorite unit. No detailed observations are made of the diorite to hornblende-rich diorite "tail".

Intruding Porphyritic Granodiorite Unit and Diorite to Hornblende-rich Diorite
Intrusions of the Quartz Monzodiorite to Granodiorite Unit into the Diorite to Hornblende-rich Diorite Unit can be observed near the contact of the Quartz Monzodiorite to Granodiorite Unit with the Diorite to Hornblende-rich Diorite Unit (Figure 3.4e, f, g, l, r). Most contacts are not straight which indicates that the host rock was not locked by solid phases, meaning that less than 70% of the melt was in solid phase when intrusion occurred.

The granodiorite dyke shown in Figure 3.5i, j originates out of the Porphyritic Granodiorite Unit, and intrudes through the Porphyritic Granodiorite Unit and continues intruding a diorite to hornblende-rich diorite sheet. Notable is that this granodiorite dyke cuts through porphyritic granodiorite intrusions in the diorite to hornblende-rich diorite sheet. This is interpreted as a product of partial melting or product of incompletely solidification of the Porphyritic Granodiorite Unit. When considering partial melting that rock consisted out of at least 20% of liquid phases. Hereby the melt could becomes mobile and intruding the sheet. This suggest that this partial melting process is a relative late stage phenomena. When considering incomplete solidification, the system was still hot and mobile enough (with less than 70% of solid phases) to form the intrusion.

5.1.3.2 Diorite to hornblende-rich diorite intrusions

Diorite to hornblende-rich intrusions are commonly large (several meters wide and tens of meters in length; Figure 3.2b). These intrusions are unstable and loose coherency by forming enclaves (Figure 3.4o; Figure 3.5a). Total loss of coherence is caused by the intrusion shown in Figure 3.5c. These observations suggested that all intruded host rocks where magmatic mobile so it could form enclaves from the intrusions. Crystallization of the host rocks existed out of less than 50% solid phases when the (hornblende-rich) diorites intruded.

5.1.3.3 Granitic Intrusions

(Leuco)granitic dykes

(Leuco)granitic dykes intruding uncorrelated to host rocks, they intrude Taft Granite (Figure 3.4y1, y2), Quart Monzodiorite to Granodiorite Units (Figure 3.3g; Figure 3.4f, p, t, u, v), Diorite to Hornblende-rich Diorite Units (Figure 3.4d, r, s1, s2) and Porphyritic Granodiorite Units (Figure 3.5k, l, m, n, o). The intrusive contacts of the dykes with respect to the host rocks are sharp and often the intrusions contain xenoliths of their host rock. The origin of the dykes can be, in almost all observed dykes, traced to Taft Granite outcrops, especially the smaller granite dykes. The abundance and intrusive character of the granitic dykes support an interpretation that these intrusions are late stage and intruding near solid (>70% solid phases) lithologies.

Double dyke

Special attention is needed to interpret the observations of Figure 3.5k, l, m, n, o. This so called double dyke intruded with sharp contact into the Porphyritic Granodiorite Unit with its diorite to hornblende-rich diorite enclaves. Petrogenetic interpretation of the double dyke is as follow: emplacement and solidification (>70% solid phases) of host rock with enclaves (e.g. Figure 3.5c); intrusion of leucogranitic dyke which stretches over several hundreds of meters (Figure 3.2b); re-using leucogranitic dyke by diorite to hornblende-rich diorite intrusion which reheat most of the leucogranitic dyke (Figure 3.5l); the inner part of the leucogranitic dyke gets assimilated resulting in a mafic-felsic mingling which varies at mineral scale (Figure 3.6 BL-15C) to decimetre scale. This assimilation by partial melting also resulted in the crenulated margins of the mafic inner layer (Figure 3.5o).

5.1.3.4 Porphyritic granodiorite and the coarse grained granodiorite intrusions

Two observations (Figure 3.5p, r) are made in the field that complicate interpretations on the relation of between the Coarse Grained Granodiorite Unit and the Porphyritic Granodiorite Unit. Figure 3.5p is interpreted as a porphyritic granodiorite dyke in the Coarse Grained Granodiorite Unit. This dyke stretches for several meters, thickness varying from several decimetres to one decimetre and the contact is irregular.

The Coarse Grained Granodiorite Unit is interpreted to be younger than the Porphyritic Granodiorite Unit, this interpretation does not correspond with the observation of the previous discussed dyke. Either the observed porphyritic dyke is a xenolith of the Porphyritic Granodiorite Unit which is dropped (by wall or roof stoping) into the Coarse Grained Granodiorite Unit, or it is a late stage facies pulsation of the Porphyritic Granodiorite Unit emplacement.

In the hypothesis that the Porphyritic Granodiorite Unit is constructed from assimilated and homogenized Taft Granite the following model can be proposed for the porphyritic granodiorite dyke. The Coarse Grained Granodiorite melt mixed and homogenized a Taft Granite xenolith which was dropped into the melt. Similar interpretations can be proposed for the observation of Figure 3.5r, which shows a coarse grained granodiorite body or intrusion in the Porphyritic Granodiorite Unit. Summarizing, the Porphyritic Granodiorite Unit and the Coarse Grained Granodiorite Unit are either interpreted as facies differences of magma injections or as a results of assimilation from the Taft Granite.

5.1.3.5 Myriad zone

The Myriad zone should be consider as a separate zone which includes granitic, leucogranitic, granodioritic and diorite to hornblende-rich diorite lithologies (e.g. Figure 3.4p, t, u, v, w, x). The follow interpretation of relative emplacement chronology can be based on field interpretations of dykes and enclaves. The host rock is Taft Granite which is intruded by diorite to hornblende-rich diorite, followed by intrusions of quartz monzodiorite to granodiorite. Partial melting of Taft Granite (over 20% liquid phases) resulted in leucogranitic dykes that intruded all previous mentioned units. Due to partial melting the Taft Granite also could assimilate xenoliths of quartz monzodiorite to granodiorite into the Taft Granite and/or leucogranite bodies. The Myriad zone is interpreted to be relative late magmatic active due to a heat source that made late stage partial melting possible.

5.1.4 Schlieren

In the literature there is a consensus that schlieren are magmatic structures that can be linked to magmatic flows. Paterson et al. (2008) interpreted layered schlieren as a feature of several magmatic pulses. Moreover, Paterson (2009) stated that schlier-complexes are magmatic flows through a crystal-mush and favours the hypothesis that such structures are related to extensive magma chambers. Barbey et al. (2007) suggest that schlieren can be attributed e.g. to assembly of differentiated magmatic pulses.

Schlieren near contact margins
Most schlieren are observed near areas which are interpreted as contact zones such as near xenoliths and contact margins (Figure 3.3b, f; Figure 3.4z1, z2; Figure 3.5t, x, y, z1, z2, z3). Figure 3.3b show resemblances with the Paterson et al. (2008) interpretation of crack-seal magmatic injections. Figure 3.5x, y, z1, z2, z3 show resemblances with the Paterson (2009) trough including mafic accumulates structures, moreover in the next paragraph.

Schlieren are interpreted by this author as mineral segregation due to a change in magmatic flow. This would imply for the previous described examples that the hot YC intruded in increments next or into the cool Taft Granite.

Schlieren structures
Figure 3.5u, v, w are of another sort of schlieren such as proposed by Paterson (2009) (Figure 5.2). Figure 3.5u shows a dyke-like structure of mafic minerals with circular features within the dyke-like structure. This is interpreted as a migration tube with little composition variety (Figure 5.2). Figure 3.5w show mafic and felsic circular shapes. The more mafic circular shapes (lower arrow in figure) form a string of the circular features. The more felsic circular shapes (upper arrow in figure) show little change in location. The mafic feature is interpreted as migrating tube and the felsic feature is interpreted as a stationary tube (Figure 5.2). Figure 3.5v show schlieren that are truncated and cut off (arrow) by other schlieren. The elongated spherical shape of the schlieren have axes that are roughly parallel. This outcrop is interpreted as a trough (Figure 5.2).
A trough is a schlieren complex recognizable by slightly elongated circular schlieren which are truncated by other elongated circular schlieren. At the most shallow part of the schlier an increase in mafic accumulates can be observed (Figure 5.2d).

This author finds resemblances between Paterson (2009) interpreted structures and the observed structures in this research. The schlieren structures are thought to be related to processes that occur in larger magmatic reservoir or crystal-mush.

5.1.5 Field Hypothesis

Field observations can be used to make a first impression of the petrogenesis. Geochemical results should verify or reject the hypothesis that originate out of this first impression. Contact relations and intrusive relations of units are used to argument in favour for the hypothesises.

The variations in the YC can be explained as several pulses that might or might not be related by magmatic processes operating at greater depth (lower crust). An alternative hypothesis is that variations are explained by variable degrees of assimilation of (parental) Taft Granite.

5.1.5.1 Hypothesis: In situ hybridization with granites

Hypothesis
A hypothesis that can be stated from the field results is as follow: The Yosemite Creek Granodiorite consists of a single magmatic batch that hybridises in situ with the Taft Granite at shallow crustal depth to form the observed YC units. In this hypothesis all YC units are an assimilation and mixing product between the Taft Granite and a mafic source such as the Diorite to Hornblende-rich Diorite Unit. Observations that coincide with this interpretation or which can be interpreted as such are stated in the next paragraph

Observations
There are no observations of the contact between the mafic end-member, the Diorite to Hornblende-rich Diorite Unit, and the Taft Granite. Between these units there is always a zone of quartz monzodiorite to granodiorite lithology. The contact of the Diorite to Hornblende-rich Diorite Unit with the surrounding Quartz Monzodiorite to Granodiorite Unit is co-magmatic which can be interpreted as two units that originate from the same magmatic increment. The occasionally porphyritic texture that is observed in the Diorite to Hornblende-rich Diorite Unit and the Quartz Monzodiorite to Granodiorite Unit can be interpreted as assimilation of Taft Granite quartz and feldspar minerals.

Hybrid: petrogenetic interpretation
The fresh increment of (hbl-rich) diorite started to assimilate and homogenize with the Taft Granite. Resulting in formation of a “hybrid” near the contact zone between the fresh increment and the (hbl-rich) diorite. This “hybrid” is classified as the Quartz Monzodiorite to Granodiorite Unit. The degree of homogenization and assimilation of Taft Granite varies per outcrop and results in different composition and grain size of the Quartz Monzodiorite to Granodiorite Unit (the hybrid). In this hypothesis the Taft Granite and the Diorite to Hornblende-rich Diorite Unit form the two end-members of a binary mixing/assimilating system (Figure 5.3a).

The Porphyritic Granodiorite Unit and Coarse Grained Granodiorite Unit do not fit within this binary mixing system. Petrogenetic interpretation for these units are stated in paragraph 5.1.5.2.

5.1.5.2 Hypothesis: Incremental growth to form the YC units.

The unit observed in the YC can also be interpreted as different magmatic pulses or increments. These increments can be related to each other at a deep (lower crustal) level or unrelated at all. Based on field observations two hypothesis can be proposed on the relationship between the increments.

Related increments

Hypothesis

Hypothesis for related increments: All YC observed units are related by source. The YC proper interacted with a parental or similar magmatic batch as the Taft Granite. The observed YC units are formed by assimilation and homogenization of the previous mentioned interaction. Differentiation into the observed units is a product of the MASH (Mixing, Assimilation, Storage, Homogenization) zone.

Observations

All the YC units show in the field a plausible interpretation of a binary mixing system between a fine grained mafic source and a coarse grained granitic source. The lithologies that are more felsic include more and bigger feldspar and quartz minerals. These minerals show strong resemblances with the feldspars and quartz minerals observed in the Taft Granite.

Related increments: petrogenetic interpretation

The petrogenesis related to the previous stated hypothesis can be envisioned in the following manner. An older granitic batch, presumably still relative hot to easy assimilation and homogenization, such as a parental Taft Granite is located in the lower crust. A fresh injection of magma resulted from subduction enters the system, this injection would be the YC proper. This fresh injection starts to assimilate and homogenize (AH) the parental Taft Granite which results in a melt with coarse grained feldspars. The felsic components of this melt escaped to the upper crust (~7 km depth) where it crystallized. This would be the Porphyritic Granodiorite Unit. After the most felsic components escaped the AH melt, a lesser coarse grained felsic component escapes to the upper crust where it crystallizes as the Coarse Grained Granodiorite Unit. The next increment would be the Quartz Monzodiorite to Granodiorite Unit which is followed by the most mafic increment the Diorite to Hornblende-rich Diorite Unit (Figure 5.3b).

This latter unit intrudes into all older increments/units resulting in reheating of the system. This leads to many of the observed intrusions. The reheating by the mafic intrusion resulted in the Myriad zone. It is plausible that stratigraphically beneath the Myriad zone the Diorite to Hornblende-rich Diorite Unit is present.

This hypothesis would be consistent with the interpretation that the observed YC is a derivative of a deep young YVIS relative. Such hypothesises are also proposed for the Taft Granite in Ratajeski et al. (2001) and for the YS in Fulmer and Kruijer (2008).

Unrelated increments

Hypothesis

Hypothesis for unrelated increments: There are several magmatic pulses that consist of unrelated magmatic batches originating from subduction magmatism. Observed incremental growth from old to young is as follow: porphyritic granodiorite, coarse-grained granodiorite, quartz monzodiorite to granodiorite and diorite to hornblende-rich diorite (occasionally feldspar porphyritic).

Observations

There are no specific observations in favour for this hypothesis which are not mentioned in previous hypothesises. The variations of composition between the units and grain sizes of the different increments can be explained by source differences. The porphyritic structure in several units suggests that Taft Granite feldspars and quartz minerals could be incorporated at source level as explained in the previous hypothesis. However the porphyritic structure inherited from the parental Taft Granite might be very local and small scale. The observed feldspars and quartz minerals responsible for the porphyritic structure might be in situ for the assimilation and mixing.

Unrelated increments: petrogenetic interpretation

Every single unit is a new fresh magma derived from the subduction system. However in such a magma "percolation" system a maturation of the melt should occur to form the observed units. This would suggest that the magmas derived from the subduction system directly enters the lower crust. An increment of this matured single magma batch escaped to the upper crust. In this hypothesis no or minor assimilation and homogenization occurred (Figure 5.3c).

In this hypothesis it might be difficult to explain why the magma batches do not interact with each other. Emplacement time of the increments is short so it might be hard not to interact at all. Moreover in Chapter 6 Conclusion and recommendation.

5.1.6 Conclusion field results

There are three hypothesis proposed to explain the formation of the Yosemite Creek Granodiorite. It is also possible that the proposed systems operated together in different degrees. The hypothesises are tested with geochemical analyses to gain more understanding on which of the processes operated and to what extent.

Geochemical research will contribute to the follow research sub-objectives:

- If all the YC units are petrogenetical linked.
- The YC units are related to Taft Granite or a young YVIS.
- The Porphyritic Granodiorite Unit and the Coarse Grained Granodiorite Unit are related to the other YC units.
- If present, define end-members of the AH trend between the Taft Granite and a YC unit.

Figure 5.1

In the figure are two processes distinguishable, partial melting and crystallization. A melt can be mobile over large distances (crustal scale) if there is 20-25% liquid phases present; ~55% of solid phases in a melt forms a randomly packed framework in which particles can sustain stress and between ~72% and 75% of solid phases the system becomes locked. Hereby this author defines a solid rock when a "melt" contains roughly 75% or more of solid phases. Modified after Vigneresse et al. (1996).

Figure 5.2

"Main structures discussed in this paper. **(a)** Stationary tubes. **(b)** Migrating tubes. **(c)** Pipes. **(d)** Troughs. **(e)** Diapirs. **(f)** Plume heads. The distinguishing features are listed in the table. Graded schlieren layers shown where developed in structures. Troughs in **(d)** include typical relationships between trough cut-offs, mineral fabrics, magma flow directions and crystal accumulations" After Paterson (2009).

Figure 5.3

Schematically representation of proposed hypothesis. Pink represents the Taft Granite, the red represents the YC Quartz Monzodiorite to Granodiorite and purple represents the Diorite to Hornblende-rich Diorite. Not to scale, no implications of relative volumes and no implications of observed location of interaction. **(a)** Assimilation and hybridization between the Taft Granite and mafic YC unit (Diorite to Hornblende-rich Diorite), indicated by white arrow. **(b)** Incremental growth with related increments. Illustrated is the MASH zone, YC proper input which assimilate and homogenizes with the parental Taft Granite. Resulting in the variation in composition and crystallization of the different increments. **(c)** Illustrated are the unrelated increments with mineral maturity location.

Figure 5.1

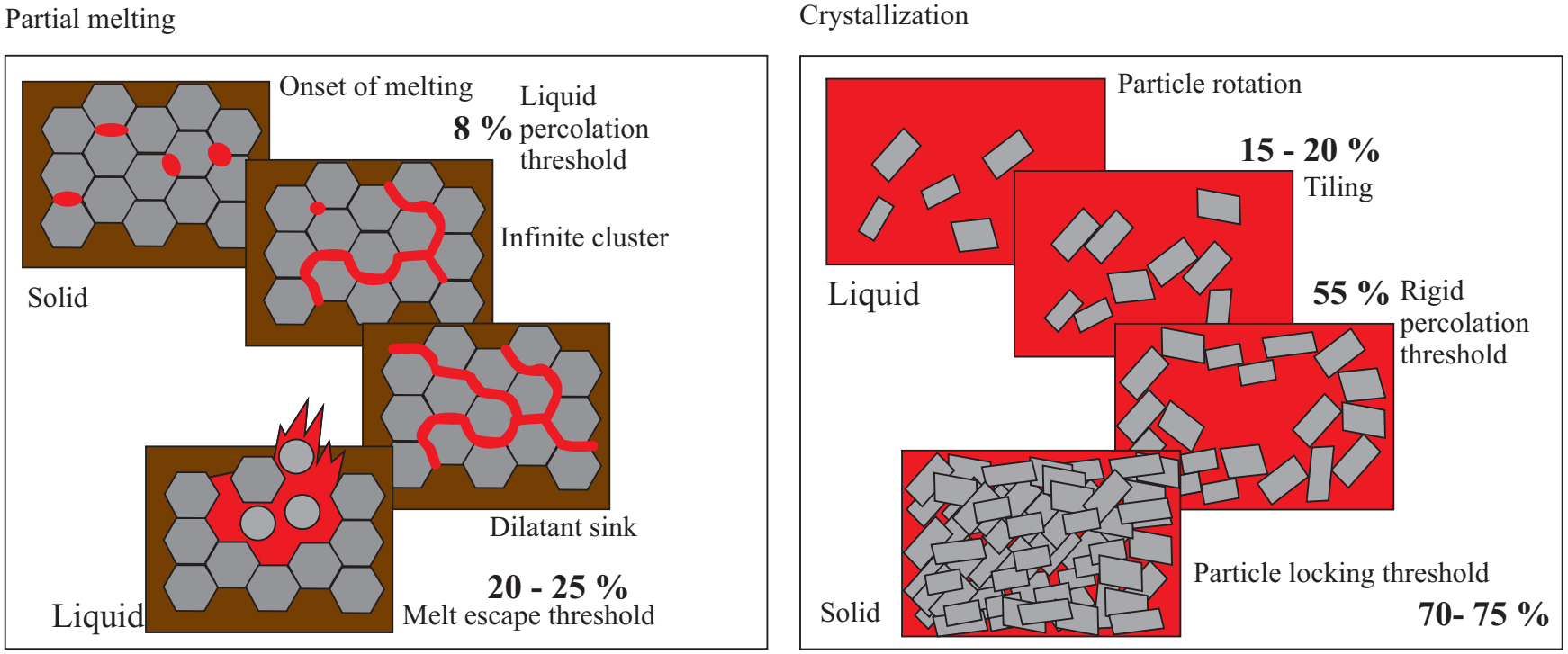
Partial melting
Onset of melting
Liquid
8 % percolation
threshold
Infinite cluster
Solid
Dilatant sink
20 - 25 %
Melt escape threshold
Liquid
a
Crystallization
Particle rotation
15 - 20 %
Tiling
Liquid
55 % Rigid
percolation
threshold
Particle locking threshold
Solid
70- 75 %
b

Figure 5.2

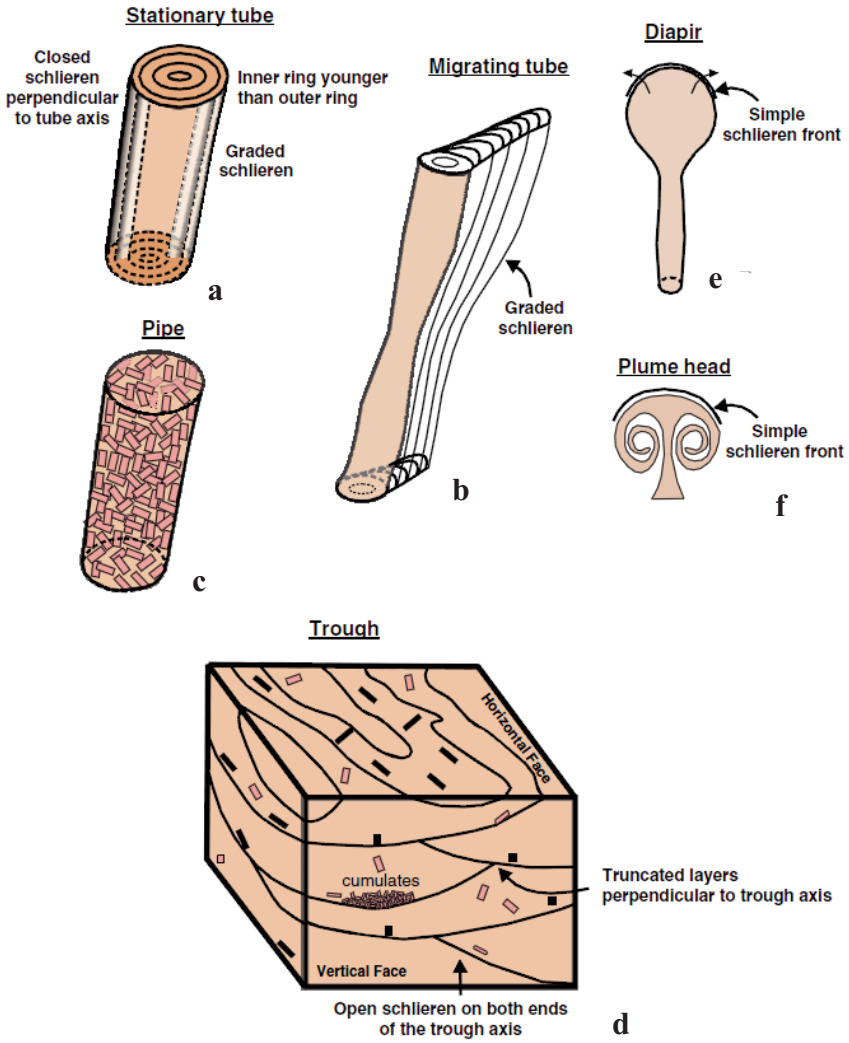

Type of Structure	Inferred Shape	Orientation	Composition	Schlieren	Magmatic lineation
Stationary Tubes	Cylinders	Steep	Distinct from and/or fractionate of host	Multi, nested rings	Steep to rarely horizontal
Migrating Tubes	Multi intersecting cylinders	Steep	Distinct from and/or fractionate of host	Multi, truncated rings	Steep to rarely horizontal
Pipes	Cylinders	Steep	Fractionate or accumulation of host minerals	Rare	Steep to rarely horizontal
Troughs	Channels	Variable	Fractionate of host	Truncated layers	Parallel trough axis
Diapirs	Spherical heads, narrow tails	Highly variable	Highly variable	Rare	Rare to variable
Plumes	Spherical heads, broad tails	Highly variable	Similar to host	Several weak layers	Rare to variable

Figure 5.3

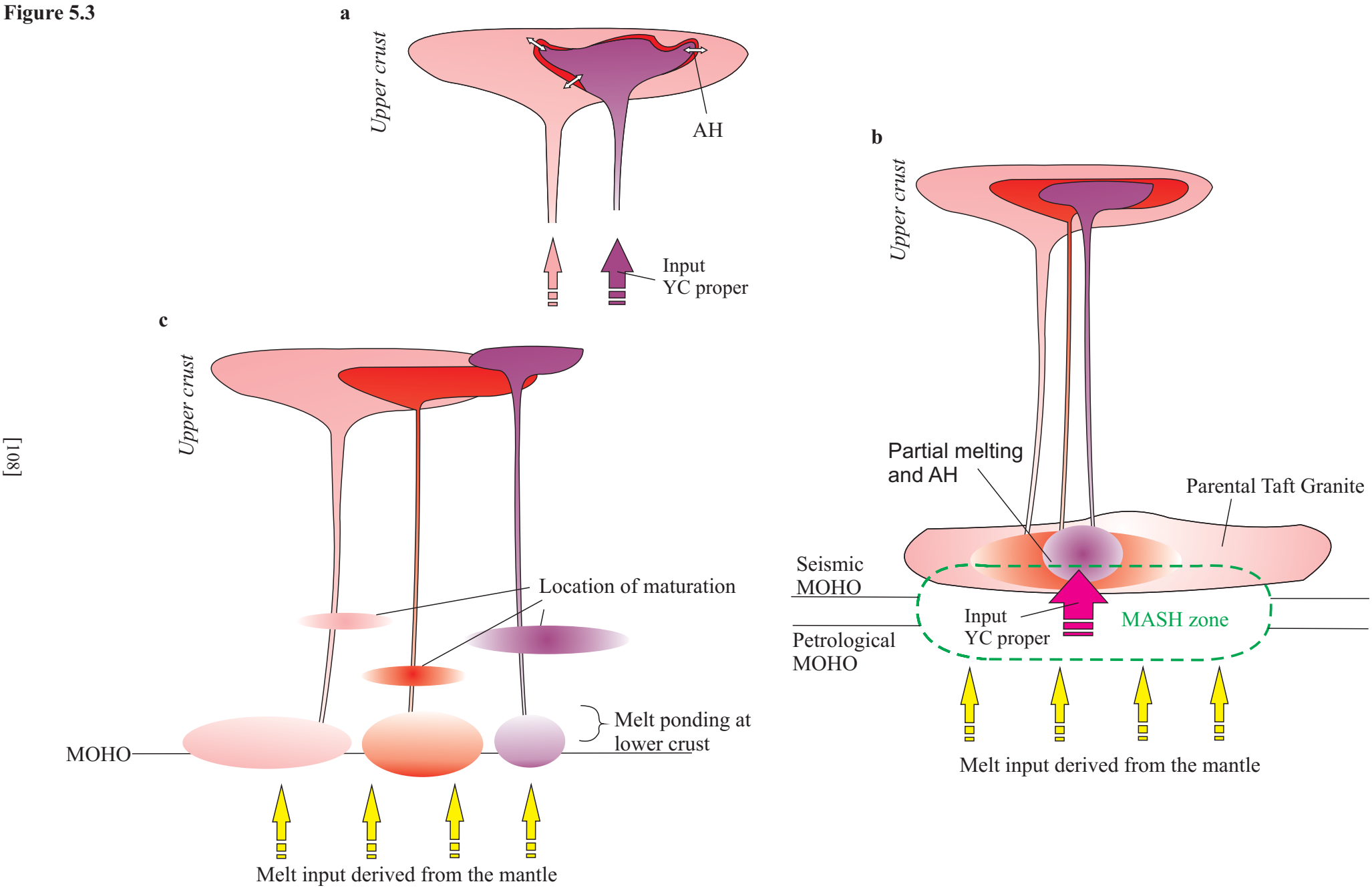
a
Upper crust
AH
Input
YC proper
b
Upper crust
Partial melting
and AH
Parental Taft Granite
Seismic
MOHO
Petrological
MOHO
Input
YC proper
MASH zone
Melt input derived from the mantle
c
Upper crust
Location of maturation
Melt ponding at
lower crust
MOHO
Melt input derived from the mantle

5.2 Geochemical results

Major and trace elements are used to test the hypothesis which are stated by use of field relations and gain possible new insights in the petrogenesis. First the major oxides are discussed and then the trace elements. Calculations are performed to argument statements and quantify processes.

5.2.1 Major elements

In this sub-section the geochemical analyses of major elements are discussed and interpreted. Starting with the TAS diagrams, AFM diagrams, Harker variation diagrams and Fenner type diagrams.

5.2.1.1 Total alkali versus silica

For a normal fractional crystallisation situation a single liquid line of descent would plot in the TAS as a straight line from gabbro to granite. When studying the whole rock data in the diagram of Figure 4.2 the observation can be made that samples are plotted in the domains of the periodotite, gabbro, monzodiorite to monzonite and granodiorite to granite.

From the TAS diagram two hypothesis can be proposed. The first hypothesis and interpretation are two liquid lines of descent (Figure 5.4, red arrows). One liquid line of descent plots from gabbro, monzodiorite, monzonite to quartz monzonite ("subalkaline"). The other liquid line of descent plots from diorite, granodiorite to granite ("Alkaline"). The liquid lines of descent from Figure 5.4 are modified after Middlemost (1993).
The second interpretation and hypothesis could be one single liquid line of descent between gabbro, diorite, granodiorite and granite (Figure 5.4, green arrow). In this interpretation a cluster of ~10 monzodiorite and quartz monzodiorite samples are enriched in alkalis.

Assuming normal liquid lines of descent one could interpreted from only the TAS diagram that two different magmatic evolving batches are present (Figure 5.4, red arrows). The second interpretation would correspond with a normal evolving trend (Figure 5.4, green arrow). The enriched (quartz) monzodiorites are then interpreted to be unrelated to the single liquid line of descent.

Notable are the alkali enriched monzodiorite enclaves. This enrichment could be explained by partial melting or fractional crystallization. Remarkable are the two granite samples, the YC TO and a YC GD, which are low in total alkali concentration and high in silica. They can be interpreted as depleted in total alkali by partial melting of granite/quartz or loss of alkalis due to separation of a volatile rich fraction late in the differentiation process.

5.2.1.2 AFM diagram

In the AFM diagram (Figure 4.3) a typical single calc-alkaline differentiation trend can be observed, which starts as a tholleiite. This liquid line of descent is related to crystal fractionation and is common for evolved subduction related igneous rocks. Minerals involved in crystal fractionation related to alkali-iron-magnesium concentrations are pyroxenes (early stage), amphiboles/hornblende and biotite. Late stage crystal fractionation are the granites with high alkali minerals such as K-feldspar and plagioclase (Winter, 2001).

5.2.1.3 Harker variation and Fenner type diagrams.

This sub-chapter comprises of several sections. In the section of the "Field units" the striking features of Figure 4.4a are discussed and interpreted. Major features and interpretations of the Harker variation diagrams and the Fenner type diagrams are discussed in paragraph "Combined samples" (Figure 5.5).

Field units

In the Harker variation diagram of the "Field units" (Figure 4.4a) a single liquid line of descent can be interpreted from the mafic to the felsic units. In all the major elements the Fine Grained Granodiorite Unit samples show enrichment or depletion with respect to the liquid line of descent. From these diagrams it is plausible that the Fine Grained Quartz Monzodiorite to Granodiorite Unit is unrelated to all the other units or a mixing/assimilation product of a mafic and felsic component.

Combined samples

In the Harker variation diagrams a normal liquid line of descent and a smaller trend line can be distinguished. These diagrams show the following relationships for the general trend: negative relation between SiO_2 and the major-oxides Al_2O_3, FeO*, CaO, TiO_2 and MgO and can be explained as fractional crystallization of plagioclase, olivine, amphibole and/or pyroxene (Figure 5.5; Winter, 2001). The major-oxides of Na_2O, K_2O and BaO show a (shallow) positive correlation with increasing silica (Figure 5.5).

The second trend line in all the Harker variation diagrams is based on a sample cluster that do not fit the normal single liquid line of descent. These outliners correspond to the Fine Grained Quartz Monzodiorite to Granodiorite Unit discussed in chapter 3 Field Observations. This smaller trend line can be interpreted as mechanical mixing between a monzodiorite and a granite (Figure 5.5) or as another batch with a different source as the normal liquid line of descent.

Major-elements in Harker variation diagrams
An integrated study of data suggest the following minerals are involved in the formation of the Yosemite Creek: plagioclase, biotite, hornblende, clinopyroxene, K-feldspar, titanite and apatite. The calculated amount of phase fractionation varies per major-element. For the same magmatic system one expects that all the fractional crystallisation phases show similar pattern for each major-element. Hence that varieties can be explained due to the arbitrary estimation of the composition of the extracted solid and changing phase composition (Figure 5.5).

The fractional crystallisation is calculated for the single liquid line of descent that ranging from gabbro to granodiorite. For an average plagioclase, with a silica concentration of 53 wt%, fractional crystallisation (FC) and extraction varies between 43% and 72% with a average of 50%. From now on statements on fractionation also include physical separation (extraction) of the phase(s) which are needed to gain the change in composition. An silicic plagioclase, with a silica concentration of 60 wt%, varies between 17% and 76% FC averaging on 62%. Hornblende FC varies between 74% and 89% averaging on 83%. FC of biotite varies between 72% and 89% with an average of 82%. The amount of K-feldspar FC varies between 22% and 67% with an average of 46%. FC of clinopyroxene is 72% and titanite FC varies between 69% and 84% and averaging on 76%. Apatite FC varies between 69% and 88% with an average of 78%.

The single liquid line of descent is controlled by the previous stated FC. For the major-oxides MgO, FeO*, CaO, TiO_2 and P_2O_5 increasing silica results in a declining single liquid line of descent. Al_2O_3 concentration varies depending upon the amount of plagioclase, biotite and hornblende FC. Na_2O and K_2O concentrations are controlled by FC of plagioclase and varies depending on the composition of the plagioclase.

Major-elements in Fenner type diagram
The Fenner type diagrams show the similar interpretation of inverse single liquid line of descent as such is interpreted for the Harker variation diagrams. The mechanical mixing trend that is interpreted for the Harker variation diagrams show less significant in the Fenner type diagrams (Figure 4.4c).

The quartz monzodiorite and granodiorite samples show an overlap in FeO*, CaO, Na_2O, TiO_2, K_2O, P_2O_5 and BaO versus MgO. This is interpreted as a result of the low amount of olivine and pyroxene in these samples. Most olivine are fractionated out of the system near 55% silica which correspond with MgO wt% of ~3.5 (Figure 4.4c).

The mafic enclaves plot near the “edges” of the single liquid line of descent. The enclaves are slightly depleted in FeO*, TiO_2 and CaO and enriched in K_2O, Na_2O and P_2O_5. This can be interpreted as enclaves that are close to their source/origin and show occasionally signatures of interaction with a more matured source (Figure 4.4c).

5.2.2 Trace-elements

In this section the trace element data are discussed and interpreted. The subsections are trace element versus silica, trace element normalization diagrams, trace element versus trace element and geochemical interpretation.

Trace element versus silica provides insights in the behaviour of the element with respect to the evolving magma batch. The trace element normalization diagrams show depletion or enrichment of a specific phase with respect to the normalised sample. Identification and quantification of fractional crystallisation can be achieved by trace element versus trace element study.

5.2.2.1 Trace element versus silica

When viewing the trace elements versus silica graphs it is striking that no “perfect” liquid lines of descent can be interpreted, such as done for the Harker variation diagram. Taking the field observations in mind the follow statements can be made which are important for further trace element interpretations.

The majority of the observed non-intrusive granitic samples are likely to be Taft Granite, except for samples collected as Coarse Grained Granodiorite and Porphyritic Granodiorite. Field results show that these granitic samples are most likely a product of mixing and/or assimilation. This means that YC GT samples can be interpreted in the trace elements versus silica graphs as a product of mixing/assimilation of a more mafic, a quartz monzodiorite or a granodiorite, sample and the Taft Granite. This is shown in Figure 5.6 by the blue arrows.

The single liquid line of descent refers to a normal evolving magma batch that is derived by extensive fractional crystallisation. When statements are made on a “mixing trend” two end-members are interpreted (quartz monzodiorite or granodiorite with a granite). Mixing products of two end-members are interpreted to plot on diagrams between the two end-members.

For conclusive interpretations on the granitic assimilation/mixing end-member see chapter 6 Conclusion and recommendation. In this section the granitic end-member is referred to as Taft Granite for sake of convenience, however no conclusive interpretation on the granitic source is meant at this stage of the discussion. A deep parental Taft Granite mixing/assimilating source is still a valid hypothesis, see 5.1.5.

Ba vs. silica
The elements Rb and Ba have similar behaviour when plotted against silica because of their similar chemical properties and substitution behaviour with potassium (Winter, 2001). The interpretation of Rb versus silica is the same as for Ba versus silica. Trends that are distinghuishable are: one evolved magmatic batch ranging from gabbro to granodiorite; one mixing line between a monzodiorite and Taft Granite and a mixing and/or assimilation between the granodiorites and an evolved granite (Figure 5.6). Ba indicates late stage fractionation of K-feldspars in the Taft Granite samples (Bouseily and Sokkary, 1976; Winter, 2001), indicated by the yellow arrows in Figure 5.6.

The normal crystal fractionation trend shows that Ba behaves less compatible for the mafic components then for felsic. The silica-rich quartz monzodiorite and the granodiorite show decrease of Ba concentrations. This is interpreted as either a mixing product between the quartz monzodiorite and the granite or as K-feldspar and biotite crystal fractionation. Quantification of the crystal fractionation is done in paragraph 5.2.2.3.

Two clusters of samples are enriched in Ba concentration, the quartz monzodiorite samples and granodiorite to granite samples. These are interpreted as enrichment due to mixing/assimilation of a high concentrated Ba Taft Granite and high Ba monzodiorite. The enrichment of de monzodiorite is a results of fractional crystallization of an average plagioclase. Between the end-members of a granodiorite and a evolved granite, samples plot that might show mixing and/or assimilation.

Another interpretation would be that the enriched Ba quartz monzodiorite samples (and possible granodiorite) are of a different source and unrelated to the normal crystal fractionation trend (Figure 5.6).

Sr vs. silica
The majority of the variation in the Sr versus silica diagram indicates evolution of typical magma suite ranging from gabbro to granodiorite (Figure 5.6). Sr reacts compatible in plagioclase crystallization. Sr behaves incompatible in the more mafic components, such as gabbros and monzodiorites, which is shown in a positive correlation with increasing silica. From 60% silica and higher plagioclase starts the fractionate, this is seen in the negative correlation with increasing silica.

The mixing trends between the granodiorite and granite in Sr concentrations show less significant than for other trace elements. The Sr concentrations might fit the geological scatter of the single liquid line of descent. However, in the diagram the envisioned mixing trend is still drawn in (Figure 5.6).

Zr vs. silica
Zr behaves incompatible except for zircon crystallization. The liquid line of descent can be interpreted as follow: a normal evolved liquid line of descent ranging from gabbro to quartz monzodiorite. The Zr enriched quartz monzodiorites (and possible Zr-rich granodiorites) are interpreted to be likely of a different source. This sample cluster consist of samples that are mafic (monzodiorite) or show interaction with mafic components in the field such as the mafic sheet of BL-13. Note that not all mafic samples (gabbros and monzodiorites) are zircon-rich.

A mixing trend is interpreted between the granodiorite and the Taft Granite. The majority of the granodiorite samples fit the mixing trend (Figure 5.6), however it is not conclusive that the granodiorite samples are a mixing product or a end-member of the liquid line of descent.

Y vs. silica
Y show compatible behaviour with garnet, other minerals that also show less incompatible behaviour with Y are amphibole, sphene and apatite. The data can be most easily interpreted as a single liquid line of descent with Y decreasing from 25 ppm to 12 ppm with increasing silica. The following interpretations can be made for Y versus silica: a normal evolved magmatic batch ranging from gabbro to granodiorite and mixing between the granodiorite and an evolved granite (Figure 5.6).

5.2.2.2 Trace element normalization diagrams

Specific trace elements concentrations and their associated minerals are already discussed in paragraph 5.2.2.1. The trace element normalization diagrams providing an overview of the trace element signatures which makes comparison between the samples and sample groups more clear (Figure 4.7). All samples are normalized to sample BL-4H which is interpreted as an typical granodiorite.

Variations in the trace element normalization diagram can be explained by fractional crystallisation or by source variation. Several elements are diagnostic for fractional crystallisation which can be specified to phases such as (Rollinson, 1993; Winter, 2001); high Rb and low K concentrations can be interpreted as amphibole extraction; Sr depletion indicates fractional crystallisation of plagioclase; P suggest fractional crystallization or addition of apatite; low Hf and Zr concentrations might indicated zircon fractional crystallization; low values of Nd and Sm are interpreted as fractional crystallisation (FC) of hornblende; depletion of the elements ranged between La and Yb can be interpreted as dominant hornblende or minor phases (titanite, garnet, allanite) extraction.

Yosemite Creek Granites
The YC GT shows in general a slightly more fractionated signature for the more incompatible REE with respect to the granodiorite (sample BL-4H). The fractionated pattern is interpreted as the result of hornblende and apatite FC. Sample BL-15A shows less FC of plagioclase than sample BL-4H. Noticeable is the low Ba concentration for BL-15B, this might be an indication that the sample/rock is extracted from an average granite source. Hence BL-15B also shows FC of zircon.
For the YC GT dykes the same interpretations with respect of fractional crystallisation can be made. However sample BL-3E and BL-4D are more depleted in Ba which might indicates that they are originated from another source rock and extracted by partial melting.

The relative flat signature of the most compatible elements for the YC GT enclave can be interpreted as assimilation and homogenization of the enclave with the granite host rock, which is the granodiorite of sample BL-4H. The enclave was hot enough and the host rock was reheated to such an extent that exchange and homogenization of the "compatible" elements where exchanged to the enclave. For BL-4H also the interpretation is made that hornblende fractionated and was extracted due the cooling effect of the granitic host rock.

Yosemite Creek Granodiorite and Tonalite
When considering FC is the driving force of the trace element signature the follow phases are involved. The Tonalite shows a depleted signature with respect to BL-4H. BL-3B, Tonalite, show no depletion or extraction of plagioclase. However, it does show FC of apatite and hornblende. The high U concentration for sample BL-3B is interpreted as no extraction of minor phases. The most obvious interpretation for sample BL-3B would be that it is of another source than sample BL-4H.

The majority of the YC GD samples show little variation with respect to the granodiorite of BL-4H with exception of sample BL-17A and sample 31I-2 SJSU. Sample BL-17A shows FC of hornblende and sample 31I-2 SJSU shows addition of plagioclase and hornblende. Sample 31I-2 SJSU also shows depletion in apatite. The GD dyke's show strong FC of hornblende. Note that the YC GD show a similar trace element signature as the YC GT. The YC TO however might be of another source.

Yosemite Creek Quartz Monzodiorite
The Quartz Monzodiorites show a dominant trace element signature which indicates FC of hornblende and minor or no FC of zircon. Sample 24A-(2)SJSU is interpreted to be of another source. The YC QM dyke shows little to no extraction of plagioclase but does show FC of hornblende, apatite and zircon. The YC QM enclave shows minor plagioclase extraction and minor to no FC of zircon and hornblende. Another interpretation for the YC QM would be that these samples are not petrogenetically related to the YC GD (sample BL-4H).

Sample BL-4C has strong resemblances with BL-4H which suggest that this sample might be wrongly classified to the YC QM group. From field classification sample BL-4C is sampled as a granodiorite this means that the CIPW classification for sample BL-4C did not suffice.

Yosemite Creek Monzodiorite and Gabbro
When considering a related source the follow FC or additions are required to gain the signature as observed for the Monzodiorite. In general minor FC of plagioclase and addition of apatite. For sample BL-2C addition of zircon is required. Samples BL-9A, BL-9B and BL-14E show FC of zircon and BL-2C and BL-9B show FC of hornblende. For BL-8D, BL-9A and BL-14E similar hornblende abundance is interpreted as for BL-4H. Another interpretation would be that the YC MD originated from another source then the BL-4H granodiorite such as observed for the YC TO and YC QM.

The YC MD dyke show slight resemblances with the other YC MD groups. When considering FC to be the cause of the trace element signature the FC of minor plagioclase and hornblende is required. Also a addition of zircon is required. For this sample an alternative interpretation can be made that this rock had another source then the granodiorite of sample BL-4H. The YC MD sheet show little to no FC of plagioclase, zircon, apatite and hornblende.

The MD enclave show two dominant trends. Little to no extraction of zircon and hornblende could be interpreted. For samples BL-13C, BL-14B and BL-18C little to no plagioclase and hornblende FC is required. The MD enclave can be interpreted to be of the same source as the YC MD and the YC MD dyke. These groups are likely not related to the YC GD BL-4H. The YC GA show one dominant signature. When considering FC: little to no FC of plagioclase, zircon, hornblende and apatite is required. These trace element signatures can also be interpreted as another source such as observed for the YC TO, YC QM and YC MD.

The Yosemite Valley Intrusive Suite
The YVIS GT shows a similar signature as for YC GT, however BL-10A and BL-11A suggest addition of plagioclase. The YVIS QM and YVIS MD show a similar signatures as BL-4H, however with addition of plagioclase. The YVIS MD shows zircon FC and addition of apatite and hornblende with respect to BL-4H. This latter signature shows resemblances with the YC GA and YC MD sheet, which also might suggest a different source than sample BL-4H.

Trace element normalization diagram review

Two distinct sources are interpreted from the trace element normalization diagrams. The YC GT, YC GT dyke, YC GT, enclave, YC GD, YC GD dyke sample BL-4G and YC QM sample BL-4C can be consider as petrogenetically related. The element variations between these groups are caused by FC such as described in the previous sections. The groups YC TO, YC GD dyke sample BL-3D, most of YC QM, YC QM dyke, YC QM enclave, YC MD dyke, YC MD sheet, YC MD enclave, YC GA and YVIS MD are interpreted to be source related and different than the previous described group. Variations between the signatures are also considered to be a product of FC. Note that YVIS GT and YVIS QM are forming the YVIS proper trace element signature. Striking is that these signatures show resemblances with the YC GD and YC GT.

Comparing these interpretations with the interpretations of the major-elements the follow analyse can be made. Either there are two unrelated magmatic batches or one magma batch which also show a mixing batch. Two unrelated magma batches correspond with the interpretations made for the major-elements, the alkaline and subalkaline trend.

Other remarks on the normalized diagrams: The YC QM trace element normalized diagram show no cluster of samples that might explain the alkaline enriched QM cluster. Note that samples 24A-(2) SJSU are two similar samples with no field observations, this would makes interpretations based on these samples weak and speculative.

5.2.2.3 Trace element versus trace element

Figure 5.7 shows the Rb vs. Nb + Y diagram which is commonly used to interpreted tectonic settings. In Figure 5.8 several mineral crystallization paths are shown, which are calculated by use of Rayleigh fractionation equation and partitioning coefficients. Specific trace elements are used in bivariant plots to quantify mineral fractionation and extraction.

Two sets of plots are shown in Figure 5.8. The first bivariant diagrams are Sr/Ba and the second diagrams are Yb/La. For the vector diagrams a common magmatic source with uniform LILE (Sr = 625; Ba = 900; Fulmer and Kruijer, 2008) and REE (La = 15; Yb = 2) concentrations is assumed as starting melt.
K-feldspar fractionation is interpreted to be late stage. By this author assumed to be fractionating after 10% plagioclase fractionation. Starting melt for K-feldspar: Ba = 625; Sr = 200; La = 16; Yb = 2.2.

Rb vs. Nb + Y, Tectonic setting
Trace elements can be used to identify the tectonic setting of igneous rocks (Pearce et al., 1984; Forster 1997). Several plots can be used, Ta versus Yb, Rb versus Nb + Ta, Rb versus Nb + Y. The most commonly used plot is the Nb versus Y. The most accurate of the three graphs is the Rb vs. Nb + Y (Pearce et al., 1984; Forster 1997; Rollinson, 1993; Winter, 2001). The samples taken for this research fall into the domain of the Volcanic Arc Granite. One gabbro and a monzodiorite dyke fall into domain of the Within Plate Granite (Figure 5.7). The origin of the granitoïds can be stated to be of a volcanic arc.

Sr vs. Ba
From the vector diagram of Figure 5.8a two hypothesis can be proposed. A dacite magmatic source which fractionation of several phases can explain all the obtained samples; or the mafic and felsic samples are not directly related to each other. The more felsic samples originated out of a dacite to rhyolite melt and the more mafic samples originate out of a basaltic melt. Trace element ratio Sr/Ba is a good indicator for plagioclase fractional crystallisation (FC). A high Sr/Ba ratio suggest no loss of plagioclase by fractional crystallisation.

The majority of the YC GT samples can be interpreted as a product of K-feldspar fractionation and extraction ranging between the 0% to 10% fractionation. Minor amount of plagioclase might also be fractionating at the same time. One YC GT sample (BL-13A) can be interpreted as a product of 20% FC of biotite and plagioclase. Sample BL-16A and BL-18A can be interpreted as a product of respectively 20% and 30% FC of plagioclase and hornblende (possible also with sphene and zircon). The YV GT enclave fits the interpretation of roughly 85% of FC of plagioclase, hornblende and sphene. However an interpretation that the YV GT enclave is of a different source than sample BL-4H is more likely.
The YC TO can be interpreted as FC of 10% biotite and K-feldspar. The YC GD fits, for the majority, a FC product of plagioclase, biotite and hornblende (and possible sphene and zircon). The biotite and plagioclase controlled fractionated samples ranging between roughly 5% to 20% of FC. The plagioclase and hornblende controlled YC GD samples ranging between the 10% and 40% of FC.

The interpretation of the YC QM, YC MD, YC GA, YVIS QM and YVIS MD depends on the hypothesis that is favoured. In the first interpretation a dacitic melt is assumed to be the origin of the all the samples. One cluster of samples of YC QM with one YC MD sample plotting near the vector of hornblende, sphene and zircon. These samples ranging between FC of ~0% to ~30%. The remaining majority of the YC QM samples and the YC MD can be interpreted as a product of FC of ~5% to 20% of plagioclase and biotite. The YC MD enclave and YC QM enclave can be interpreted as a product of 10% K-feldspar and biotite FC.

When assuming the second hypothesis with a basaltic melt all the mafic samples plot as a product of FC of the phases plagioclase, clinopyroxene and hornblende. However clinopyroxene is assumed to have no to minor contribution.
The majority of the monzodiorite and gabbros plot between 50% and ~80% FC of plagioclase, clinopyroxene and hornblende. The quartz monzodiorites ranging between 70% and ~95% of FC of plagioclase and hornblende. One YC MD enclave has 100% FC of plagioclase. Remaining enclaves plot between ~40% to ~70% of FC of plagioclase and hornblende.

Figure 5.8c shows Sr vs. Ba diagram with field unit classifications. The (quartz) monzodiorite cluster from Figure 5.8a can be interpreted as the Fine Quartz Monzodiorite to Granodiorite Unit which is derived meanly from hornblende FC and extraction.

La vs. Yb
Two hypothesis are tested such as previous stated in the section Sr vs. Ba. All the samples originate out of one dacitic melt; or two different source melts can explain for the sample, a dacite to rhyolite melt for felsic samples and a basaltic melt for the mafic melts.

In Figure 5.8b several phases are plotted in the vector diagram. Concerning the first hypothesis the follow interpretations can be made. The YC GT samples plot for the majority between 40% zircon, plagioclase and K-feldspar FC. YC GT samples BL-15A and BL-15B, the double dyke, can be interpreted as a product of 30% FC of biotite and hornblende. All the YC GD sample can be interpreted as FC product of zircon, plagioclase and K-feldspar which ranging between the ~0% and 70%.

For the (quartz) monzodiorite and gabbro samples two interpretations are possible. For the first hypothesis the quartz monzodiorites show great scatter. Two samples can be in interpreted as 10% to 35% of FC of biotite and or plagioclase. Three YC MD samples can be interpreted as a product of 10% to 40% FC of hornblende and biotite, which also might be influenced by apatite and sphene FC. Samples 24A-(2)SJSU have very high La concentrations which can be interpreted as 95% FC of zircon, K-feldspar and plagioclase. No field data is at hand to explain these high values.
The second hypothesis results in a general interpretation that the mafic samples can be a product of 70% to 95% of FC of clinopyroxene, and might be strongly influenced by plagioclase and hornblende FC. The monzodiorite samples plot near 85% of the phases.

From Figure 5.8c Yb vs. La it is shown that the most samples are controlled by hornblende and/or plagioclase FC. No deviating samples clusters are present, which might suggest that all the samples are related. Another interpretation could be that only the Porphyritic Granodiorite and Coarse Grained Granodiorite are related and are showing minor overlap with the Fine Grained Quartz Monzodiorite to Granodiorites.

5.2.3 Geochemical Hypotheses

Geochemical study provides two hypotheses on the petrogenesis. Validation of this hypothesises are discussed in this section. Final conclusions are presented in Chapter 6 Conclusion and Recommendation. Major distinction between the two hypothesis is that the basaltic/gabbroic melt in hypothesis 1 unrelated and in hypothesis 2 related to the "felsic" YC units.

5.2.3.1 Hypothesis 1: Two normal magmatic FC batches

Hypothesis
Based on the major-element variations and field relations the hypothesis is that the field area is dominated by two major magma suites; one mafic to moderate felsic and one moderate felsic to felsic. The two batches can be described as an "alkaline" batch and a "subalkaline" batch.

Observations
From the Total Alkali versus Silica diagram two magmatic batches can be observed. The alkaline batch ranging from periodotite (gabbro) to monzonite. The subalkaline batch ranging from diorite to granite. These separate batches are less visible in Harker variation diagrams and Fenner type diagrams. However, a trend is distinguishable between the gabbro and monzonites and between the quartz monzodiorite and granites. Two magmatic batches are also distinguishable from trace element study, the granodiorites and granites originating from a dacitic melt and the gabbro, monzodiorites and quartz monzodiorites originating from a basaltic melt. Trace element normalization diagrams support to hypothesis of two batches, a mafic (alkaline) and a felsic (subalkaline) batch.

Petrogenesis
The petrogenesis that can be deduced from this hypothesis is as follow. A dacitic melt forms in the MASH zone. This melts starts to fractionate plagioclase, (biotite) and hornblende. In the MASH zone the melt is assimilating and homogenizing with a parental YVIS Taft Granite source. This process leads to the increments that finale form the granodiorites and granites when emplaced in the upper crust.
In the lower crust a basaltic melt intrudes which is of another source than the previous described melt. This melt underwent extensive FC of plagioclase, pyroxene, and hornblende. Residual melts escapes and are emplaced in the upper crust. From this source a batch escapes, now of a more dacitic composition, and underwent extensive fractionalisation of hornblende and addition of zircon and plagioclase. The latter two (residual) phases are interpreted to be inherited from an earlier melt.

5.2.3.2 Hypothesis 2: Two magmatic batches, a normal FC batch and a mechanical mixing batch

Hypothesis

Two magmatic batches can be observed in major-elements. The first batch is a single liquid line of descent from gabbro to quartz monzodiorite. The second batch are the granodiorites and granites which are thought to be a mechanical mixing product between a quartz monzodiorite and a YVIS granite.

Observations

From Total Alkali versus Silica diagram a mixing trend can be observed. Harker variation diagrams and Fenner type diagrams support this hypothesis, by a single liquid line of descent and a mixing product between the quartz monzodiorite and granite. Trace elements versus silica are interpreted to show a strong mixing product between the quartz monzodiorite and the YVIS granites. Trace element normalization diagrams show two clear element signatures, a mafic one and a felsic one. The mafic signatures show clear distinction with respect to the felsic samples (granodiorites and granites). The felsic samples show a similar trace element signatures as is observed for the YVIS granites.

Petrogenesis

The Medium Grained Quartz Monzodiorite to Granodiorite, Coarse Grained Granodiorite and Porphyritic Granodiorite (roughly grouped in YC GD and YC GT) are a deep crustal mixing product between a YVIS granitic source and the Diorite to Hornblende-rich Diorite (YC GA, YC MD and YC QM).

The Yosemite Creek mafic (GA, MD and QM / Diorite to Hornblende-rich Diorite) melts evolves, probably at or in the lower crust, and intrudes in the upper crust. During emplacement several injections of these melts, with different composition due to maturation, are intruding in each other and the earlier emplaced felsic units. This mafic group consist out of two batches one normal liquid line of descent and one batch with residual phases, see next paragraph.

Remark on hypothesis

The samples of Ten Lakes locality, the Fine Grained Quartz Monzodiorite to Granodiorite, show a strong depleted hornblende signature. On very local scale the Yosemite Creek underwent fractional crystallization of hornblende and addition of zircon and plagioclase (e.g. sample BL-8E). This local FC process of hornblende can be explained by cooling and addition of residual phases of earlier extracted melts. Hornblende is a phase that is easily separated from the melt during cooling of a magma.

A good comparison can be made between sample BL-8D and BL-8E. The normal liquid line of descent is represented by BL-8D and BL-8E represents the “residual” batch (field classification: Fine Grained Quartz Monzodiorite to Granodiorite Unit).

Figure 5.4

Total Alkali versus silica diagram for plutonic rocks. Blue arrow indicates Alkaline and subalkaline divide (after Winter, 2001). The normal liquid lines of descents are indicated with red arrows, modified after Middlemost (1993). Green arrow indicates one single liquid line of descent.

Figure 5.5

Interpretations of the major element graphs. Illustrated are the lever rule phase quantification between solid-parent-daughter relation.

Figure 5.6

Trace elements versus silica. Plotted are Ba, Sr, Zr and Y versus silica.

Figure 5.7

Trace elements for interpretation of the tectonic setting. See text for explanation.

Figure 5.8

Trace elements versus trace elements in vector diagram. Phase vector diagrams showing fractional crystallization. The direction of the lines showing the compositional change in the residual liquid when the specified phase is progressively removed during fractional crystallization (Rollinson, 1993). **(a)** Sr versus Ba. **(b)** Yb versus La. **(c)** Sr versus Ba and Yb versus La for field classified units.

Figure 5.4

Total Alkali versus silica diagram

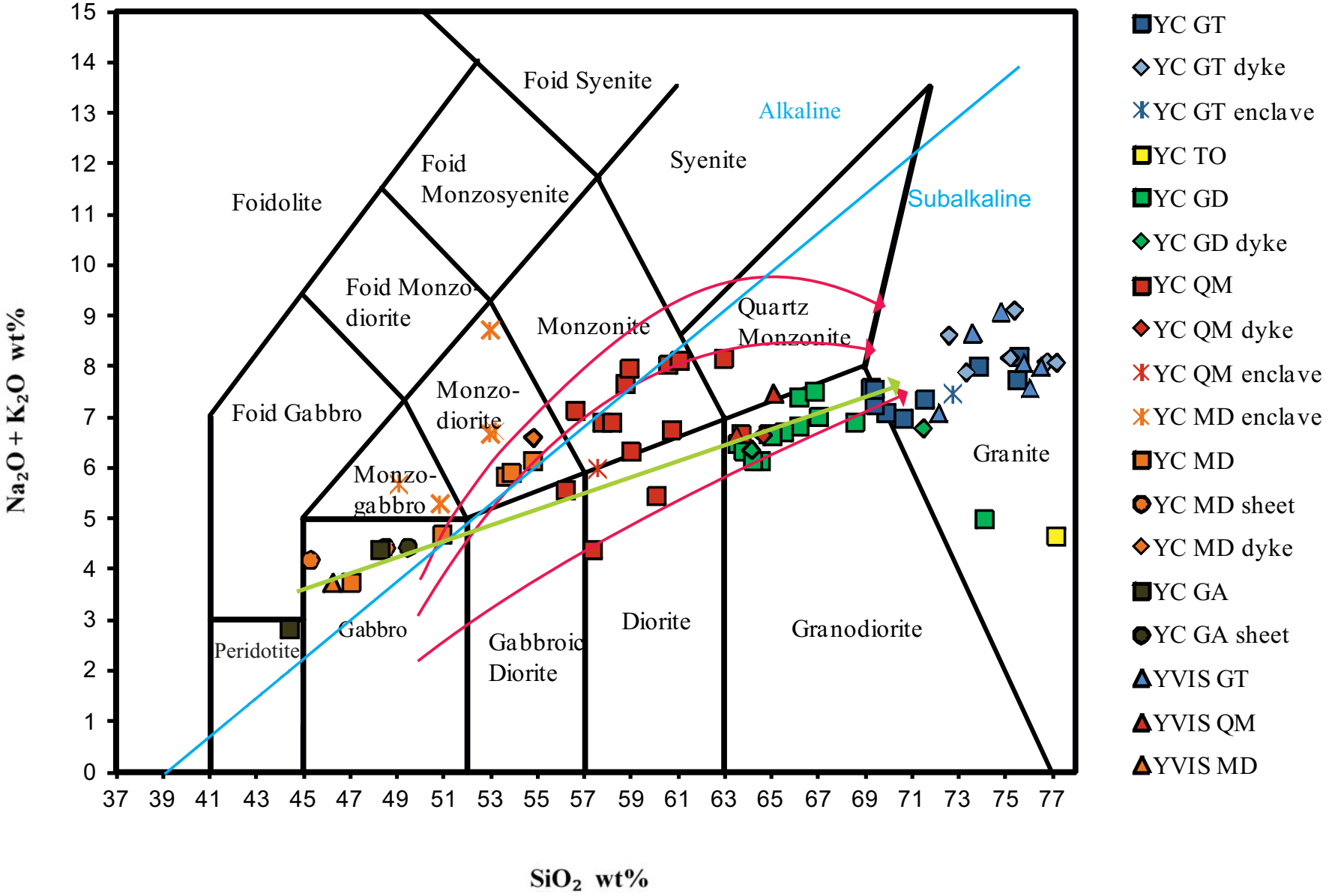

Figure 5.5

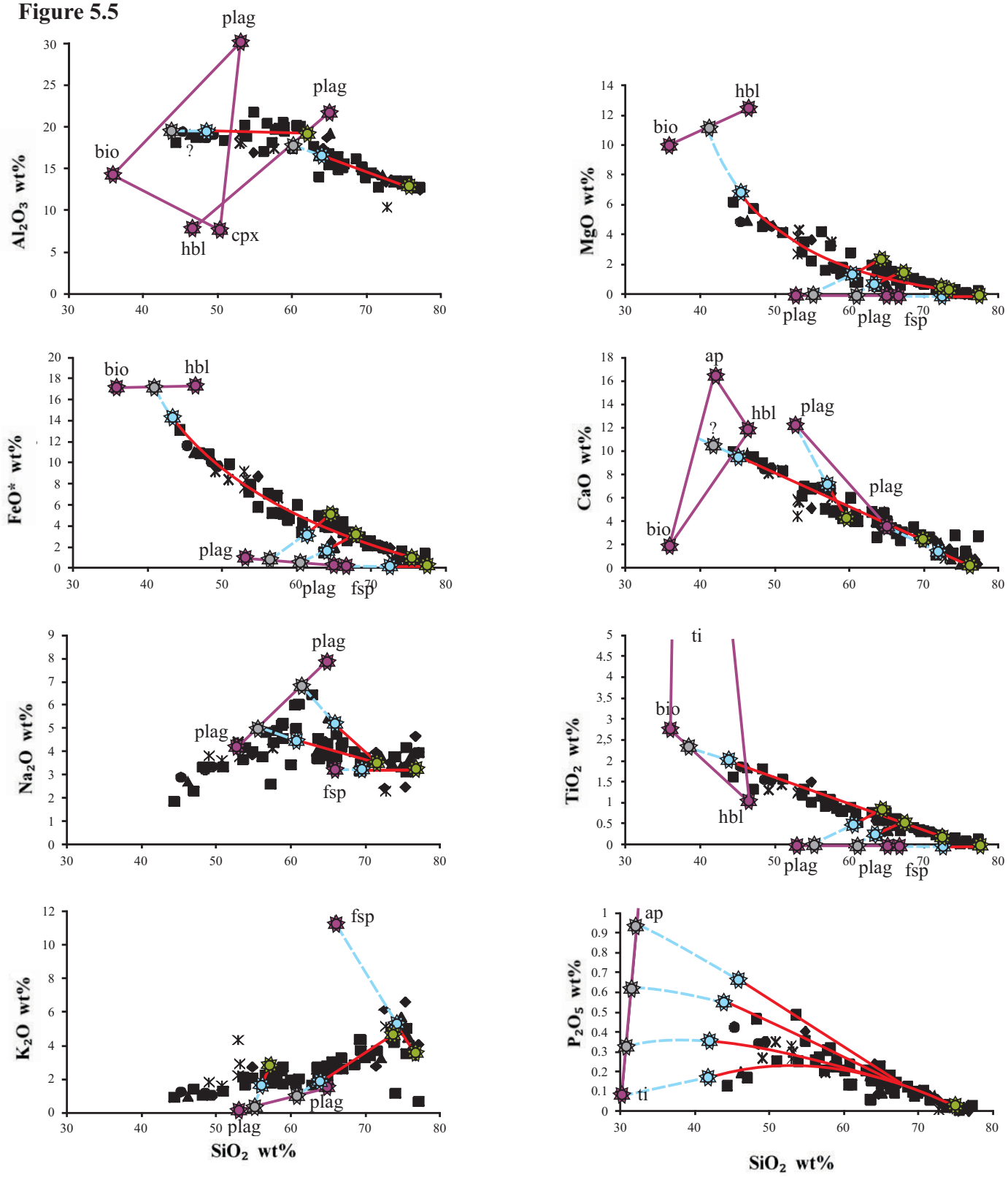

bulk mineral extract line

bulk mineral extract line of triangle

control line extracted phase - parent melt

control line parent - daughter

extracted phase

parent

daughter

extracted solid

Figure 5.6

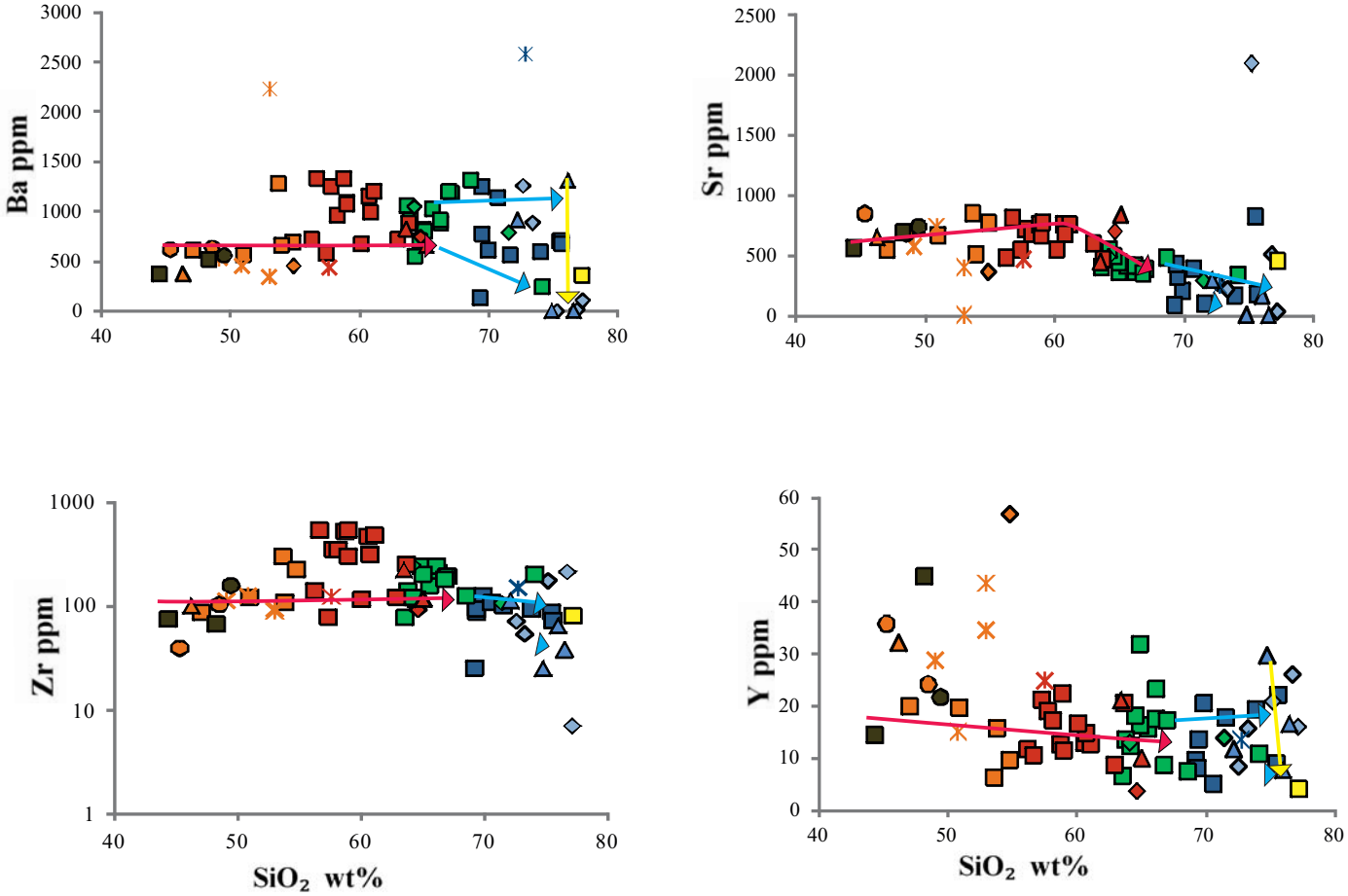

Figure 5.7

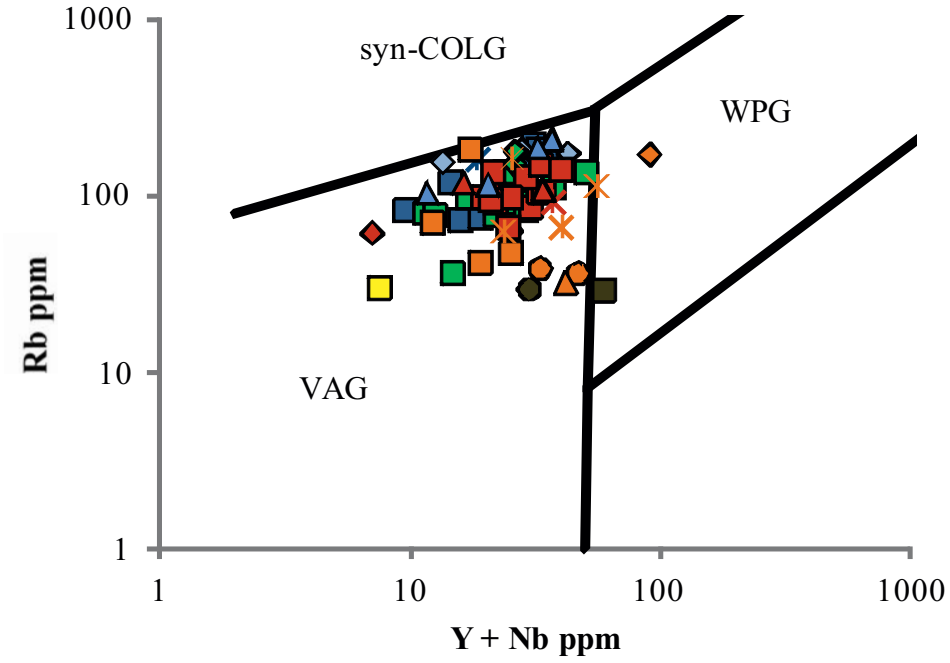

Figure 5.8a

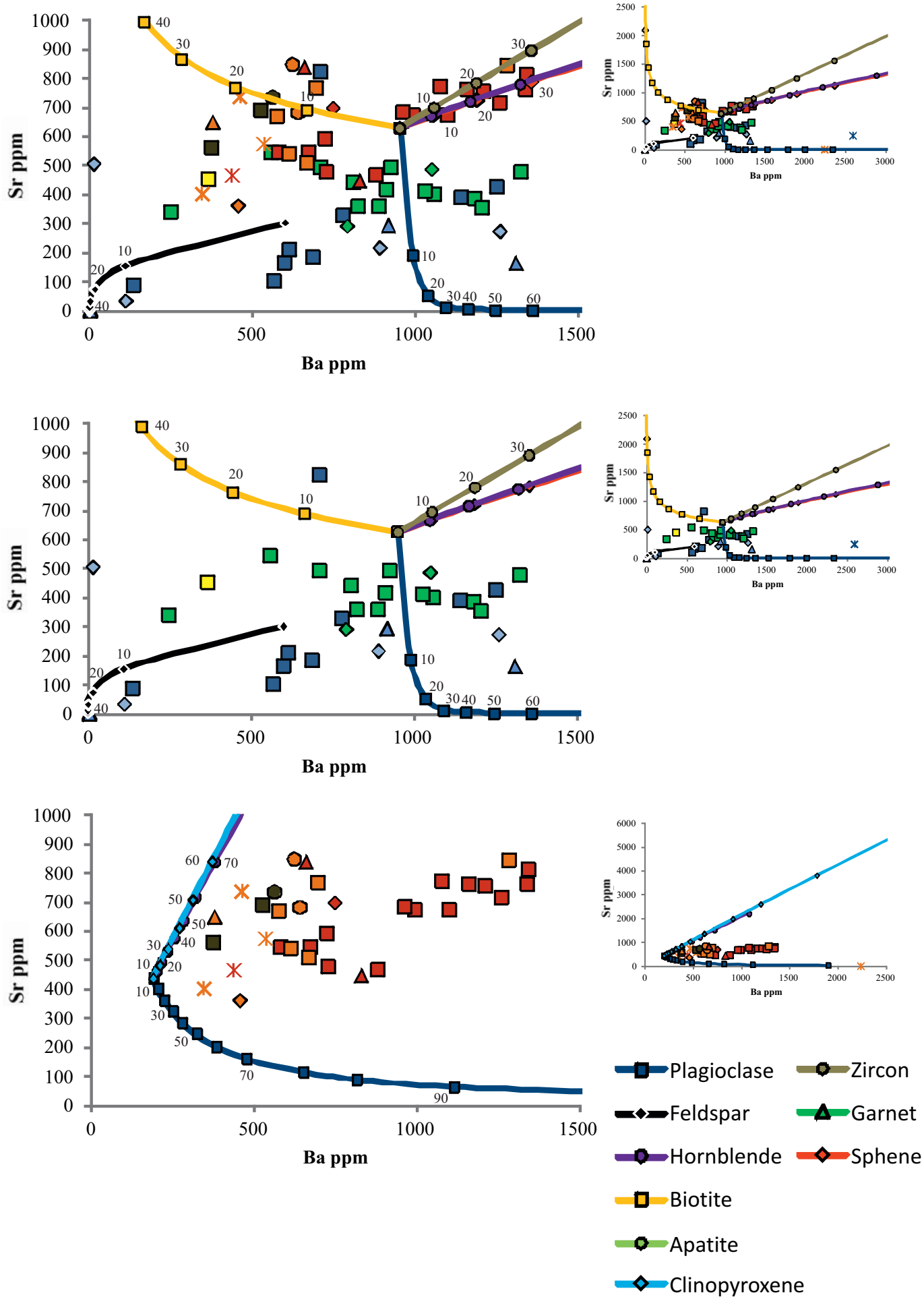
Sr ppm
Ba ppm
Plagioclase
Zircon
Feldspar
Garnet
Hornblende
Sphene
Biotite
Apatite
Clinopyroxene

Figure 5.8b

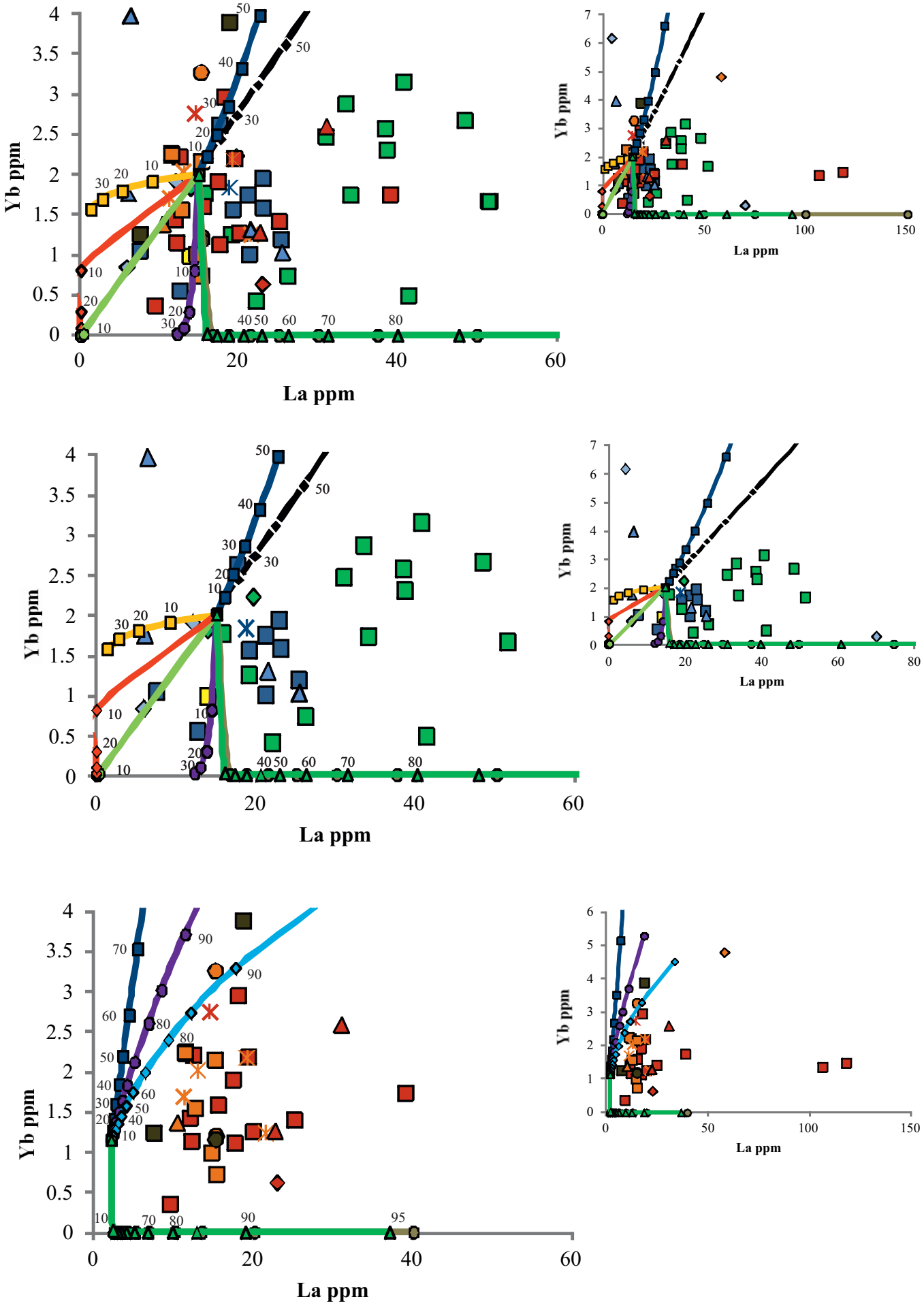
Yb ppm
La ppm
0
20
40
60
0.5
1
1.5
2
2.5
3
3.5
4
50
40
30
20
10
70
80
90
95
0
50
100
150
5
6
7

Figure 5.8C

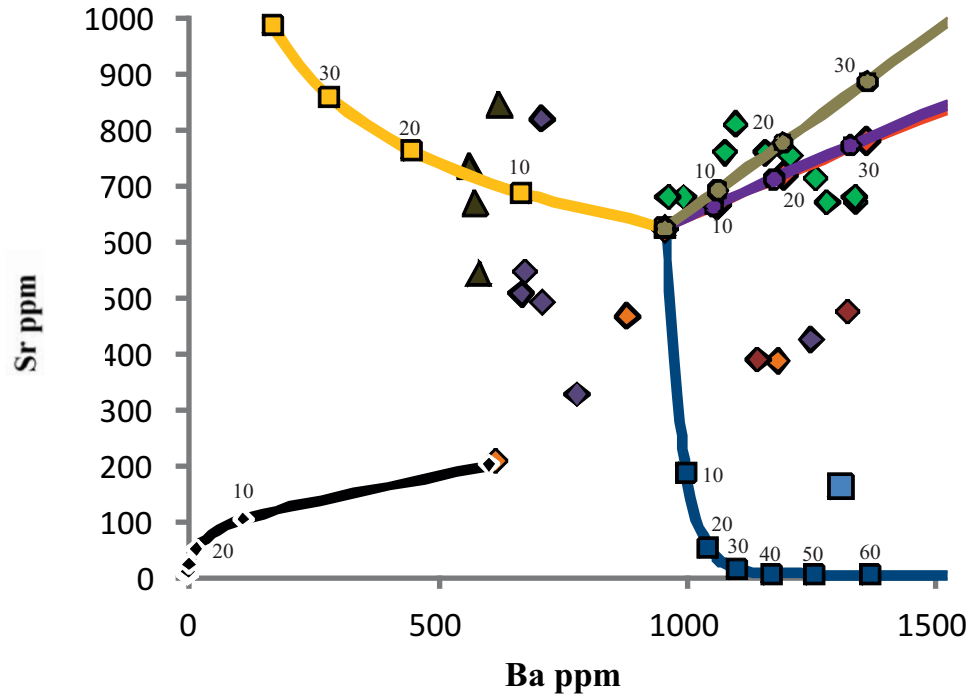

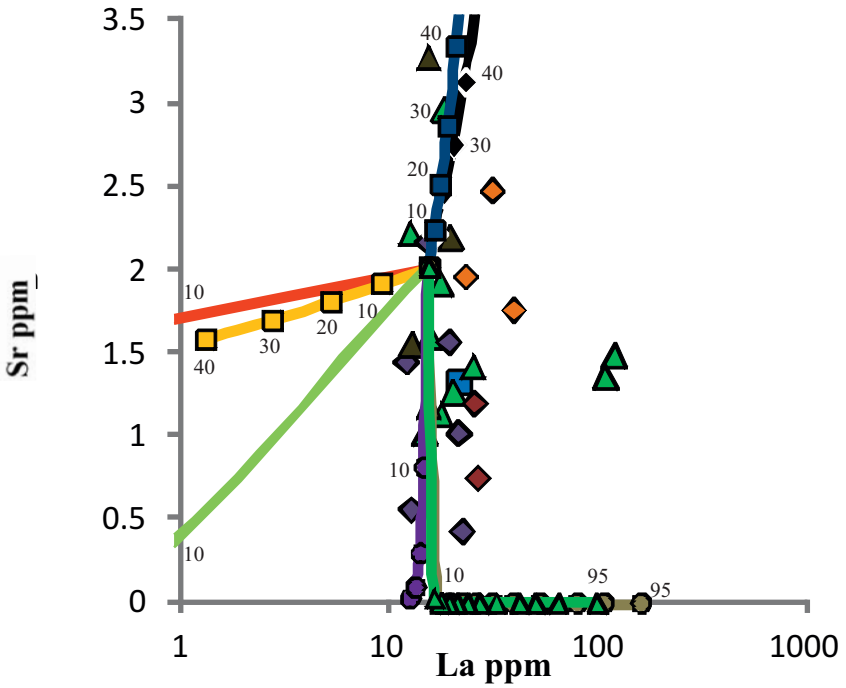

Granite Fine Qm-GD Medium Qm-GD

Coarse GD Porphyritic GD (hbl) diorite

5.3 Summary Discussion

Key observations and interpretations are summarised in the next paragraphs. First section is on field results and the second section is on geochemical results. The latest section sums up all the hypothesis discussed in the Discussion.

5.3.1 Field results

The Quartz Monzodiorite to Granodiorite Unit is interpreted to intrude into the Taft Granite which results in assimilation of Taft Granite. The observed features of Taft Granite incorporated into the YC are interpreted to be small scale wall and roof stoping. The origin of the Quartz Monzodiorite to Granodiorite Unit could be either a separate YC increment or a assimilation and homogenization product between the Taft Granite and the Diorite to Hornblende-rich Diorite Unit.
The Coarse Grained Granodiorite Unit and the Porphyritic Granodiorite Unit are interpreted to be related in composition and petrogenesis. The textural difference between the two units are caused by either emplacement related differences or by assimilation of (parental) Taft Granite.

Enclaves and xenoliths are used to make interpretations on the liquid/solid state of the rocks. The follow trend is distinguishable, granite enclaves and xenoliths are partially molten however they remained in a relative solid state. Enclaves and xenoliths of the Quartz Monzodiorite to Granodiorite Unit and the Diorite to Hornblende-rich Diorite units contained between 20% and 50% of solid phases when emplaced.

Intrusive relations show that mafic (diorite and hornblende-rich diorite) intrusions are generally near co-magmatic with the host-rock. This might be due to late stage intrusion or due to partial melting of the host-rock. Felsic (granitic and granodiorite) intrusions have sharp contacts which is interpreted to be late stage phenomena in a relative cold system.

The majority of the schlieren are observed in the Coarse Grained Granodiorite Unit and Porphyritic Granodiorite Unit. These structures are interpreted to be related to relative large scale magma chambers. Schlieren observed in the other units are interpreted as mineral segregation due to changing magmatic flow.

5.3.2 Geochemical results

The TAS diagram gives an insight in the possible relationships between different batches of magma. The data can be explained by a single liquid line of descent with an cluster of alkaline enriched samples. Another explanation would be two magmatic batches, one “alkaline” and one “subalkaline” batch.

Harker variation diagram and Fenner type diagram show a single liquid line of descent with a quart monzodiorite cluster that does not fit the liquid line of descent. This is thought to be either a mixing result between an enriched/depleted monzodiorite and granite, the result of crystal fractionation or source related. Using the lever-rule it is possible to quantify the relevant phases. From this analyses it is seen that fractionation of plagioclase, biotite and hornblende are the dominant phases that characterises the Yosemite Creek units.

From trace element study two magmatic source batches are distinguished, a “normal trend” and a Ba and Zr enriched cluster of samples. Also, trace elements versus silica show the role of mixing between the granodiorites and granites. This mixing produces all the YC GT’s. Also is shown from these graphs is that plagioclase and zircon are important phases for the REE and LILE.

The calculation of the amount of mineral fractionation using Rayleigh fractional crystallization shows that a dacitic melt with extensive crystal fractionation can explain, quantify and characterize the felsic Yosemite Creek units and there evolution. Extensive FC of a basaltic melt can explain the more mafic YC units.

Combining the Rayleigh FC calculations with the trace element normalized diagrams two batches are distinguishable. A basaltic melt that evolves by extensive FC of plagioclase, clinopyroxene and hornblende forming the units: YC TO, YC GD dyke sample BL-3D, most of YC QM, YC QM dyke, YC QM enclave, YC MD dyke, YC MD sheet, YC MD enclave, YC GA and YVIS MD. A dacitic melt with FC of plagioclase, biotite, hornblende, zircon and feldspar forming the units: YC GT, YC GT dyke, YC GT, enclave, YC GD, YC GD dyke sample BL-4G and YC QM sample BL-4C. The latter magmatic batch show strong resemblances with the YVIS Taft Granite trace element signature.

5.3.3 Hypothesises on petrogenesis

Three hypothesis are proposed to explain the observed field relations. The first hypothesis is that the Taft Granite was intruded by the Diorite to Hornblende-rich Diorite Unit (in this situation YC proper). All the observed (quartz) monzodiorite rocks are a product of in-situ assimilation and homogenization between the Taft Granite and the YC proper. The second hypothesis is incremental growth with petrogenetically related increments. All the YC units are a product of assimilation and homogenization between a parental Taft Granite (or other granite source) in the MASH zone. The third hypothesis is that all the observed units are a product of different increments with unrelated magmatic reservoirs or source origin.

There are two hypothesis proposed to explain the observed geochemical data. The first hypothesis is that all the mafic units (periodotite/gabbro to quartz monzodiorite) are source related. With the second magmatic batch ranging from diorite to granite. Both batches are unrelated to each other.
The second hypothesis considers the same alkaline (mafic) batch as for hypothesis 1. The second batch in Hypothesis 2 is interpreted as a mixing product between quartz monzodiorite and granite. End-members of this deep crustal mixing product are the “mafic” YC quartz monzodiorite and the (parental) YVIS Taft Granite.
For both hypothesis the follow interpretation is made. The “relative enriched/depleted” quartz monzodiorite sample cluster (or Fine Grained Quartz Monzodiorite to Granodiorite samples) are a product of extensive hornblende FC with inheritance of residual phases of earlier melt. This increment is derived from the Diorite to Hornblende-rich Diorite (mafic YC).

6 Conclusion and recommendation

This study is performed to construct a petrogenesis of the Yosemite Creek Granodiorite, which was previous studied by Huber et al. (1989), Petsche (2008) and Johnson (unpublished). An attempted is made to characterise the units of the Yosemite Creek Granodiorite.

The research objective was to gain more insight in the evolution of the Yosemite Creek and thereby into crustal arc formation in general. Field and geochemical study should provide the information needed. The research objectives is divided in several studies as stated in the introduction. All the objectives are achieved and are discussed below. In chapter 6.1 the research questions are answered and the research hypothesis is discussed.

6.1 Overall conclusion

The overall conclusion discussed below is based on combined field and geochemical study. The research questions of the introduction are answered and proven. The hypothesis on the formation and characterization of the Yosemite Creek Granodiorite is tested, see 6.1.3. All the conclusions are based on the most favourable model.

6.1.1 Conclusions of field and geochemical study

From field observations a model is proposed that coincides with the most favourable hypothesis that rises from the field and geochemical study. This model is revered to as “Incremental growth with related increments” and “Hypothesis 2” in the geochemical discussion.

From geochemical study there can be stated that the Diorite to Hornblende-rich Diorite Unit (YC GA and YC MD) and Fine Grained Quartz Monzodiorite to Granodiorite Unit (YC MD and YC QM) are petrogenetically related by source. The Fine Grained Quartz Monzodiorite to Granodiorite Unit (YC MD) originate from another batch that underwent extensive hornblende fractional crystallisation and addition of the residual phases of plagioclase and zircon which were derived from another melt. The Medium Grained Quartz Monzodiorite to Granodiorite Unit (YC GD), Coarse Grained Granodiorite (YC GD and YC GT) and the Porphyritic Granodiorite (YC GD and YC GT) are petrogenetically related. All the samples of the YC GT and YC GD are a mixing product between the YC QM and a (parental) YVIS GT (Taft Granite).

6.1.2 Validation of the hypothesis stated in the introduction

In this section the hypothesis of the introduction is discussed and subjected to validation. The hypothesis stated is:

"The YC consists of several pulses originating from one magma batch. Different magma pulses are partial assimilate and reactivating the older Taft Granite unit. The oldest YC pulses are highly felsic and record the most assimilation. The younger the pulse the more mafic the intrusion become and the lesser assimilation occurs."

The hypothesis is valid however concerning the assimilation no hard conclusive statements can be made. Isotope study should verify if the Medium Grained Quartz Monzodiorite to Granodiorite, Coarse Grained Granodiorite and Porphyritic Granodiorite are a mixing/assimilation product of the Yosemite Creek and the (parental) YVIS Taft Granite. The YC does consists out of several pulses or increments: the Medium Grained Quartz Monzodiorite to Granodiorite; Coarse Grained Granodiorite; Porphyritic Granodiorite; the Diorite to Hornblende-rich Diorite and the Fine Grained Quartz Monzodiorite to Granodiorite. The most units are related to one magma batch originated from the MASH zone. The Diorite to Hornblende-rich Diorite and the Fine Grained Quartz Monzodiorite to Granodiorite are interpreted to be of another source, originated from the mantle.

6.1.3 Research questions

In this section the research questions stated in the introduction are answered. Doing so, a conclusive interpretation and characterization of the Yosemite Creek Formation is achieved.

- Does the YC consist of one magma batch?

No, the YC consists out of several identifiable units. Units identified are the Diorite to Hornblende-rich Diorite, the Fine Grained Quartz Monzodiorite to Granodiorite, Medium Grained Quartz Monzodiorite to Granodiorite, Coarse Grained Granodiorite and Porphyritic Granodiorite. In Figure 3.2a (Geological Map of Ten Lakes and vicinity) respectively referred to as Kyd, Kyd and Kymt, Ky, Kyc and Kyp. Diorite to Hornblende-rich Diorite and Fine Grained Quartz Monzodiorite to Granodiorite can be consider as a separate batch. The Medium Grained Quartz Monzodiorite to Granodiorite, Coarse Grained Granodiorite and Porphyritic Granodiorite can be considered as one batch.

- What are the origins of the YC magma batches?

The favoured model of "Incremental growth with related increments" suggests that all the increments/batches are a product of a MASH zone. The origin of all the batches is the lower crust near the MOHO. In the MASH zone (parental) Taft Granite mixes with fresh Yosemite Creek melt, which results in the melts belonging to the Medium Grained Quartz Monzodiorite to Granodiorite Unit, Coarse Grained Granodiorite Unit and Porphyritic Granodiorite Unit. Some YV GT rocks can be an in-situ mixing product located in the upper crust between Yosemite Creek and Taft Granite. The Diorite to Hornblende-rich Diorite are originated from the lower crust. The Fine Grained Quartz Monzodiorite to Granodiorite originated from the Diorite to Hornblende-rich Diorite and underwent extensive fractional crystallisation of hornblende in the lower crust. When rising to the upper crust it assimilated residual zircon and plagioclase phases of an earlier melt.

- Does the YC magma batch assimilate wall-rock on a major scale?

Yes, the YC magma batches assimilate wall-rock on major scale. Evidence is found in the field by observations of Taft Granite which mixes with the Yosemite Creek units. Granites subscribed to the YC GT can be a mixing product between the YC and (parental) Taft Granite. The incorporation of zircons and plagioclase into the Fine Grained Quartz Monzodiorite to Granodiorite Unit can be considered as wall-rock assimilation. So, wall-rock assimilation does contribute to the characteristic of the Yosemite Creek units and wall-rock assimilation did played a major role in the formation of the YC batches.

- To what extent does hybridization occur between the different units?

It is concluded that there is a high amount of hybridization between the units. Hybridization can be concluded from the (parental) YVIS Taft Granite interaction in the deeper crust and incorporation of residual phases in the Fine Grained Quartz Monzodiorite to Granodiorite Unit. Isotope study is required to quantify the hybridization process between the units.

6.2 Petrogenetic model of the Yosemite Creek Formation

The favoured petrogenetic model is shown in Figure 6.1 which is a cartoonish impression of the MASH zone, evolution of the melt and emplacement of the increments.

Melt derived from subduction zone enters the lower crust where it ponds. The lower crust becomes partial molten. Host rock and fresh melt interacts (mixing, assimilation, storage and homogenization =MASH). Within the MASH zone assimilation and homogenization between the “fresh” YC and the (parental) YVIS Taft Granite occurs. This results in a dacitic melt that will form the granitic and granodioritic melts after FC. These melts escape into the crust due to the greater buoyancy of the melt. Before emplacement the major phases fractionated are plagioclase, biotite and hornblende. Minor compositional differences result in subtly different phase relations and cause the compositional varieties.

A second melt batch enters the MASH zone. Little interaction with melts and host rock occurs. Extensive fractional crystallization of hornblende, clinopyroxene and plagioclase changes the composition of the melt. The Fine Grained Quartz Monzodiorite to Granodiorite Unit is a magma batch that is derived from the Diorite to Hornblende-rich Diorite and underwent extensive hornblende fractionation. These two units intrude the previous described granitic and granodioritic emplaced increments.

The Yosemite Creek Granodiorite (Huber et al., 1989) suite is constructed by emplacement of the several increments. The source of these increments is envisioned to be the dacitic and gabbroic melt that underwent crystal fractionation in the lower crust and a gabbroic/quartz monzodiorite melt that underwent extensive fractional crystallization.

6.3 Recommendation

An isotope study is required to validate the petrogenetic model in relation to crustal assimilation and homogenization in the MASH zone. Sr, Nd and Hf isotope study is recommended to detect and to quantify the assimilation and quantification with a parental Taft Granite or young YVIS unit. A conclusive relationship between the Fine Grained Quartz Monzodiorite to Granodiorite Unit and the Diorite to Hornblende-rich Diorite can be more specified.

Isotopic recommendation:

- Prove isotopic distinction between the gabbroic derived and dacitic derived increments, e.g. respectively samples BL-13F and BL-2D with BL-4H, BL17A and BL-18D.

- Prove petrogenetic similarity between granitic sample trough out the research area, e.g. samples BL-6A, BL-12A, BL-13A, BL-16A and BL-18A.

- Prove assimilation and homogenization between the YC and YVIS by isotopic similarity between YC GT and YVIS GT, e.g. sample BL-15B and BL-10A.

- Quantify hybridization (relation) between the petrologically related YC units.

- Study conclusive relationship between the Diorite to Hornblende-rich Diorite Unit and the Fine Grained Quartz Monzodiorite to Granodiorite Unit, e.g. respectively sample BL-8B and BL-14D.

- Indentify possible zircon and plagioclase inheritance of the Fine Grained Quartz Monzodiorite to Granodiorite.

- Quantify wall-rock assimilation by studying the YC GT enclave (sample BL-4A) which is interpreted to have been partial assimilated and homogenized by YC granodiorite.

- Indentify sample 24A-(2)SJSU and its relation to YC GD samples.

Figure 6.1

Cartoonish impression of conclusive model. Integrated are the interpreted field and geochemical conclusions. Abbreviations: Kt = Taft Granite, Kyd = Diorite to Hornblende-rich Diorite and Fine Grained Quartz Monzodiorite to Granodiorite, Ky = Medium Grained Granodiorite, Kyc = Coarse Grained Granodiorite, Kyp = Porphyritic Granodiorite, FC = fractional crystallization, AH = assimilation and homogenization, MASH zone = mixing – assimilating – storage – homogenization zone, YVIS = Yosemite Valley Intrusive Suite, YC GD – Yosemite Creek Granodiorite. Abbreviations are adopted from Figure 3.2a to make minor implications on emplacements with respect to the geological map. Figure is not to scale. **(a)** Modified after Saleeby at al. (2003), envisioned is the cartoonish impression implemented in a more realistic sketch of the Sierra Nevada lithosphere. **(b)** Cartoonish impression of the final petrological model.

Figure 6.1a

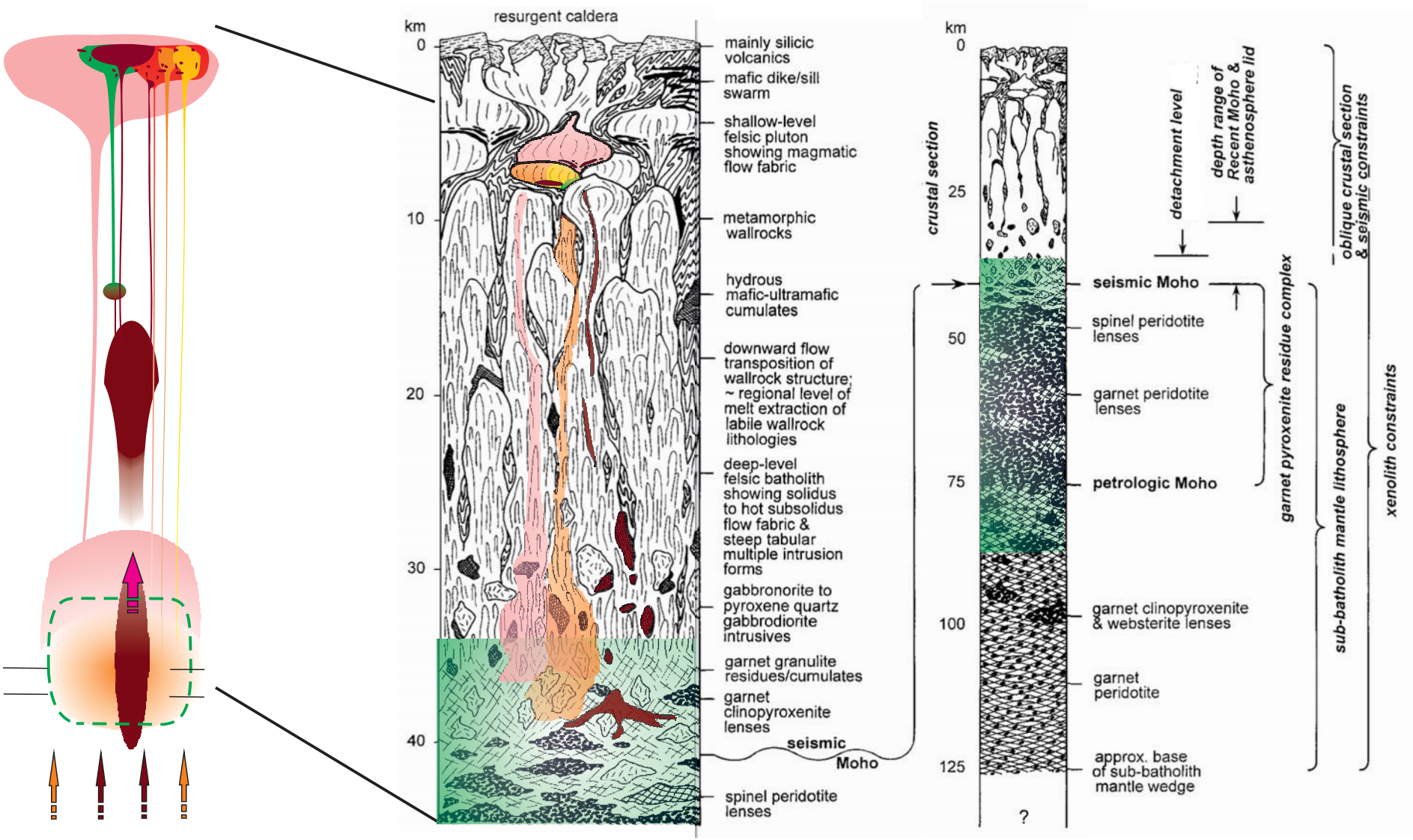
resurgent caldera
km
0
10
20
30
40
mainly silicic volcanics
mafic dike/sill swarm
shallow-level felsic pluton showing magmatic flow fabric
metamorphic wallrocks
hydrous mafic-ultramafic cumulates
downward flow transposition of wallrock structure; ~ regional level of melt extraction of labile wallrock lithologies
deep-level felsic batholith showing solidus to hot subsolidus flow fabric & steep tabular multiple intrusion forms
gabbronorite to pyroxene quartz gabbrodiorite intrusives
garnet granulite residues/cumulates
garnet clinopyroxenite lenses
seismic Moho
spinel peridotite lenses
crustal section
km
0
25
50
75
100
125
?
detachment level
depth range of Recent Moho & asthenosphere lid
seismic Moho
spinel peridotite lenses
garnet peridotite lenses
petrologic Moho
garnet clinopyroxenite & websterite lenses
garnet peridotite
approx. base of sub-batholith mantle wedge
garnet pyroxenite residue complex
sub-batholith mantle lithosphere
oblique crustal section & seismic constraints
xenolith constraints

Figure 6.1b

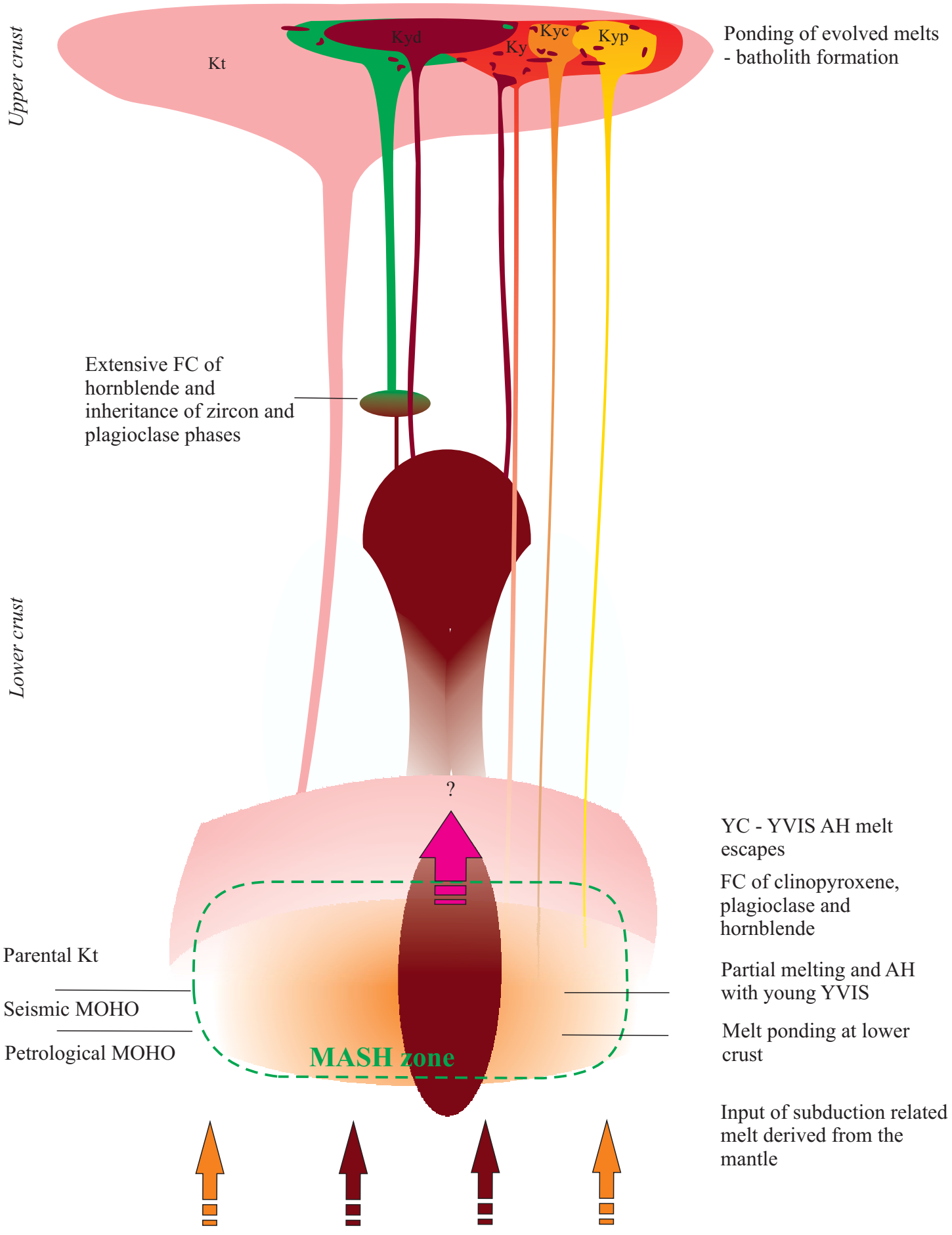
Upper crust
Lower crust
Kt
Kyd
Ky
Kyc
Kyp
Ponding of evolved melts - batholith formation
Extensive FC of hornblende and inheritance of zircon and plagioclase phases
?
YC - YVIS AH melt escapes
FC of clinopyroxene, plagioclase and hornblende
Parental Kt
Partial melting and AH with young YVIS
Seismic MOHO
Melt ponding at lower crust
Petrological MOHO
MASH zone
Input of subduction related melt derived from the mantle

References cited:

Adamuszek M., John T., Dabrowski M., Podladchikov Y. Y., Gertisser R. (2009) *Assimilation and diffusion during xenoliths-magma interaction: a case study of the Variscan Karkonosze Granite*, Bohemian Massif, Mineral Petrology 97:203-222

Allaby A. and Allaby M. (1993) *Oxford Dictionary of Earth Sciences*, Oxford University press, second edition

Annen C., Blundy J. D., Sparks S. J. (2006) *The Genesis of Intermediate and Silicic Magmas in Deep Crustal Hot Zones*, Journal of Petrology, Volume 47, Number 5, Pages 505-539

Ashwal L. D. (1982) *Mineralogy of mafic and Fe-Ti oxide-rich differentiates of the Marcy anorthosite massif*, Adirondacks, New York, American Mineralogist, Volume 67, pages 14-27

Bachmann O. and Bergantz G. W. (2004) *On the Origin of Crystal-poor Rhyolites: Extracted from Batholithic Crystal Mushes*, J. Petrology 45(8): 1565-1582

Bachmann O. and Bergantz G. W. (2006) *Gas percolation in upper-crustal silicic crystal mushes as a mechanism for upward heat advection and rejuvenation of near-solidus magma bodies*, Journal of Volcanology and Geothermal Research, Volume 149, Issues 1-2

Baker D. R. (1991) *Interdiffusion of hydrous dacitic and rhyolitic melts and the efficacy of rhyolite contamination of dacitic enclaves*, Springer-Verslag, Contribution of Mineralogy and Petrology, 106:462-473

Barbey P., Gasquest D., Pin C., Bourgeix A. L. (2007) *Igneous banding, schlieren and mafic enclaves in calc-alkaline granites: The Budduso pluton (Sardinia)*, ScienceDirect, Lithos 104:147-163

Bartley J. M., Coleman D. S., Glazner, A F. (2006) *Incremental pluton emplacement by magmatic crack-seal*, Transactions of the Royal Society of Edinburgh: Earth Sciences, 97, 383–396, 2008

Bateman P. C. and Chappell B. W. (1979*) Crystallization, fractionation, and solidification of the Tuolumne Intrusive Series, Yosemite National Park, California*, Geol Soc Am Bull 90, 465-482.

Bateman P. C. (1992) Plutonism *in the central part of the Sierra Nevada batholith, California*, U.S. Geological Survey Professional Paper 1483.

Burgess S. D. and Miller J. S. (2008) *Construction, solidification and internal differentiation of a large felsic arc pluton: Cathedral Peak granodiorite, Sierra Nevada Batholith*, Geological Society, London, Special Publications v. 304; p. 203-233

Calkins F. C. (1930) *The granitic rocks of the Yosemite region, in Matthes*, F. E., ed., Geologic history of the Yosemite Valley: U.S. Geol. Survey Prof Paper 160, 0 120-129

Chen J. H. and Moore J. G. (1982) *Uranium-Lead isotopic ages from the Sierra Nevada Batholith, California*, Journal of Geophysical Researcr, Vol. 87, No. B6, Pages 4761-4784

Coleman D.S., Bartley J.M., and Glazner A.F. (2005) *Field evidence for the assembly of the Half Dome pluton by amalgamation of small intrusions*, Geological Society of America Abstracts with Programs, v. 37, no. 4, p. 71.

Coleman D.S., and Glazner A.F., (1997) *The Sierra crest magmatic event: rapid formation of juvenile crust during the Late Cretaceous in California*, International Geology Review, v. 39, p. 768–787.

Coleman D.S., Gray W., and Glazner A.F. (2004) *Rethinking the emplacement and evolution of zoned plutons: geochronologic evidence for incremental assembly of the Tuolumne Intrusive Suite, California*, Geology, v. 32, no. 5, p. 433–436

Deer W. S., Howie R. A., Zussman J. (1966) *An Introduction to the Rock-forming Minerals*, Longman Group Limited, London

El Bouseily A. M. and El Sokkary A. A. (1975) *The relation between Rb, Ba and Sr in granitic rocks*, Elsevier Scientific Publishing Company, Amsterdam, Chemical Geology, 16:207-219

Jellinek, A.M., and DePaolo, D.J., 2003, *A model for the origin of large silicic magma chambers: Precursors of caldera-forming eruptions*, Bulletin of Volcanology, v. 65, p. 363–381.

Johnson (unpublished) *Structure, construction, and emplacement of Cretaceous plutons in the Central Sierra Nevada Batholith*, San Jose State University, Graduate Thesis

Forster H. J., Tischendorf G., Trumbell R. B. (1997) *An evulation of the Rb vs. (Y + NB) discrimination diagram to infer tectonic setting of silicic igneous rocks*, Elsevier, Lithos 40: 261-293

Frey A. F., Chappell B. W., Roy S. D. (1978) *Fractionation of rare-earth elements in the Tuolumne Intrusive Series, Sierra Nevada batholith, California*, Geological Society of Amerika, Volume 6: 239-242.

Fulmer E. C. and Kruijer T. (2008) *The Nature of Batholith Formation: Detailed field, geochemical and isotopic constrains on the assembly of the Sentile Granodiorite*, Sierra Nevada Batholith, USA, Vrije Universiteit Amsterdam.

Glazner A. F., Bartley J. M. (2006) *Is stoping a volumetrically significant pluton emplacement process?*, Geol Soc Am Bull 118(9–10):1185–1195

Glazner A.F., Bartley, J.M., Coleman D.S., Gray W.M., and Taylor R.Z. (2004) *Are plutons assembled over millions of years by amalgamation from small magma chambers?*, GSA Today, v. 14, no. 4/5, p. 4–11.

Glazner A. F., Coleman D. S., Bartley J. M. (2008) *The tenuous connection between high-silica rhyolites and granodiorite plutons*, The Geological Society of America, Inc, Geology; 36; 183-186

Gray W, Glazner A. F., Coleman D. S., Bartley J. M. (2008) *Long-term geochemical variability of the Late Cretaceous Tuolumne Intrusive Suite, central Sierra Nevada, California*, Geol Soc Lond Special Publ 304:183–201

Gray W., Glazner A. F., Coleman D. S., and Bartley J. M. (2008) *Long-term geochemical variability ofthe Late Cretaceous Tuolumne Intrusive Suite, central Sierra Nevada, California. Dynamics of Crustal Magma Transfer, Storage and fentiation*, Geological Society, London, Special Publications, 33 4183–201.

Grove T. L., Elkins-Tanton L. T., Parman S. W., Chatterjee N., Müntener O., Gaetani G. A. (2003) *Fractional crystallization and mantle-melting controls on calc-alkaline differentiation trends*, Springer-Verslag, Contribution to Mineralogy and Petrology, 145:515-533

Grove T. L., Gerlach D. C., Sando T. W. (1982) *Origin of Calc-Alkaline Series Lavas at Medicine Lake Volcano by Fractionation, Assimilation and Mixing*, Springer-Verslag, Contributions to Mineralogy and Petrology, 80:160-182

Hildreth W. (1979) *The Bishop Tuff; evidence for the origin of compositional zonation in silicic magma chambers, in Chapin, C.E., and Elston, W.E., eds., Ash-flow tuffs*, Geological Society of America Special Paper 180, p. 43–75.

Huber N.K., Bateman P.C., Wahrhaftig C., (1989) *Geologic map of Yosemite National Park and vicinity, California*, U.S. Geological Survey Map I-1874, 1:125,000.

Huber C., Bachmann O., Manga M. (2009) *Homogenization processes in silicic magma chambers by stirring and mushification (latent heat buffering)*, Earth and Planetary Science Letters 283 38–47

Johannsen A. J. (1939) *A Descriptive Petrography of the Igneous Rocks (5 Volumes)*, University of Chicago Press, Chigaco

Johnson B. R., and Glazner A. F. (2010) *Formation of K-feldspar megacrysts in granodioritic plutons by thermal cycling and late-stage textural coarsening*, Contrib Mineral Petrol: 159:599–619

Johnson B. R., Glazner A. F. (2009) *Formation of K-feldspar megacrysts in granodioritic plutons by thermal cycling and late-stage textural coarsening*, Springer-Verlag, Contrib Mineral Petrol 159:599–619.

Kemp A. I. S., Hawkesworth C. J., Foster G. L., Paterson B. A., Woodhead J. D., Hergt J. M., Gray C. M., Whitehouse M. J. (2007) *Magmatic and Crustal Differentiation History of Granitic Rocks from Hf-O Isotopes in Zircon,* Science 315, 980

Klimm K., Holtz F., King P. L. (2008) *Fractionation vs. magma mixing in the Wangrah Suite A-type granites, Lachlan Fold Belt, Australia: Experimental contstraints,* Elsevier, Lithos, 102:415-434

Kotková J. (2007) *High-pressure granulites of the Bohemian Massif: recent advances and open questions*, Journal of Geoschiences, 52: 45-71

Kistler R., W., (1973) *Geological map of the Hetchy Hetchy reservoir quadrangle, Yosemite National Park, California,* United States Geological Survey.

Kistler R.W., Chappell B.W., Peck D.L., and Bateman P.C., (1986) *Isotopic variation in the Tuolumne intrusive suite, central Sierra Nevada, California,* Contributions to Mineralogy and Petrology, v. 94, p. 205–220

Kistler R. W., Chappell B. W., PeckD. L., and Bateman P. C. (1986) *Isotopic variation in the Tuolumne Intrusive Suite, central Sierra Nevada, California,* Contrib. Mineral. Petr. 9944, 205-220

Kistler R.W., and Fleck R.J., (1994) *Field guide for a transect of the central Sierra Nevada, California: Geochronology and isotope geology,* U.S. Geological Survey Open-File Report, v. 94-267, 53p

Lackey J. S., Valley J. W., Chen J. H., Stockli D. F. (2008) *Dynamic Magma Systems, Crustal Recycling, and Alteration in the Central Sierra Nevada Batholith: the Oxygen Isotope Record*, Journal Of Petrology Vol. 49 No. 7 Pages 1397-1426

Lackey J. S., Valley J.W., and Saleeby J. B. (2005) *Supracrustal input to magmas in the deep crust of Sierra Nevada batholith: evidence from high-d18O zircon,* Earth and Planetary Science Letters 235, 315-330.

Lackey J. S., Valley J. W., and Hinke H. J. (2006) *Deciphering the source and contamination history of peraluminous magmas using d18O of accessory minerals: examples from garnet-bearing granitoids of the Sierra Nevada batholith,*. Contributions to Mineralogy and Petrology 151, 20-44.

Lipman P. W., (2007) Incremental assembly and prolonged consolidation of Cordilleran magma chambers: Evidence from the Southern Rocky Mountain volcanic field: Geosphere, v. 3, p. 42–70

Matzel J., Mundil R., Paterson S., Renne P., Nomade S., (2005) *Evaluating pluton growth models using high resolution geochronology: Tuolumne Intrusive Suite, Sierra Nevada, CA,* Geological Society of America Abstracts with Programs 37, 131.

McCarthy T. S., Groves D. I. (1979) *The Blue Tier Batholith, Northeastern Tasmania,* Springer-Verslag, Contribution to Mineralogy and Petrology, 71:193-209

Menand T. (2007) *The mechanics and dynamics of sills in layered elastic rocks and their implications for the growth of laccoliths and other igneous complexes,* Earth and Planetary Science Letters 267 93–99

Middlemost E. A. K. (1994) *Naming materials in the magma/igneous rock system,* Elsevier Earth-Science Reviews 37:215-224

Miller J. S. (2008) *Assembling a pluton…one increment at a time,* The Geological Society of America. Geology: v. 36 ; no. 6; p. 511–512

Miller J. S., Matzel J. E. P., Miller C. F., Burgess S. D., and Miller R. B. (2007) *Zircon growth and recycling during the assembly of large, composite arc plutons,* Journal of Volcanology and Geothermal Research, v. 167, p. 282–299

Mills R. D., Glazner A. F., Coleman D. S. (2009) *Scale of pluton/wall rock interaction near May Lake, Yosemite National Park, CA, USA,* Contrib Mineral Petrol 158:263–281

Mills, R. D., Glazner, A. F., Coleman, D. S., (2009) *Scale of pluton/wall rock interaction near Mary Lake, Yosemite National Park, CA, USA*, Springer, Mineral Petrology, 158: 263-281.

Pearce J. A., Harris N. B. W., Tindle A. G. (1984) *Trace Element Discrimination Diagrams for the Tectonic Interpretation of Granitic Rocks,* Oxford Journals, Journal of Petrology, Volume 24, Part 4, page 956-983

Petsche J. M. (2008) *Structure of the Sentinel Granodiorite, Yosemite National Park, California,* San Jose State University, Graduate Thesis.

Paterson S. R., Zak J., and Janousek V. (2008) *Growth of complex sheeted zones during recycling of older magmatic units into younger: Sawmill Canyon area, Tuolumne batholith, Sierra Nevada, California,* Journal of Volcanology and Geothermal Research 177, 457-484.

Paterson S. R. (2009) *Magmatic tubes, pipes, troughs, diapirs, and plumes: Late-stage convective instabilities resulting in compositional diversity and permeable networks in crystal-rich magmas of the Tuolumne batholith, Sierra Nevada, California*, Geological Society of America, volume 5:496-527

Peck D.L., (2002) *Geologic map of the Yosemite Quadrangle, central Sierra Nevada, California,* U.S. Geological Survey Map I-2751, 1:62,500.

Ratajeski K., Glazner A.F., and Miller B.V. (2001) *Geology and geochemistry of mafic and felsic plutonic rocks in the Cretaceous intrusive suite of Yosemite Valley, California,* Geological Society of America Bulletin, v. 113, p. 1486–1502

Rollinson H. R. (1993) *Using Geochemical Data: Evaluation, Presentation, Interpretation,* Pearson Education Limited, Essex England

Saleeby J., Ducea M., Clemens-Knott D. (2003) *Production and loss of high-density batholithic root, southern Sierra Nevada, California,* American Geophysical Union, Tectonics, Volume 22, number 6, 1064

Sano Y., Terada K., Fukuoka T. (2002) *High mass resolution ion microprobe analysis of rare earth elements in silicate glass, apatite and ziecon: lack of matric dependency,* Chemical Geology, 184:217-230

Schlotz R., and Uhlig S. (2006) *Introduction to X-ray Fluorescence Analysis (XRF),* Bruker AXS GmbH, Karlruhe, West Germany

Schweickert R. A., Bogen N. L., Girty G. H., Hanson R. E., Merguerian C. (1984) *Timing and structural expression of the Nevada orogeny, Sierra Nevada, California,* Geological Society of America Bulletin, v. 95, p. 967-979

Streckeisen A. L. (1974) *Classification and Nomenclature of Plutonic Rocks. Recommendations of the IUGS Subcommission on the Systematics of Igneous Rocks. Geologische Rundschau. Internationale Zeitschrift für Geologie,* Stuttgart. Vol.63, p.773-785

Solgadi F., Sawyer E. W. (2008) *Formation of Igneous Layering in Granodiorite by Gravity Flow: a Field, Microstructure and Geochemical Study of the Tuolumne Intrusive Suite at Sawmill Canyon, California,* Journal Petrology, volume 46: 2009-2042.

Titus S. J., Clark R., Tikoff B. (2005) *Geologic and geophysical investigation of two fine-grained granites, Sierra Nevada Batholith, California; evidence for structural controls on emplacement and volcanism,* Geol Soc Am Bull 117(9–10):1256–1271

Venezky D. Y., Rutherford M. J. (1999) *Petrology and Fe-Ti oxide reequilibration of the 1991 Mount Unzen mixed magma*, Elsevier, Journal of Volcanology and Geothermal Research 89: 213-230

Vogel T. A., Hidalgo P. J., Patino L., Tefend K. S. (2008) *Evaluation of magma mixing and fractional crystallization using whole-rock chemical analyses: Polytopic vector analyses,* American Geophysical Union, Geochemistry Geophysics Geosystems, Volume 9, Number 4, ISSN: 1525-2027

Vigneresse J. L., Barbey P., Cuney M. (1996) *Rheological Transitions During Partial Melting and Crystallization with Application to Felsic Magma Segregation and Transfer, Oxford Journals,* Journal of Petrology, Volume 37, Number 6, Pages 1579-1600

Watson E. B (1980) *Apatite and Phosphorus in Mantle Source Regions: An Experimental Study of Apatite/Melt equilibria at pressures to 25 kBar,* Elsevier, Earth and Planetary Science Letters, 51:322-335

Winter J. D. (2001) *An Introduction to Igneous and Metamorphic Petrology,* Prentice Hall, New Jersey

Workman R. K., Hart S. R. (2005) *Major and trace element composition of the depleted MORB mantle (DMM),* Elsevier, Earth and Planetary Science Letters, 231:53-72

Žák J., Paterson S. R., Janoušek V. (2009) *The Mammoth Peak sheeted complex, Tuolumne batholith, Sierra Nevada, California: a record of initial growth or late thermal contraction in a magma chamber?*, Contrib Mineral Petrol 158:447–470

Samples, location on the geological map of Johnson (unpublished) and classification by use of CIPW normative mineral calcualtion

Sample name	Unite	Map Formation	Rock Classification
5E SJSU	YC	medium-grained granodiorite to tonalite	Granodiorite
5G SJSU	YC	medium-grained granodiorite to tonalite	Granodiorite
11C SJSU	YC	coarse-grained granodiorite	Granodiorite
11F SJSU	YC	porphyritic granodiorite	Granodiorite
19J SJSU	YC	Myriad zone intruding Taft and El Cap	Quartz Monzodiorite
20B SJSU	YC	coarse-grained granodiorite	Granodiorite
23B SJSU	YC	medium-grained granodiorite to tonalite	Granite
24A SJSU	YC	medium-grained granodiorite to tonalite	Quartz Monzodiorite
24A-2 SJSU	YC	medium-grained granodiorite to tonalite	Quartz Monzodiorite
25B SJSU	YC	Taft granite	Monzodiorite
31C SJSU	YC	coarse-grained granodiorite	Granodiorite
31H SJSU	YC	coarse-grained granodiorite	Granodiorite
31I-2 SJSU	YC	Myriad zone intruding Taft granite	Granodiorite
33F SJSU	YC	mafic quartz diorite to diorite	Gabbro
34C SJSU	YC	Myriad zone intruding Taft granite	Quartz Monzodiorite
35I SJSU	YC	Myriad zone intruding Taft granite	Granite
37A SJSU	YVIS	El Capitan: Mt. Hoffman granodiorite	Granodiorite
37D SJSU	YVIS	El Capitan: Mt. Hoffman granodiorite	Granite
37G SJSU	YVIS	El Capitan: Mt. Hoffman granodiorite	Quartz Monzodiorite
40B SJSU	YVIS	El Capitan: Equigranular granite	Quartz Monzodiorite

Sample name	Unite	Map Formation	Field Classification	
BL-1A	YC	medium-grained granodiorite to tonalite	mafic diorite	Quartz Monzodiorite
BL-1B	YC	medium-grained granodiorite to tonalite	hybrid	Quartz Monzodiorite
BL-1C	YC	medium-grained granodiorite to tonalite	taft	Granite
BL-2A	YC	mafic quartz diorite to diorite	taft (felsic dyke)	Granite
BL-2B	YC	mafic quartz diorite to diorite	mafic sheet	Monzodiorite
BL-2C	YC	mafic quartz diorite to diorite	hybrid	Monzodiorite
BL-2D	YC	mafic quartz diorite to diorite	hornblenderich diorite	Gabbro
BL-3A	YC	Taft granite	mafic sheet	Gabbro
BL-3B	YC	Taft granite	diorite	Tonalite
BL-3C	YC	Taft granite	hybrid	Quartz Monzodiorite
BL-3E	YC	Taft granite	granite dyke	Granite
BL-3D	YC	Taft granite	hybrid dyke	Granodiorite
BL-3F	YC	Taft granite	taft	Granite
BL-4A	YC	medium-grained grano	taft xenolith	Granite
BL-4C	YC	medium-grained granodiorite to tonalite	granodiorite	Quartz Monzodiorite
BL-4D	YC	medium-grained granodiorite to tonalite	pegmatite dyke	Granite
BL-4E	YC	medium-grained granodiorite to tonalite	mafic enclave	Monzodiorite
BL-4G	YC	medium-grained granodiorite to tonalite	diorite/tonalite dyke	Granodiorite
BL-4H	YC	medium-grained granodiorite to tonalite	granodiorite	Granodiorite
BL-6A	YC	medium-grained granodiorite to tonalite	porpheritic gran.	Granodiorite
BL-7A	YS	porphyritic granodiorite	sentinel	Granodiorite
BL-8A	YC	mafic quartz diorite to diorite	mafic body	Monzodiorite
BL-8B	YC	mafic quartz diorite to diorite	diorite	Quartz Monzodiorite
BL-8C	YC	mafic quartz diorite to diorite	granite dyke	Granite
BL-8D	YC	mafic quartz diorite to diorite	porpheritic gran.	Monzodiorite
BL-8E	YC	mafic quartz diorite to diorite	hybrid	Quartz Monzodiorite
BL-8F	YC	mafic quartz diorite to diorite	taft	Granite
BL-8G	YC	mafic quartz diorite to diorite	diorite	Quartz Monzodiorite
BL-9A	YC	mafic quartz diorite to diorite	granodiorite	Monzodiorite
BL-9B	YC	mafic quartz diorite to diorite	diorite	Monzodiorite
BL-10A	YC	Taft granite	taft	Granite
BL-11A	YC	Taft granite	leucogranite	Granite
BL-12A	YC	Myriad zone intruding Taft granite	leucogranite	Granite
BL-12B	YC	Myriad zone intruding Taft granite	granodiorite	Quartz Monzodiorite
BL-13A	YC	porphyritic granodiorite	porpheritic gran.	Granodiorite
BL-13B	YC	porphyritic granodiorite	mafic enclave	Monzodiorite
BL-13C	YC	porphyritic granodiorite	diorite dyke	Quartz Monzodiorite
BL-13D	YC	porphyritic granodiorite	granite dyke	Granite
BL-13E	YC	porphyritic granodiorite	leucogranite dyke	Granite
BL-13F	YC	porphyritic granodiorite	diorite dyke	Monzodiorite
BL-14A	YC	porphyritic granodiorite	porpheritic gran.	Quartz Monzodiorite
BL-14B	YC	porphyritic granodiorite	mafic enclave	Monzodiorite
BL-14C	YC	porphyritic granodiorite	enclave+porph. gran.	Monzodiorite
BL-14D	YC	porphyritic granodiorite	porpheritic gran.	Quartz Monzodiorite
BL-14E	YC	porphyritic granodiorite	granodiorite	Monzodiorite
BL-15A	YC	porphyritic granodiorite	leucogranite	Granite
BL-15B	YC	porphyritic granodiorite	porpheritic gran.	Granite
BL-16A	YC	porphyritic granodiorite	porpheritic gran.	Granite
BL-17A	YC	porphyritic granodiorite	granodiorite	Granodiorite
BL-17B	YC	porphyritic granodiorite	mafic enclave	Quartz Monzodiorite
BL-18A	YC	porphyritic granodiorite	granodiorite	Granite
BL-18C	YC	porphyritic granodiorite	mafic enclave	Monzodiorite
BL-18D	YC	porphyritic granodiorite	porpheritic gran.	Granodiorite

Results of CIPW normative mineral calculation (wt%)

Sample	q	an	hy	ab	or	ap	il	c	mt	di	ol	ne
5E SJSU	18.712	15.339	7.1494	41.124	15.661	0.278	0.8926	0.2846	0.551	0	0	0
5G SJSU	20.064	19.227	6.7575	37.993	13.533	0.3244	1.1205	0.3282	0.6525	0	0	0
11C SJSU	27.227	14.078	3.7821	35.37	18.261	0.1622	0.4558	0.4091	0.2755	0	0	0
11F SJSU	19.472	20.206	9.4954	32.154	16.015	0.417	1.1585	0.4299	0.6525	0	0	0
19J SJSU	4.8879	19.879	9.8083	44.932	16.37	0.5329	1.584	1.2806	0.7829	0	0	0
20B SJSU	19.448	15.514	11.859	33.001	16.842	0.5329	1.5004	0.4635	0.8409	0	0	0
23B SJSU	32.862	6.0706	1.9269	32.662	25.352	0.0463	0.2849	0.6115	0.174	0	0	0
24A SJSU	6.6785	19.227	6.7501	52.039	12.056	0.3244	1.0826	1.2879	0.5655	0	0	0
24A-2 SJSU	6.7732	19.128	6.613	52.124	12.41	0.3244	1.0466	1.0529	0.551	0	0	0
25B SJSU	0	37.916	8.9271	0.8764	6.0869	0.4634	3.6085	0	1.8269	8.971	16.425	0
31C SJSU	22.271	13.939	9.8278	32.747	18.438	0.4402	1.2155	0.3976	0.725	0	0	0
31H SJSU	21.763	16.219	9.3213	31.139	18.615	0.3707	1.1585	0.7622	0.6525	0	0	0
31I-2 SJSU	41.193	13.744	3.101	33.085	7.0325	0.0695	0.3419	1.1624	0.261	0	0	0
33F SJSU	0	33.723	4.5763	28.77	6.2642	1.089	3.5136	0	1.7689	7.0446	13.253	0
34C SJSU	4.3905	23.968	10.895	42.139	13.769	0.6487	1.8232	1.5113	0.8554	0	0	0
35I SJSU	33.748	5.3628	3.8657	32.239	22.87	0.139	0.4748	0.9577	0.3335	0	0	0
37A SJSU	23.483	11.65	5.3174	37.316	20.27	0.2317	0.6647	0.6327	0.435	0	0	0
37D SJSU	31.944	9.8459	3.9285	32.662	19.738	0.1854	0.4558	0.9462	0.3045	0	0	0
37G SJSU	17.439	19.148	9.8567	35.031	15.779	0.4402	1.3105	0.2614	0.725	0	0	0
40B SJSU	15.687	19.24	3.9818	46.878	11.878	0.2317	0.6457	1.1291	0.319	0	0	0
BL-1A	12.9867	32.2637	17.5907	22.4235	10.6373	0.48656	2.08914	0.39776	1.11643	0	0	0
BL-1B	4.8507	14.078	7.9665	53.816	9.8691	0.4634	1.4624	0	0.7829	6.7117	0	0
BL-1C	35.609	4.5327	1.4691	30.547	26.889	0.0463	0.1519	0.6049	0.1305	0	0	0
BL-2A	35.753	3.6893	1.339	29.024	29.016	0.0463	0.1519	0.8504	0.1305	0	0	0
BL-2B	0	34.083	7.8823	28.177	7.2097	0.8109	3.0387	0	1.6819	5.6827	11.435	0
BL-2C	3.6898	27.938	16.861	31.901	13.06	1.1585	2.317	1.1886	1.1889	0	0	0
BL-2D	0	39.613	5.5263	16.416	5.7914	0.3012	3.2097	0	2.894	8.5986	18.367	0
BL-3A	0	34.547	11.327	29.108	6.4415	0.8341	2.9818	0	1.5949	5.1609	8.0072	0
BL-3B	44.084	13.447	2.5288	33.847	4.0185	0.0695	0.2849	0.6465	0.2175	0	0	0
BL-3C	10.478	23.9	10.858	39.601	10.519	0.6024	1.6143	1.645	0.7829	0	0	0
BL-3E	37.777	1.4073	1.0005	34.27	24.466	0.0463	0.057	0.9003	0.087	0	0	0
BL-3D	19.624	15.994	10.125	36.639	12.41	0.5561	1.5004	2.4419	0.7105	0	0	0
BL-3F	32.307	3.7885	1.0618	30.462	31.38	0.0463	0.1519	0.7014	0.1015	0	0	0
BL-4A	52.726	0	1.5057	7.8694	33.744	0.0232	0.1709	3.8293	0.145	0	0	0
BL-4C	16.486	18.65	10.067	39.516	12.469	0.3707	1.2345	0.4684	0.7395	0	0	0
BL-4D	34.825	3.5223	0.9775	39.939	20.388	0.057	0.057	0.1898	0.1015	0	0	0
BL-4E	0	20.25	0	33.579	26.416	0.7878	2.45	0	1.2614	0.0434	12.89	2.3452
BL-4G	31.519	10.838	4.4258	34.524	16.842	0.1854	0.5318	0.811	0.3335	0	0	0
BL-4H	22.29	14.449	7.3204	37.993	15.779	0.3475	0.8736	0.3881	0.551	0	0	0
BL-6A	29.098	10.807	5.4213	32.916	20.093	0.2317	0.6647	0.3398	0.4205	0	0	0

Sample	q	an	hy	ab	or	ap	il	c	mt	di	ol	ne
BL-7A	19.487	21.3	9.1948	34.101	13.178	0.4866	1.2155	0.4102	0.638	0	0	0
BL-8A	0	41.1	3.9558	18.616	7.7416	1.0195	3.6845	0	1.9284	0	12.905	0
BL-8B	7.5539	22.383	11.647	38.247	14.951	0.7182	1.8232	1.8224	0.8554	0	0	0
BL-8C	32.744	7.6424	1.7737	30.716	26.239	0.0695	0.1899	0.4714	0.145	0	0	0
BL-8D	0	31.815	16.707	28.854	7.9189	0.6024	3.0198	0	1.6094	6.7223	2.743	0
BL-8E	11.42	21.054	9.3346	42.901	10.46	0.5561	1.4624	2.1072	0.696	0	0	0
BL-8F	37.408	5.1776	1.2823	32.239	22.929	0.0463	0.1329	0.6648	0.1305	0	0	0
BL-8G	7.0694	22.318	11.338	42.562	11.76	0.7414	1.6903	1.6719	0.8409	0	0	0
BL-9A	0	37.579	5.8565	20.308	8.569	0.3939	2.6019	0	1.7979	7.8996	14.987	0
BL-9B	3.2236	31.383	13.159	34.354	12.647	0.8341	1.9752	1.5129	0.9134	0	0	0
BL-10A	32.825	1.5561	1.12	28.939	34.453	0.0463	0.057	0.9129	0.1015	0	0	0
BL-11A	37.862	1.3576	0.9565	33.931	24.348	0.0463	0.057	1.346	0.087	0	0	0
BL-12A	35.191	5.6398	1.4242	26.824	30.08	0.0232	0.1899	0.4885	0.1305	0	0	0
BL-12B	5.5058	21.566	9.3873	44.001	15.07	0.5329	1.5574	1.6415	0.7395	0	0	0
BL-13A	26.958	13.616	5	30.631	22.516	0.1854	0.6457	0.1204	0.348	0	0	0
BL-13B	0	29.666	7.8672	31.731	9.9282	0.8341	2.8108	0	1.3774	8.5349	7.2518	0
BL-13C	17.939	23.324	5.4573	38.331	13.119	0.2085	0.6077	0.5766	0.406	0	0	0
BL-13D	33.576	4.4649	0.7477	21.239	39.476	0	0.076	0.3338	0.087	0	0	0
BL-13E	30.59	6.1069	3.8984	21.07	36.876	0.139	0.4748	0.5412	0.3045	0	0	0
BL-13F	1.904	21.233	20.123	33.424	16.488	0.9499	2.9248	0	1.4354	1.5308	0	0
BL-14A	13.01	26.475	14.201	29.531	11.531	0.4866	1.7283	0	0.9714	1.7194	0	0
BL-14B	0	30.795		28.201	11.11	0.6256	2.545	0	1.5079	6.9413	0	0
BL-14C	0	24.444	11.991	32.747	17.552	0.6951	2.488	0	1.3629	1.6346	7.0778	0
BL-14D	4.6654	24.722	6.6022	32.577	10.46	0.6024	2.2411	0	1.1599	6.6022	0	0
BL-14E	0	27.916	16.987	36.047	10.105	0.6024	2.5829	0	1.2759	4.3768	0.1186	0
BL-15A	34.581	6.9297	0.9385	35.708	21.275	0.0232	0.1519	0.2913	0.1015	0	0	0
BL-15B	25.73	13.436	5.5391	27.331	26.239	0.2317	0.7217	0.3662	0.406	0	0	0
BL-16A	25.866	13.436	5.5391	27.247	26.18	0.2317	0.7217	0.3834	0.406	0	0	0
BL-17A	23.735	16.48	6.6446	34.016	17.138	0.278	0.8167	0.4277	0.464	0	0	0
BL-17B	5.8255	23.751	15.994	35.708	10.992	0.4634	1.8802	0	1.0874	4.3104	0	0
BL-18A	29.739	12.428	4.6969	30.885	20.506	0.2549	0.6077	0.5346	0.348	0	0	0
BL-18C	0	22.583	4.7457	38.247	14.183	0.6256	2.393	0	1.4934	4.0697	11.663	0
BL-18D	18.381	21.07	10.643	32.916	13.533	0.417	1.3674	0	0.7395	0	0	0

q	Quartz	**il**	Ilmenite
an	Anorthite	**c**	Corundum
hy	Hypersthene	**mt**	Magnetite
ab	Albite	**di**	Diopside
or	Orthoclase	**ol**	Olivine
ap	Apatite	**ne**	Nepheline

XRF Whole rock composition for major-elements

Sample serie code	Sample name	SiO2	Na2O+K2O	TiO2	Fe2O3	FeO*	MgO	Al2O3	CaO	Na2O	K2O	P2O5	BaO	MnO	Total
YC GT	23B SJSU	73.882	8.001	0.144	1.138	1.024	0.186	13.571	1.231	3.791	4.210	0.024	0.068	0.036	98.28
	BL-6A	69.907	7.069	0.338	2.816	2.534	0.697	13.937	2.241	3.774	3.295	0.093	0.070	0.068	97.24
	BL-13A	69.431	7.254	0.329	2.355	2.119	0.809	14.842	2.782	3.533	3.721	0.076	0.088	0.055	98.02
	BL-15A	75.471	7.732	0.084	0.660	0.594	0.035	13.516	1.393	4.172	3.560	0.006	0.016	0.022	98.94
	BL-15B	69.238	7.563	0.376	2.743	2.468	0.866	15.213	2.806	3.185	4.378	0.098	0.142	0.040	99.09
	BL-16A	69.392	7.558	0.376	2.749	2.474	0.867	15.220	2.807	3.182	4.376	0.098	0.142	0.040	99.25
	BL-18A	70.653	6.985	0.314	2.360	2.124	0.698	14.569	2.602	3.582	3.403	0.105	0.130	0.042	98.46
	35I SJSU	71.565	7.338	0.235	2.151	1.935	0.383	12.779	1.105	3.640	3.698	0.058	0.063	0.070	95.75
	BL-12A	75.589	8.197	0.100	0.908	0.817	0.099	13.168	1.143	3.145	5.052	0.013	0.079	0.025	99.32
YC GT dyke	BL-4D	76.760	8.097	0.033	0.648	0.583	0.000	12.864	0.700	4.680	3.417	0.001	0.003	0.060	99.15
	BL-2A	75.200	8.173	0.079	0.892	0.803	0.061	12.901	0.759	3.363	4.810	0.020	0.213	0.017	98.31
	BL-8C	73.309	7.888	0.094	1.024	0.921	0.167	13.734	1.547	3.550	4.338	0.031	0.102	0.015	97.91
	BL-13D	75.376	9.115	0.040	0.561	0.505	0.001	13.215	0.897	2.494	6.621	0.004	0.016	0.011	99.24
	BL-13E	72.589	8.619	0.245	2.090	1.881	0.507	13.448	1.289	2.458	6.161	0.059	0.145	0.039	99.03
	BL-3E	77.174	8.079	0.025	0.544	0.489	0.048	12.382	0.310	3.993	4.086	0.023	0.014	0.076	98.67
YC GT enclave	BL-4A	72.750	7.460	0.080	0.880	0.792	0.090	10.400	0.840	2.310	5.150	0.010		0.020	92.54
YC TO	BL-3B	77.177	4.649	0.146	1.481	1.333	0.251	12.781	2.729	3.970	0.679	0.028	0.043	0.028	99.31
YC GD	11C SJSU	63.578	6.471	0.213	1.664	1.497	0.527	14.061	2.608	3.721	2.750	0.058	0.109	0.042	89.33
	20B SJSU	64.901	6.660	0.777	5.683	5.114	1.907	15.433	3.382	3.847	2.813	0.228	0.094	0.137	99.20
	31C SJSU	66.214	6.826	0.628	4.856	4.369	1.461	14.907	2.990	3.780	3.046	0.182	0.100	0.106	98.27
	31H SJSU	65.564	6.685	0.595	4.377	3.938	1.524	15.813	3.404	3.602	3.083	0.158	0.116	0.085	98.32
	5E SJSU	66.170	7.382	0.459	3.730	3.356	0.952	16.476	3.195	4.774	2.608	0.115	0.103	0.098	98.68
	5G SJSU	64.994	6.626	0.575	4.386	3.947	1.357	16.846	3.969	4.385	2.241	0.141	0.092	0.095	99.08
	BL-4H	67.014	7.001	0.454	3.750	3.374	0.990	15.602	3.037	4.393	2.608	0.147	0.135	0.086	98.22
	11F SJSU	63.821	6.335	0.593	4.368	3.930	1.582	16.562	4.199	3.701	2.634	0.174	0.104	0.081	97.82
	BL-17A	68.563	6.899	0.427	3.231	2.907	1.083	16.172	3.467	4.008	2.891	0.122	0.152	0.054	100.17
	BL-18D	64.541	6.144	0.720	5.087	4.577	1.969	16.514	4.683	3.870	2.274	0.179	0.081	0.095	100.01
	31I-2 SJSU	74.099	4.978	0.178	1.737	1.563	0.328	13.580	2.746	3.819	1.159	0.034	0.028	0.027	97.74
	37A SJSU	66.826	7.488	0.338	2.859	2.573	0.599	15.163	2.374	4.213	3.275	0.096	0.135	0.069	95.95
	BL-7A	64.211	6.138	0.629	4.314	3.882	1.539	16.946	4.484	3.953	2.185	0.204	0.063	0.092	98.62
YC GD dyke	BL-4G	71.483	6.775	0.274	2.226	2.003	0.614	14.258	2.239	3.990	2.785	0.080	0.090	0.073	98.11
YC GD dyke	BL-3D	64.153	6.349	0.783	4.863	4.376	1.726	17.471	3.494	4.276	2.073	0.237	0.114	0.076	99.27

Sample serie code	Sample name	SiO2	Na2O+K2O	TiO2	Fe2O3	FeO*	MgO	Al2O3	CaO	Na2O	K2O	P2O5	BaO	MnO	Total
YC QM	24A SJSU	60.607	8.019	0.555	3.776	3.398	0.813	20.211	3.973	6.020	1.999	0.135	0.129	0.079	98.30
	24A-2 SJSU	61.089	8.104	0.539	3.709	3.337	0.814	20.102	3.964	6.045	2.059	0.135	0.135	0.077	98.67
	BL-1A	57.366	4.374	1.083	7.608	6.846	3.257	18.198	6.657	2.602	1.772	0.207	0.063	0.134	98.95
	BL-1B	62.938	8.156	0.781	5.502	4.951	1.974	17.717	4.804	6.462	1.694	0.205	0.080	0.092	102.25
	BL-4C	63.703	6.658	0.639	5.012	4.510	1.471	16.950	3.897	4.586	2.072	0.156	0.101	0.129	98.72
	BL-8B	57.754	6.879	0.938	5.806	5.224	1.838	19.721	4.802	4.409	2.470	0.307	0.140	0.093	98.28
	BL-8E	60.740	6.751	0.756	4.753	4.277	1.445	19.818	4.498	5.001	1.750	0.236	0.110	0.111	99.22
	BL-8G	58.203	6.879	0.876	5.702	5.131	1.718	19.875	4.824	4.926	1.953	0.318	0.107	0.146	98.65
	BL-14A	60.105	5.445	0.901	6.627	5.963	2.771	17.440	5.963	3.452	1.993	0.204	0.075	0.102	99.63
	BL-14D	56.221	5.547	1.166	7.861	7.073	4.222	17.080	6.845	3.798	1.749	0.258	0.074	0.178	99.45
	34C SJSU	56.661	7.123	0.932	5.737	5.162	1.590	20.462	5.065	4.849	2.274	0.270	0.149	0.082	98.07
	BL-12B	58.760	7.640	0.813	5.072	4.564	1.348	20.573	4.581	5.130	2.510	0.224	0.151	0.054	99.22
	19J SJSU	58.968	7.950	0.799	5.297	4.766	1.328	19.983	4.241	5.224	2.726	0.226	0.124	0.115	99.03
	BL-3C	58.995	6.308	0.827	5.231	4.707	1.810	19.551	5.032	4.569	1.739	0.256	0.116	0.064	98.19
YC QM dyke	BL-13C	64.647	6.647	0.318	2.748	2.473	0.788	18.685	4.742	4.464	2.183	0.088	0.084	0.038	98.79
YC QM enclave	BL-17B	57.567	5.987	0.973	7.380	6.641	3.538	17.408	6.007	4.156	1.831	0.197	0.048	0.164	99.27
YC MD enclave	BL-4E	52.985	8.715	1.254	8.441	7.595	2.699	19.124	4.423	4.360	4.355	0.328	0.249	0.216	98.44
	BL-13B	50.836	5.286	1.441	9.290	8.359	4.183	18.360	8.306	3.652	1.634	0.349	0.051	0.136	98.24
	BL-14B	49.078	5.679	1.315	10.162	9.144	4.642	19.342	8.070	3.838	1.841	0.268	0.058	0.184	98.80
	BL-14C	53.189	6.726	1.284	9.279	8.349	4.328	18.221	5.625	3.803	2.923	0.298	0.080	0.178	99.21
	BL-18C	52.968	6.678	1.239	10.141	9.125	3.846	18.008	5.789	4.442	2.236	0.264	0.040	0.201	99.17
YC MD	BL-2C	53.633	5.843	1.191	8.000	7.198	2.846	20.256	6.152	3.683	2.160	0.486	0.136	0.069	98.61
	BL-8D	50.958	4.678	1.567	10.964	9.865	4.139	18.410	8.246	3.357	1.321	0.254	0.062	0.126	99.40
	BL-9A	47.051	3.746	1.335	12.090	10.879	5.743	18.809	9.478	2.335	1.411	0.169	0.062	0.151	98.64
	BL-9B	54.824	6.143	1.027	6.428	5.784	2.256	21.781	6.735	4.022	2.121	0.355	0.077	0.145	99.77
	BL-14E	53.865	5.895	1.343	8.738	7.862	3.526	18.852	6.939	4.206	1.689	0.252	0.076	0.125	99.61
YC MD sheet	BL-2B	48.521	4.423	1.557	11.243	10.116	4.807	18.764	8.469	3.236	1.187	0.341	0.068	0.160	98.35
	BL-8A	45.296	4.182	1.877	12.903	11.610	4.862	19.449	9.496	2.913	1.269	0.424	0.066	0.199	98.75
YC MD dyke	BL-13F	54.829	6.600	1.509	9.657	8.689	3.640	16.948	5.085	3.866	2.734	0.402	0.051	0.186	98.91
YC GA	33F SJSU	48.268	4.389	1.822	11.990	10.789	4.559	18.782	8.970	3.342	1.047	0.464	0.056	0.197	99.50
	BL-2D	44.397	2.817	1.632	14.553	13.095	6.197	18.127	9.893	1.875	0.942	0.128	0.040	0.153	97.94
YC GA sheet	BL-3A	49.463	4.435	1.540	10.753	9.676	4.568	19.082	8.506	3.368	1.067	0.349	0.060	0.140	98.90
YVIS GT	BL-1C	75.766	8.062	0.082	0.931	0.838	0.090	12.976	0.933	3.562	4.500	0.015	0.129	0.032	99.02
	BL-8F	76.039	7.569	0.072	0.840	0.756	0.058	12.823	1.054	3.748	3.821	0.019	0.151	0.025	98.65
	BL-3F	73.591	8.656	0.078	0.700	0.630	0.061	13.377	0.765	3.498	5.158	0.021	0.085	0.020	97.35
	BL-10A	74.801	9.081	0.026	0.650	0.585	0.022	13.166	0.336	3.356	5.725	0.021	0.001	0.097	98.20
	BL-11A	76.506	7.982	0.034	0.557	0.501	0.006	12.654	0.299	3.937	4.045	0.023	0.000	0.095	98.16
	37D SJSU	72.153	7.071	0.239	2.026	1.823	0.520	14.267	2.056	3.791	3.280	0.077	0.105	0.057	98.57
YVIS QM	37G SJSU	63.504	6.657	0.677	4.872	4.384	1.487	16.576	4.016	4.046	2.611	0.183	0.093	0.103	98.17
	40B SJSU	65.093	7.461	0.339	2.183	1.964	0.535	19.226	3.957	5.473	1.988	0.095	0.076	0.050	99.02
YVIS MD	25B SJSU	46.240	3.734	1.847	12.225	11.000	4.961	19.080	9.780	2.737	0.997	0.198	0.040	0.150	98.25

XRF Whole rock trace element compositions (ppm) selection of LILE-REE

Sample serie code	Samples	Rb	Ba	Th	U	Nb	Ta	K	La	Ce	Pb	Pr	Sr	P	Nd	Sm	Zr	Hf	Ti	Dy	Y	Er	Yb
Conversion Factor								8301						4365					5995				
YC GT	23B SJSU	157.08	594.64	22.21	8.4	14.71	0.62	34947.21	21.1	36.97	28.96	3.27	165.86	104.76	14.45	2.32	95.55	1.75	863.28	-3.18	19.43	-0.72	1.75
	BL-6A	152.74	611.93	12.89	4.63	9.5	0	27351.80	22.88	37.3	11.39	4.07	210.3	405.95	13.44	2.92	129.61	2.14	2026.31	-1.63	20.5	0.26	1.95
	BL-13A	134.99	775.31	17.16	6.53	9.99	1.06	30888.02	19.11	31.45	20.1	2.65	328.92	331.74	10.27	1.96	91.19	2.06	1972.36	-2.65	13.52	-0.28	1.56
	BL-15A	72.44	704.99	2.06	2.9	6.78	0	29551.56	12.57	21.02	6.53	2.88	821.66	26.19	8.15	2.69	90.33	2.94	503.58	2.45	8.81	0.2	0.55
	BL-15B	75.5	132.41	20.9	29.99	9.16	1.07	36341.78	7.5	11.15	29.42	0.68	90.68	427.77	4.62	0.81	26.04	-0.22	2254.12	-4.67	9.68	-1.34	1.05
	BL-16A	118.42	1246.68	10.08	3.23	6.33	0	36325.18	21.23	23.37	18.25	2.59	426.57	427.77	3.02	1.06	96.97	1.85	2254.12	-3.54	8.04	-1.38	1.01
	BL-18A	83.07	1139.18	8.21	2.12	4.44	0.27	28248.30	25.26	28.16	13.76	3.16	391.77	458.33	4.79	1.45	110.13	2.48	1882.43	-4.77	5.05	-1.12	1.19
	35I SJSU	196.26	562.98	25.89	7.29	13.17	0.23	30697.10	23.04	45.46	27.29	3.92	101.72	253.17	18.62	3.03	104.93	1.96	1408.83	-3.02	17.75	-0.73	1.58
	BL-12A	184.09	682.26	47.38	9.4	10.17	1.14	41936.65	17.6	29.21	28.46	2.95	185.41	56.75	9.13	2.31	75.37	1.6	599.50	-2.76	22.07	-0.37	2.62
YC GT dyke	BL-4D	175.29	11.53	3.79	1.92	16.42	4.42	28364.52	4.24	12.5	15.15	0.65	505.95	4.37	5.83	1.34	219.85	2.42	197.84	-2.81	25.98	0.8	6.16
	BL-2A	63.84	0	57.05	21.21	4.35	4.08	39927.81			97.37		2095.58	87.30			181.36	9.43	473.61	-0.14	20.75	4.61	0
	BL-8C	89.38	888.22	9.36	9.8	13.32	2	36009.74	11.99	14.17	24.98	0.88	216.47	135.32	2.55	0.54	55.44	0.64	563.53	-3.82	15.53	-0.94	1.91
	BL-13E	156.47	1258.07	82.3	11.38	5.03	0.06	51142.46	70.09	103.17	25.48	10.94	274.25	257.54	30.65	5.68	73.35	1.36	1468.78	-3.2	8.28	-0.84	0.3
	BL-3E	183.38	108.39	3.09	3.7	11.72	2.49	33917.89	5.81	14.94	12.31	0.89	34.86	100.40	6.69	1.49	7.27	-1.16	149.88	-4.77	15.87	-1.3	0.84
YC GT enclave	BL-4A	161.95	2583.81	21.62	5.71	4.92	0	42750.15	18.7	13.57	21.29	1.79	251.02	43.65	0	0	153.9	4.63	479.60	-2.84	13.49	-0.62	1.84
YC TO	BL-3B	30.72	363.81	4.1	2.44	3.42	0	5636.38	13.84	15.17	9.57	1	454.34	122.22	2.98	0.64	82	1.76	875.27	-5.51	4	-1.97	0.99
YC GD	11C SJSU	79.77	1055.67	5.9	1.58	4.93	4.3	22827.75	15.67	16.52	16.02	2.2	401.75	253.17	3.69	1.37	79.19	3.8	1276.94	-4.29	6.55	2.49	1.77
	20B SJSU	136.05	821.39	11.71	5.29	18.17	4.37	23350.71	40.58	86.27	12.96	9.01	360.1	995.22	35.6	6.57	245.28	7.23	4658.12	1.63	31.82	4.11	3.15
	31C SJSU	111.72	887.12	19.32	3.64	13.75	0	25284.85	48.31	80.26	13.78	8.45	358.77	794.43	28.13	5.03	215.37	4.73	3764.86	0.61	23.25	1.24	2.67
	31H SJSU	106.16	1025.16	15.03	2.43	10.91	0	25591.98	33.95	57.97	15.61	5.71	413.52	689.67	19.38	3.84	163.12	3.55	3567.03	-1.13	15.61	0.43	1.74
	5E SJSU	99.12	908.94	14.36	2.11	10.69	4.11	21649.01	38.33	73.33	15.12	7.41	418.5	501.98	25.92	4.85	247.44	7.43	2751.71	-0.54	17.6	3.17	2.58
	5G SJSU	122.2	805.46	13.62	3.34	8.82	0	18602.54	38.58	64.7	14.13	7.07	441.22	615.47	23.39	4.53	211.05	5.12	3447.13	0.66	16.1	0.89	2.31
	BL-4H	92.99	1180.1	8.84	2.34	9.03	0.6	21649.01	30.92	56.17	12.83	6.15	388.88	641.66	18.4	4.28	199.01	4.58	2721.73	-0.2	17.22	0.42	2.47
	11F SJSU	83.4	922.27	10.77	2.33	8.2	2.74	21864.83	33.42	47.78	13.95	5.59	494.31	759.51	15.82	3.4	143.5	5.16	3555.04	0.6	13.65	2.63	2.87
	BL-17A	78.45	1321.25	6.8	8.03	5.09	0	23998.19	26.1	26.31	13.64	2.98	477.28	532.53	1.02	0.94	129.61	2.55	2559.87	-3.73	7.26	-0.71	0.74
	BL-18D	85.01	706.53	7.3	2.67	10.66	0.25	18876.47	22.07	41.34	9.85	4.47	493.9	781.34	16.91	3.32	119.65	2.5	4316.40	-2.09	18.14	-0.07	0.42
	31I-2 SJSU	36.66	245.2	20.35	2.26	3.74	0	9620.86	51.41	118.33	15.52	9.98	341.97	148.41	49.1	6.98	208.27	4.38	1067.11	-3.23	10.84	-0.2	1.67
	37A SJSU	97.19	1202.56	18.05	3.43	8.36	0	27185.78	41.23	69.03	16.72	6.62	353.84	419.04	23.23	4.02	188.72	3.99	2026.31	-3.8	8.62	-1.18	0.49
	BL-7A	77.89	555.26	7.99	3.36	9.43	0.55	18137.69	19.05	36.15	12.21	3.75	544.89	890.46	15.45	3.24	123.37	3.05	3770.86	-1.93	12.21	-0.69	1.25
YC GD dyke	BL-4G	152.78	788.61	15.05	7.6	12.07	0.21	23118.29	19.6	32.15	18.83	3.03	292.14	349.20	8.79	2.07	109.63	2.24	1642.63	-2.64	13.83	0.07	2.23
YC GD dyke	BL-3D	179.89	1048.25	5.16	7.45	13.16	0.21	17207.97	13.88	26.33	12.99	2.53	487.59	1034.51	5.76	2.04	254.17	5.36	4694.09	0.36	12.82	0.16	1.82
YC QM	24A SJSU	101.43	1156	35.03	2.94	10.92	0	16593.70	118.16	195.34	14.72	20.17	762.33	589.28	63.62	10.57	481.29	11.72	3327.23	-2.3	12.85	1.62	1.48
	24A-2 SJSU	102.24	1205.53	34.15	2.55	10.94	0	17091.76	106.32	171.04	14.24	17.93	756.41	589.28	55.84	9.45	497.2	12.57	3231.31	-2.2	12.69	1.15	1.35
	BL-1A	87.85	578.23	7.08	5.59	8.74	1.1	14709.37	19.33	43.8	10.02	5.19	544.23	903.56	21	4.32	81.63	2.4	6492.59	3.76	21.25	0.96	2.19
	BL-1B	100.13	721.45	3.73	2.89	10.66	0	14061.89	9.44	17.49	8.15	1.82	594.95	894.83	6.08	1.74	125.76	2.43	4682.10	-2.43	8.64	-1.3	0.37
	BL-4C	106.78	876.5	12.15	3.8	11.88	0	17199.67	38.93	64.09	12.42	6.91	468.35	680.94	21.73	4.44	261.98	5.51	3830.81	-0.53	20.64	0.26	1.75
	BL-8B	104.81	1255.61	3.55	1.89	14.59	0	20503.47	17.33	29.8	11.93	3.09	716.06	1340.06	6.69	2.11	362.38	8.26	5623.31	2.6	18.92	2.02	1.91
	BL-8E	128.54	990.07	3.25	2.5	13.89	0.34	14526.75	12.49	22.71	12.48	2.36	674.1	1030.14	5.73	1.87	325.91	7.64	4532.22	-0.42	14.78	0.99	2.21
	BL-8G	149.42	959.26	3.99	3.62	15.72	1.54	16211.85	15.45	27.48	10.29	2.98	682.51	1388.07	7.55	2.33	362.13	8.1	5251.62	-0.45	17.21	0.48	1.59
	BL-14A	66.69	670.64	4.63	2.41	7.97	0	16543.89	11.91	26.81	10.31	3.19	548.1	890.46	11.75	2.98	119.79	2.94	5401.50	2.11	16.6	1.09	1.44
	BL-14D	134.88	722.49	0.89	0.78	9.84	0	14518.45	12.17	20.47	8.61	2.52	477.63	1126.17	6.25	2.36	144.93	3.22	6990.17	2.68	11.62	0.88	1.15
	34C SJSU	93.16	1337.31	4.49	2.03	11.02	0	18876.47	17.57	34.17	10.72	3.36	812.35	1178.55	9.82	2.72	548.51	12.76	5587.34	-0.54	10.51	1.19	1.12
	BL-12B	97.45	1335.62	5.42	3.53	12	0	20835.51	25.01	39.24	12.04	4.34	762.22	977.76	9.68	2.71	537.82	12.67	4873.94	-0.01	12.7	1.57	1.41
	19J SJSU	139.55	1095.63	7.67	5.03	17.43	0	22628.53	18.04	34.73	14.38	3.81	672.35	986.49	10.45	2.73	552.19	13.45	4790.01	0.37	22.41	2.07	2.96
	BL-3C	94.77	1073.3	6.15	7.42	9.52	0	14435.44	19.99	37.58	11.76	3.72	773.76	1117.44	12.9	2.82	311.91	7.93	4957.87	0.11	11.4	0.06	1.26
YC QM dyke	BL-13C	61.69	745.24	23.98	3.62	3.34	0	18121.08	22.89	29.76	14.57	2.85	697.46	384.12	6.93	1.69	94.72	2.38	1906.41	-3.67	3.63	-1.58	0.63
YC QM enclave	BL-17B	93.17	435.16	1.52	1.11	11.95	0	15199.13	14.42	37.02	9.22	4.51	466.79	859.91	19.86	4.2	127.25	3.06	5833.14	2.85	24.85	1.43	2.76
YC MD enclave	BL-4E	164.56	2230.93	21.68	21.07	36.98	0	36150.86	11.23	19.95	31.9	2.95	6.83	1431.72	1.98	2.42	96.03	5.07	7517.73	4.36	43.51	1.61	1.7
	BL-13B	63.4	459.04	6.83	2.53	8.33	0	13563.83	21.46	44.06	9.26	5.46	738.08	1523.39	21.87	4.5	129.84	3.57	8638.80	5.19	15.02	0.63	1.25
	BL-14B	66.79	532.81	1.31	0.51	11.25	0	15282.14	12.96	45.28	10.09	6.07	574.64	1169.82	26.89	5.93	116.58	3	7883.43	6.34	28.67	1.96	2.03
	BL-18C	114.72	342.31	5.89	6.23	20.49	1.32	18561.04	19.08	50.91	10.97	6.19	402.56	1152.36	28.12	5.48	91.27	1.69	7427.81	7.67	34.52	1.5	2.19

Sample serie code	Samples	Rb	Ba	Th	U	Nb	Ta	K	La	Ce	Pb	Pr	Sr	P	Nd	Sm	Zr	Hf	Ti	Dy	Y	Er	Yb
Conversion Factor								8301						4365					5995				
YC MD	BL-2C	70.66	1278.96	2.43	0.88	5.78	0	17930.16	14.63	23.06	7.37	2.63	846.08	2121.39	5.35	2.02	304.4	7.58	7140.05	0.36	6.3	0.2	1.01
	BL-8D	42.73	570.75	3.14	1.03	7.41	0	10965.62	12.68	34.6	6.77	4.48	672.1	1108.71	17.61	4.38	126.39	3.21	9394.17	5.13	19.69	0.67	1.55
	BL-9A	47.69	609.48	1.77	0.5	5.35	0	11712.71	11.38	27.9	5.06	3.82	541.71	737.69	14.6	4.06	89.04	1.83	8003.33	5.17	19.83	1.39	2.25
	BL-9B	183.8	693.25	2.35	2.36	7.53	0	17606.42	15.22	23.9	7.35	2.41	767.8	1549.58	4.14	1.88	228.56	3.98	6156.87	0.14	9.6	-3.4	0.74
	BL-14E	61.22	664.48	1.43	0.44	9.64	0.01	14020.39	15.12	30.68	7.08	3.99	509.71	1099.98	14.18	3.58	111.75	2.76	8051.29	1.72	15.69	0.91	2.16
YC MD sheet	BL-2B	38.97	637.1	1.21	0.33	8.53	0	9853.29	15.24	43.67	5.66	5.08	682.5	1488.47	24.52	4.94	106.67	3.05	9334.22	5.63	24.13	1.76	1.21
	BL-8A	36.7	619.55	0.34	0	10.6	0.68	10533.97	15.18	54.84	5.41	7.05	847.87	1850.76	31.89	7.13	40.8	2.32	11252.62	10.51	35.74	2.63	3.27
YC MD dyke	BL-13F	172.04	453.06	19.73	15.31	33.16	5.12	22694.93	58.23	129.38	11.27	15.19	361.93	1754.73	63.13	10.55	296.09	7.75	9046.46	9.11	56.76	3.54	4.8
YC GA	33F SJSU	29.39	524.72	1.79	0	13.93	0.28	8691.15	18.68	71.08	7.73	8.12	692.04	2025.36	40.77	8.5	68.64	3.07	10922.89	11.09	44.86	3.71	3.9
	BL-2D	75.93	371.84	1.49	0	4.58	0	7819.54	7.52	17.2	3.19	2.4	563.96	558.72	10.18	3.31	77.1	2.24	9783.84	6.63	14.28	0.27	1.25
YC GA sheet	BL-3A	29.83	559.13	1.77	0	8	0	8857.17	15.2	43.21	5.9	5.27	735.98	1523.39	22.75	5.09	162.09	4.89	9232.30	4.67	21.61	1.87	1.17
YVIS GT	BL-8F	104.1	1306.43	12.39	3.46	3.94	0	31718.12	21.43	22.24	26.36	2.52	163.29	82.94	0.88	0.95	65.86	0.91	431.64	-4.18	7.62	-1.24	1.31
	BL-10A	211.07	0	8.08	7.08	6.67	0.17	47523.23	6.32	9.57	27.17	-0.04	6.88	91.67	4.18	0.41	25.65	0.19	155.87	-2.8	29.71	-0.17	3.97
	BL-11A	187.22	0	11.62	12.41	15.58	0.65	33577.55	5.99	13.09	17.89	0.48	1.95	100.40	5.38	1.13	39.31	0.35	203.83	-4.98	16.45	-1.41	1.76
	37D SJSU	116.81	914.84	16.43	4.36	8.59	0.23	27227.28	25.37	41.13	23.08	4.24	294.69	336.11	14.43	3	115.84	2.24	1432.81	-2.71	11.66	-0.65	1.03
YVIS QM	37G SJSU	108.96	826.7	13.66	3.25	12.66	0	21673.91	30.97	65.32	12.12	6.32	446.39	798.80	26.23	5.12	227.98	5.63	4058.62	0.97	21.03	1.12	2.6
	40B SJSU	118.24	656.31	5.26	2.74	6.25	0.5	16502.39	22.61	39.75	14.57	3.7	836.99	414.68	14.19	2.5	120.32	3.05	2032.31	-1.51	9.94	-0.57	1.28
YVIS MD	25B SJSU	32.69	375.77	1.05	0.48	9.4	0	8276.10	10.41	37.74	6.77	5.02	649.01	864.27	23.17	5.56	102.02	3.37	11072.77	6.38	32.09	1.51	1.38

XRF Whole rock trace element compositions (ppm) Spel, VCCBS and (selection) Metals

		Spel									VCrCoBaSc						Metals					
Sample serie code	**Sample name**	**Mo**	**Nb**	**Y**	**Zr**	**Sr**	**U**	**Rb**	**Th**	**Pb**	**V**	**Cr**	**Co**	**Ba1**	**Sc**	**Er1**	**Hf1**	**Ga**	**Zn**	**W**	**Cu**	**Ni**	**Total**
YC GT	23B SJSU	28.20	14.71	19.43	95.55	165.86	8.40	157.08	22.21	28.96	9.12	3.33	-5.63	594.64	3.38	-6.07	2.75	14.40	28.25	-1.67	2.45	5.78	94.20
	BL-6A	1.65	9.50	20.50	129.61	210.30	4.63	152.74	12.89	11.39	32.12	3.62	1.04	611.93	6.55	-4.84	0.36	15.92	46.61	0.10	1.37	6.27	93.15
	BL-13A	1.42	9.99	13.52	91.19	328.92	6.53	134.99	17.16	20.10	41.10	4.60	0.29	775.31	5.52	-6.06	0.77	16.33	48.87	-0.57	2.59	7.33	93.85
	BL-15A	0.74	6.78	8.81	90.33	821.66	2.90	72.44	2.06	6.53	176.67	15.58	26.93	704.99	13.61	2.17	2.33	22.97	127.78	2.97	27.65	35.50	87.29
	BL-15B	1.85	9.16	9.68	26.04	90.68	29.99	75.50	20.90	29.42	3.97	1.94	-7.22	132.41	1.96	-6.23	-2.10	15.37	18.33	-1.16	2.01	5.55	91.35
	BL-16A	1.32	6.33	8.04	96.97	426.57	3.23	118.42	10.08	18.25	49.77	6.78	0.84	1246.68	5.25	-5.46	-0.33	15.81	47.68	-0.45	2.90	7.25	92.11
	BL-18A	1.50	4.44	5.05	110.13	391.77	2.12	83.07	8.21	13.76	33.43	2.08	-1.46	1139.18	4.89	-4.85	0.54	15.40	51.19	-0.29	2.07	43.27	90.92
	35I SJSU	3.18	13.17	17.75	104.93	101.72	7.29	196.26	25.89	27.29	16.47	3.16	-2.11	562.98	4.00	-5.03	1.74	16.69	64.36	-0.37	2.29	5.79	94.57
	BL-12A	1.82	10.17	22.07	75.37	185.41	9.40	184.09	47.38	28.46	6.64	2.95	-6.78	682.26	3.40	-4.23	-0.80	13.42	20.74	-1.26	1.09	5.96	93.94
YC GT dyke	BL-4D	0.33	16.42	25.98	219.85	505.95	1.92	175.29	3.79	15.15	2.70	1.69	-8.07	11.53	1.93	-4.51	0.59	19.54	16.58	-1.16	0.66	5.52	93.06
	BL-2A	78.58	4.35	20.75	181.36	2095.58	21.21	63.84	57.05	97.37	1.71	1.08	-5.58	-33.46	0.09	-8.61	-2.68	0.42	8.43	-21.84	44.06	5.34	-3.21
	BL-8C	1.58	13.32	15.53	55.44	216.47	9.80	89.38	9.36	24.98	10.91	1.38	-5.28	888.22	3.26	-6.31	-1.11	15.92	19.68	-0.53	2.32	6.20	92.44
	BL-13E	2.29	5.03	8.28	73.35	274.25	11.38	156.47	82.30	25.48	29.95	4.40	-2.26	1258.07	2.67	-6.00	-0.68	12.34	40.12	0.32	1.54	6.83	93.49
	BL-3E	2.37	11.72	15.87	7.27	34.86	3.70	183.38	3.09	12.31	5.70	1.07	-7.06	108.39	2.32	-7.91	-2.59	17.82	10.97	-0.73	1.05	5.64	91.14
YC GT enclave	BL-4A	1.39	4.92	13.49	153.90	251.02	5.71	161.95	21.62	21.29	17.96	1.59	-6.73	2583.81	1.81	-5.37	2.73	11.28	20.07	-0.74	1.82	6.50	
YC TO	BL-3B	0.92	3.42	4.00	82.00	454.34	2.44	30.72	4.10	9.57	15.05	1.14	-4.88	363.81	2.84	-6.53	-0.25	13.29	28.18	-0.73	1.23	5.37	93.12
YC GD	11C SJSU	2.45	4.93	6.55	79.19	401.75	1.58	79.77	5.90	16.02	26.32	3.89	-2.53	1055.67	5.05	-5.15	0.97	15.31	42.88	0.79	3.53	6.76	96.42
	20B SJSU	2.08	18.17	31.82	245.28	360.10	5.29	136.05	11.71	12.96	79.53	7.39	9.83	821.39	13.48	-0.50	5.64	19.58	122.28	1.86	4.24	7.85	94.14
	31C SJSU	2.18	13.75	23.25	215.37	358.77	3.64	111.72	19.32	13.78	69.77	6.43	6.72	887.12	9.81	-0.51	2.19	18.59	100.95	-0.51	3.38	7.46	94.72
	31H SJSU	2.68	10.91	15.61	163.12	413.52	2.43	106.16	15.03	15.61	70.55	7.24	6.77	1025.16	9.94	-1.76	1.43	18.68	88.37	0.11	13.50	9.85	95.35
	5E SJSU	1.53	10.69	17.60	247.44	418.50	2.11	99.12	14.36	15.12	42.47	7.96	2.22	908.94	8.36	-3.33	4.44	18.11	82.75	1.31	5.28	7.76	92.96
	5G SJSU	2.06	8.82	16.10	211.05	441.22	3.34	122.20	13.62	14.13	69.24	5.31	5.51	805.46	11.02	-0.23	3.46	18.51	77.12	-0.61	22.13	6.93	95.34
	BL-4H	2.62	9.03	17.22	199.01	388.88	2.34	92.99	8.84	12.83	40.42	2.30	2.38	1180.10	8.51	-2.06	2.74	18.39	79.99	-0.41	2.85	5.86	93.79
	11F SJSU	2.27	8.20	13.65	143.50	494.31	2.33	83.40	10.77	13.95	75.10	7.95	7.30	922.27	10.14	-2.16	3.72	18.59	81.27	1.12	8.14	9.02	94.64
	BL-17A	0.92	5.09	7.26	129.61	477.28	8.03	78.45	6.80	13.64	48.26	12.96	1.53	1321.25	6.49	-4.50	0.66	17.45	63.45	-0.10	2.37	6.91	90.39
	BL-18D	1.27	10.66	18.14	119.65	493.90	2.67	85.01	7.30	9.85	89.87	8.80	8.79	706.53	10.57	-0.38	2.14	20.06	87.07	1.51	8.61	11.03	90.14
	31I-2 SJSU	2.54	3.74	10.84	208.27	341.97	2.26	36.66	20.35	15.52	24.42	3.98	-2.68	245.20	4.34	-6.37	2.32	14.19	24.71	-1.69	6.65	8.21	95.94
	37A SJSU	1.92	8.36	8.62	188.72	353.84	3.43	97.19	18.05	16.72	25.85	2.91	-0.44	1202.56	7.46	-4.49	4.62	17.20	60.06	-0.37	2.13	5.59	96.10
	BL-7A	0.71	9.43	12.21	123.37	544.89	3.36	77.89	7.99	12.21	69.60	4.50	6.20	555.26	9.39	-2.88	2.51	20.47	90.03	0.55	4.11	7.17	92.90
YC GD dyke	BL-4G	1.17	12.07	13.83	109.63	292.14	7.60	152.78	15.05	18.83	23.18	2.75	-1.75	788.61	4.91	-5.17	0.86	15.75	49.78	-0.63	1.32	6.05	92.67
YC GD dyke	BL-3D	0.30	13.16	12.82	254.17	487.59	7.45	179.89	5.16	12.99	82.12	3.79	7.79	1048.25	8.25	-1.66	4.68	22.03	94.08	0.88	6.38	6.68	89.18
YC QM	24A SJSU	-0.30	10.92	12.85	481.29	762.33	2.94	101.43	35.03	14.72	11.63	1.26	-0.03	1156.00	7.68	-2.50	8.87	23.13	109.52	-0.14	1.99	5.28	94.10
	24A-2 SJSU	1.23	10.94	12.69	497.20	756.41	2.55	102.24	34.15	14.24	12.29	1.75	0.51	1205.53	7.73	-3.28	9.47	23.02	107.27	0.29	1.98	5.65	93.89
	BL-1A	0.75	8.74	21.25	81.63	544.23	5.59	87.85	7.08	10.02	178.03	8.91	20.38	578.23	19.56	1.09	3.03	20.79	122.62	1.77	15.13	13.43	94.80
	BL-1B	0.27	10.66	8.64	125.76	594.95	2.89	100.13	3.73	8.15	101.27	5.30	10.57	721.45	9.44	-2.14	2.20	21.29	91.86	0.63	16.37	8.59	93.32
	BL-4C	0.19	11.88	20.64	261.98	468.35	3.80	106.78	12.15	12.42	67.96	4.54	6.39	876.50	10.66	-2.36	4.72	19.90	101.13	0.21	6.76	6.22	90.81
	BL-8B	-0.86	14.59	18.92	362.38	716.06	1.89	104.81	3.55	11.93	44.11	1.83	7.63	1255.61	9.69	-0.39	7.18	25.05	109.53	0.55	6.49	5.93	91.97
	BL-8E	-0.69	13.89	14.78	325.91	674.10	2.50	128.54	3.25	12.48	40.89	1.36	5.08	990.07	8.46	-1.58	6.61	23.85	98.39	0.59	14.61	5.94	92.42
	BL-8G	-0.65	15.72	17.21	362.13	682.51	3.62	149.42	3.99	10.29	41.07	1.23	7.18	959.26	9.01	-1.26	7.52	24.66	125.96	0.97	10.93	5.40	89.04
	BL-14A	0.83	7.97	16.60	119.79	548.10	2.41	66.69	4.63	10.31	139.58	10.92	16.69	670.64	15.12	-0.78	2.56	20.70	99.23	0.73	17.27	10.60	93.22
	BL-14D	0.45	9.84	11.62	144.93	477.63	0.78	134.88	0.89	8.61	186.89	17.01	25.12	722.49	20.56	3.60	4.18	24.55	169.94	1.87	32.23	21.46	91.11
	34C SJSU	-0.88	11.02	10.51	548.51	812.35	2.03	93.16	4.49	10.72	41.32	1.89	6.76	1337.31	11.36	-1.02	10.77	24.77	111.16	0.65	6.46	5.59	92.79
	BL-12B	-1.81	12.00	12.70	537.82	762.22	3.53	97.45	5.42	12.04	36.66	2.30	4.14	1335.62	8.76	-0.63	11.15	25.39	104.55	0.99	4.78	5.77	91.14
	19J SJSU	-0.35	17.43	22.41	552.19	672.35	5.03	139.55	7.67	14.38	33.34	2.64	5.21	1095.63	10.17	0.47	14.82	23.98	103.46	1.06	7.41	5.92	94.48
	BL-3C	-0.85	9.52	11.40	311.91	773.76	7.42	94.77	6.15	11.76	77.46	4.11	9.41	1073.30	9.05	-3.05	5.96	24.43	101.13	0.83	10.72	7.31	92.29

		Spel									VCrCoBaSc						Metals					
Sample serie code	**Sample name**	**Mo**	**Nb**	**Y**	**Zr**	**Sr**	**U**	**Rb**	**Th**	**Pb**	**V**	**Cr**	**Co**	**Ba1**	**Sc**	**Er1**	**Hf1**	**Ga**	**Zn**	**W**	**Cu**	**Ni**	**Total**
YC QM dyke	BL-13C	0.58	3.34	3.63	94.72	697.46	3.62	61.69	23.98	14.57	47.59	5.41	0.46	745.24	5.00	-5.21	-0.13	20.40	49.52	-0.32	1.74	7.49	92.66
YC QM enclave	BL-17B	1.03	11.95	24.85	127.25	466.79	1.11	93.17	1.52	9.22	163.28	31.67	18.72	435.16	17.49	0.50	3.02	21.27	140.76	0.76	57.45	19.33	91.46
YC MD enclave	BL-4E	0.56	9.64	15.69	111.75	509.71	0.44	61.22	1.43	7.08	173.68	94.68	22.71	664.48	18.22	2.93	3.31	21.82	133.25	1.44	39.10	37.15	92.64
	BL-13B	0.67	8.33	15.02	129.84	738.08	2.53	63.40	6.83	9.26	224.51	34.31	26.09	459.04	20.51	3.55	4.78	24.18	138.40	1.55	35.03	16.54	94.53
	BL-14B	0.20	11.25	28.67	116.58	574.64	0.51	66.79	1.31	10.09	231.37	9.64	28.69	532.81	27.76	7.66	4.37	24.05	142.69	2.27	49.43	11.70	93.87
	BL-18C	2.51	20.49	34.52	91.27	402.56	6.23	114.72	5.89	10.97	180.86	2.24	22.38	342.31	27.67	2.71	3.75	26.10	174.56	1.82	84.86	17.51	90.00
YC MD	BL-2C	-1.12	5.78	6.30	304.40	846.08	0.88	70.66	2.43	7.37	132.82	6.97	17.96	1278.96	9.37	0.37	7.41	25.24	119.42	1.45	17.08	9.33	91.74
	BL-8D	3.52	4.58	14.28	77.10	563.96	0.10	75.93	1.49	3.19	462.03	8.26	52.43	371.84	32.46	8.63	4.23	21.34	139.42	3.11	40.53	15.63	95.40
	BL-9A	0.14	5.35	19.83	89.04	541.71	0.50	47.69	1.77	5.06	328.11	15.20	42.61	609.48	27.26	8.12	4.70	22.48	126.32	2.74	44.42	19.06	91.74
	BL-9B	-0.15	7.53	9.60	228.56	767.80	2.36	183.80	2.35	7.35	77.66	1.33	11.66	693.25	8.83	-1.85	5.26	25.30	125.66	21.77	147.83	5.65	90.01
YC MD sheet	BL-2B	-0.25	8.53	24.13	106.67	682.50	0.33	38.97	1.21	5.66	268.62	4.93	32.01	637.10	26.92	7.11	3.72	24.13	138.87	2.71	30.06	13.78	95.45
	BL-8A	-0.41	10.60	35.74	40.80	847.87	-0.51	36.70	0.34	5.41	258.00	4.29	27.91	619.55	30.90	10.18	3.15	27.00	173.86	3.21	30.95	10.71	91.29
YC MD dyke	BL-13F	1.62	33.16	56.76	296.09	361.93	15.31	172.04	19.73	11.27	168.52	10.78	22.95	453.06	19.02	5.23	7.96	25.27	181.31	1.75	12.28	10.84	94.91
YC GA	33F SJSU	1.40	13.93	44.86	68.64	692.04	-0.81	29.39	1.79	7.73	261.98	2.10	34.89	524.72	31.58	9.45	3.81	24.98	171.39	1.55	37.27	8.97	96.65
YC GA sheet	BL-3A	-0.86	8.00	21.61	162.09	735.98	-0.03	29.83	1.77	5.90	273.54	6.81	39.82	559.13	24.88	5.08	5.22	23.58	141.38	2.43	59.61	15.18	95.38
YVIS GT	BL-8F	1.72	3.94	7.62	65.86	163.29	3.46	104.10	12.39	26.36	5.57	1.40	-6.68	1306.43	1.19	-6.98	-0.24	12.20	22.55	-1.28	1.41	6.34	92.79
	BL-10A	2.30	6.67	29.71	25.65	6.88	7.08	211.07	8.08	27.17	1.42	1.43	-7.52	-1.06	1.22	-6.24	-1.45	16.37	25.66	-0.43	0.55	6.06	91.87
	BL-11A	2.29	15.58	16.45	39.31	1.95	12.41	187.22	11.62	17.89	1.48	1.51	-7.74	-6.76	1.52	-7.28	-1.43	16.59	19.90	-0.36	0.54	5.20	92.77
	37D SJSU	2.53	8.59	11.66	115.84	294.69	4.36	116.81	16.43	23.08	21.86	4.13	-2.06	914.84	4.54	-3.86	-0.29	14.87	50.80	-0.35	1.57	5.42	96.28
YVIS QM	37G SJSU	2.66	12.66	21.03	227.98	446.39	3.25	108.96	13.66	12.12	74.71	5.05	7.37	826.70	12.85	0.42	3.61	19.57	89.55	0.77	5.46	6.67	95.42
	40B SJSU	0.54	6.25	9.94	120.32	836.99	2.74	118.24	5.26	14.57	24.69	2.94	-2.78	656.31	4.66	-3.24	1.34	21.43	51.85	1.57	6.76	6.08	93.78
YVIS MD	25B SJSU	1.41	9.40	32.09	102.02	649.01	0.48	32.69	1.05	6.77	338.69	3.78	33.59	375.77	38.79	8.57	3.88	24.58	133.61	3.18	34.66	8.51	95.64

Composition of solid phases, used for the lever-rule calculations

phase	SiO2	Al2O3	MgO	FeO	CaO	Na2O	TiO2	K2O	P2O5	BaO	Paper
plagioclase average	52.96	29.72	0	0.84	12.28	4.21	0	0.13	0	0	Deer et al., 1966
plagioclase silisic	65	22	0	0	4	8	0	2	0.00	0	Klimm et al., 2008
feldspar	66	19	0	0	0	3	0	11	0.00	0	Klimm et al., 2008
hornblende	46	8	13	17	12	1	1	1	0.00	0	McCarthy et al., 1979
biotite	36	14	10	17	2	0	3	8	0.00	0	McCarthy et al., 1979
clinopyroxene	51	8	16	3	20	1	1	0	0.00	0	Workman et al., 2005
clinopyroxene	*53*	*6*	*31*	*6*	*2*	*0*	*0*	*0*	*0.00*	*0*	*Workman et al., 2005*
spinel	0	58	19	13	0	0	0	0	0.00	0	Workman et al., 2005
olivine	41	0	49	10	0	0	0	0	0.00	0	Workman et al., 2005
titanite	30	1	0	1	28	0	37	0	0.10	0	Fulmer and Kruijer, 2008
ilmenite	0	0	3	53	0	0	40	0	0.00	0	Venezky et al., 1999
magnetite	*0*	*2*	*2*	*81*	*0*	*0*	*11*	*0*	*0.00*	*0*	*Venezky et al., 1999*
magnetite	0	0	2	45	0	0	53	0	0.00	0	Ashwal, 1982
apatite	41.89	12.47	9.03	9.43	16.55	1.37	2	0.2	4.94	0	Watson, 1980

Lever-rule calculation

major-element	Phase(s)		SD	SP	%D	%S
Al	plag-hbl		23	6	26	74
	plag-bio-c	best guess	25	7	28	72
Fe	bio-hbl		65	7	11	89
	plag_av		14	8	57	43
	plag_si		11	5	45	55
	feld		15	8	53	47
Na	plag_av		23	7	30	70
	plag_si		20	9	45	55
	feld		15	5	33	67
K	plag_av		8	4	50	50
	plag_si		21	5	24	76
	feld		27	21	78	22
Mg	bio-hbl		58	13	22	78
	plag_av		14	8	57	43
	plag_si		10	3	30	70
	feld		15	8	53	47
Ca	ap-bio-hbl	best guess	42	5	12	88
	plag_av		19	11	58	42
	plag_si		12	10	83	17
Ti	bio-hbl		49	8	16	84
	plag_av		14	8	57	43
	plag_si		10	4	40	60
	feld		15	8	53	47
P	ti-ap1		61	16	26	74
	ti-ap2		62	15	24	76
	ti-ap3		63	17	27	73
	ti-ap4		67	21	31	69
CaO enclave			17	10	59	41
K2O enclave			18	4	22	78

S	solid
D	daugther
P	parent
%	amount phase

Partition Coefficients

Rollinson, 1993	basalt				
		Plagioclase	Hornblende	Clinopyroxene	Garnet
	Rb	0.071	0.29	0.31	0.042
	Sr	1.83	0.46	0.06	0.012
	Ba	0.23	0.42	0.026	0.023
	K	0.17	0.96	0.038	0.015
	La	0.19	0.25	0.056	0.026
	Yb	0.067	0.49	0.542	35.6

Rollinson, 1993	Andesite						
		Plagioclase	Hornblende	Clinopyroxene	Orthopyroxene	Garnet	Allanite
	Rb	0.53	0.04	0.02	0.022	0.01	
	Sr	1.6	0.2	0.08	0.032		
	Ba	0.155	0.1	0.02	0.013		
	K	0.117	0.33	0.02	0.014	0.01	
	La	0.302	0.5	0.047	0.031	0.076	1495.4
	Yb	0.041	2.1	0.633	0.0254	53	100.7

Bachmann et al., 2005	Dacite												
		Plagioclase	Feldspar	Biotite	*Biotite*	Hornblende	Apatite	Sphene	Zircon	Zircon	Allanite	Garnet	Quartz
	Rb	0.01	0.7	3.2	*2*	0		0.01				0.009	0.041
	Sr	12.5	7.4	0.447	*0.1*	0.4		0.37		0.01		0.015	
	Ba	0.61	17.1	25.533	*4.4*	0.08		0.01		0.01		0.017	
R	**K**	0.263				0.081						0.2	
	La	0.4	0.06	5.713	*0.01*	1.4	36	113	0.00046	0.1	1495.4	0.39	0.015
	Yb	0.01	0.03	1.473	*0.03*	9.6	48	393	325	465	100.7	43.475	0.017
Paper			R		S			F	F	F	R	R	

Starting melts in Rayliegh calculations are based on EM1 and EM2 of Vogel et al., 2008

Fulmer and Kruijer, 2008	F
Rollinson, 1993	R
Sano et al., 2002	S